University of Massachusetts Amherst
ScholarWorks@UMass Amherst

Doctoral Dissertations 1896 - February 2014

1-1-1979

Dynamic mechanical property studies of segmented polyurethanes and epoxy resins/

George Albert Senich
University of Massachusetts Amherst

Follow this and additional works at: https://scholarworks.umass.edu/dissertations_1

Recommended Citation
Senich, George Albert, "Dynamic mechanical property studies of segmented polyurethanes and epoxy resins/" (1979). *Doctoral Dissertations 1896 - February 2014*. 648.
https://scholarworks.umass.edu/dissertations_1/648

This Open Access Dissertation is brought to you for free and open access by ScholarWorks@UMass Amherst. It has been accepted for inclusion in Doctoral Dissertations 1896 - February 2014 by an authorized administrator of ScholarWorks@UMass Amherst. For more information, please contact scholarworks@library.umass.edu.

UMASS/AMHERST

312066 0015 5990 4

DYNAMIC MECHANICAL PROPERTY STUDIES OF SEGMENTED POLYURETHANES AND EPOXY RESINS

A Dissertation Presented

By

GEORGE ALBERT SENICH, JR.

Submitted to the Graduate School of the
University of Massachusetts in partial fulfillment
of the requirements for the degree of

DOCTOR OF PHILOSOPHY

February 1979

Polymer Science and Engineering

© George Albert Senich, Jr. 1979

All Rights Reserved

Army Materials and Mechanics Research Center
Contract DAAG-46-77-C-0031

Army Research Office
Grant DAAG-29-77-G-0055

DYNAMIC MECHANICAL PROPERTY STUDIES OF SEGMENTED POLYURETHANES AND EPOXY RESINS

A Dissertation Presented

By

GEORGE ALBERT SENICH, JR.

Approved as to style and content by:

William J Mac Knight

Dr. William J. MacKnight
Chairperson of Committee

Richard J. Farris

Dr. Richard J. Farris, Member

Richard S. Stein

Dr. Richard S. Stein, Member

William J Mac Knight

Dr. William J. MacKnight
Department Head
Polymer Science and Engineering

To my parents, for getting me going
when the going got tough
and Brown and Henderson, who summed
it up in a song.

ACKNOWLEDGMENTS

Many individuals have contributed to the successful completion of this dissertation. Above all, I am indebted to Professor William J. MacKnight for timely advice, encouragement, and guidance throughout this research endeavor. I wish to express my appreciation to Professor Richard J. Farris and Professor Richard S. Stein, who as members of the dissertation committee offered many helpful criticisms and suggestions.

I have benefited from numerous conversations with Dr. Richard Neumann, particularly concerning the material presented in the first two chapters. Dr. N.S. Schneider kindly provided many of the materials examined and discussed his work on epoxy resins and polyurethane elastomers at length. I am grateful for their interest.

My thanks to Dr. K. Krishnan of Digilab for assistance in carrying out the FT-ir studies and to Mr. Jack Carroll for making instrument time available. Thanks also to Mr. David Henderson for his assistance with the thermal analyzer experiments.

I would like to acknowledge the time and talents expended on behalf of this research by many of my fellow graduate students. Their friendship will always be remembered.

Special thanks go to Chuck and Nancy Ryan, who spared me from an onerous residency at the Drake during the completion of this dissertation.

Finally, I wish to thank the Department of Polymer Science and

Engineering, the Materials Research Laboratory, the Army Research Office and the Army Materials and Mechanics Research Center for supporting my studies at the University of Massachusetts.

PREFACE

This dissertation is presented in six chapters. Each chapter includes an introduction, discussing the pertinent literature, and a self-contained reference section. In Chapter I, the technique of dynamic spring analysis is discussed and experimental findings compared to results obtained from other dynamic methods of measuring moduli to determine the applicability of the technique. The origin of a relaxation process above the glass transition, evident in Chapter I, is the subject of Chapter II. Utilization of this phenomenon in a kinetic study of the curing reaction of epoxy resins is detailed in Chapter III. A study of phase segregation in a series of segmented polyurethane elastomers is presented in Chapter IV. Dynamic mechanical testing is employed extensively in this examination. Chapter V discusses an infrared thermal study of the hydrogen bonding equilibria in a particular block polyurethane. Suggestions for future work are outlined in the last chapter. Some of the material presented in Chapters I through IV has been previously published.

ABSTRACT

Dynamic Mechanical Property Studies of Segmented Polyurethanes and Epoxy Resins

(February 1979)

George Albert Senich, Jr.

B.S., Case Western Reserve University
M.S., University of Massachusetts
Ph.D., University of Massachusetts

Directed by: Professor William J. MacKnight

The technique of dynamic spring analysis (DSA) is employed to obtain the storage and loss modulus of polystyrene in the glassy and rubbery region of viscoelastic response. The results are compared to dynamic shear moduli by time temperature superposition and show that DSA can be used to semi-quantitatively predict moduli in the rubbery region. The technique as constituted is not sensitive to modulus changes below the glass transition temperature.

An apparent irreversible relaxation process above the glass transition temperature in DSA determinations is attributable to solvent evaporation from incompletely dried films. Studies on carefully prepared polystyrene samples exhibit a repeatable dynamic mechanical loss dispersion well above T_g, analogous to the T_{ll} process observed by torsional braid analysis. A model which predicts that any composite sample consisting of an elastic support and a viscous liquid must produce such a relaxation, devoid of molecular origin, is proposed. Measurements on

4,000 molecular weight polystyrene and glycerol confirm these predictions while direct viscometric studies of the former material show that only simple liquid-like response is observed in a comparable temperature frequency region.

The curing behavior of two commercially formulated epoxy resins composed of the tetrafunctional amine dicyandiamide and with differing epoxy components, 4,4'-bisglycidylphenyl-2,2'-propane and the tetraglycidyl ether of methylene dianiline, is characterized by DSA. This technique is well suited to the determination of the onset of gelation under isothermal conditions but is not useful for monitoring later stages of reaction. The activation energy for curing of the two resins is about 87 kJ/mole. Rate constants for the first order curing reaction are given. Additional studies of films cured below the ultimate T_g show that two relaxations can be observed upon heating. The first relaxation occurs near the original isothermal cure temperature with a low activation energy, about 250 kJ/mole, whereas the second relaxation occurs near the ultimate T_g, with an activation energy of 500 to 650 kJ/mole. These activation energies provide a unique method of characterizing the molecular mobility of epoxy resins at various states of cure.

The dynamic mechanical response of several segmented polyurethanes, consisting of either 2,4- or 2,6-toluene diisocyanate (TDI), 1,4-butanediol (BD) and 1000 or 2000 molecular weight poly(tetramethylene oxide) (PTMO), is studied as a function of diisocyanate structure, diisocyanate content and PTMO molecular weight and related

to the degree of phase segregation present in these elastomers. The symmetrical 2,6-TDI isomer and longer TDI-BD (hard segment) and PTMO sequence lengths promote phase segregation in these materials. The glass transition temperature of the PTMO phase is strongly influenced by the purity of the phase and the overall degree of crystallinity. The high temperature relaxation, corresponding to the glass transition in 2,4-TDI copolymers and melting in the 2,6-TDI copolymers, is directly related to the average hard segment length, while the plateau modulus between these relaxation regions is strongly dependent upon hard segment content. Comparison of block polyurethane relaxations to the corresponding loss process of TDI-BD and TDI-PTMO copolymers indicates that short block length and a significant degree of intersegmental mixing contribute to poor phase organization in the block polyurethanes.

Thermal analysis of hydrogen bonding in block polyurethanes is studied by Fourier Transform infrared spectroscopy. The ratio of hydrogen bonded to free absorbance is determined to be 4.6 for the N-H stretch and 1.05 for the C=O stretch of a 2,6-TDI polyurethane. The heat of hydrogen bond dissociation is determined to be about 21 kJ/mole for bonding to either the urethane carbonyl or other acceptor sites. A large amount of interfacial material is thought to preclude observation of discontinuities in the hydrogen bonding equilibria caused by the hard segment glass transition.

TABLE OF CONTENTS

Page

ACKNOWLEDGMENTS v

PREFACE vii

ABSTRACT viii

LIST OF TABLES xiii

LIST OF FIGURES xiv

Chapter

I. DYNAMIC SPRING ANALYSIS 1

- Introduction 1
- Experimental 4
  - Samples 4
  - Dynamic Mechanical Measurements 4
  - Melt Rheology Measurements 8
- Theory 8
- Results 12
- Discussion 30
- Conclusions 37
- References 38

II. DISPERSIONS ABOVE THE GLASS TRANSITION IN SUPPORTED SYSTEMS . 40

- Introduction 40
- Experimental 43
  - Samples 43
  - Measurements 43
- Theory 45
- Results 49
  - Solvent Induced Relaxations 49
  - Other Relaxations Above the Glass Transition 61
- Discussion 71
- Conclusions 76
- References 78

Chapter Page
III. A DYNAMIC MECHANICAL STUDY OF THE CURING REACTION OF TWO EPOXY RESINS 80

Introduction 80
Experimental 81
Samples 81
Measurements 81
Results 87
Isothermal Cures 87
Partially Cured Thin Films 107
Discussion 114
Isothermal Cures 114
Partially Cured Thin Films 120
Conclusions 122
References 124

IV. PHASE SEGREGATION IN TOLUENE DIISOCYANATE BLOCK POLYURETHANES 126

Introduction 126
Experimental 129
Samples 129
Characterization 130
Results 137
Hard and Soft Segments 137
2,4-TDI Polyurethanes 148
2,6-TDI Polyurethanes 165
Discussion 191
Hard and Soft Segment Polymers 191
The α Relaxation of 2,4-T-1P 192
Soft Segment Relaxations 194
Hard Segment Relaxations 201
Degree of Phase Segregation 206
Effects of Phase Segregation on Modulus 208
Conclusions 211
References 214

V. FOURIER TRANSFORM INFRARED THERMAL ANALYSIS OF A BLOCK POLYURETHANE 216

Introduction 216
Experimental 219
Results 220
Discussion 240
Conclusions 249
References 250

VI. SUGGESTIONS FOR FUTURE WORK 252

APPENDIX 255

LIST OF TABLES

Table Page

1-1. Comparison of Spring Constants Determined by Several Methods 13
2-1. Summary of Polystyrene Relaxations 55
2-2. Slopes and Viscosities of 4000 $\overline{M}_n$ Polystyrene from RMS Data 67
2-3. Products of Frequency and Viscosity for 4000 $\overline{M}_n$ Polystyrene and Glycerol at the Loss Tangent Maximum 70
3-1. Isothermal Cure Times for Resin I 93
3-2. Isothermal Cure Times for Resin II 94
3-3. Chemical Activation Energies for Epoxy Cures 99
3-4. Comparison of Chemical Activation Energies Determined by Several Methods 101
3-5. Rate Constants for Epoxy Cures 106
3-6. Transition Temperatures and Activation Energies for Partially Cured Resin II Films 117
4-1. Toluene Diisocyanate Polyurethane Compositions 133
4-2. Relaxations of Hard and Soft Segment Polymers 149
4-3. Relaxations of 2,4-TDI Block Polyurethanes 157
4-4. Relaxations of 2,6-TDI Block Polyurethanes 168
4-5. Relaxations of Thermally Treated 2,6-TDI Polyurethanes . . . 186
5-1. Variation of Hydrogen Bonding with Temperature 239

LIST OF FIGURES

Figure		Page
1-1.	Schematic Representation of a DSA Composite Sample	6
1-2.	Temperature Variation of Relative Spring Modulus and Loss Tangent	16
1-3.	Storage and Loss Modulus of Polystyrene from DSA as a Function of Temperature	19
1-4.	Composite Loss Tangent of Polystyrene from DSA as a Function of Temperature	21
1-5.	Elastic Stress Strain Response of Polystyrene from ERD at Several Temperatures	24
1-6.	Viscous Stress Strain Response of Polystyrene from ERD at Several Temperatures	26
1-7.	Time Temperature Superposition of Storage Moduli from DSA and ERD	29
1-8.	Time Temperature Superposition of Loss Moduli from DSA and ERD	32
1-9.	Comparison of the Polystyrene Loss Tangent Determined from DSA and a Thin Film	36
2-1.	Spring-Dashpot Model Proposed to Account for the T_{ll} Relaxation	47
2-2.	Loss Tangent for Sample C-2 During the Initial Thermal Scan	51
2-3.	Loss Tangent for Sample C-2 During the Second Thermal Scan	53
2-4.	Gas Chromatograph Trace of Vapors Evolved During Thermal Analysis	58
2-5.	Concentration of Organic Vapors Evolved During Thermal Analysis	60
2-6.	Temperature Variation of the Loss Tangent for 4000 $\overline{M}_n$ Polystyrene	63
2-7.	Loss Modulus vs. Frequency for 4000 $\overline{M}_n$ Polystyrene	65
2-8.	Temperature Variation of the Loss Tangent for Glycerol	69
2-9.	Temperature Variation of the Loss Tangent for Polystyrene of Several Molecular Weights	73
3-1.	Chemical Structure of Epoxy Resin I	83
3-2.	Chemical Structure of Epoxy Resin II	85
3-3.	Variation of Resin I Storage and Loss Modulus with Time at 80.2°C	89
3-4.	Loss Tangent vs. Time for Resin II at Several Cure Temperatures	92
3-5.	Arrhenius Plots for the Resin I Curing Reaction	96
3-6.	Arrhenius Plots for the Resin II Curing Reaction	98
3-7.	Viscosity vs. Time for Several Resin I Cures	103
3-8.	Viscosity vs. Time for Several Resin II Cures	105

Figure Page

3-9. Temperature Variation of the Storage and Loss Modulus of Resin I Cured at 79°C 109
3-10. Temperature Variation of the Loss Tangent of Resin I Cured at 79°C 111
3-11. Temperature Variation of the Storage and Loss Modulus of Resin II Cured at 83°C 113
3-12. Loss Tangent of Resin II vs. Temperature for Several Cure Temperatures 116
4-1. Structure of the Block Polyurethane Elastomers 132
4-2. Thermal History of Compression Molded Polyurethane Films . . 135
4-3. DSC Thermograms of Hard Segment Polymers 140
4-4. Temperature Variation of the Storage and Loss Modulus of 2,6-TDI/BD 142
4-5. Temperature Variation of the Storage and Loss Modulus of 2,6-TDI/PTMO 145
4-6. DSC Thermograms of Soft Segment Polymers 147
4-7. Storage and Loss Modulus for Two Compositions of 2,4-T-1P as a Function of Temperature 151
4-8. Comparison of Dynamic Mechanical and DSC or TMA Transition Temperatures for 2,4-T-1P and 2,4-T-2P 153
4-9. Storage and Loss Modulus for Three Compositions of 2,4-T-2P as a Function of Temperature 155
4-10. Temperature Variation of DSA Storage and Loss Modulus of 2,4-T-1P-60 159
4-11. Frequency Variation of DSA Loss Modulus and Loss Tangent of 2,4-T-1P-60 162
4-12. Temperature Variation of DSA Storage and Loss Modulus of 2,4-T-2P-43 164
4-13. Storage and Loss Modulus for Three Compositions of 2,6-T-1P as a Function of Temperature 167
4-14. Comparison of Dynamic Mechanical and DSC or TMA Transition Temperatures for 2,6-T-1P 170
4-15. Storage and Loss Modulus for Four Compositions of 2,6-T-2P as a Function of Temperature 173
4-16. Loss Tangent for Four Compositions of 2,6-T-2P as a Function of Temperature 175
4-17. Temperature Variation of the Storage and Loss Modulus of 2,6-T-1P-31 and 2,6-T-2P-33 177
4-18. DSC Thermograms of 2,6-T-1P-31 and 2,6-T-2P-33 180
4-19. Comparison of Dynamic Mechanical and DSC or TMA Transition Temperatures for 2,6-T-2P 182
4-20. Comparison of 2,6-T-2P-43 Dynamic Mechanical Response on Initial and Second Determination 185
4-21. Comparison of 2,6-T-2P-43 Loss Tangent on Initial and Second Determination 188
4-22. Activation Energy of the 2,6-T-2P α_s Relaxation as a Function of Composition for Two Determinations 190

Figure Page

4-23. Inverse Temperature Variation of the Normalized Loss Modulus of the 2,4-T-2P α_s Relaxation 196
4-24. Inverse Temperature Variation of the Normalized Loss Modulus of the 2,6-T-1P α_s Relaxation 199
4-25. Reciprocal Average Hard Segment Length vs. Inverse Temperature for the 2,6-TDI δ Relaxation 204
4-26. Temperature Variation of the Storage and Loss Modulus of 2,4-T-2P-43 and 2,6-T-2P-43 210
5-1. Infrared Spectrum of 2,6-T-2P-43 222
5-2. Infrared Spectra of 2,6-T-2P-43 in the N-H and C=O Stretching Region at Two Temperatures 225
5-3. Normalized Integrated Absorbance vs. Temperature for N-H and C=O Stretch 227
5-4. Difference Spectrum in the N-H Stretching Region 231
5-5. Difference Spectrum in the C=O Stretching Region 233
5-6. Integrated Absorbance of the Difference Spectra vs. Temperature for Four Absorptions 236
5-7. Van't Hoff Plot for 2,6-T-2P-43 Hydrogen Bonding Equilibria 242

CHAPTER I

DYNAMIC SPRING ANALYSIS

Introduction

The study of the viscoelastic properties of materials with insufficient strength to be analyzed by normal tensile testing methods has presented experimental problems to those studying elastomeric materials, crosslinking reactions, low molecular weight polymers, and other systems of low modulus. Many techniques have been developed which are capable of aiding the experimenter in such a viscoelastic analysis. A brief discussion of several of these methods will be given here.

The rheological response of materials can be studied by many viscometric techniques. The Rheometrics mechanical spectrometer (RMS) is capable of rheological characterization in cone and plate and parallel plate geometries in both steady state and dynamic experiments (1). Solid samples can be evaluated in a bending beam test to temperatures just above the glass transition or melting temperature. A complete determination from solid to melt is usually impossible with a single sample geometry and the quantity of a sample required is often prohibitively large, typically 1 to 10 g.

Other attempts to obtain information on dynamic viscoelastic properties of rubbery polymers and polymer melts have focused upon modification of the Rheovibron. A study of the rheological properties of styrene-ethylene oxide block copolymers by Erhardt and coworkers (2) included a modification of the Rheovibron DDV-II which produced a dynamic shearing mode of deformation between parallel plates. Shah and Darby (3) have employed the Rheovibron DDV-III in a study of dynamic moduli of polymer melts by modification to give a shear deformation between two sets of parallel plates. A similar modification was employed by Murayama (4) with the more common Rheovibron DDV-II.

Studies have also been conducted by using inert substrates as supports for materials of low modulus. Polystyrene films (5) and cylinders (6), cellulose blotter paper (7), cellulose filter strips (8), and quartz filaments (9) have all been used as substrates in various evaluations of mechanical behavior. A supported sample technique which has been extensively applied is torsional braid analysis (TBA), developed by Gillham and coworkers (10-12). The sample is prepared by mounting a glass fiber braid impregnated with the material of interest in a conventional torsion pendulum instrument. The relative rigidity, equal to the square of the inverse of the period of free oscillation, and the mechanical damping index, proportional to the logarithmic decrement, are obtained as a function of temperature and are related to the storage and loss modulus response of the sample. TBA studies of the viscoelastic behavior of many polymers at high temperatures, curing reactions of numerous types, and the effect of additives and aging upon polymer viscoelastic properties have been carried out. This method of analysis suffers from several disadvantages, the principal ones being a lack of quantitative information about the complex modulus and its loss and storage components, the inability of frequency to be varied over a wide range, and the variability of the frequency during a test.

An interesting approach to monitoring the curing reaction of a thermosetting resin was described by Naganuma and coworkers (13,14). In this method, termed dynamic spring analysis (DSA), the crosslinking reaction was studied by application of the small oscillating displacement of the Rheovibron to a spiral spring, used to contain the sample, and the change in rigidity with temperature was followed. This technique was subsequently employed in a study of commercial adhesive curing, radical polymerization, and solvent evaporation from a polymer solution (15). The authors also favorably compared the viscoelastic response of polycarbonate obtained by DSA to that resulting from a thin film analyzed in the tensile mode on the Rheovibron, and obtained the dynamic viscoelastic response of polystyrene and high density polyethylene in a demonstration of the versatility of this method of analysis.

In previously published treatments of DSA data, no attempt to obtain the complex modulus or its storage and loss components was made. The relative modulus of the polymer-spring sample to the spring alone is the only measure of strength discussed. This quantity is similar to the relative rigidity parameter defined as a measure of strength in TBA in that neither variable is an absolute measure of the modulus of a material. This work will show how the storage and loss modulus can be obtained from DSA by the assumption of a model for the deformation. With the aid of the time-temperature superposition principle, moduli obtained in this manner from polystyrene test samples will be compared to those available from an analysis with the RMS to show the applicability of DSA. Portions of this work have been previously published (16).

Experimental

Samples. The HH101 atactic polystyrene used throughout this work was supplied by the Monsanto Company. The molecular weight characteristics of this polymer are as follows: $\overline{M}_n = 9.0\text{-}9.5 \times 10^4$, $\overline{M}_w = 2.6\text{-}2.8 \times 10^5$, $\overline{M}_z = 4.7\text{-}5.0 \times 10^5$ g/mole. To insure purity of the polymer, the polystyrene pellets were first dissolved in toluene, then precipitated with an amount of methanol eight to ten times the initial volume and dried under vacuum for three days at 90°C.

Dynamic mechanical measurements. The helical springs used in DSA studies, made of steel music wire, were obtained from the National Camera Supply Corporation. Several copper springs were made by winding 26 gauge armature wire about a rod of appropriate diameter. The spring ends were bent at a right angle so that they could be inserted into small holes drilled in the center of the gripping surfaces of the Rheovibron clamps to minimize slippage effects. In preparation of a sample for DSA, the spring was first cleaned in a chromic acid solution, then inserted in a clamping device and stretched to achieve a pitch P of 0.1 mm. A solution of polystyrene in toluene, typically 0.04 g/ml, was applied dropwise and the solvent allowed to evaporate before another drop was added. As this procedure progressed, the polymer formed a thin, continuous film between turns of the helically coiled spring. Application of about 10 to 15 mg of material was required at a temperature of 55°C and over a three hour period, after which the sample was dried under vacuum. A schematic representation of a sample prepared in this manner is shown in Figure 1-1. Thin film samples

Figure 1-1. Schematic Representation of a DSA Composite Sample.

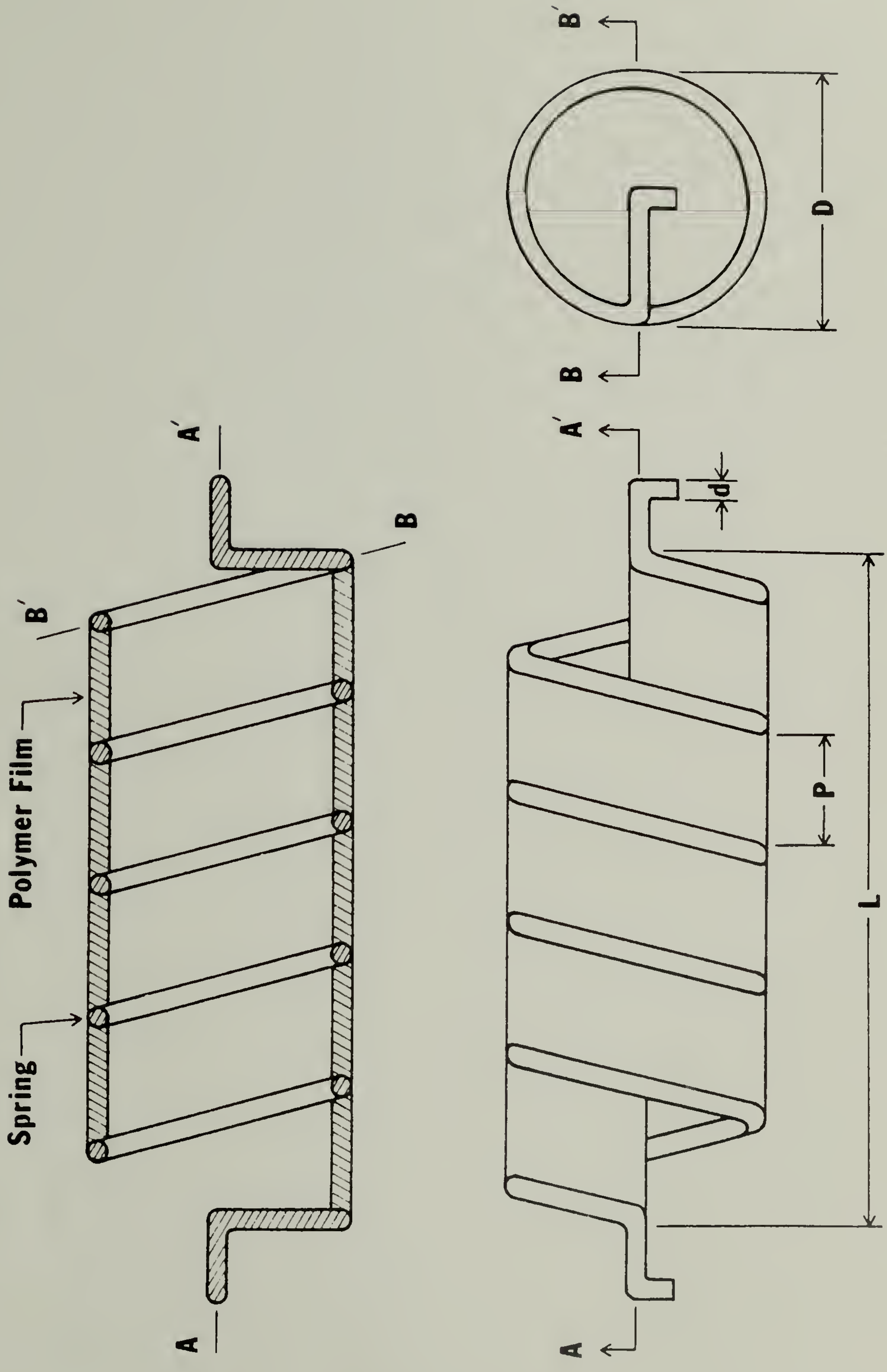
Spring
Polymer Film
A
A´
B
B´
P
L
D
d

tested were compression molded at 160°C under 3 MPa pressure and allowed to cool slowly to room temperature. An appropriate length of a 0.3 mm thick film was evaluated by standard procedures with the Rheovibron.

The Rheovibron DDV-IIB, with a slight modification to the clamps as previously described, was employed in all DSA experiments and in the tensile mode for thin films. Samples were analyzed in a nitrogen atmosphere from ambient to about 240°C at a nominal heating rate of 1.5°C/min at frequencies of 3.5, 11, and 110 Hz. Temperature was determined by a copper-constantan thermocouple junction placed near the sample in the heating oven and connected to a Leeds and Northrup 8691-2 millivolt potentiometer or a platinum resistance thermometer placed under the sample with the output displayed on an Omega Engineering model 250A digital thermometer.

The data were corrected for instrument compliance as discussed by Massa (17). This correction should be applicable at all temperatures for DSA studies since deformation of the samples in the clamps does not occur. Inertial corrections were found to be small even at 110 Hz and they were neglected in this analysis. Several computer programs were employed to facilitate data reduction. Dsafig was used to calculate and plot modulus and loss tangent results determined from DSA data. Vibfig served a similar purpose for the thin film determinations. Arrhea was employed to calculate apparent activation energies to the 95% confidence level from the Arrhenius dependence of log(frequency) on inverse temperature. Copies of these programs and instructions for their use can be found in the Appendix.

Melt rheology measurements. Samples were prepared in the form of one inch diameter discs by compression molding at 220°C and 3 MPa pressure. Polystyrene discs 0.8 mm thick were prepared in this manner and later dried under vacuum at 175°C for 42 hours. Three discs were required to attain the minimum sample thickness.

The RMS, a refinement of the orthogonal rheometer (18), was used in the eccentric rotating disc (ERD) mode to obtain the shear modulus of the polystyrene discs. A platten diameter of 25 mm and sample thickness of 2.0 to 2.5 mm were employed throughout. A temperature range of 120 to 180°C inclusive was examined. Strains within the range of 0.2 to 35% were used, depending upon the temperature and rotational speed, but operation was always maintained within the linear range of stress-strain response. Three or more determinations of the stress as a function of strain at a given temperature and frequency were conducted to verify that the range of strains examined was within the linear region. Nominal rotational speeds of 0.1, 0.4, 1, 4, and 10 r/s in both directions of upper platten rotation were employed. A theoretical treatment of the ERD mode of the RMS, a discussion of reduction of data, and an outline of the procedure to correct the data for instrument compliance has been given by Macosko and Davis (19).

Theory

In previous work by Naganuma et al. (13), an attempt was made to outline a method of analysis for the behavior of the polymer-spring composite in order to obtain the modulus of the polymer as a function of temperature at a given frequency. It was found necessary to expand upon this analysis in order to obtain the storage and loss components of the polymer modulus. The central feature of the analysis by Naganuma, the assumption of a parallel model to describe the behavior of the composite under an applied oscillating strain, was retained.

For the two component system of the spring s and the polymer p the modulus of the composite c can be expressed as:

$$M_c^* = M_s^* + M_p^* \tag{1-1}$$

where M_k^* denotes the complex modulus of each component. The complex modulus can be expressed as the product of two terms, the magnitude and the phase information, allowing equation 1-1 to be rewritten as:

$$|M_p^*|\exp(i\delta_p) = |M_c^*|\exp(i\delta_c) + |M_s^*|\exp(i\delta_s) \tag{1-2}$$

The real and imaginary terms can be separately equated to yield expressions for the storage and loss moduli. An additional quantity, the relative modulus M_r, can be defined as the ratio of the magnitude of the composite modulus to that of the spring modulus or in terms of an equation:

$$M_r = |M_c^*|/|M_s^*| \tag{1-3}$$

If the contribution of the spring to the composite loss behavior is small, the storage and loss moduli can be obtained from the following expressions:

$$M_p' = |M_s^*|\ [M_r\cos(\delta_c) - 1] \tag{1-4}$$

$$M_p'' = |M_s^*|\ M_r\sin(\delta_c) \tag{1-5}$$

The loss tangent of the supported polymer is given by the equation:

$$\tan(\delta_p) = \frac{M_p''}{M_p'} \qquad (1\text{-}6)$$

The relative modulus and loss tangent behavior of the composite can be directly obtained from the Rheovibron analysis. The equation used to calculate the complex modulus from the Rheovibron data can be found in the instruction manual for the instrument (20) and is shown below:

$$|E^*| = \frac{2L \times 10^8}{A(DF - K)S}\ \mathrm{Pa} \qquad (1\text{-}7)$$

where E* is the dynamic complex tensile modulus, L is the sample length, S the sample cross sectional area, A the amplitude of the deformation, DF the resultant force, and K the instrument compliance correction. Provided that the spring and composite have the same length and cross sectional area, the relative modulus can be expressed as:

$$M_r = \frac{A_s(DF_s - K)}{A_c(DF_c - K)} \qquad (1\text{-}8)$$

The composite and spring length and cross sectional area will be equal if a spring evaluated alone at a length and pitch identical to the final composite values is used in preparation of the polymer-spring composite sample.

The modulus of the supporting spring can be calculated from equation 1-7 if the length and the sample cross sectional area are known. The length under consideration should involve only the coil or active segment of the spring, not the ends, which merely provide a means to secure the coil to the instrument clamps. The sample length is then the distance between the ends of the stretched coil. The cross sectional area can be found by consideration of the total area of contact between the spring and the polymer sample. Provided that the film thickness and wire diameter d are comparable, the cross sectional area can be approximated by the area of an annulus, with inner diameter equal to the coil diameter less twice the wire diameter and outer diameter equal to the coil diameter D. The actual area of contact extends over a helix of n turns so that the total area of polymer-spring contact can be approximated by the area of the annulus multiplied by the number of turns of the spring. The length and cross sectional area expressed in terms of measurable dimensions of the spring are given in equations 1-9 and 1-10 respectively.

$$L = n(P + d) \tag{1-9}$$

$$S = n\pi d(D - d) \tag{1-10}$$

Combination of equations 1-7, 1-9 and 1-10 gives an expression for the spring modulus:

$$M_s' = \frac{2(P + d) \times 10^8}{\pi d(D - d)A(DF - K)} \text{ Pa} \tag{1-11}$$

This expression is valid if the loss of the spring is small compared to that of the composite.

Results

A check of the measured spring constant as compared to that calculated from theory is desirable to insure that the technique can be correctly applied. The force F applied to a helical spring can be related to the deformation x by the equation:

$$F = kx \tag{1-12}$$

where k represents the spring constant. From an experiment conducted on the Rheovibron both the dynamic force and the oscillating displacement were determined for several springs. Spring constants were also determined in a static test by hanging weights on the end of a vertically mounted spring and determining the displacement with a cathetometer. For helical extension or compression springs, the spring constant can be calculated from an equation given by Faupel (21):

$$k = Gd^4/8nD^3 \tag{1-13}$$

where G is the shear modulus of the material which forms the spring. Experimental and calculated values for several springs are compared in Table 1-1. In general the experimentally determined and theoretically calculated values differ by a small amount. These discrepancies could arise from variations in wire and coil diameter and effects of the spring ends on the uniform distribution of the applied displacement. These effects were not taken into account in the analysis, but the agreement between theory and experiment is reasonable nevertheless.

Variation of the spring modulus and loss tangent with tempera-

TABLE 1-1

COMPARISON OF SPRING CONSTANTS DETERMINED BY SEVERAL METHODS

SPRING*	WIRE DIAMETER (mm)	COIL DIAMETER (mm)	NUMBER OF TURNS	SPRING CONSTANT (N/m)		
				CALCULATED	DYNAMIC	STATIC
S-1	0.39	2.75	20	434	472	--
S-2	0.30	3.30	20	159	224	233
S-3	0.25	3.30	23	63	--	70
S-4	0.20	2.79	46	21	--	21
S-5	0.20	2.79	16	61	--	59

*S-1 from copper wire, all others steel.

ture is an important consideration as it is desirable that the spring respond elastically at all temperatures with minimal change in strength. To characterize the temperature dependence of these spring properties, spring S-2 was evaluated from 30 to 250°C on the Rheovibron at 110 Hz. As an aid in the interpretation of these results, the relative spring modulus S_r can be defined as the ratio of the spring modulus at any temperature to the spring modulus at the initial temperature. A plot of the variation of S_r and the loss tangent with temperature for this spring is given in Figure 1-2. It is evident that the loss tangent is small and virtually independent of temperature while the relative spring modulus decreases slightly with increasing temperature. Since S_r at 253°C shows less than a 7% drop from the initial value, the spring modulus was assumed to remain constant during a composite test. Identical results were obtained when the experiment was repeated, an indication that these properties are not dependent upon the thermal history of the spring.

The type of modulus that can be obtained from dynamic spring analysis has not yet been specified. An examination of the degree of deformation expected from a typical spring can prove to be useful for this purpose. The oscillating displacement in the direction of the spring axis can be calculated for tensile deformation. Using data obtained for the spring S-2, a value of 15.8 μm was obtained for the total dynamic tensile displacement. The total angular deflection θ of one end of the spring with respect to the other can be calculated from a method given by Wahl (18) for an elementary analysis as:

Figure 1-2. Temperature Variation of Relative Spring Modulus and Loss Tangent for Spring S-2.

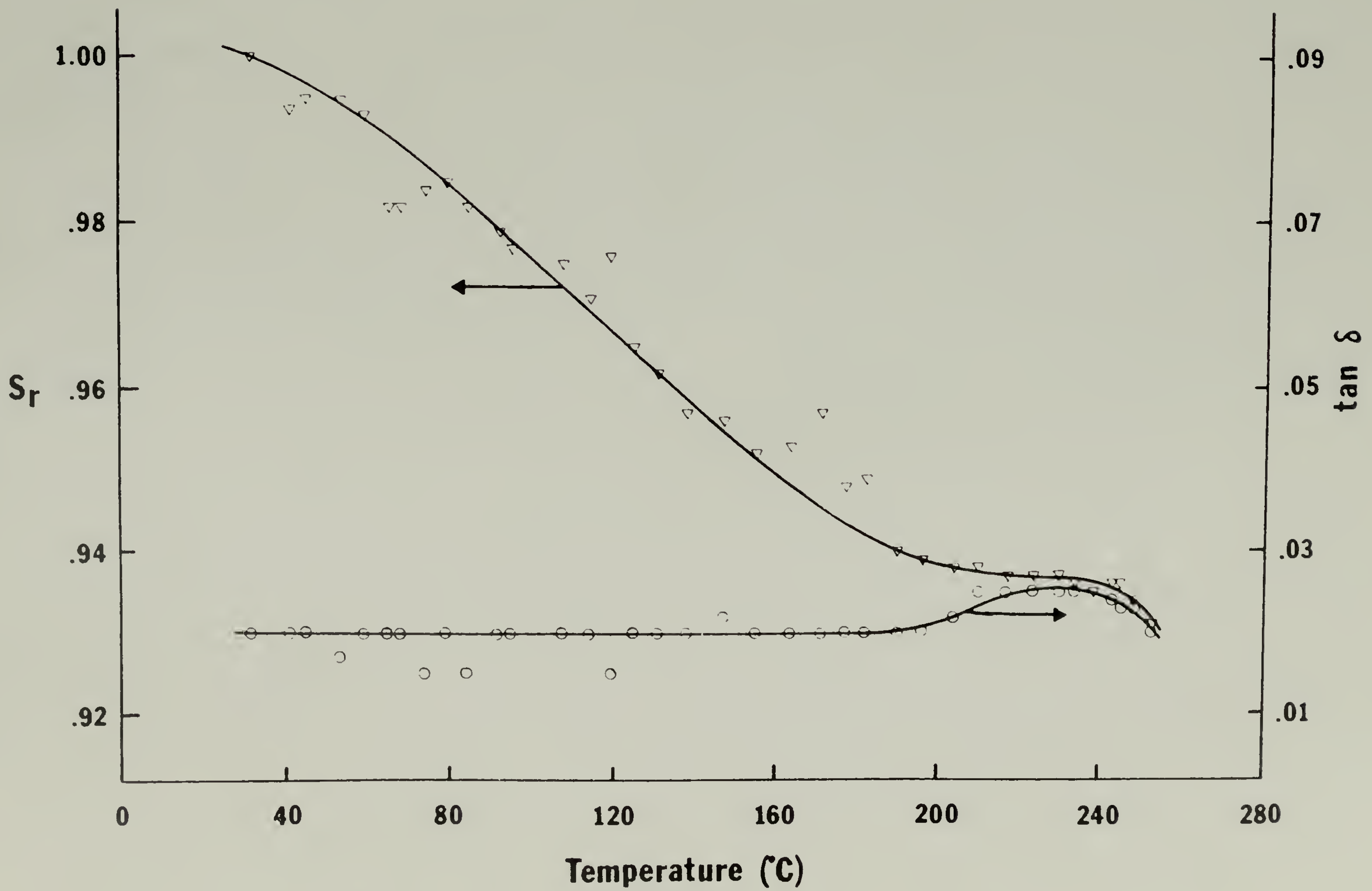
S_r
1.00
.98
.96
.94
.92
tan δ
.09
.07
.05
.03
.01
0
40
80
120
160
200
240
280
Temperature (°C)

$$\theta = 8nFD^3/Gd^4 \tag{1-14}$$

provided a shear modulus of the spring material, the applied load F, and certain geometrical characteristics of a given spring are available. Again for spring S-2, a total angular deflection of 22.2 μm was obtained. These results indicate that both tensile and shear deformation take place in the Rheovibron so the modulus obtained will be mixed in character, neither pure tensile nor shear. As can be seen from a comparison of equations 1-13 and 1-14, any attempt to reduce the amount of shear deformation will result in an increase in the spring constant and a loss in sensitivity to variation of the polymer modulus in the composite sample. The values of moduli obtainable by DSA should lie somewhere between shear moduli obtained from ERD analysis in the RMS and tensile moduli determined with a thin film sample on the Rheovibron over the same temperature region.

DSA samples were prepared by the technique outlined in the experimental section. Steel springs with the dimensions of S-2 in Table 1-1 were employed throughout. A typical supported polystyrene sample with a polymer volume fraction of 0.352 displayed the viscoelastic response shown in Figure 1-3 for the storage and loss modulus and in Figure 1-4 for the composite loss tangent when heated to well above the glass transition temperature. The glass transition relaxation was found to occur over the range of 108 to 120°C as determined from the loss modulus maxima. An apparent activation energy of 390 kJ/mole ± 15% was determined for this transition, in good agreement with that reported by Baker and coworkers (23) in a dielectric relaxation study of poly-

Figure 1-3. Storage and Loss Modulus of Polystyrene from DSA as a Function of Temperature at Three Frequencies.

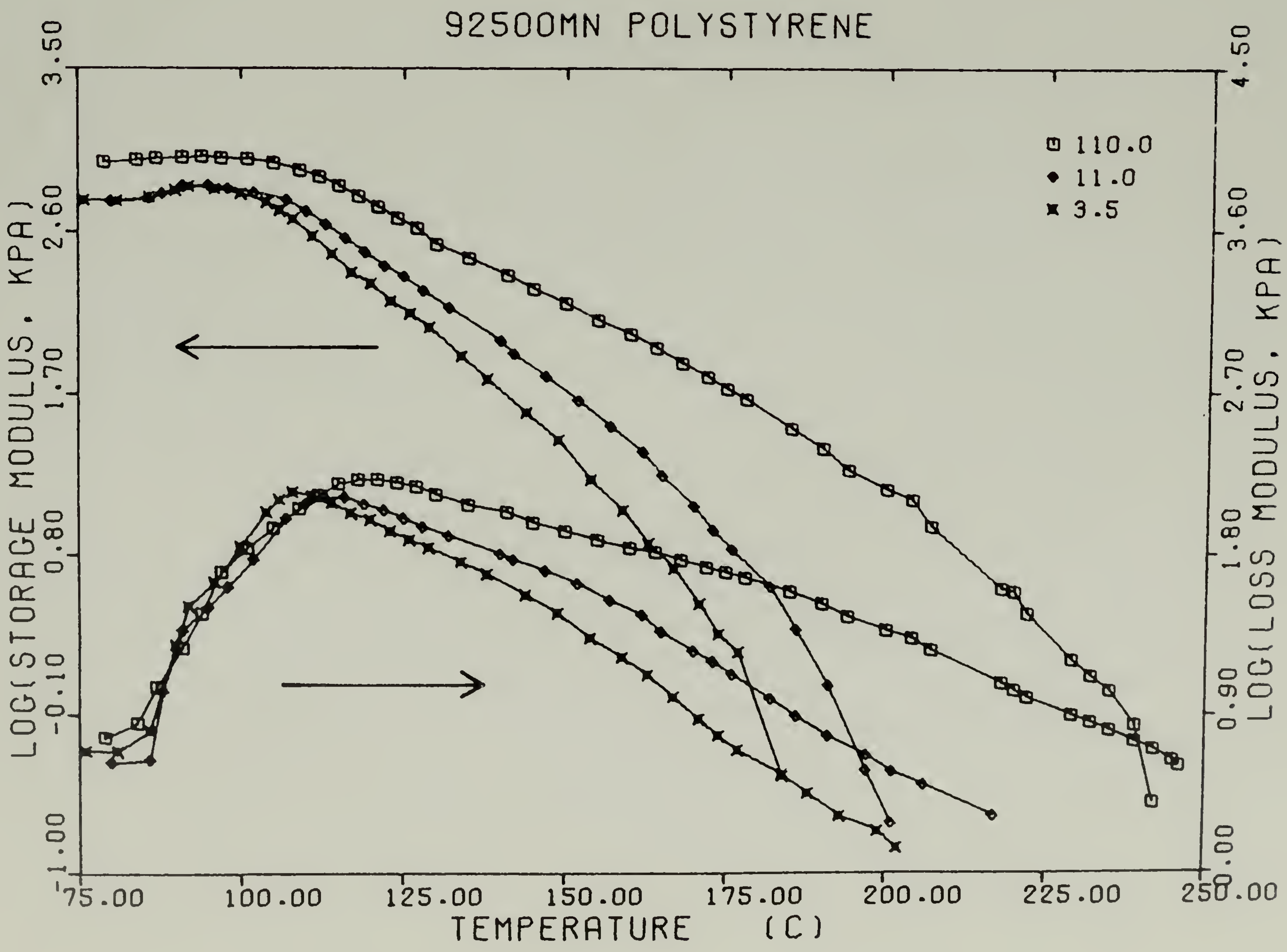
92500MN POLYSTYRENE
110.0
11.0
3.5
LOG(STORAGE MODULUS, KPA)
3.50
2.60
1.70
0.80
-0.10
-1.00
LOG(LOSS MODULUS, KPA)
4.50
3.60
2.70
1.80
0.90
0.00
75.00
100.00
125.00
150.00
175.00
200.00
225.00
250.00
TEMPERATURE (C)

Figure 1-4. Composite Loss Tangent of Polystyrene from DSA as a Function of Temperature at Three Frequencies.

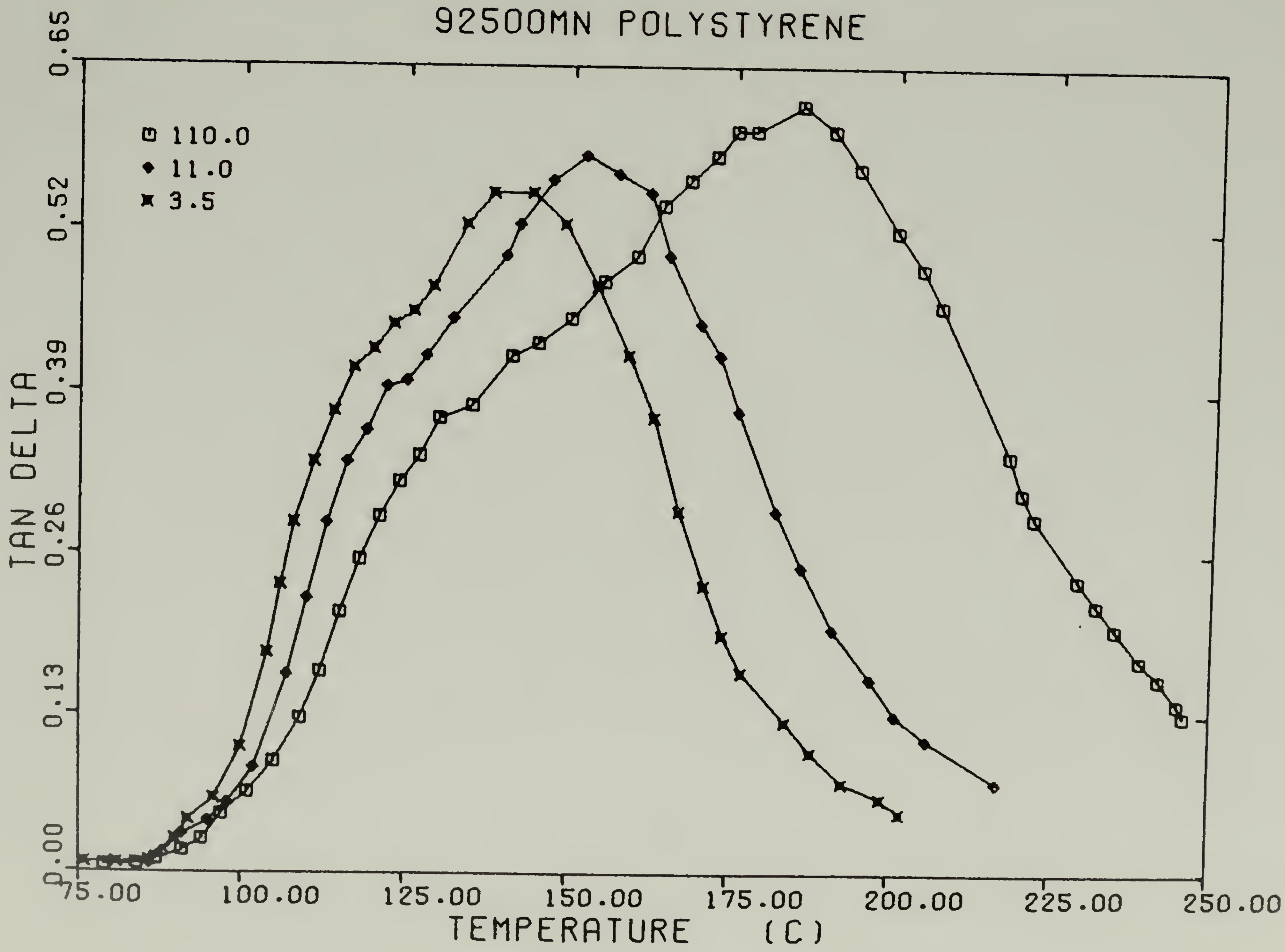
92500MN POLYSTYRENE
110.0
11.0
3.5
TAN DELTA
0.00
0.13
0.26
0.39
0.52
0.65
TEMPERATURE (C)
75.00
100.00
125.00
150.00
175.00
200.00
225.00
250.00

styrene, 360 kJ/mole.

In order to obtain the storage and loss components of the shear modulus of polystyrene at various temperatures and frequencies, a study of the material in the ERD mode of the RMS was undertaken. Two orthogonal stresses can be determined from an ERD analysis. The stress in the direction of the platten offset, σ_y, results from elastic forces which act in a direction opposite to the centerline displacement. A plot of σ_y vs. strain will yield the storage modulus as its slope. The x direction stress results from forces of viscous dissipation. The loss modulus can be obtained from a plot of this stress vs. strain. Typical plots of σ_y and σ_x vs. strain at several frequencies as a function of temperature are shown in Figures 1-5 and 1-6, respectively. The linear relationship between stress and strain over the region of strain examined is confirmed by this data. It is evident that an increase in rotational speed or frequency at constant temperature, or a decrease in the test temperature at constant frequency causes the modulus to increase.

Information about the storage and loss modulus as a function of temperature for polystyrene samples analyzed by ERD and DSA cannot be directly compared owing to the different frequency range covered and the mode of operation of the two techniques. The DSA experiments were conducted at three constant frequencies, 3.5, 11, and 110 Hz, as a function of temperature. ERD experiments were performed at a constant temperature between 120 and 180°C and with varying rotational speeds from 0.1 to 10 r/s, corresponding to frequencies in the range of 0.016 to 1.6 Hz. As the frequency ranges studied for each technique

Figure 1-5. Elastic Stress Strain Response of Polystyrene Samples Analyzed by ERD at Several Temperatures.

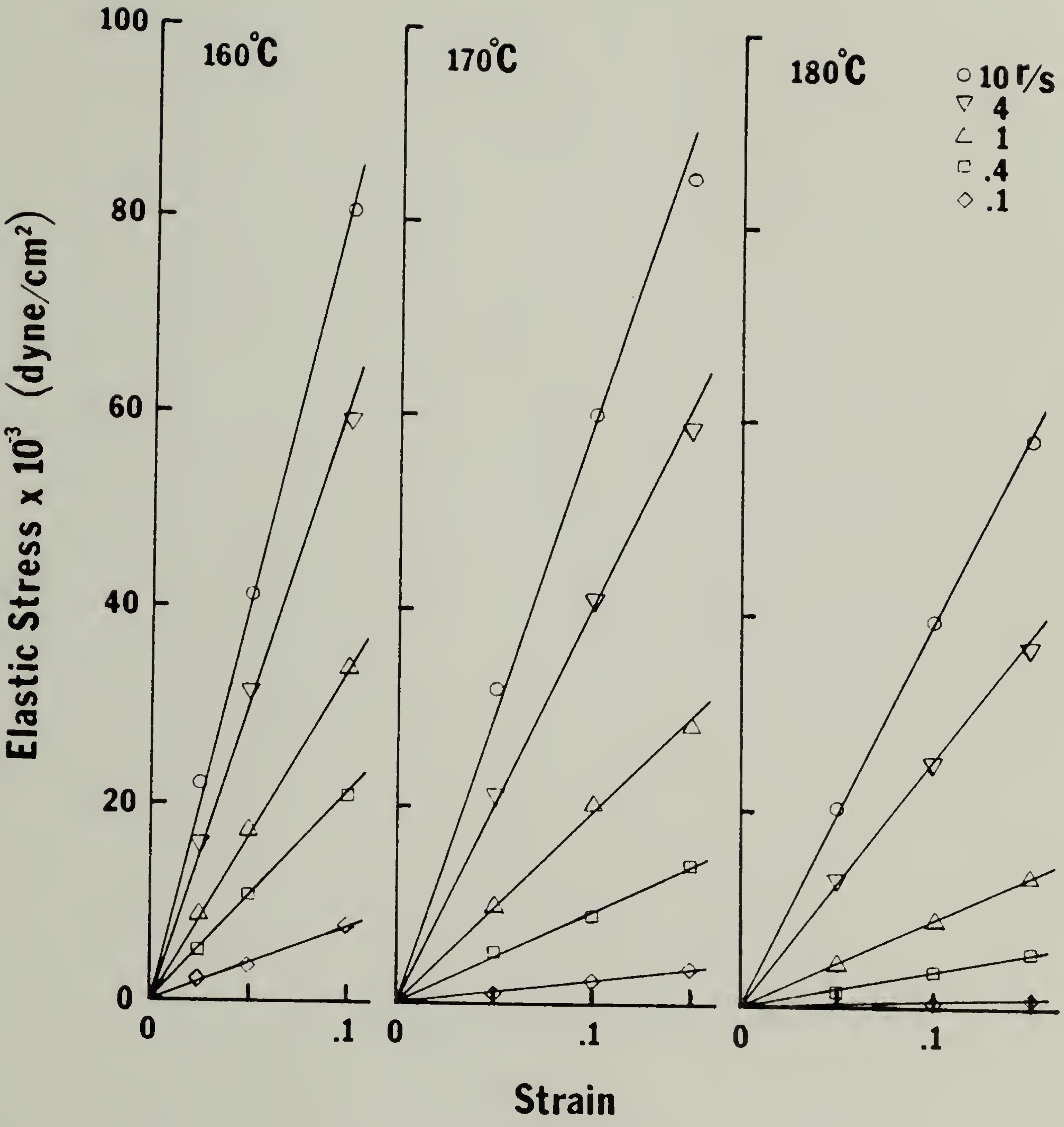
Elastic Stress x 10^{-3} (dyne/cm^2)
100
80
60
40
20
0
160°C
170°C
180°C
○ 10 r/s
▽ 4
△ 1
□ .4
◇ .1
0
.1
0
.1
0
.1
Strain

Figure 1-6. Viscous Stress Strain Response of Polystyrene Samples Analyzed by ERD at Several Temperatures.

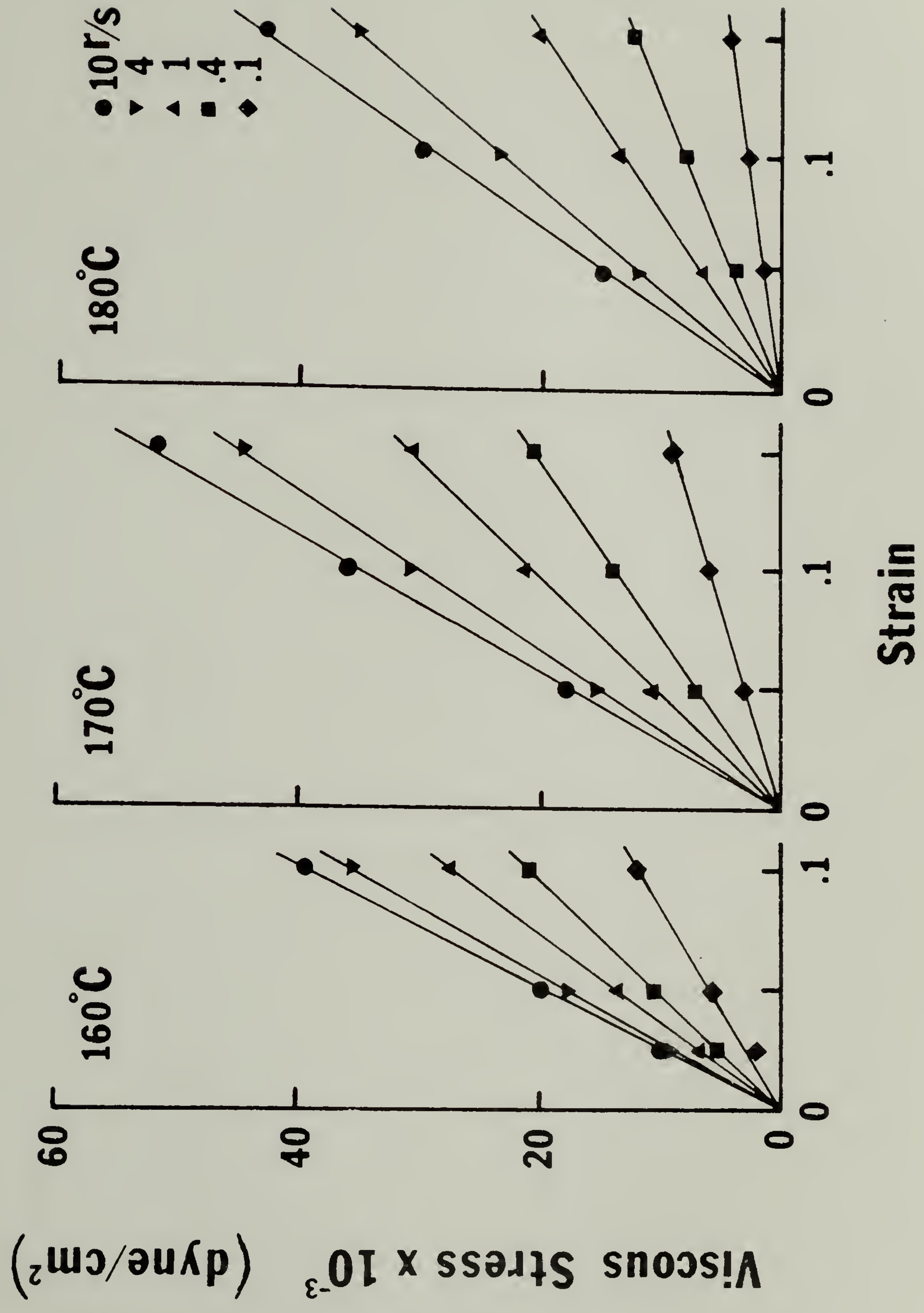
Viscous Stress x 10⁻³ (dyne/cm²)
0
20
40
60
Strain
0
.1
160°C
170°C
180°C
● 10 r/s
▼ 4
▲ 1
■ .4
◆ .1

did not overlap, it is not possible to compare the modulus information obtained from the two techniques without resorting to the time temperature superposition principle. The shift factors for superposition, a_T, can be determined from the temperature of the experiment by the WLF equation (24):

$$\log a_T = \frac{C_1(T - T_g)}{C_2 + T - T_g} \qquad (1\text{-}15)$$

For polystyrene, the WLF constants were determined by Plazek (25) to be $C_1 = 13.3$, and $C_2 = 47.5$, while 100°C was taken for T_g. An additional correction for the temperature dependence of entropy elasticity (26) was included to normalize the modulus values at any temperature to those at the reference temperature.

The storage modulus data obtained from both techniques were shifted with the WLF equation to produce the plot of reduced storage modulus vs. shifted frequency shown in Figure 1-7. The figure shows that the modulus determined by DSA is about half an order of magnitude lower than the shear modulus over the entire frequency range. The storage modulus obtained from DSA is a mixed modulus, since both tensile and shear deformation occur, and should be at most a factor of three greater than the shear modulus for the polymer in the rubbery region (27). The overall discrepancy between the moduli determined by DSA and ERD is about an order of magnitude. Both sets of results have a similar dependence on shifted frequency and are roughly parallel except at lower values of the shifted frequency. The DSA data points show some scatter when compared to the ERD results, which clearly lie

Figure 1-7. Time Temperature Superposition of Storage Moduli Obtained from DSA and ERD Response of Polystyrene.

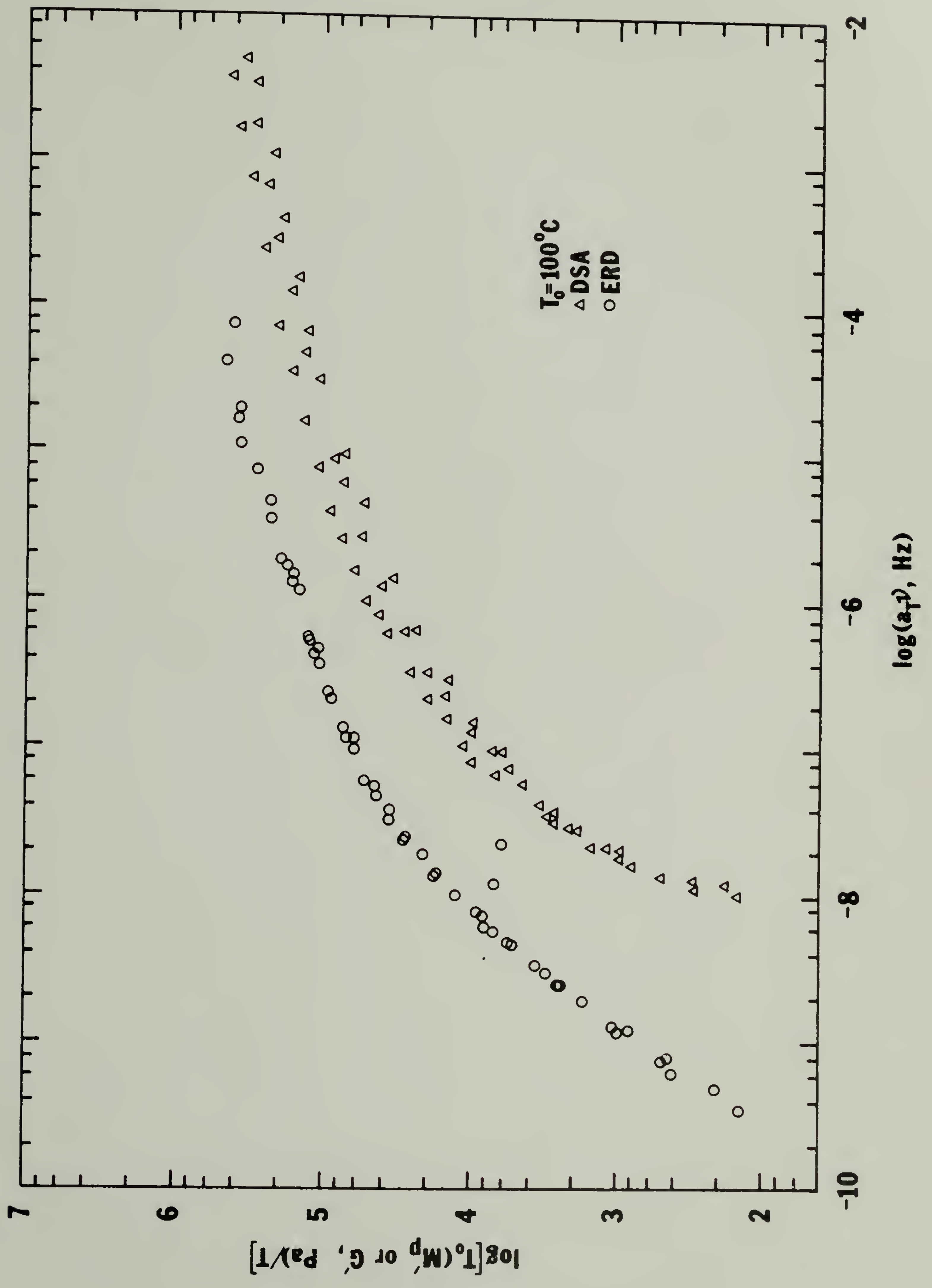
T₀=100°C
△DSA
○ERD
log[T₀(M′p or G′, Pa)/T]
7
6
5
4
3
2
-10
-8
-6
-4
-2
log(aTν, Hz)

on a single curve. It is evident that the storage modulus obtained from DSA is a qualitative approximation of the shear modulus of the polymer in the region above T_g.

The agreement between loss moduli obtained from the two techniques is similar as can be noted from Figure 1-8, a plot of loss modulus as a function of shifted frequency. A smaller region of concurrence of the moduli occurs in the range of shifted frequency below 4×10^{-6} Hz.

Discussion

A significant advantage of the DSA technique is the small amount of material required, on the order of 10 to 15 mg. Few methods are available for characterizing the viscoelastic response of such minute samples. A drawback is the difficulty in controlling the weight of material deposited. A small variation can make a significant change in the polymer volume fraction and cause the film thickness to differ from the wire diameter. The model assumes that these dimensions are identical and that the film is uniform. In actuality, this situation can be difficult to achieve.

The agreement of the magnitude of the storage and loss moduli between DSA and a tensile mode test on the Rheovibron is poor at ambient temperature. The storage modulus of a polystyrene sample analyzed in the tensile mode of the Rheovibron at 25°C was found to be about 2.6 GPa. The same polymer evaluated by DSA yielded a storage modulus of about 0.8 MPa. Part of this discrepancy can be accounted for by the mixed nature of the storage modulus obtained from DSA, this modulus

Figure 1-8. Time Temperature Superposition of Loss Moduli Obtained from DSA and ERD Response of Polystyrene.

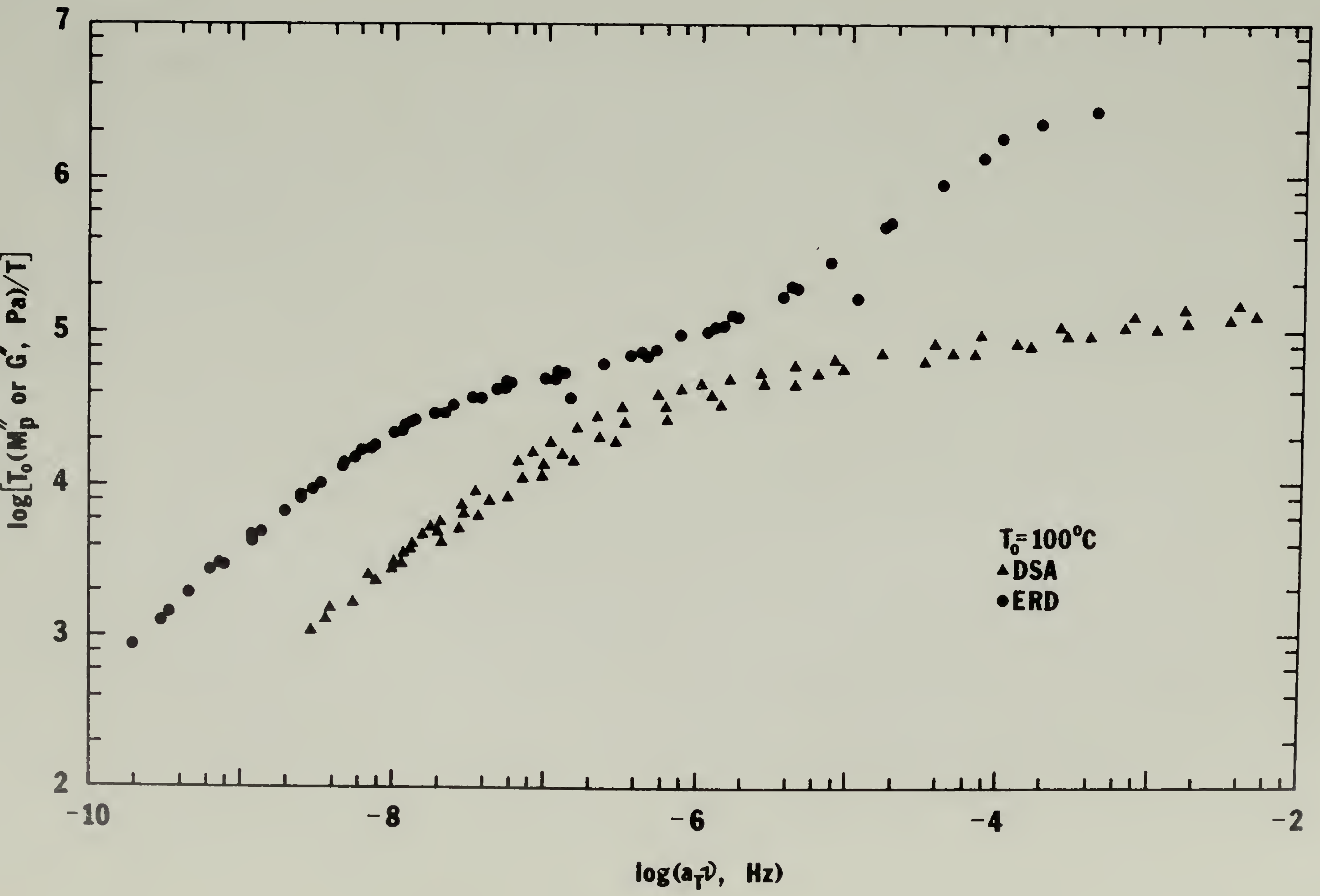
7
6
5
4
3
2
-10
-8
-6
-4
-2
log[T$_o$(M$_p''$ or G$''$, Pa)/T]
log(a$_T$ν, Hz)
T$_o$= 100°C
▲DSA
●ERD

being intermediate between the tensile and shear modulus values. At most, however, the mixed nature of the DSA storage modulus could account for a factor of three differences between the DSA and tensile storage moduli. A similar disparity in the loss modulus values was also apparent.

A possible explanation for the thousand-fold discrepancy remaining is a change in the nature of the deformation which occurs in a polymer-spring composite when the polymer can be characterized as glasslike in behavior. The high modulus glassy polymer can cause the applied oscillating deformation to act on the spring ends rather than on the coil. The shape of the spring ends can change by small deformations at bends in the wire, accommodating the small displacement with less expenditure of energy than would be necessary to deform the coil and the polymer film between its turns. This type of behavior was not taken into account in the previous analysis outlined. The spring ends were assumed to be rigid supports. As the glass transition temperature of the polymer is approached, the polymer modulus will decline and the oscillating deformation will then act on the coil and the polymer film.

The contribution of the ends of the spring was experimentally determined by evaluating several springs which had been soldered together over the entire coil region. When the correction was applied to composite sample data in the region of glasslike polymer response, the moduli obtained varied widely and erratically with temperature. This is no doubt due to the nature of the correction, which is comparable to dynamic force values obtained for the composite in this region and results in a small numerical value for the difference between the two. The lack of rigidity of the spring ends precludes the quantitative use of DSA to determine the moduli of glassy materials. This is not a serious problem, as glassy polymers can be routinely analyzed on the Rheovibron in the tensile mode.

The large differences in moduli determined from DSA and thin film experiments can be overcome to an extent by comparison of the loss tangent response of both techniques in the glass transition region. The loss tangent of the polymer in a DSA experiment is different from that of the composite and can be determined as shown in equation 1-6. The DSA and conventional thin film results are compared in Figure 1-9. It is evident that both processes are sensitive to the polystyrene glass transition at about 110°C. The DSA data show the presence of an additional relaxation process above the glass transition. A discussion of this phenomenon can be found in Chapter II.

Several problems are inherent in the comparison of DSA and ERD data with the aid of the time temperature superposition principle. At low shifted frequencies the DSA data becomes less accurate as the composite modulus closely approaches that of the supporting spring and as the temperature of measurement exceeds the limit of applicability of the WLF equation. At high shifted frequencies the ERD analysis becomes less accurate owing to difficulties in maintaining the no slip condition at the platten surfaces for a glassy sample. Additional simplifications due to the assumption of a parallel model that neglect any interfacial effects and complications which arise out of the mixed character of the modulus obtainable by DSA further reduce the possibil-

Figure 1-9. Comparison of the Polystyrene Loss Tangent Determined from DSA (diamonds) and a Thin Film (squares) as a Function of Temperature at 11 Hz.

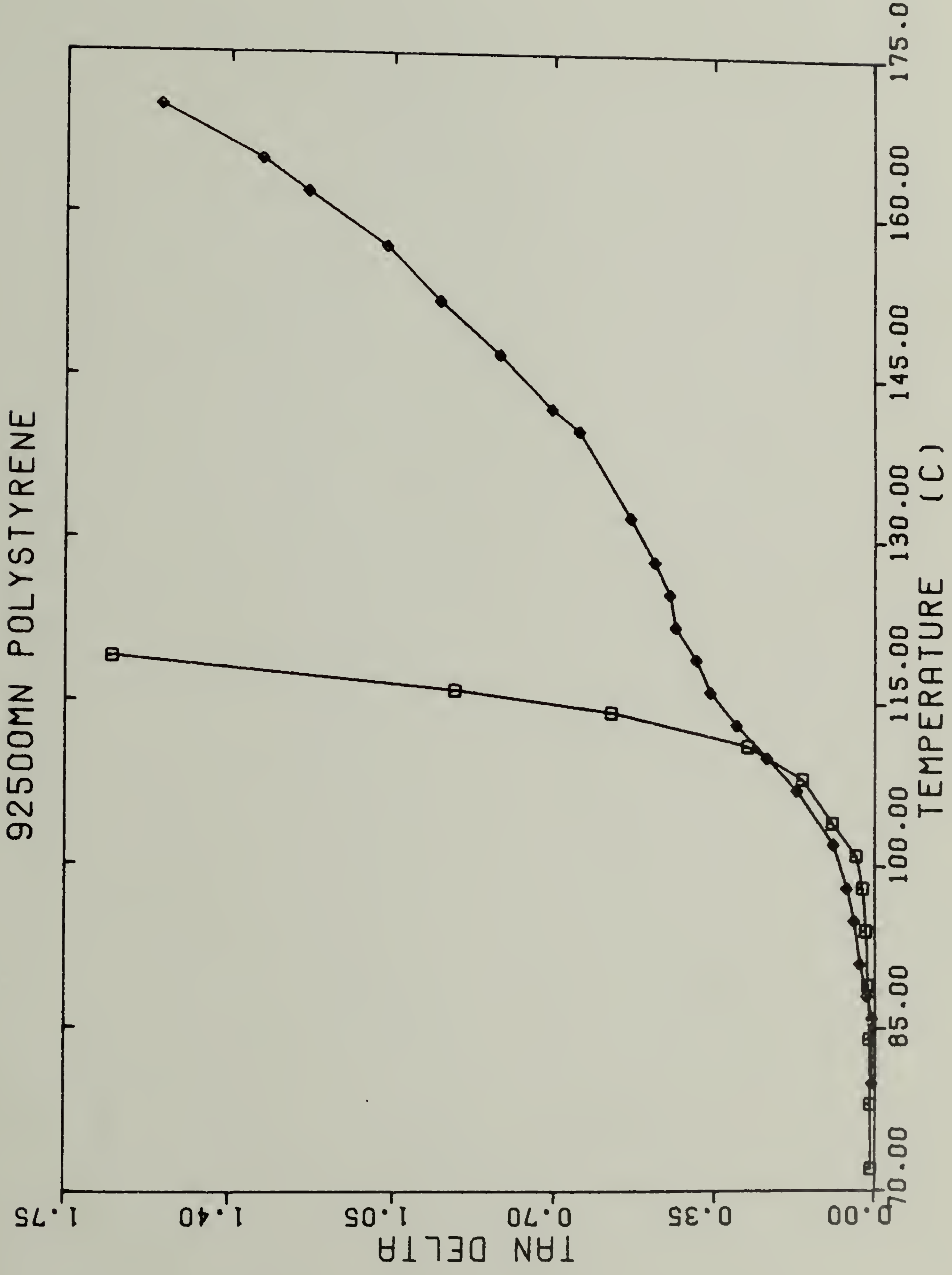
92500MN POLYSTYRENE
TAN DELTA
0.00
0.35
0.70
1.05
1.40
1.75
TEMPERATURE (C)
70.00
85.00
100.00
115.00
130.00
145.00
160.00
175.00

ity for exact agreement between the two techniques. However, the method of DSA can clearly be used to obtain semiquantitative predictions of the dynamic storage and loss moduli of polymers above the glass transition temperature in addition to providing information on loss processes and their frequency dependence.

Conclusions

Dynamic spring analysis, a technique of supported dynamic viscoelastic testing, has been shown to be a valuable tool for evaluation of dynamic mechanical properties, particularly if only small quantities of a material are available. From an assumption of a simple parallel model for the composite deformation, the storage and loss moduli and the loss tangent as a function of temperature can be derived from a straightforward treatment of the Rheovibron data. The deformation has been shown to be both tensile and shear in nature, but the loss and storage moduli agree qualitatively with shear modulus data in the region of rubbery response, as compared by time temperature superposition. DSA provides a method for obtaining the loss tangent and, semiquantitatively, the moduli of a polymeric material above the glass transition temperature. In the glass transition region, the method can provide information on the temperature and frequency dependence of the glass to rubber relaxation. The magnitude of the storage and loss moduli determined in this region and below T_g are not comparable to those determined by conventional methods, as the supports for the composite make a significant contribution to the overall response.

REFERENCES

1. J.M. Starita and C.W. Macosko, S.P.E.J., 27, 38 (1971).
2. P.F. Erhardt, J.J. O'Malley, and R.G. Crystal, Polymer Preprints, 10(2), 812 (1969).
3. B.H. Shah and R. Darby, Polym. Eng. Sci., 16, 46 (1976).
4. T. Murayama, J. Appl. Polym. Sci., 19, 3211 (1975).
5. K.H. Illers, Rheol. Acta, 3, 194 (1964).
6. J.M. Crissman, J. Appl. Phys., 45, 4190 (1974).
7. J.A. Faucher, J.V. Koleske, E.R. Santee, J.J. Stratta, and C.W. Wilson, J. Appl. Phys., 37, 3962 (1966).
8. J.M.G. Cowie, Amer. Chem. Soc., Prepr., Div. Org. Coat. Plas. Chem., 38, 284 (1978).
9. H. Thurn, Kolloid-Z., 173, 72 (1960).
10. A.F. Lewis and J.K. Gillham, J. Appl. Polym. Sci., 6, 422 (1962).
11. J.K. Gillham, CRC Crit. Revs. Macromol. Sci., 1, 83 (1972).
12. J.K. Gillham, AIChE Journal, 20, 1066 (1974).
13. S. Naganuma, T. Sakurai, Y. Takahashi, and S. Takahashi, Kobunshi Kagaku, 29, 105 (1972).
14. S. Naganuma, T. Sakurai, Y. Takahashi, and S. Takahashi, Shikizai Kyokaishi, 45, 297 (1972).
15. S. Naganuma, T. Sakurai, Y. Takahashi, and S. Takahashi, Kobunshi Kagaku, 29, 519 (1972).
16. G.A. Senich and W.J. MacKnight, J. Appl. Polym. Sci., 22, 2633 (1978).
17. D.J. Massa, J. Appl. Phys., 44, 2595 (1973).
18. B. Maxwell and R.P. Chartoff, Trans. Soc. Rheology, 9, 41 (1965).

19. C.W. Macosko and W.M. Davis, Rheol. Acta, 13, 814 (1974).

20. "Rheovibron DDV-II Instruction Manual 17," Tokyo Baldwin Co., Tokyo (1969).

21. J.H. Faupel, "Engineering Design," p. 212, John Wiley & Sons, New York (1964).

22. A.M. Wahl, "Mechanical Springs," p. 230, McGraw-Hill Book Co., New York (1963).

23. E.B. Baker, R.P. Auty, and G.J. Ritenour, J. Chem. Phys., 21, 159 (1953).

24. M.L. Williams, R.F. Landel, and J.D. Ferry, J. Amer. Chem. Soc., 77, 3701 (1955).

25. D.J. Plazek, J. Phys. Chem., 69, 3480 (1965).

26. J.J. Aklonis, W.J. MacKnight, and M. Shen, "Introduction to Polymer Viscoelasticity," p. 48, Wiley-Interscience, New York (1972).

27. Ibid., p. 10.

CHAPTER II

DISPERSIONS ABOVE THE GLASS TRANSITION IN SUPPORTED SYSTEMS

Introduction

Polymer molecules in the amorphous state commonly exhibit a transition from a vitreous to a mobile state as the temperature of the system is raised. The glass transition is observed as a change in slope of a volume-temperature or enthalpy-temperature plot or as a loss maximum in a dynamic mechanical experiment. At the glass transition temperature, short range molecular motions begin but long range cooperative motions are greatly restricted by the presence of strong local interactions between neighboring chains, chemical bonds in crosslinked rubbers, or entanglement networks in high molecular weight linear polymers (1). The formation of an entanglement network is evident by a plateau region in the storage modulus after its marked decline over the glass transition region, the exact modulus and length of the plateau depending strongly on the polymer molecular weight (2). The molecular weight at which the entanglement network forms is proportional to the critical molecular weight (M_c), determined from the change in the dependence of viscosity η on weight average molecular weight as follows:

$$\eta = B\bar{M}_w^{\,a} \qquad (2\text{-}1)$$

where a equals 1 below M_c weight and 3.4 above (3). A plateau region in the storage modulus above T_g is not expected when an entanglement network does not form, below M_c.

As temperature is increased (or frequency decreased) still further at a molecular weight above M_c, the entanglement network is no longer capable of inhibiting translation of one chain relative to another. This process is manifested in a further decline in the storage modulus and an accompanying relaxation maximum in the loss modulus, behavior which is predicted from theory and sometimes observed experimentally (4). Two relaxation maxima would therefore be expected in a plot of the loss modulus or loss tangent vs. temperature for an amorphous polymer above M_c, the first corresponding to the glass to rubber relaxation, the second to the onset of flow. The second relaxation maximum is often difficult to characterize, as viscous flow of the polymer precludes its complete measurement by many techniques (5).

Interest has recently revived in the T_{ll} transition of amorphous polymers. This transition occurs above the glass transition temperature and is thought to correspond to a transition from a "fixed fluid" to a "true liquid," the former state prohibiting relative translation of the centers of gravity of polymer chains which readily occurs in a true liquid (6). Such an interpretation corresponds to the entanglement slippage relaxation discussed previously. Other arguments have been made in favor of a third order thermodynamic transition at T_{ll} (7). The T_{ll} transition has been observed most commonly for polystyrene, however, other amorphous polymers (8) and block copolymers (9) also display the phenomenon. The subject has been copiously reviewed

(10-15). Recent publications contend that the T_{11} transition is a kinetic flow phenomenon rather than a thermodynamic transition (16) or an artifact of the measurement procedure and not of molecular origin (17). It is the latter point to which this chapter is addressed.

Torsional braid analysis (TBA), a supported sample dynamic mechanical technique discussed in Chapter I, has been employed in many studies of the T_{11} transition in polystyrene (6,18,19). Major findings of these investigations will be briefly discussed. Both T_g and T_{11} relaxation maxima are observed for narrow molecular weight distribution polystyrene samples of 600 to 111,000 molecular weight (6). Below the critical molecular weight of polystyrene, about 35,000, T_{11} is observed at 1.1 to 1.2 times T_g, both in °K. Above M_c, T_{11} increases steeply as molecular weight increases. The sharpness of the T_{11} loss peak decreases with increasing molecular weight and dispersity. The transition is suggested to correspond to an isoviscous state of 10^4 to 10^5 poise. Subsequent studies of polydisperse blends of monodisperse polystyrenes show that the single T_{11} observed is linearly related to $\overline{M}_n^{-1}$ when both components are below M_c (18). For blends with one component above and one below M_c, or both components above M_c, the T_{11} transition occurs independently for each. Plasticized polystyrene exhibits a decrease in T_{11} proportional to the amount of diluent in a manner similar to the behavior of T_g (19). In addition, a relaxation above T_{11}, designated T_{11}', is found to be present in the plasticized samples.

The study described here was undertaken to ascertain the origin of relaxations observed by DSA above the glass transition of polystyrene. Some of the results reported in this chapter have been previously published (20,21).

Experimental

Samples. Several polystyrene samples were employed in this study. Monodisperse samples ($\bar{M}_w/\bar{M}_n < 1.1$) with $\bar{M}_n$ equal to 4000, 19,800, 37,000 and 233,000 g/mole were obtained from the Pressure Chemical Company. An additional monodisperse polymer of 2000 $\bar{M}_n$ was obtained from Arrow Laboratories. These materials were used without further purification. A sample of Monsanto HH101 polystyrene resin having the following molecular weight characteristics was also studied: $\bar{M}_n = 9.0\text{-}9.5 \times 10^4$, $\bar{M}_w = 2.6\text{-}2.8 \times 10^5$. To insure purity of this sample, the polystyrene pellets were first dissolved in toluene, then precipitated with an amount of methanol eight to ten times the initial volume and dried under vacuum for three days at 90°C. Technical grade glycerol, supplied by Eastman Organic Chemicals, was also employed.

Measurements. The helical steel springs used in DSA studies were 20 turns in length with a wire diameter of 0.3 mm and a coil diameter of 3.3 mm. Polystyrene composite samples were prepared by deposition from solution onto a spring stretched to a pitch of 0.1 mm, described in detail in Chapter I. Toluene was employed as the solvent. The conditions under which the samples were dried will be discussed in the text. A glycerol sample was prepared by depositing the liquid with a hypodermic syringe onto a spring which was held stretched in the clamps of the Rheovibron. All samples were analyzed at several frequencies in a dry nitrogen atmosphere at a nominal heating rate of 1.5°C/min with a Rheovibron DDV-IIB Dynamic Viscoelastometer. Some samples were also studied while cooling from elevated temperatures at a nominal rate of 2°C/min.

A comprehensive interfaced pyrolysis-gas chromatographic peak identification system was employed to detect the evolution of solvent vapors during heating. Samples were prepared in the same manner as for DSA analysis. A length of 1.6 mm outer diamter aluminum tube was used to support the ends of the spring in the extended position. Samples were placed in a Spex MP-3 Multipurpose Thermal Analyzer and heated at a rate of 4-8°C/min to 250°C under a flowing helium atmosphere. The evolved gases were passed through a thermal conductivity detector (TCD) and a flame ionization detector, then trapped on a glass bead column maintained at 77°K. Upon completion of heating, the trapped gases were backflushed into a Varian 2700 Gas Chromatograph and passed through a 153-cm-long column of 1.5% OV-101 on Chromosorb G, 100-120 mesh. A Norcon 201 Infrared Prism Spectrometer was used to record spectra of substances which gave rise to peaks on the GC trace. Uden and co-workers (22) have given a thorough description of the entire system and its capabilities.

The Rheometrics mechanical spectrometer (RMS) was employed in the dynamic cone and plate mode to obtain the loss and storage shear moduli of 4000 $\overline{M}_n$ polystyrene as a function of frequency at constant temperature. A 25 mm diameter plate and a 0.1 rad cone were used throughout. The powdered polymer sample was introduced onto the pre-heated plattens and allowed to liquify before the proper cone gap was fixed. A strain of 2% was used in all the determinations. At frequencies greater than 1 Hz, a ten cycle average was used for each modulus determination. At all frequencies the moduli were obtained from an average of at least ten measurements. Temperature was maintained constant to within 1°C by the instrument temperature controller.

The computer program Dsafig was employed to calculate and plot results derived from DSA experiments. A copy of this program and instructions for its use can be found in the Appendix.

Theory

The mechanical model shown in Figure 2-1 was formulated to characterize the response of the composite sample used in DSA. The model can be generalized to other supported sample techniques by replacing the Hookean moduli E_i with the appropriate moduli. The model consists of spring 1 in series with Voigt element 2, spring 2 in parallel with a dashpot of viscosity η. Spring 1 arises from the contribution of the ends of the spring uncoated by polymer, as discussed in Chapter I. When the polymer is rigid, its dynamic tensile modulus can be added to E_2 since it is in parallel with E_2. In the region of viscous response, however, the behavior of the composite is that of a dashpot with the spring coils being driven through the liquid of viscosity η. The area of viscous dissipation is of interest in this discussion.

The complex tensile compliance of Voigt element 2 is given by the expression (23):

$$D_2^* = D_2' - iD_2'' \tag{2-2}$$

Figure 2-1. A Spring-Dashpot Model Proposed to Account for the T_{11} Relaxation.

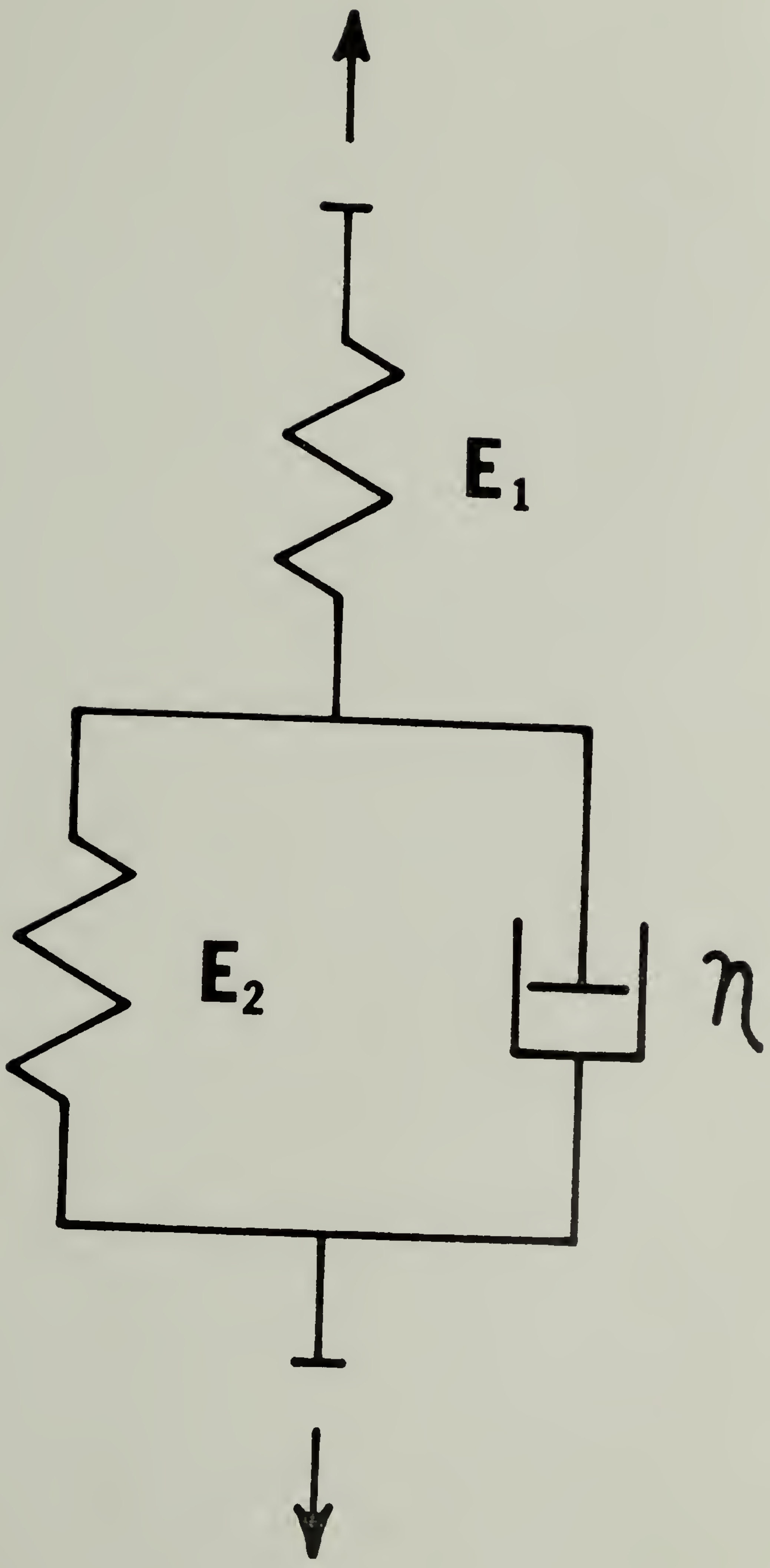
E_1
E_2
η

where $D_2' = 1/E_2(1 + x)^2$, $D_2'' = xD_2'$, $x = \omega\eta/E_2$, and ω is the angular frequency. For spring 1, the following relation holds:

$$D_1^* = D_1' - iD_1'' \tag{2-3}$$

where $D_1' = 1/E_1$ and $D_1'' = 0$. Since spring 1 and Voigt element 2 are in series, the complex compliance of the composite D^* can be written as:

$$D^* = D_1^* + D_2^* \tag{2-4}$$

The complex compliance of the composite can also be written as:

$$D^* = D' - iD'' \tag{2-5}$$

$$D^* = D_1' + D_2' - iD_2'' \tag{2-6}$$

where the real and imaginary parts are additive due to the series arrangement. The loss tangent of the composite can be expressed by:

$$\tan(\delta_c) = D''/D' \tag{2-7}$$

$$\tan(\delta_c) = \frac{x}{1 + \frac{E_2}{E_1}(1 + x^2)} \tag{2-8}$$

At the maximum in $\tan(\delta_c)$, $d(\tan(\delta_c))/dx$ is equal to zero and the following equation holds:

$$\eta_{max} = \frac{E_2}{2\pi\nu}\left(1 + \frac{E_1}{E_2}\right)^{1/2} \tag{2-9}$$

where ν is the frequency in Hertz. This expression can be rewritten as:

$$\eta_{max}\nu = C \tag{2-10}$$

where C is a constant dependent only on the elastic moduli of the supporting elements. The model predicts that at a fixed frequency a maximum in $\tan(\delta_c)$ will occur at the viscosity η_{max}; that the T_{11} damping maximum corresponds to an isoviscous state.

Results

Solvent induced relaxations. Several samples were prepared from solution for DSA studies and dried at 90 to 95°C under vacuum for up to 24 hours. Figure 2-2 shows the loss tangent behavior of sample C-2 during the first heating experiment. The plot shows a T_g relaxation near 130°C and a second broad loss peak well above the glass transition region. Further analysis of sample C-2 revealed that the transition above T_g could not be reproduced upon reheating as indicated by the loss tangent plot in Figure 2-3. The loss modulus behavior is similar to that of the loss tangent in that only a single relaxation attributable to the glass transition is present. This relaxation occurs about 8°C lower than the position observed during the first heating. An activation energy of 440 kJ/mole ± 20% was calculated from the loss modulus peak, in agreement with the results of Baker and coworkers (24) who report 360 kJ/mole. Similar results were obtained from a composite prepared with polystyrene of molecular weight 233,000 and narrow molecular weight distribution, sample C-3. Upon first heating, a glass to rubber relaxation was observed in a loss modulus vs. temperature plot

Figure 2-2. Composite Loss Tangent by DSA for Sample C-2 During the Initial Thermal Scan at Three Frequencies.

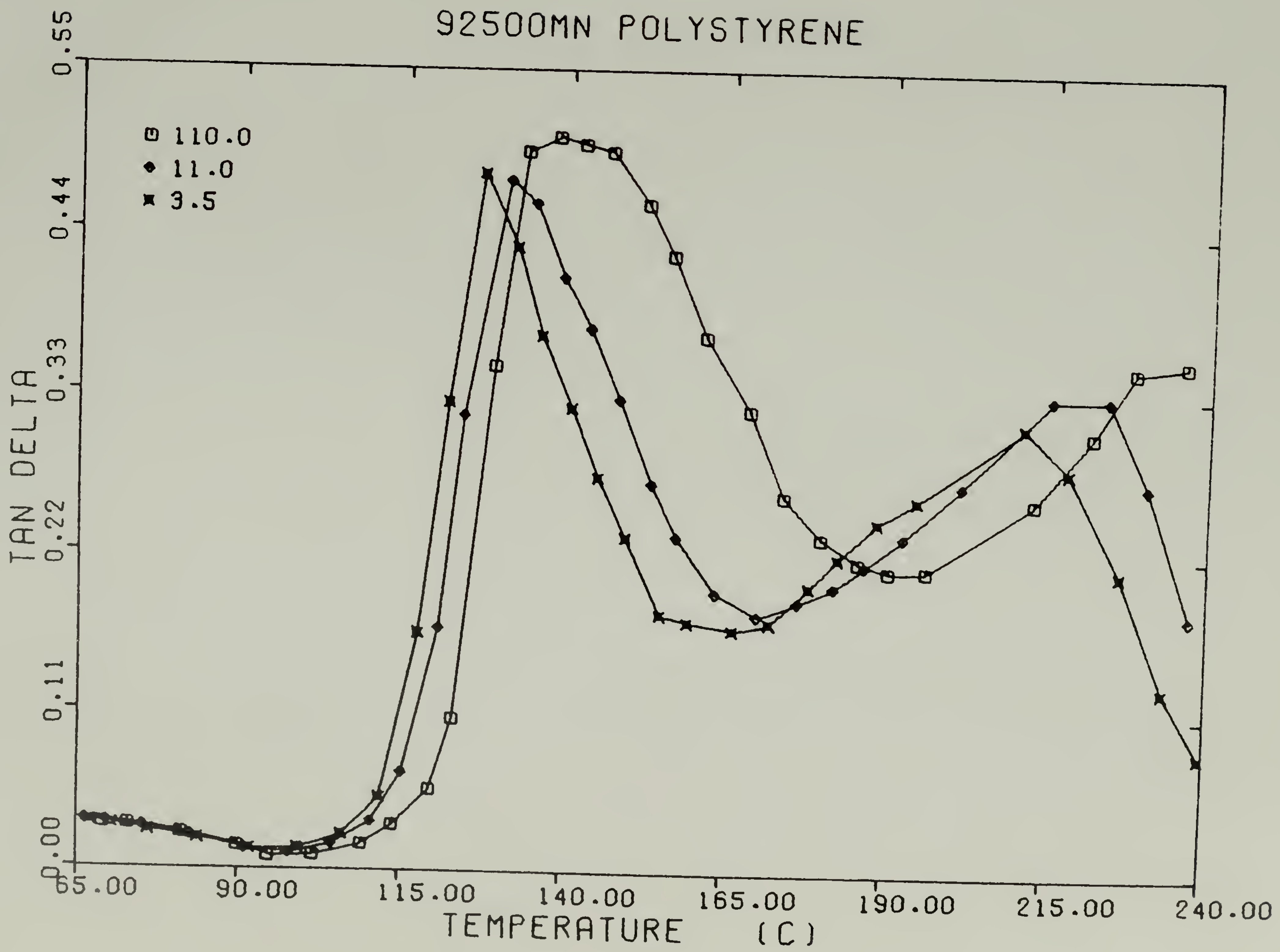
92500MN POLYSTYRENE
110.0
11.0
3.5
TAN DELTA
0.00
0.11
0.22
0.33
0.44
0.55
65.00
90.00
115.00
140.00
165.00
190.00
215.00
240.00
TEMPERATURE (C)

Figure 2-3. Composite Loss Tangent by DSA for Sample C-2 During the Second Thermal Scan at Three Frequencies.

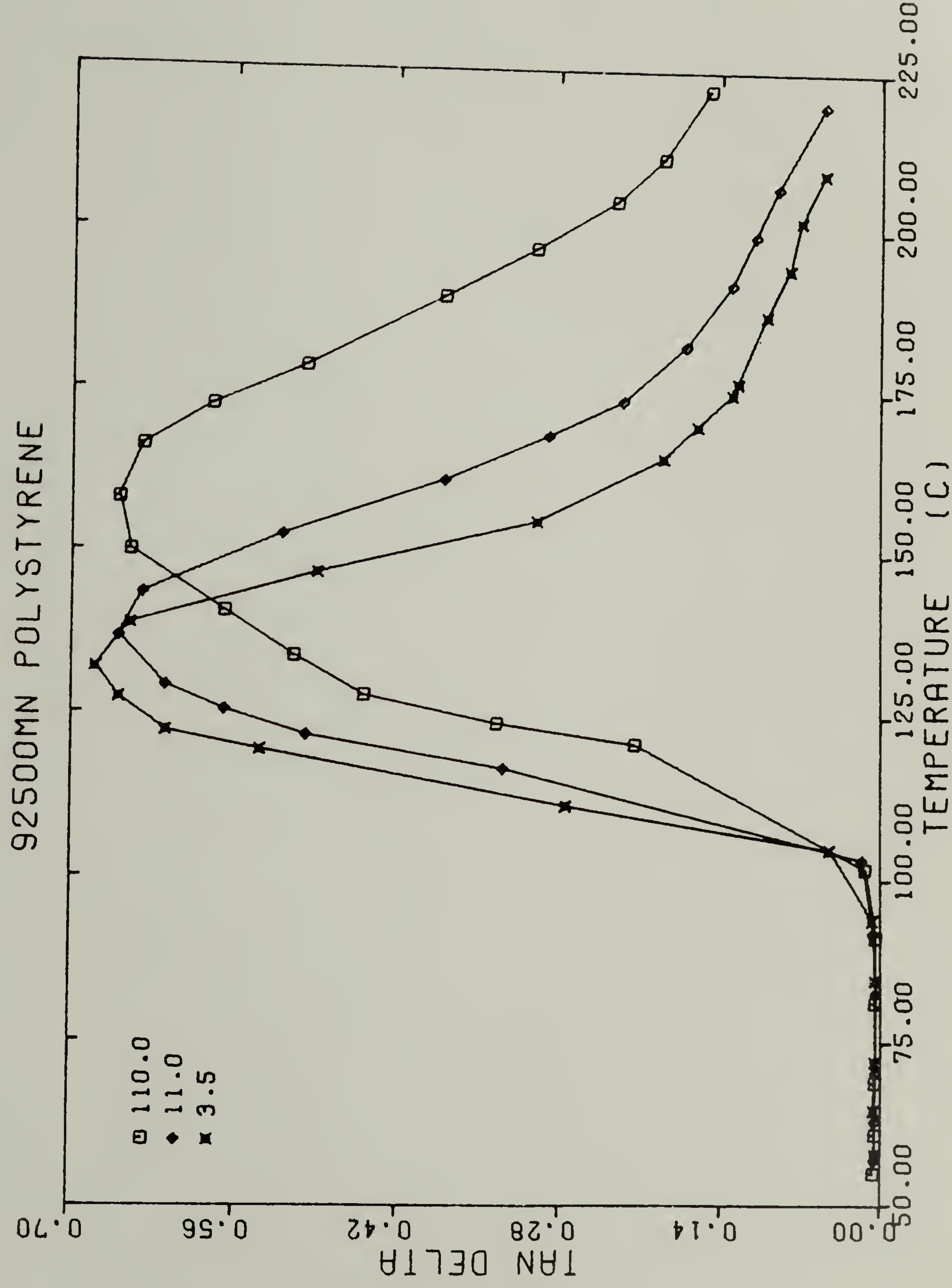
92500MN POLYSTYRENE
TAN DELTA
0.00
0.14
0.28
0.42
0.56
0.70
TEMPERATURE (C)
50.00
75.00
100.00
125.00
150.00
175.00
200.00
225.00
110.0
11.0
3.5

as well as a very broad transition above T_g. When the sample was rerun, no higher temperature transition was evident. Sample C-1 exhibited a loss process above T_g which appeared as a broad shoulder on the high temperature side of the T_g relaxation peak for the loss modulus during the first heating of the sample. Data subsequently collected while cooling sample C-1 until ambient temperature was reached showed the T_g transition at the same position observed upon heating and no evidence of a higher temperature transition. Results obtained from DSA evaluation of these samples are summarized in Table 2-1. The glass transition temperature does not show a significant variation between samples owing to the relatively high molecular weight of all the polymers studied. The samples display a relaxation above T_g only during the first analysis. Subsequent DSA evaluations upon either cooling from the first run or reheating after the sample had cooled to ambient temperature reveal no higher temperature transitions.

The unusual viscoelastic behavior displayed by some of the polystyrene DSA samples above T_g is thought to be attributable to the loss of monomer or solvent from the polymer. This seems likely for several reasons. The high temperature loss peak could not be reproduced upon reheating, indicating that a unique event had occurred. The complete evolution of solvent vapors upon heating during the first analysis could explain why the relaxation was not observed when the experiment was repeated. The composite sample studied in Chapter I, which did not display irregular behavior above T_g, was dried under vacuum at 170°C while the other samples were all dried below the glass transition temperature of polystyrene. As the drying procedure was the only

TABLE 2-1

SUMMARY OF POLYSTYRENE RELAXATIONS AS DETERMINED FROM LOSS MODULUS MAXIMA

SAMPLE	MOLECULAR WEIGHT $\overline{M}_n \times 10^{-3}$	ANALYSIS*	T_g TRANSITION (°C)			TRANSITION ABOVE T_g (°C)		
			FREQUENCY (Hz)			FREQUENCY (Hz)		
			3.5	11	110	3.5	11	110
C-1	37	1H	117	121	132	140	150	168
		1C	115	119	134	N**	N	N
C-2	90-95	1H	124	128	133	188	202	211
		2H	116	119	126	N	N	N
C-3	233	1H	109	113	119	210	215	222
		2H	106	109	117	N	N	N

*1H = first heating; 1C = cooling after first heating; 2H = second heating.

**N = none observed.

significant difference in the preparation of these DSA samples, incomplete drying of C-1, C-2, and C-3 could have caused the unusual behavior of these samples.

A test for evolution of volatile organic compounds was undertaken with the Spex MP-3 thermal analyzer. All samples studied in this manner were prepared with HH101 resin and were dried near T_g in a procedure similar to that used in preparation of C-2. The samples were evaluated *in situ*, as the sample chamber of the MP-3 proved to be of adequate diameter. A sample evaluated by heating at a rate of 8°C/min from 35 to 220°C showed the first presence of organic vapors at 70°C. The highest concentration was observed at 138°C but a small amount of material could still be detected at 200°C. A gas chromatograph trace of the material collected over the course of the run, shown in Figure 2-4, indicates that several small peaks and one major component are present. An infrared spectrum of the most abundant compound had prominent bands at 3.3, 3.4, 6.7, 9.4, 9.7, 13.5, and 14.7μ. These positions are similar to the locations of major absorptions in the infrared spectrum of toluene, the solvent used in sample preparation. No absorption could be noted at 10.1, 11.1, and 12.9μ, the most intense maxima in the IR spectrum of styrene.

A second sample was analyzed in order to make a quantitative determination of the amount of material evolved during heating. This sample was heated at 4°C/min to 215°C, then cooled to ambient temperature and reheated at the same rate. The results are shown in Figure 2-5. During the first run, the TCD detector recorded the presence of organic material from about 60 to 190°C with the highest concentration

Figure 2-4. Gas Chromatograph Trace of Vapors Evolved During a Thermal Analyzer Study to 220°C.

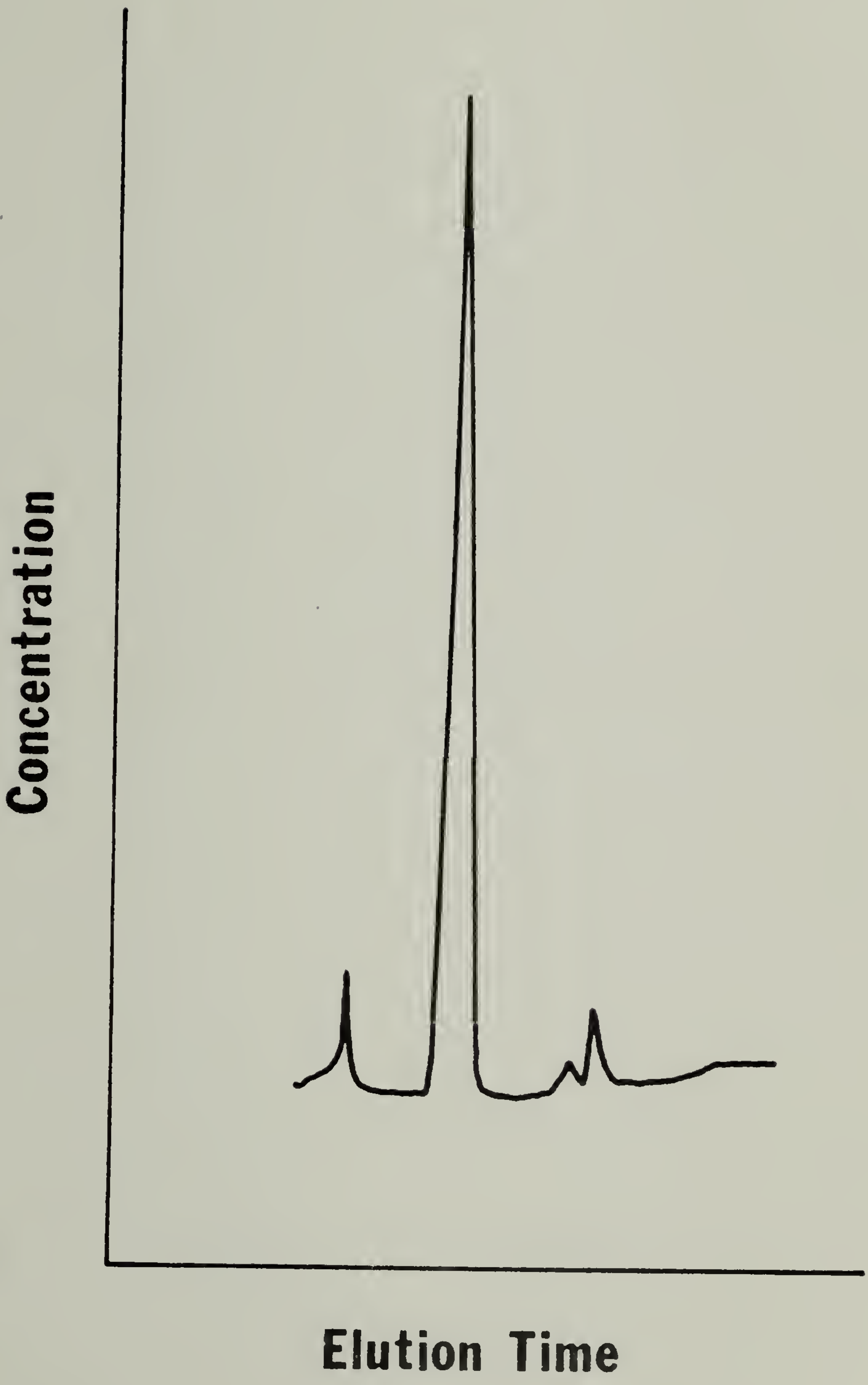
Concentration
Elution Time

Figure 2-5. Concentration (Arbitrary Units) of Organic Vapors Evolved During a Thermal Analyzer Study as a Function of Temperature for (1) First Heating Run, (2) Second Heating Run (Baseline Displaced for Clarity).

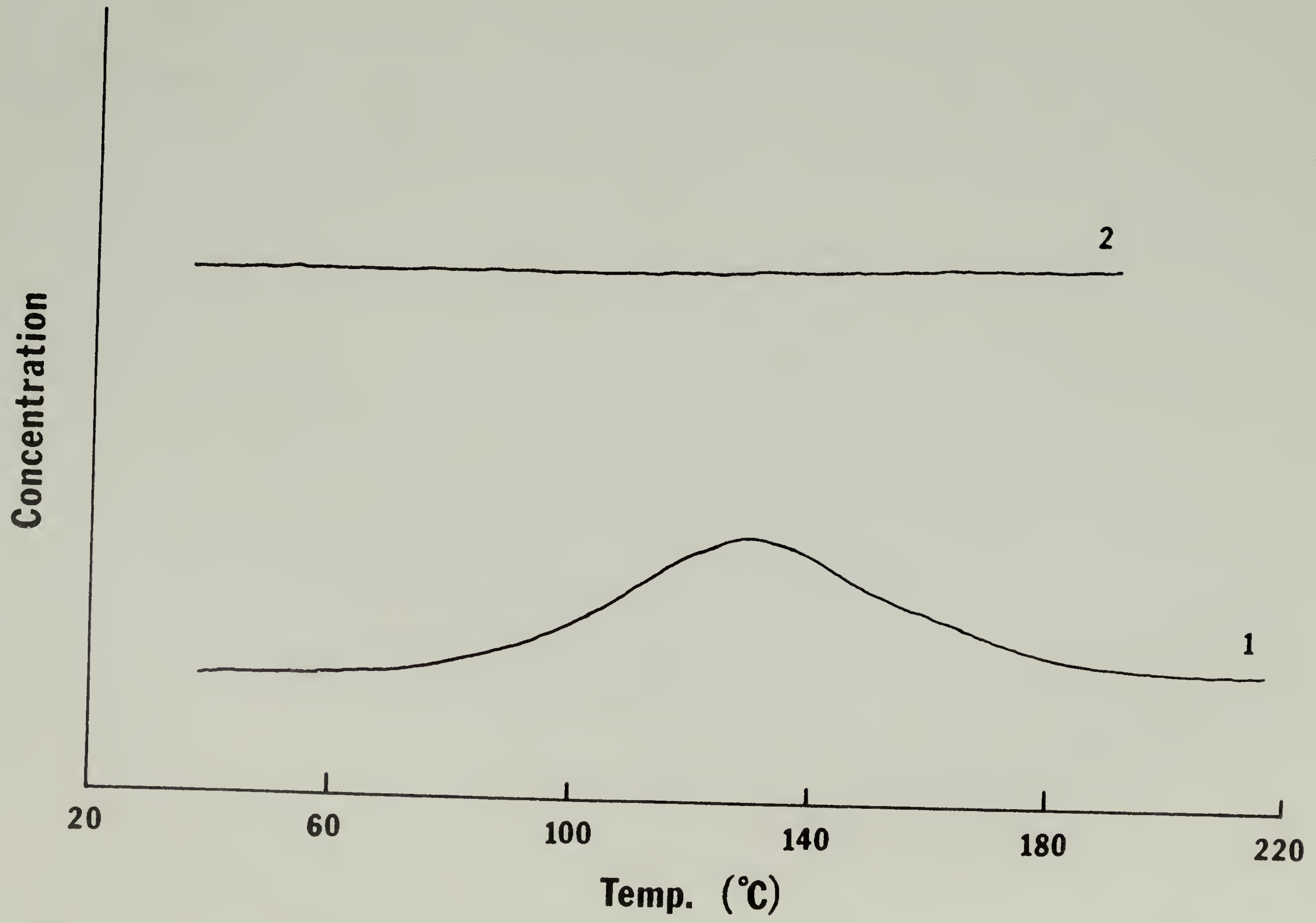
Concentration
2
1
20
60
100
140
180
220
Temp. (°C)

at 125°C. No organic compounds were detected in the inert gas stream during the second heating. A sample of neat toluene injected into the GC gave a peak with the same position as the major peak in the GC of the evolved gases, confirming the identiciation of the major component of the GC trace as toluene. Several injections were used to obtain a calibration curve for peak height as a function of toluene concentration. From this curve it was estimated that about 1.7 μl of toluene was released during the first heating. This amount is approximate, but was used to estimate the concentration of solvent which remained in the dried sample to be about 8% by weight.

Other relaxations above the glass transition. Several low molecular weight polystyrene composite samples were prepared from toluene solution and dried at 30°C above their glass transition temperatures for at least 72 hr under vacuum to avoid any residual solvent effects. An HH101 resin sample was dried for 17 hr at 160°C under vacuum.

The composite loss tangent, $\tan(\delta_c)$, obtained from a DSA study of 4000 molecular weight polystyrene, is shown in Figure 2-6. No relaxation is evident near the glass transition temperature, determined to be 77°C from DSC experiments (25). A loss maximum which increases in temperature with increasing frequency occurs at 119°C at 3.5 Hz and 125°C at 11 Hz. The same material studied in the dynamic cone and plate mode of the RMS gave the response shown in Figure 2-7. Only the loss modulus, G", is shown, as G' and therefore $\tan(\delta)$ could not be determined accurately by this method. These data cover the same temperature/frequency domain in which a loss maximum was evident when the

Figure 2-6. DSA Composite Loss Tangent for 4000 $\bar{M}_n$ Polystyrene as a Function of Temperature at Four Frequencies.

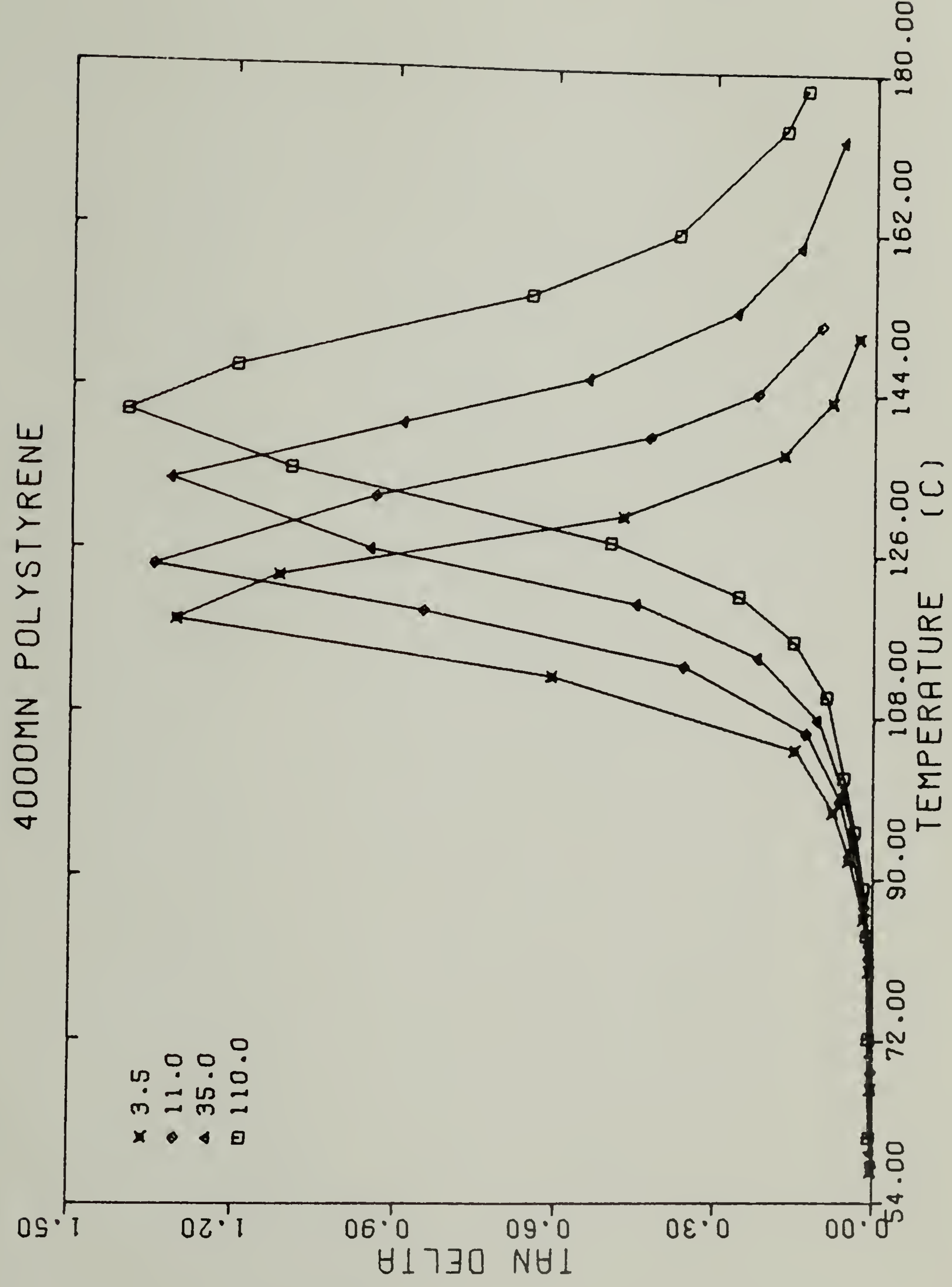
4000MN POLYSTYRENE
TAN DELTA
1.50
1.20
0.90
0.60
0.30
0.00
TEMPERATURE (C)
54.00
72.00
90.00
108.00
126.00
144.00
162.00
180.00
3.5
11.0
35.0
110.0

Figure 2-7. Log G" versus Log ν for 4000 $\overline{M}_n$ Polystyrene at Four Temperatures.

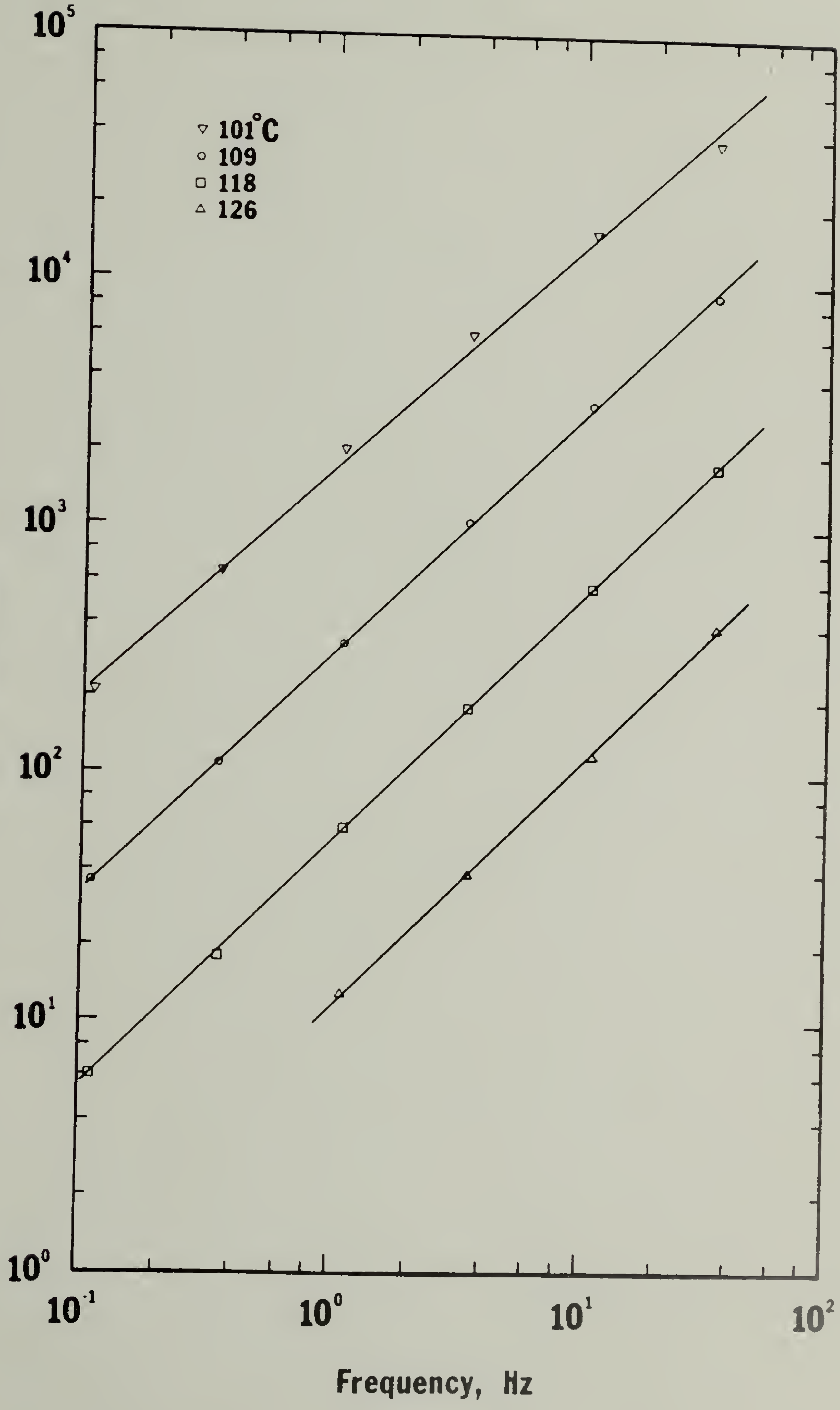
▽ 101°C
○ 109
□ 118
△ 126
10^5
10^4
10^3
10^2
10^1
10^0
G'', kPa.
10^-1
10^0
10^1
10^2
Frequency, Hz

same material was examined by DSA in Figure 2-6. No relaxation process is present in the RMS results. The response of the 4000 $\overline{M}_n$ polystyrene sample is that of a simple liquid of Newtonian viscosity η, which can be described by the relations (26):

$$G'' = \omega\eta \tag{2-11}$$

$$\log(G'') = \log(\nu) + \log(2\pi\eta) \tag{2-12}$$

A linear least squares fit of the data at each temperature resulted in the parameters given in Table 2-2. Values of the slope indicate that in this temperature region the polymer behaves as a simple fluid, corresponding to unit slope, with some slight deviations evident at the lowest temperature. Since no relaxation process is observed by direct measurement in the RMS, the DSA dispersion above T_g in Figure 2-6 cannot be of molecular origin.

Additional DSA experiments were conducted on glycerol with the results displayed in Figure 2-8. A series of well-defined maxima are evident at temperatures above the glass transition, estimated by Schulz (27) to be -90°C. Crystallization is sometimes possible above T_g but was not detected in the storage modulus results. The mechanical model previously discussed predicts from equation 2-10 that the viscosity-frequency product will be constant at the $\tan(\delta_c)$ relaxation maximum for a given composite sample. This product has been evaluated for 4000 $\overline{M}_n$ polystyrene and glycerol and is given in Table 2-3. The results confirm the prediction of equation 2-10, as the fluctuations in $\eta\nu$ are within the error caused by ±1°C error in T_{max}. This

TABLE 2-2

SLOPES AND VISCOSITIES FOR 4000 $\overline{M}_n$ POLYSTYRENE FROM A LEAST SQUARES FIT OF RMS DATA

TEMPERATURE (°C)	SLOPE*	η (kPa•s)
126	0.995 ± 1.5%	1.8
118	0.993 ± 1.0%	8.5
109	0.969 ± 1.0%	48.0
101	0.913 ± 3.0%	270.0

*To the 95% confidence level.

Figure 2-8. DSA Composite Loss Tangent for Glycerol as a Function of Temperature at Four Frequencies.

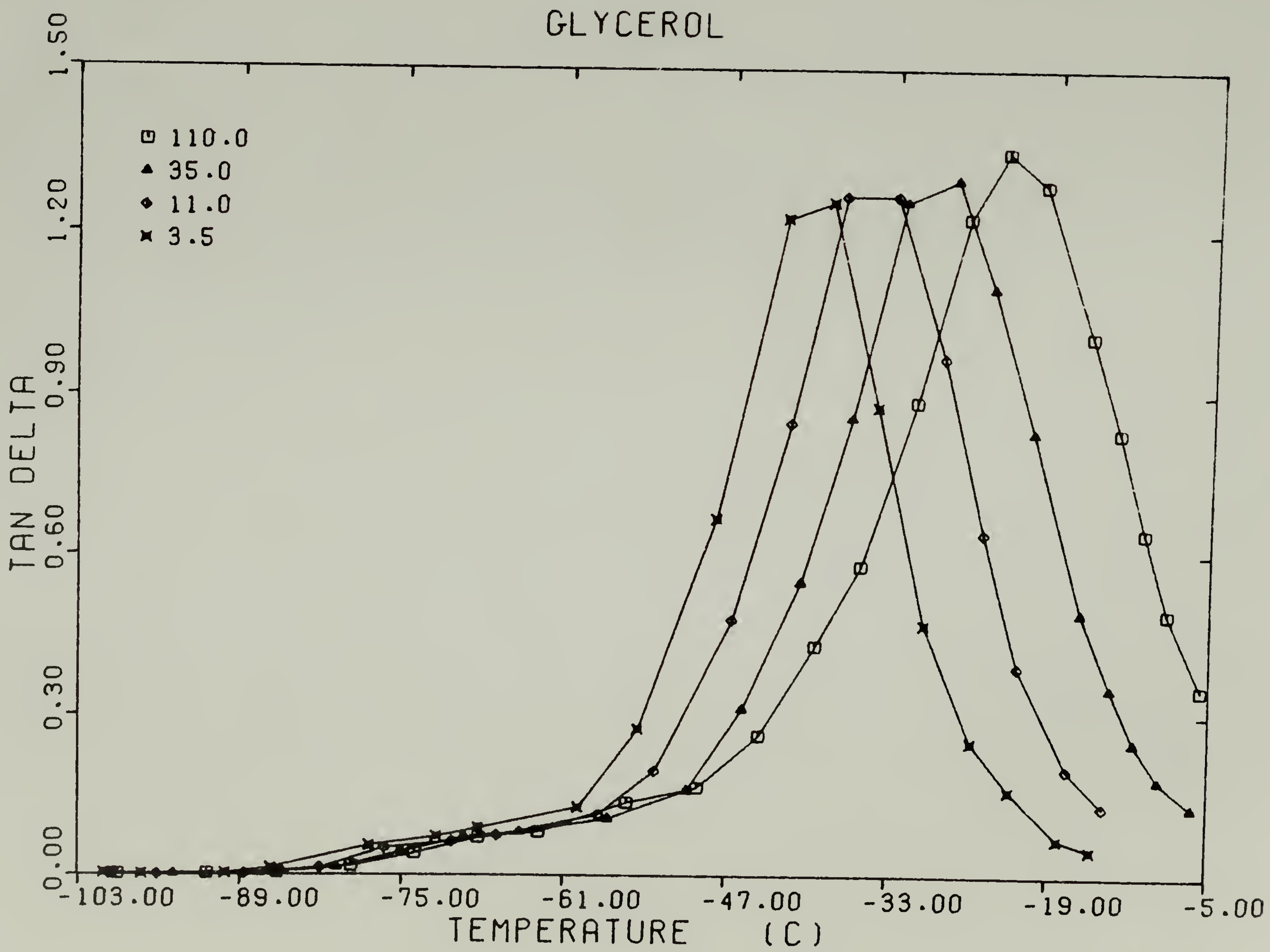
GLYCEROL
110.0
35.0
11.0
3.5
TAN DELTA
0.00
0.30
0.60
0.90
1.20
1.50
TEMPERATURE (C)
-103.00
-89.00
-75.00
-61.00
-47.00
-33.00
-19.00
-5.00

TABLE 2-3

PRODUCTS OF FREQUENCY AND VISCOSITY FOR 4000 $\overline{M}_n$ POLYSTYRENE AND GLYCEROL AT TEMPERATURES WHERE TAN(δ_c) IS A MAXIMUM AS DETERMINED BY DSA

MATERIAL	T_{max} (°C)	ν (Hz)	η (kPa·s)*	$\eta\nu$ (kPa)
4000 $\overline{M}_n$ Polystyrene	142	110	0.20	22
	134	35	0.58	20
	125	11	2.2	24
	119	3.5	6.2	22
Glycerol	-23	110	0.20	22
	-30	35	0.60	21
	-35	11	1.5	17
	-41	3.5	5.9	21

*The 4000 $\overline{M}_n$ polystyrene literature values were obtained by means of an empirical equation relating viscosity, temperature, and molecular weight found in reference (28). Glycerol literature values from reference (29).

uncertainty can result in considerable error in the selection of the literature viscosity.

DSA results from a series of polystyrene molecular weights are presented in Figure 2-9. The polymers are monodisperse with the exception of 92,500 $\bar{M}_n$ polystyrene. The temperature of $\tan(\delta_c)_{max}$ increases with increasing molecular weight for the monodisperse materials. The two highest molecular weight samples display a prominent shoulder on the low temperature side of the main relaxation maximum. This shoulder corresponds to the true glass to rubber relaxation associated with T_g and is due to the formation of an entanglement network at these molecular weights, above M_c for polystyrene (30). The higher temperature loss processes for 37,000 and 92,500 $\bar{M}_n$ polystyrene and the relaxation maxima for the three lower molecular weight materials correspond to the dispersion predicted from the mechanical model in Figure 2-1.

Discussion

The evolution of solvent during heating of polystyrene samples dried at temperatures near T_g for less than 24 hours has been clearly shown by thermal analysis. It is likely that this release of solvent causes a loss phenomenon above T_g to be observed when similarly prepared samples are analyzed by DSA. The absence of solvent evolution upon reheating during thermal analysis is consistent with the failure of the high temperature loss peak to be reproduced upon repetition of the DSA experiments. The mechanism of the loss process above T_g is not certain, but can be envisioned as a conversion of the mechanical energy input into heat necessary to volatilize the solvent. A process requir-

Figure 2-9. DSA Composite Loss Tangent for Polystyrene at 11 Hz as a Function of Temperature for Five Molecular Weights. $\overline{M}_n \times 10^{-3}$ indicated in legend.

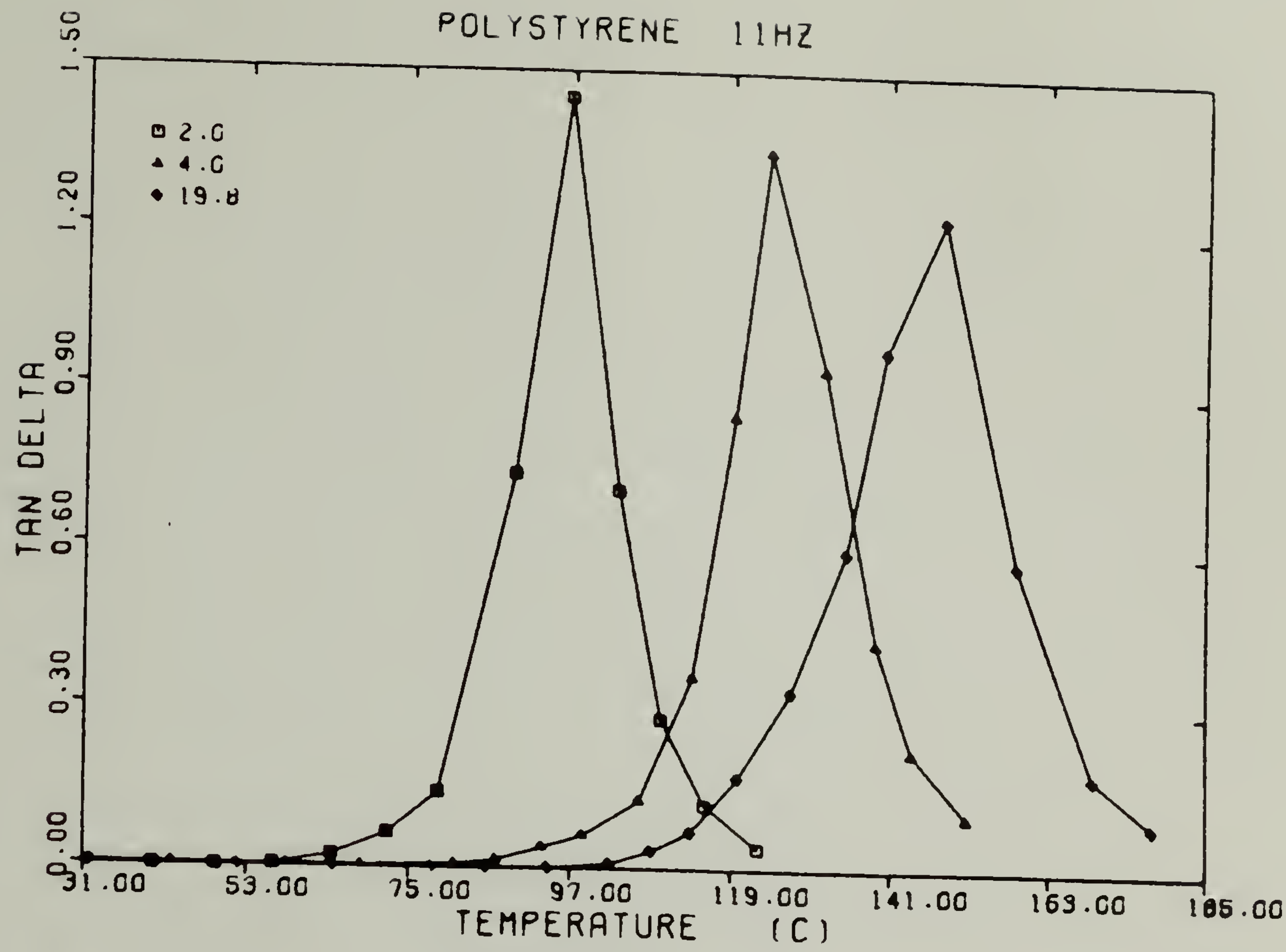
POLYSTYRENE 11HZ
2.0
4.0
19.8
TAN DELTA
0.00
0.30
0.60
0.90
1.20
1.50
31.00
53.00
75.00
97.00
119.00
141.00
163.00
185.00
TEMPERATURE (C)

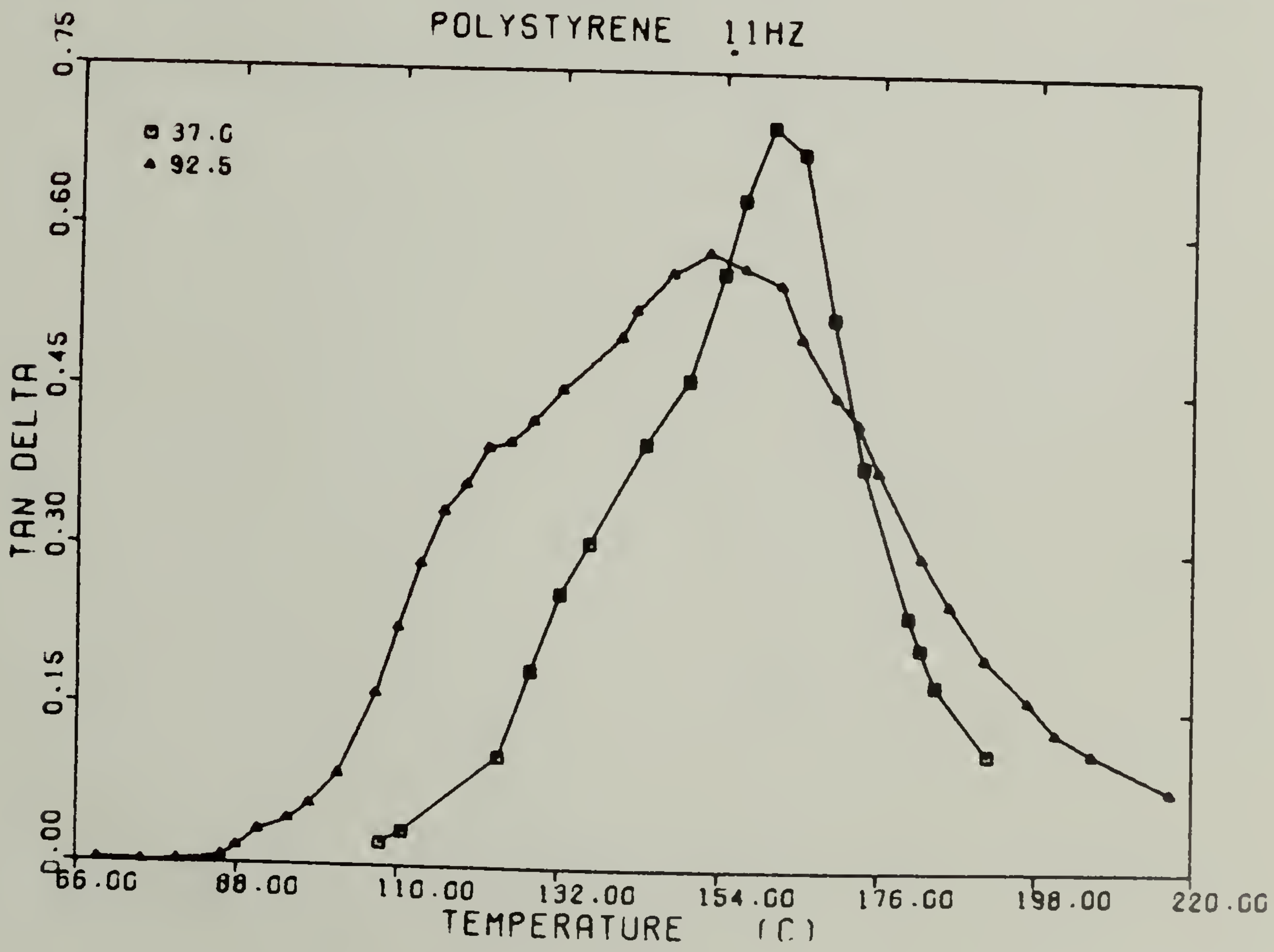
POLYSTYRENE 11HZ
37.0
92.5
TAN DELTA
0.00
0.15
0.30
0.45
0.60
0.75
66.00
88.00
110.00
132.00
154.00
176.00
198.00
220.00
TEMPERATURE (C)

ing the formation of new surface area, in the form of small solvent bubbles, and their transportation to the surface of the polymer could also account for a one time expenditure of energy.

It is interesting to consider the variation of the solvent release relaxation phenomenon with polymer molecular weight. Sample C-1, composed of polystyrene of lowest molecular weight studied, shows the earliest onset of the phenomenon while C-3, of highest molecular weight, gives the highest temperature pseudorelaxation. Sample C-2, of intermediate number average molecular weight, exhibits a transition between that of the two narrow distribution polystyrenes analyzed. This variation can be explained by the high sensitivity of melt viscosity to molecular weight above M_c as shown in equation 2-1. The rate of diffusion of an organic solvent in a molten polymer should be higher, and the temperature at which evolution is complete should be lower for a lower molecular weight polymer, as diffusion occurs more readily in a lower viscosity polymer melt. This relation was found to hold for the loss phenomenon above T_g, which occurred with a similar dependence on the molecular weight of the polymer sample.

The dependence of the solvent induced relaxation on molecular weight is similar to the variation T_{11} with number average molecular weight reported by Gillham and coworkers (19). However, another report (6) states that identical values of the T_{11} transition are obtained after any number of consecutive heating and cooling cycles below degradation temperatures. This indicates that solvent release is unlikely to be responsible for the T_{11} loss maximum observed in TBA experiments.

A more plausible explanation for the T_{11} relaxation found by TBA arises from the mechanical model presented in Figure 2-1. The relaxation which occurs for low molecular weight polystyrenes has been shown to arise from the composite nature of the specimen and not from any molecular dissipative mechanism. The coated braid in TBA experiments is also a composite sample and the model should be equally applicable to this technique above the glass transition or melting temperature of the supported component. The elastic constants of the TBA system will of course differ from those of a DSA composite as will the frequency of measurement. The viscosity at the relaxation maximum and therefore the location of the relaxation maxima during a temperature scan would also be expected to differ for an analysis of the same material by the two methods, as is apparent from equation 2-9.

These physical differences in the two techniques were taken into account in a study of the isothermal curing of two epoxy resins, discussed in detail in Chapter III. The constant C in equation 2-10 was determined from the temperatures of the T_{11} relaxation maxima for various molecular weight polystyrenes given in reference (13) by applying an empirical equation from reference (28) to obtain the viscosity at the T_{11} maximum. An average value of 3 kPa was determined for C. The frequency was assumed to be constant at each T_{11} maximum, as no frequency data are given. If the frequency at the T_{11} maximum is the same as that at the epoxy isothermal curing maximum, then the viscosity of the epoxy resin is known at the time of the curing maximum. Plots of viscosity vs. time of cure constructed from DSA and TBA data on the same resins (Figures 3-7 and 3-8) show good agreement between the TBA and DSA curing maxima when the cure temperatures are the same. This suggests that the origins of the DSA and TBA T_{ll} and curing maxima are identical and lie in the composite nature of the testing methods.

The isoviscous state at T_{ll} proposed by Stadnicki and coworkers (6) is indeed realized if the elastic constants and frequency of measurement are identical for all TBA experiments. This is evident from equation 2-9. Equally evident is the fact that the viscosity at the isoviscous state can be varied at will for any series of experiments by changing E_1, E_2, or ν or any combination of these variables.

Finally it should be emphasized that the T_{ll} relaxation found by DSA has no molecular significance as the point of onset of entanglement slippage or as a transition from a fixed to a true fluid. Such transitions might best be observed from experiments on the pure material of interest and not by a supported viscoelastic technique with relaxation mechanisms inherent to the composite nature of the specimens required. Such viscoelastic techniques are not without merit however. Chapter III presents a study in which the DSA technique proved to be extremely useful in studying the curing kinetics of epoxy resins.

Conclusions

Relaxation processes in DSA experiments above the glass transition temperature have been shown to be caused by the evolution of solvent from incompletely dried samples. Such relaxations are not reversible or repeatable. In thoroughly dried samples, a repeatable relaxation has been observed which has been shown to be an artifact attributable to the composite nature of the specimen. Predictions of a mechanical model that the relaxation will be observed when the sample viscosity reaches the critical value have been found to hold from experimental studies. The occurrence of this relaxational phenomenon depends only on the viscosity not on the molecular nature of the supported material. The relaxation has been shown to occur for polystyrene polymers of various molecular weights, both above and below M_c, and for glycerol. The explanation for this relaxation is thought to also apply to the T_{11} relaxation observed by TBA, another supported sample technique of viscoelastic analysis. The isoviscous state observed at T_{11} is predicted from the mechanical model advanced to explain the DSA relaxation. Any supported sample technique can be expected to show such a T_{11} relaxation, independent of the nature of the supported material and having no molecular basis.

REFERENCES

1. J.J. Aklonis, W.J. MacKnight, and M. Shen, "Polymer Viscoelasticity," p. 39, Wiley-Interscience, New York (1972).

2. J.D. Ferry, "Viscoelastic Properties of Polymers," p. 424, John Wiley and Sons, New York (1970).

3. Ibid., p. 269.

4. Ibid., p. 282.

5. L.E. Nielsen, "Mechanical Properties of Polymers and Composites," Vol. 1, p. 163, Marcel Dekker, New York (1974).

6. S.J. Stadnicki, J.K. Gillham, and R.F. Boyer, J. Appl. Polym. Sci., 20, 1245 (1976).

7. R.F. Boyer, J.B. Enns, and J.K. Gillham, Polymer Preprints, 18(2), 462 (1977).

8. E.A. Sidorovitch, A.I. Marei, and N.S. Gashtol'd, Rubber Chem. Tech., 44, 166 (1971).

9. E.A. Sidorovitch, G.N. Pavlov, and A.I. Marei, Polym. Sci. USSR, 16, 993 (1974).

10. R.F. Boyer, Rubber Chem. Tech., 36, 1303 (1963).

11. R.F. Boyer, J. Polym. Sci. C., 11, 267 (1966).

12. R.F. Boyer in "Polymeric Materials," p. 277, E. Baer and S.V. Radcliffe, eds., American Society for Metals, Metals Park, OH (1975).

13. J.K. Gillham and R.F. Boyer, J. Macromol. Sci. Phys., B13, 497 (1977).

14. R.F. Boyer, Amer. Chem. Soc., Prepr., Div. Org. Coat. Plas. Chem., 38, 379 (1978).

15. Ibid., p. 387.

16. G.D. Patterson, H.E. Bair, and A.E. Tonelli, J. Polym. Sci. C., 54, 249 (1976).

17. L.E. Nielsen, Polym. Eng. Sci., 17, 713 (1977).

18. C.A. Glandt, H.K. Toh, J.K. Gillham, and R.F. Boyer, J. Appl. Polym. Sci., 20, 1277 (1976).

19. J.K. Gillham, J.A. Benci, and R.F. Boyer, Polym. Eng. Sci., 16, 357 (1976).

20. G.A. Senich and W.J. MacKnight, J. Appl. Polym. Sci., 22, 2633 (1978).

21. R.M. Neumann, G.A. Senich, and W.J. MacKnight, Polym. Eng. Sci., 18, 624 (1978).

22. P.C. Uden, D.E. Henderson, and R.J. Lloyd, J. Chromatogr., 126, 225 (1976).

23. J.J. Aklonis, W.J. MacKnight, and M. Shen, p. 152.

24. E.B. Baker, R.P. Auty, and G.J. Ritenour, J. Chem. Phys., 21, 159 (1953).

25. P.S. Alexandrovich, private communication.

26. J.D. Ferry, p. 249.

27. A.K. Schulz, Z. Naturforsch, 9A, 944 (1954).

28. T.G. Fox and P.J. Flory, J. Polym. Sci., 14, 315 (1954).

29. "Handbook of Chemistry and Physics," p. F-40, The Chemical Rubber Co., Cleveland, OH (1972-73).

30. J.D. Ferry, p. 409.

CHAPTER III

A DYNAMIC MECHANICAL STUDY OF THE CURING REACTION OF TWO EPOXY RESINS

Introduction

Several techniques are available which allow the dynamic mechanical properties of epoxy resins to be studied during the actual curing process. Torsional braid analysis, TBA, has been shown by Gillham (1,2) to be a useful method for characterizing the curing behavior of epoxy resins through both the gelation and vitrification stages of the reaction. Viscosity and dynamic shear measurements have been employed by Mussatti and Macosko (3) to determine the order, rate constants and activation energy for a network forming epoxy reaction. The method of dynamic spring analysis, DSA, was proposed by Naganuma and coworkers (4) as a viscoelastic technique employing the Rheovibron Dynamic Viscoelastometer with the sample coated on small metal springs. The technique was initially applied to a curing study of a butylated melamine resin but subsequent work by the same authors showed the versatility of the method by examining the crosslinking of commercial adhesives (5) as well as the curing of modified phenolic resins and tung oil (6). The present work focuses on the extension of the DSA technique to a study of the crosslinking of two epoxy resins. Application of a model described in Chapter I allows both storage and loss moduli to be obtained as a function of time for the curing system. Knowledge of the viscosity at the T_{11} loss maximum at each frequency, as discussed in Chapter II, has facilitated the determination of kinetic parameters of the curing reactions. Additional characterization of unsupported resin films cured at several temperatures has also been carried out on the Rheovibron employing conventional methods of analysis. The study described in this chapter has been previously published (7,8).

Experimental

Samples. Two commercially formulated epoxy resins are identical to those used in a recent DSC and TBA study (9,10), where more detailed sample composition information can be found. Resin I consists of novolac resin (a phenol-formaldehyde prepolymer), a difunctional epoxy, 4,4'-bisglycidylphenyl-2,2'-propane (A), the tetrafunctional amine dicyandiamide (DICY, C), a urea type accelerator (D), and a small amount of monofunctional epoxy (B) as shown in Figure 3-1. Resin II consists of a tetrafunctional epoxy, the tetraglycidyl ether of methylene dianiline (A), and the tetrafunctional amine DICY (B), in addition to a urea type accelerator (C), shown schematically in Figure 3-2. The recommended cure for both resins is two hours at 127°C with no postcure. Epoxy resin II was supplied as a 50% by weight solution in methylene chloride.

Measurements. The curing reaction was followed by the technique of dynamic spring analysis (DSA) in conjunction with the Rheovibron DDV-IIB

Figure 3-1. Chemical Structures of the Components of Epoxy Resin I.

RESIN I

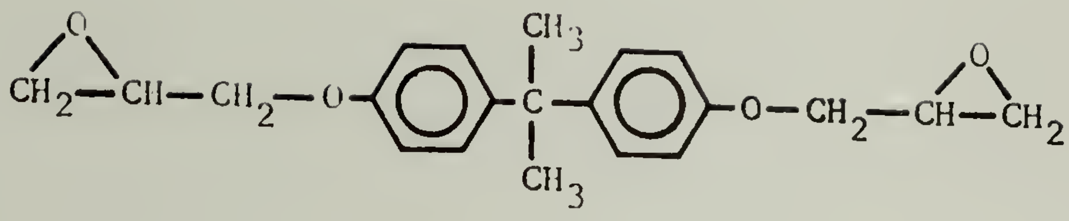

A, EPON 828

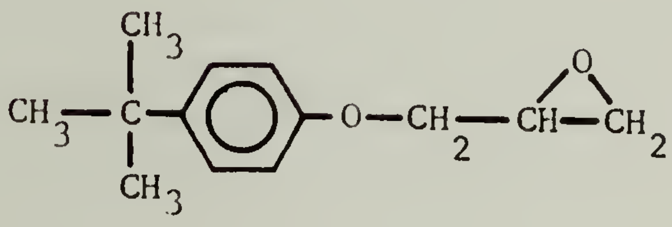

B

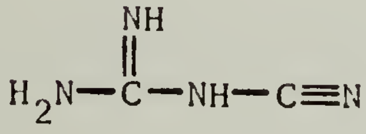

$$H_2N-\overset{\overset{\displaystyle NH}{\|}}{C}-NH-C\equiv N$$

C, DICY

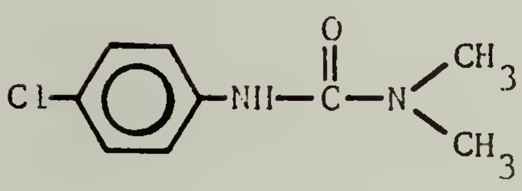

D, MONURON

Figure 3-2. Chemical Structures of the Components of Epoxy Resin II.

RESIN II

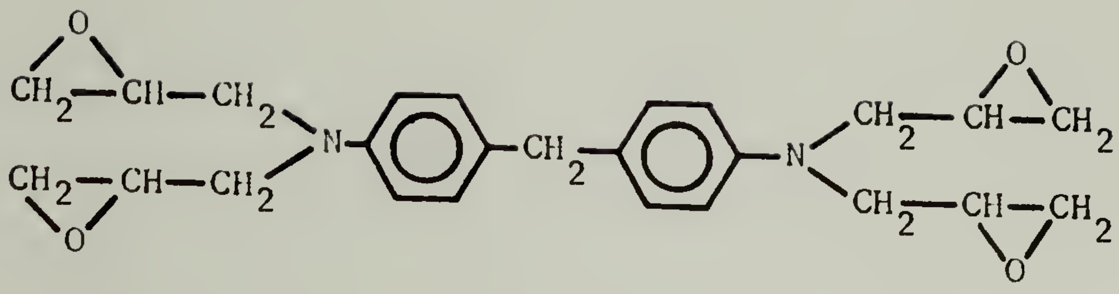

A

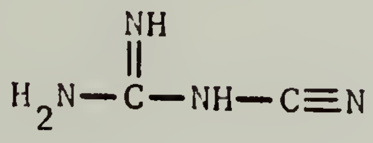

$$H_2N-\overset{\overset{NH}{\|}}{C}-NH-C\equiv N$$

B, DICY

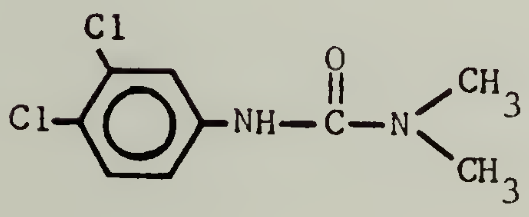

C, DIURON

Dynamic Viscoelastometer, as described previously in Chapter I. A 0.30 mm diameter steel wire spring, 3.3 mm in outer diamter and twenty turns in length, was placed in the Rheovibron and stretched to achieve a pitch of 0.1 mm. The Rheovibron temperature chamber was then brought to a constant cure temperature, T_c, and the epoxy resin sample applied with a hypodermic syringe as a 50% by weight solution in methylene chloride. Evaporation of the methylene chloride occurred very rapidly, resulting in the deposition of an uncured epoxy film. The viscoelastic response of the composite was followed in a dry nitrogen atmosphere as a function of time from the moment of sample application. About 15 mg of epoxy sample was required for each curing study.

Thin film epoxy samples were prepared by compression molding 0.25 mm thick samples under pressures of 2.3-2.9 MPa at a constant cure temperature. Resin II was subjected to room temperature drying in a vacuum oven to remove most of the methylene chloride before molding. The epoxy films were removed from the press after the desired time at T_c had been attained. These samples were analyzed in the Rheovibron DDV-IIB by standard procedures at nominal heating rates of 1.5°C/min in a dry nitrogen atmosphere. DSA and Rheovibron measurements were made sequentially at frequencies of 3.5, 11, 35, and 110 Hz with the exact time or temperature noted when the measurement was made.

Several computer programs were utilized to facilitate data reduction. Isofig was used to compute and plot isothermal cure data. Vibfig was similarly employed to analyze the thin film temperature scans. Ratecon served to determine first order rate constants from isothermal cure data. Arrhea was used to calculate Arrhenius activation energies for relaxations observed during the thin film temperature scans. Copies of these programs and instructions for their use can be found in the appendix.

Results

Isothermal cures. Several cures of each resin system were carried out over the temperature range of 80 to 110°C by the DSA technique. Figure 3-3 is typical of the data collected and shows the storage and loss modulus of resin I at several frequencies as a function of the natural logarithm of time for a cure at 80.2°C. The analysis required to obtain the storage and loss modulus of the epoxy as discussed in Chapter I was modified slightly be elimination of the volume fraction terms from the parallel model assumed. For this case, the defining parallel model equation can be written as:

$$M_c = M_p + M_s \tag{3-1}$$

where M_c is the composite modulus, M_s the spring modulus, and M_p the polymer modulus. The frequency dependence of the loss peaks in Figure 3-3 indicates that the phenomenon occurs first at high frequency and last at the lowest frequency studied. Corresponding to the loss peak in M_p'', the storage modulus M_p' shows an increase from about 0.1 kPa to 1000 kPa, over a relatively short time interval. The final level of the storage modulus is about that expected for a lightly crosslinked rubbery network.

In isothermal cures at fixed frequency, the position of the

Figure 3-3. Storage and Loss Modulus at Four Frequencies of Resin I as a Function of Logarithmic Time for an 80.2°C Cure.

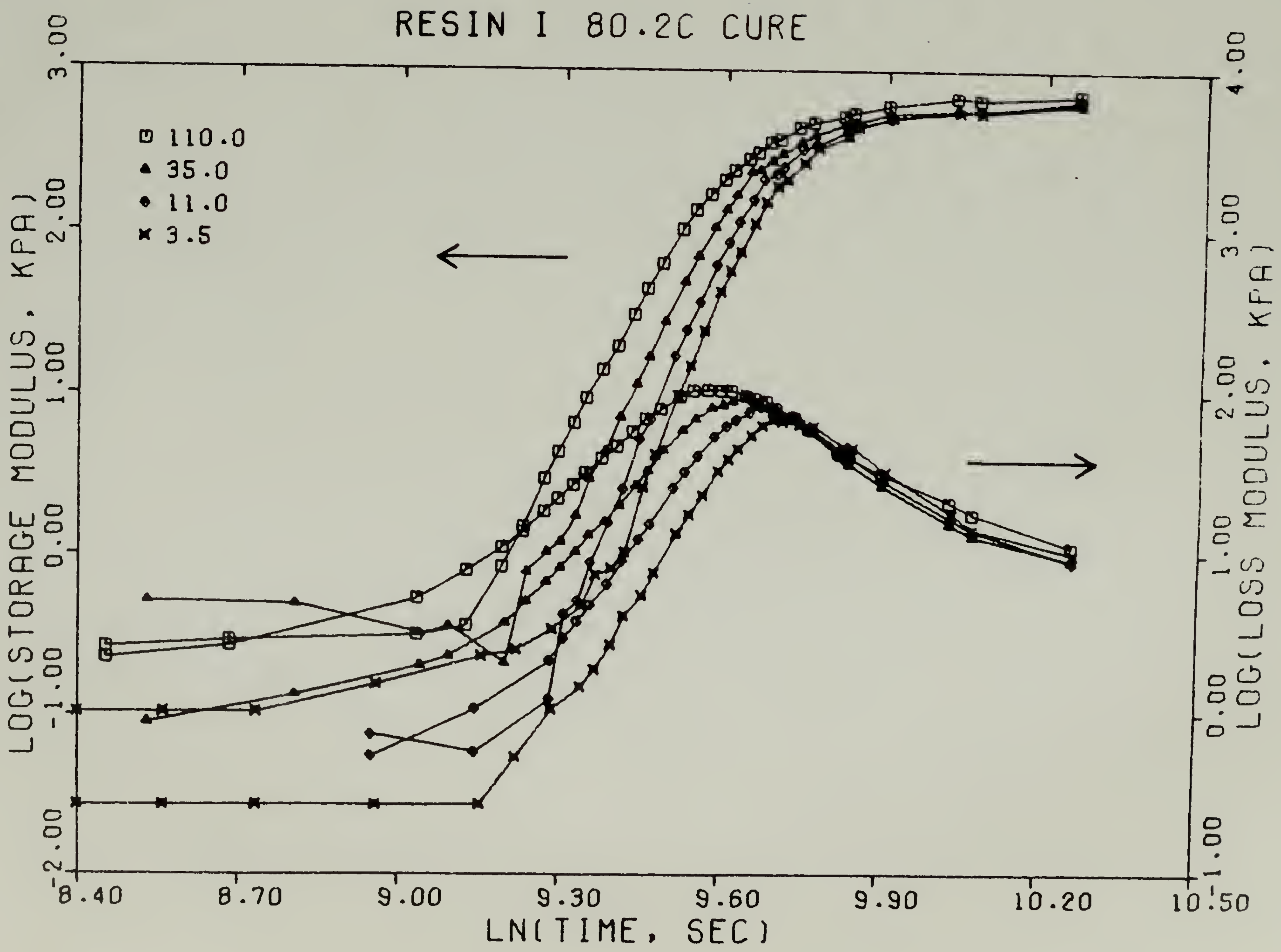
RESIN I 80.2C CURE
110.0
35.0
11.0
3.5
LOG(STORAGE MODULUS, KPA)
-2.00
-1.00
0.00
1.00
2.00
3.00
LOG(LOSS MODULUS, KPA)
-1.00
0.00
1.00
2.00
3.00
4.00
LN(TIME, SEC)
8.40
8.70
9.00
9.30
9.60
9.90
10.20
10.50

loss maximum was found to vary with the temperature at which the epoxy sample was cured. Figure 3-4 shows a plot of the composite tan(δ) at 110 Hz for four resin II samples cured at temperatures between 80 and 110°C. It is apparent that the highest T_c results in the earliest onset of the loss peak associated with the curing process. Isothermal cure times for resin I and II reactions at several temperatures are given in Tables 3-1 and 3-2, respectively. This information can be used to calculate an activation energy for the epoxy curing process in the following manner. The velocity constant k for a chemical reaction varies with temperature according to the Arrhenius relation:

$$\ln(k) = -H_a/RT + C \qquad (3\text{-}2)$$

where H_a is the activation energy of the reaction. Since the velocity constant is inversely proportional to the time of reaction independent of the order of the reaction (11), the elapsed time to the loss modulus maximum t_{max} was used as a convenient measure of the rate of reaction at each temperature and for each frequency.

$$\ln(t_{max}) = H_a/RT + C' \qquad (3\text{-}3)$$

The slope of a plot of $\ln(t_{max})$ vs. 1/T can then be used to determine the activation energy. Such plots are shown in Figure 3-5 for resin I and in Figure 3-6 for resin II. For each frequency, the data can be seen to fit a straight line quite well. A linear least squares fit was used to determine the activation energy for both resins at each frequency. These results are summarized in Table 3-3 for both materials. Activation energies determined from the position of the tan(δ) loss

Figure 3-4. Loss Tangent at 110 Hz vs. Logarithmic Time for Resin II at Several Cure Temperatures.

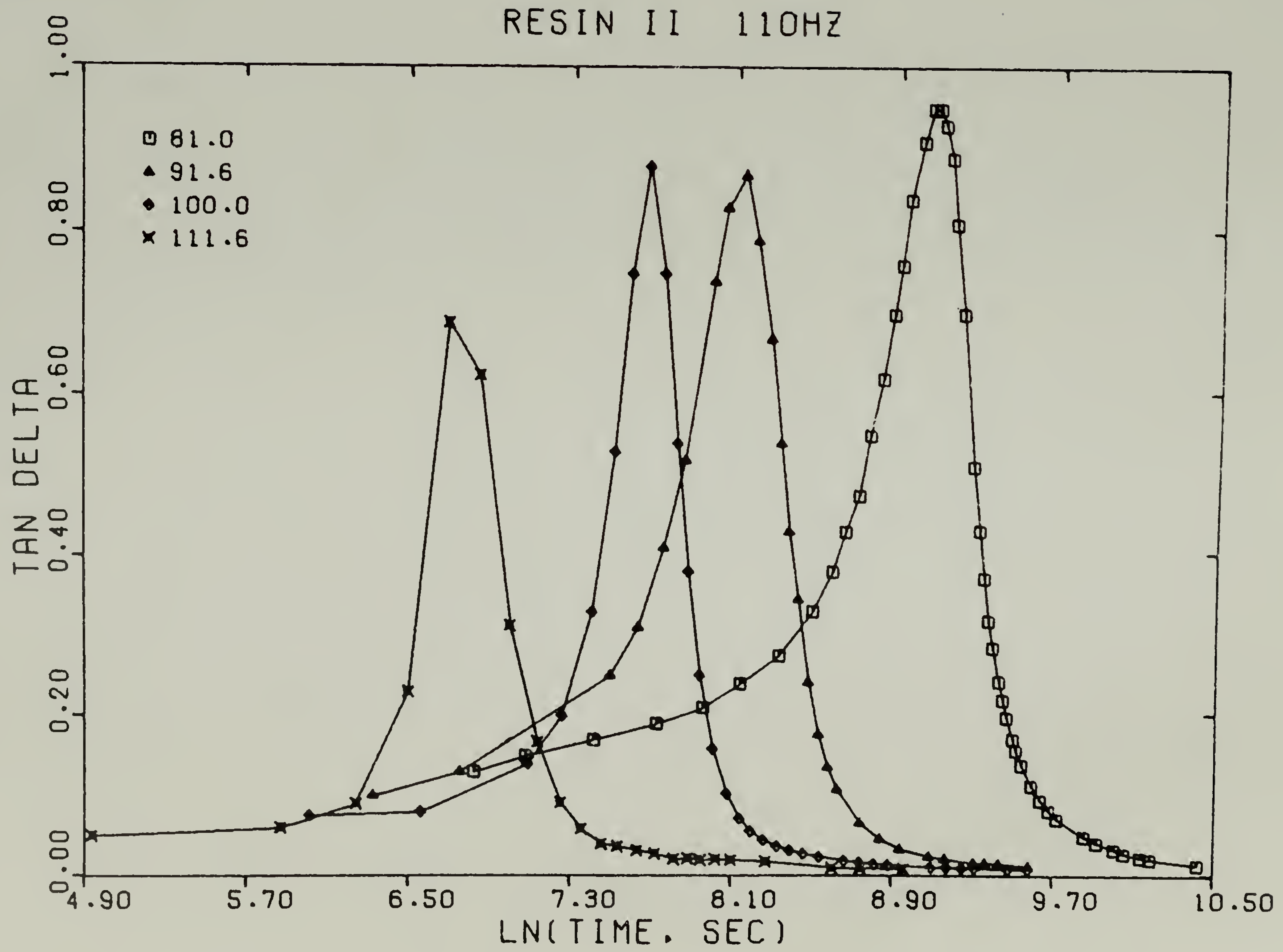
RESIN II 110HZ
81.0
91.6
100.0
111.6
TAN DELTA
0.00
0.20
0.40
0.60
0.80
1.00
4.90
5.70
6.50
7.30
8.10
8.90
9.70
10.50
LN(TIME, SEC)

TABLE 3-1

ISOTHERMAL CURE TIMES FOR RESIN I

CURE TEMPERATURE (°C)	FREQUENCY (Hz)	ln (time,sec)	
		at M''_{max}	at $\tan(\delta)_{max}$
108.0	110	7.367	7.136
	35	7.401	7.212
	11	7.522	7.242
	3.5	7.563	7.258
99.4	110	8.075	7.847
	35	8.117	7.923
	11	8.193	7.960
	3.5	8.261	8.018
90.2	110	8.778	8.651
	35	8.839	8.699
	11	8.880	8.750
	3.5	8.909	8.784
80.2	110	9.576	9.411
	35	9.627	9.496
	11	9.688	9.553
	3.5	9.739	9.597

TABLE 3-2

ISOTHERMAL CURE TIMES FOR RESIN II

CURE TEMPERATURE (°C)	FREQUENCY (Hz)	ln (time,sec) at M''_{max}	ln (time,sec) at $\tan(\delta)_{max}$
111.6	110	6.987	6.726
	35	7.021	6.793
	11	7.063	6.841
	3.5	7.101	6.876
100.0	110	7.836	7.668
	35	7.890	7.727
	11	7.926	7.776
	3.5	8.002	7.833
91.6	110	8.355	8.107
	35	8.441	8.216
	11	8.492	8.294
	3.5	8.552	8.361
81.0	110	9.219	9.072
	35	9.338	9.222
	11	9.405	9.263
	3.5	9.467	9.335

Figure 3-5. Arrhenius Plots at Four Frequencies for the Determination of Activation Energies for the Resin I Curing Reaction.

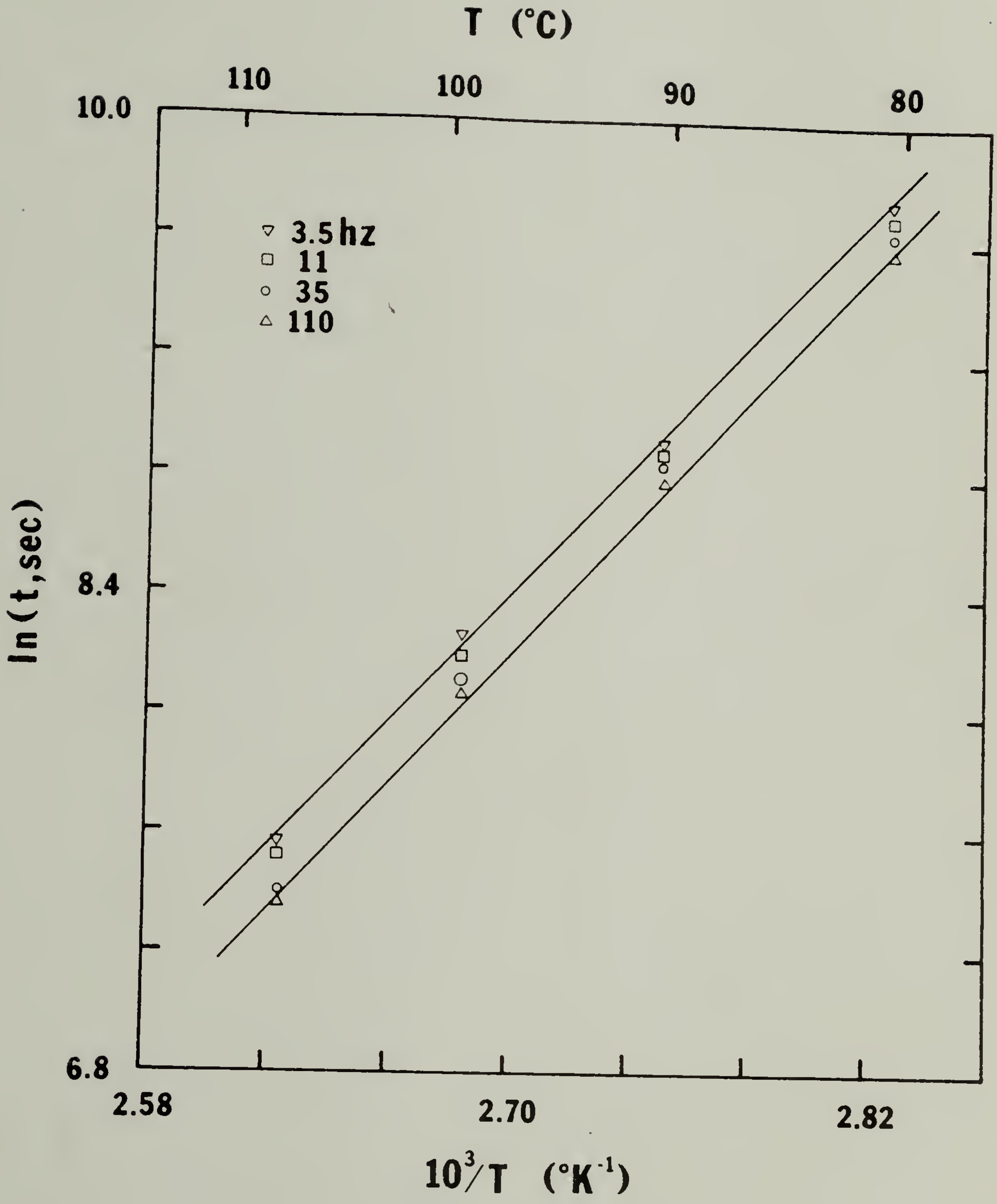
T (°C)
110
100
90
80
10.0
8.4
6.8
ln(t,sec)
▽ 3.5 hz
□ 11
○ 35
△ 110
2.58
2.70
2.82
$10^3/T$ (°K^{-1})

Figure 3-6. Arrhenius Plots at Four Frequencies for the Determination of Activation Energies for the Resin II Curing Reaction.

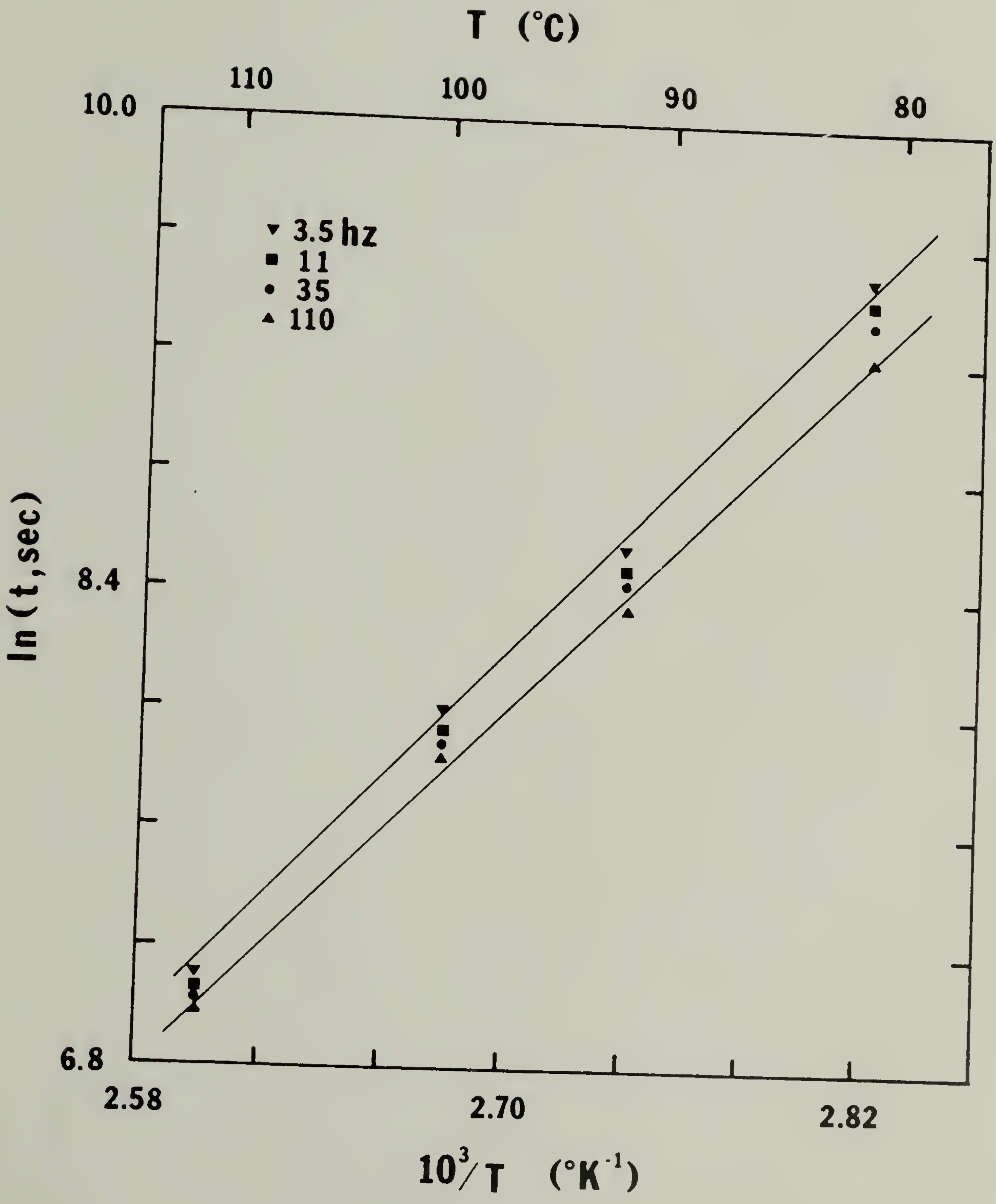
T (°C)
110
100
90
80
10.0
8.4
6.8
ln (t, sec)
▼ 3.5 hz
■ 11
● 35
▲ 110
2.58
2.70
2.82
10³/T (°K⁻¹)

TABLE 3-3

CHEMICAL ACTIVATION ENERGY FROM DSA FOR EPOXY CURES

FREQUENCY (Hz)	RESIN I H_a (kJ/mole)	RESIN II H_a (kJ/mole)
110	88.5 ± 4.1*	81.8 ± 5.0*
35	89.4 ± 4.7	85.0 ± 4.5
11	86.8 ± 2.3	86.0 ± 4.3
3.5	86.8 ± 4.2	86.6 ± 5.2
Average	87.9 ± 2.8	84.9 ± 4.6

*From the loss modulus maximum, to the 95% confidence level.

maximum differ by 5% or less from those cited in Table 3-3. Chemical activation energies determined by DSA are in good agreement with determinations by other methods on the same samples, as indicated in Table 3-4, as well as with the results obtained from other studies of epoxy resins cured with DICY (12,13).

A rate constant for the curing reaction can be evaluated by a method proposed by Mussatti and Macosko (3) in which the viscosity is plotted against the reaction time required to reach that viscosity at a constant temperature. Since DSA experiments were conducted at four frequencies and the viscosity frequency product is constant at the tan(δ) loss maximum as discussed in Chapter II, four reaction times to a known viscosity level are available. From this data, plots of logarithmic viscosity, data given in Table 2-3, as a function of reaction time for each isothermal cure were constructed, as shown in Figures 3-7 and 3-8 for resins I and II, respectively. A logarithmic variation of viscosity with time indicates that the reaction is first order and the slope of such a plot is equal to the overall rate constant. The rate constant measured is thought to be complex in nature as it is dependent upon particle size, solubility and degree of mixing of the DICY component (13) as well as the extent of various side reactions which are possible in the system (14). Rate constants determined for each resin at each cure temperature by a linear least squares fit are given in Table 3-5.

The rate constants for isothermal curing can be used to determine the activation energy of the curing reaction from a plot of the logarithm of the rate constant vs. the inverse cure temperature as

TABLE 3-4

COMPARISON OF THE CHEMICAL ACTIVATION ENERGY OF CURING DETERMINED BY SEVERAL METHODS

ANALYSIS	RESIN I H_a (kJ/mole)	RESIN II H_a (kJ/mole)
DSA	87.9	84.9
TBA*	81.6	85.4
DSC*	84.9	84.9

*From reference 9.

Figure 3-7. Logarithmic Viscosity vs. Time for Several Resin I Isothermal Cure Temperatures. Filled points from DSA, open point from TBA at 100°C.

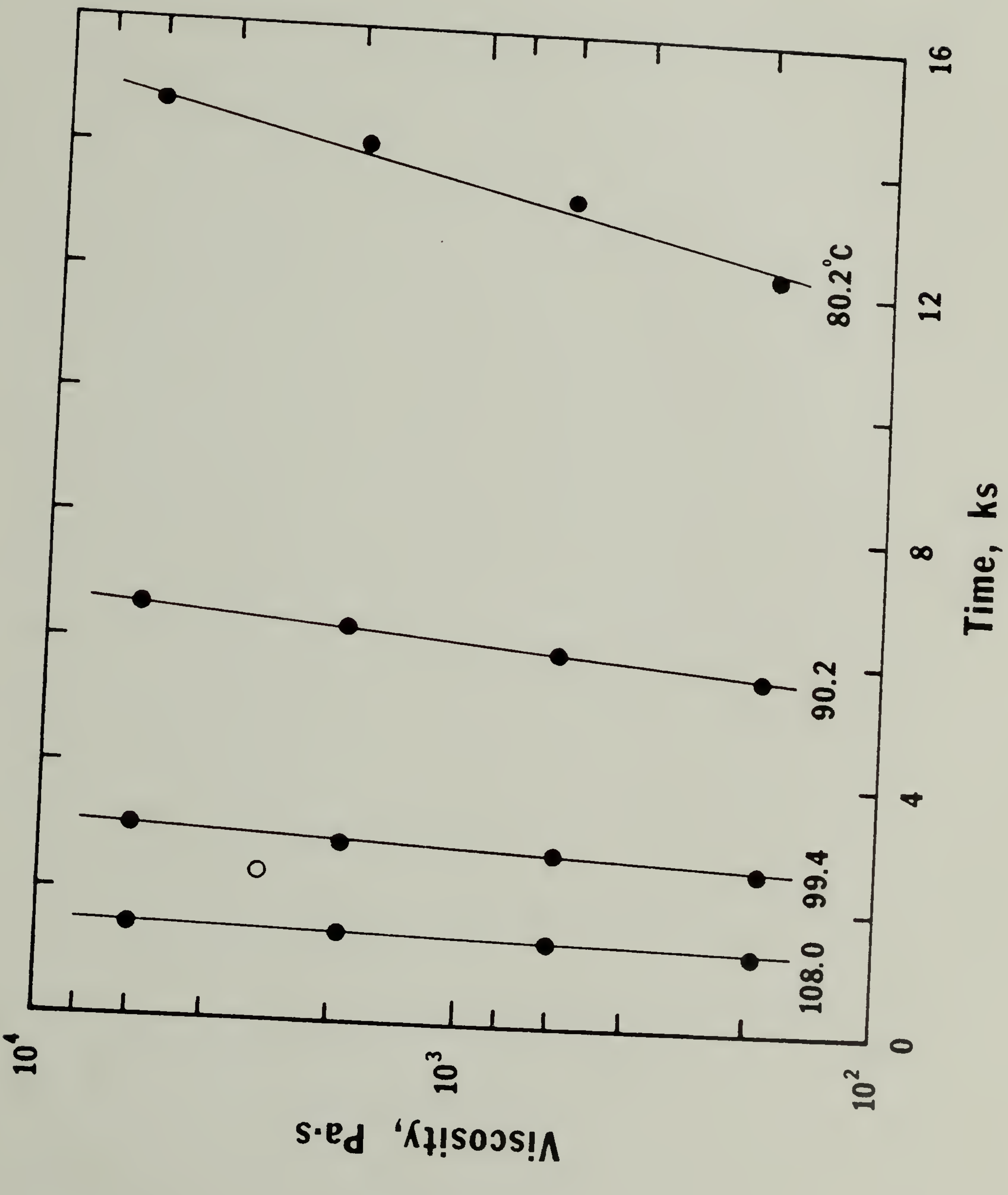
Viscosity, Pa·s
10^4
10^3
10^2
Time, ks
0
4
8
12
16
108.0
99.4
90.2
80.2°C

Figure 3-8. Logarithmic Viscosity vs. Time for Several Resin II Isothermal Cure Temperatures. Filled points from DSA, open points from TBA (O̍ 112, -O 102, O̩ 92, O- 82°C).

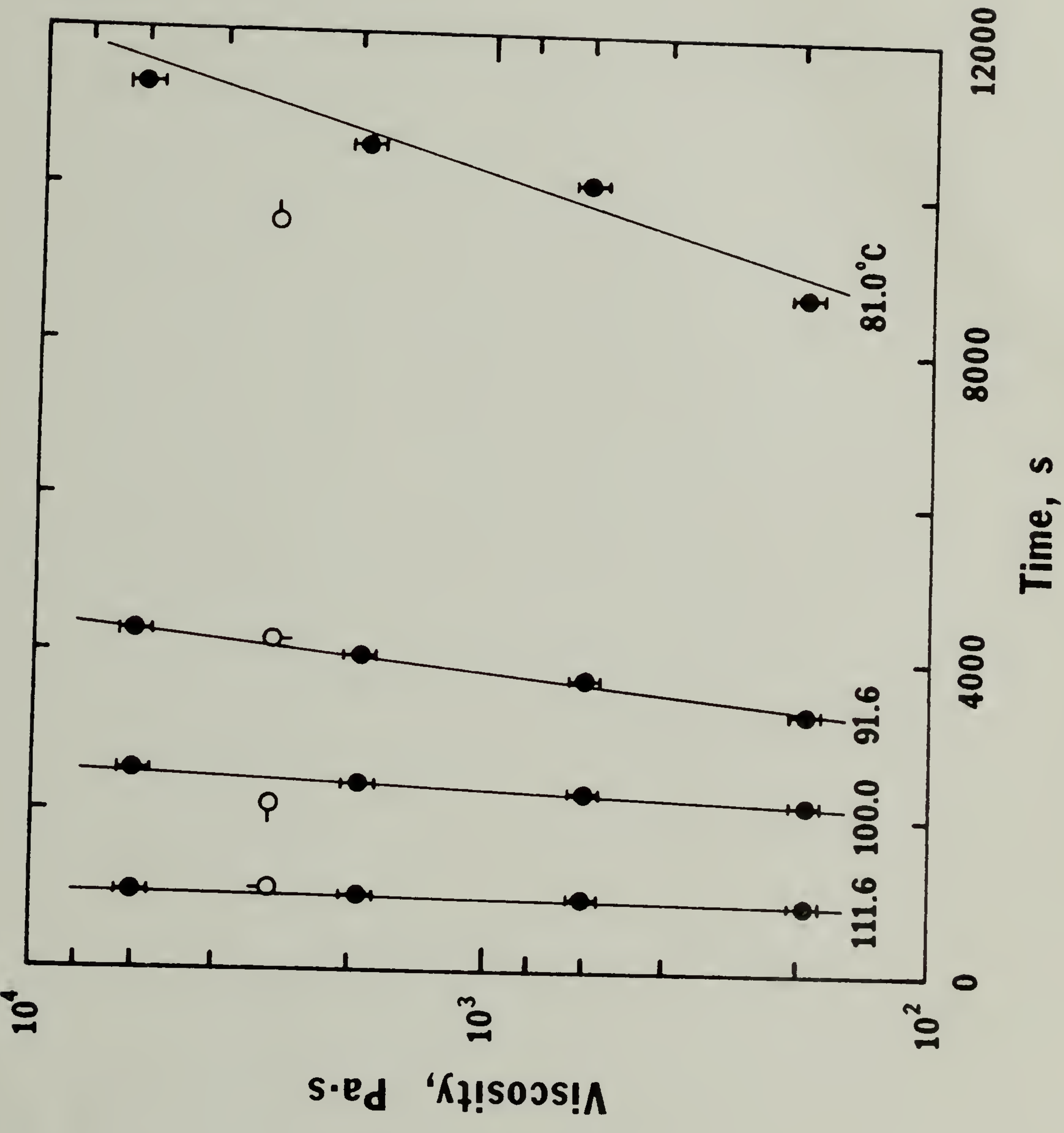
Viscosity, Pa·s
10^4
10^3
10^2
0
4000
8000
12000
Time, s
111.6
100.0
91.6
81.0°C

TABLE 3-5

RATE CONSTANTS FOR EPOXY CURES FROM DSA

SAMPLE	TEMPERATURE OF CURE (°C)	RATE CONSTANT $k \times 10^3$ (sec^{-1})
Resin I	108.0	8.5 ± 4.3*
	99.4	3.2 ± 0.6
	90.2	1.8 ± 0.2
	80.2	0.59 ± 0.11
Resin II	111.6	11.0 ± 2.0
	100.0	3.9 ± 0.3
	91.6	1.6 ± 0.2
	81.0	0.57 ± 0.21

*Calculated from time to reach $\tan(\delta)_{max}$, to the 95% confidence level.

indicated in equation 3-2. A linear least squares fit of the data in Table 3-5 gave an activation energy to the 95% confidence level of 104 ± 17 kJ/mole for resin I and 111 ± 26 kJ/mole for resin II. The greater degree of error in the activation energies obtained from the rate constants compared to those obtained from the time to the loss maxima can be attributed to the necessity of performing two least squares fits in the former procedure.

Partially cured thin films. Data were collected on cured epoxy films to characterize the behavior of the partially cured resin beyond its gel point. Figures 3-9 and 3-10 show the dynamic mechanical relaxation behavior of a sample of resin I cured at 79°C for 260 min. Two relaxations can be observed upon initial heating, the first at about 80°C and a second at 128°C, both at 3.5 Hz. The first softening loss peak gives an apparent activation energy, determined from the dependence of ln(frequency) on 1/T, of 330 ± 70 kJ/mole while the process near 130°C has an activation energy of about 500 ± 40 kJ/mole. The sample was continuously heated to over 200°C, then cooled while observing its dynamic mechanical response. Upon cooling only a single relaxation in the vicinity of 145°C was observed. The value of $T_{g\infty}$ for resin I, the limited T_g which could be reached with a network cured for long times at high temperatures, appeared to be 140°C at 3.5 Hz and 148°C at 110 Hz based on results from several determinations.

The dynamic mechanical behavior of a resin II sample cured at 83°C is shown in Figure 3-11. A T_g' relaxation at 84°C (3.5 Hz) is indicated in the figure by a broad maximum in E". The storage modulus

Figure 3-9. Storage and Loss Modulus at Four Frequencies as a Function of Temperature for Resin I Cured at 79°C.

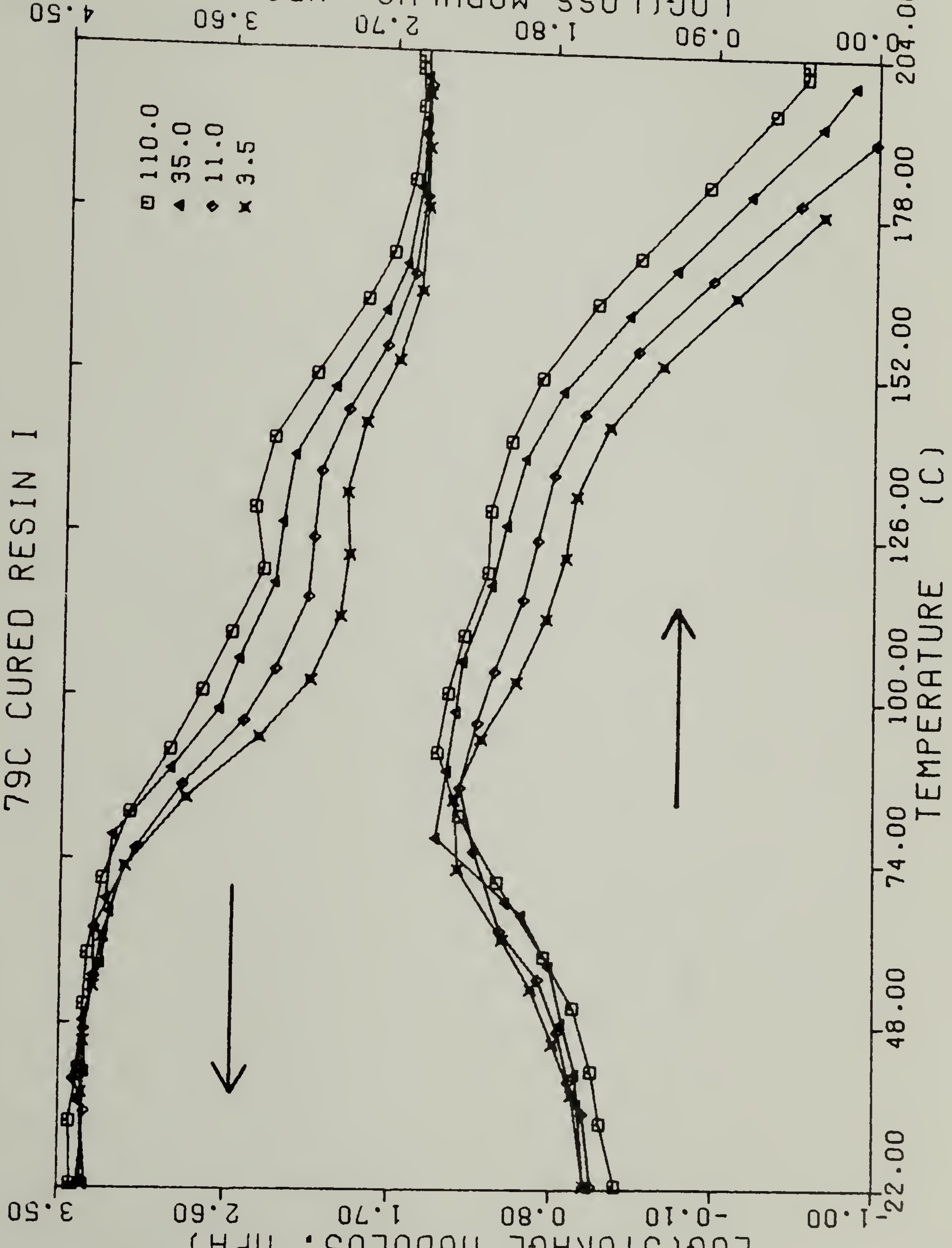
79C CURED RESIN I
⊡ 110.0
▲ 35.0
◆ 11.0
✖ 3.5
LOG(STORAGE MODULUS, MPA)
3.50
2.60
1.70
0.80
-0.10
-1.00
LOG(LOSS MODULUS, MPA)
4.50
3.60
2.70
1.80
0.90
0.00
TEMPERATURE (C)
22.00
48.00
74.00
100.00
126.00
152.00
178.00
204.00

Figure 3-10. Loss Tangent at Four Frequencies as a Function of Temperature for Resin I Cured at 79°C.

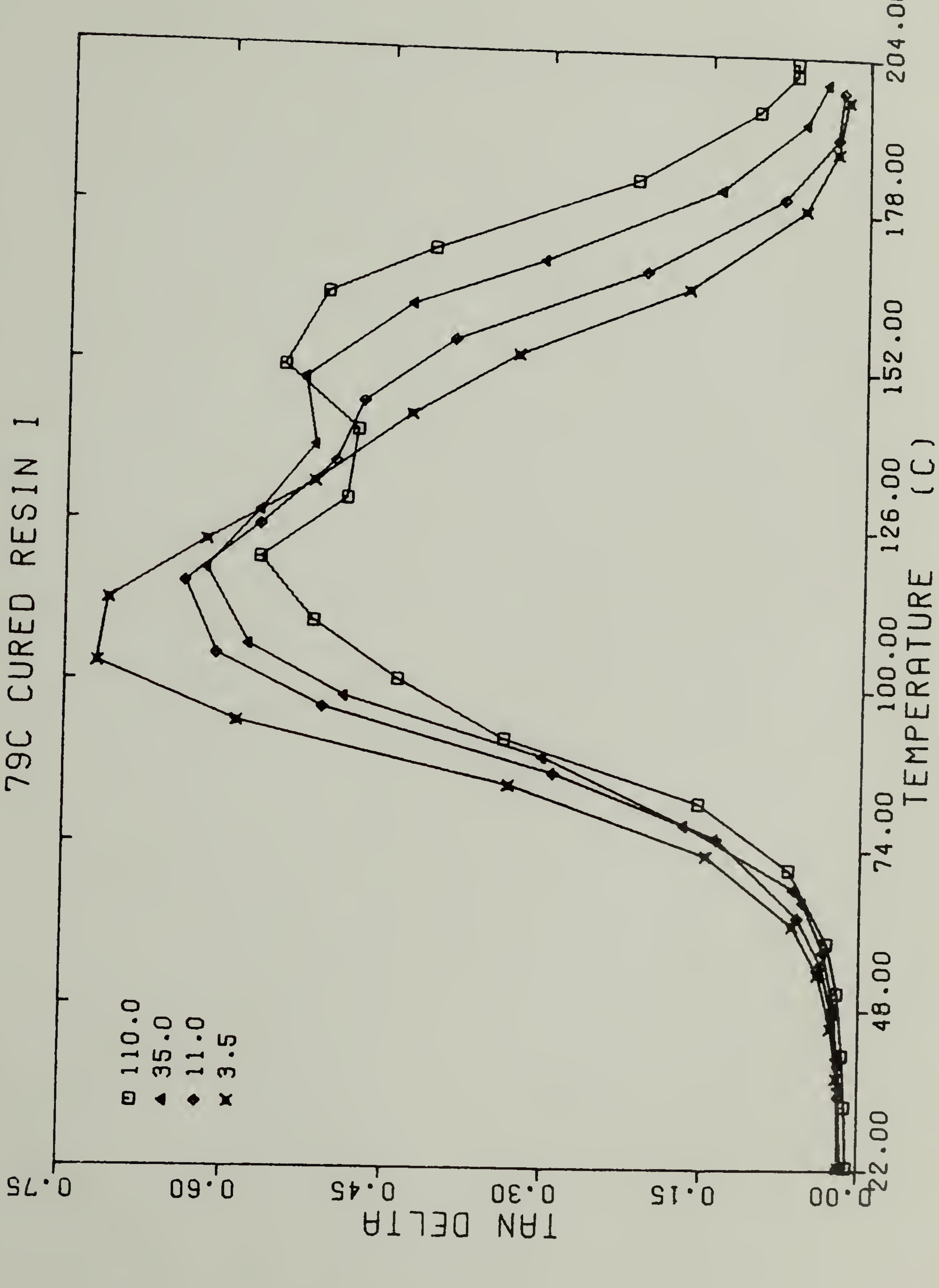
79C CURED RESIN I
□ 110.0
▲ 35.0
◆ 11.0
✕ 3.5
TAN DELTA
0.00
0.15
0.30
0.45
0.60
0.75
TEMPERATURE (C)
22.00
48.00
74.00
100.00
126.00
152.00
178.00
204.00

Figure 3-11. Storage and Loss Modulus at Four Frequencies as a Function of Temperature for Resin II Cured at 83°C.

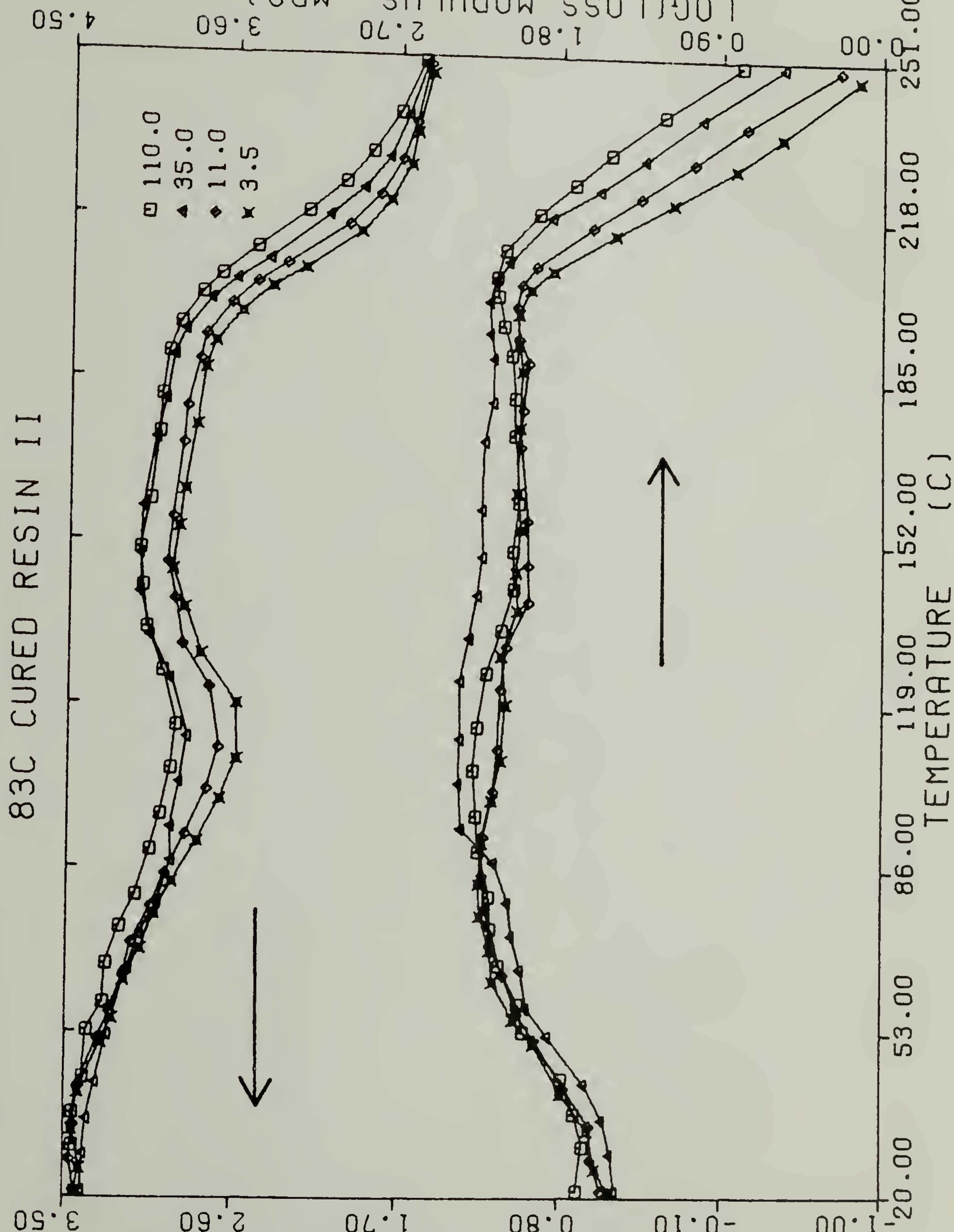
83C CURED RESIN II
□ 110.0
▲ 35.0
◆ 11.0
✕ 3.5
LOG(STORAGE MODULUS, MPA)
3.50
2.60
1.70
0.80
-0.10
-1.00
LOG(LOSS MODULUS, MPA)
4.50
3.60
2.70
1.80
0.90
0.00
TEMPERATURE (C)
20.00
53.00
86.00
119.00
152.00
185.00
218.00
251.00

also shows a gradual drop of about an order of magnitude followed by a gradual rise as the sample undergoes additional reaction and forms a more highly cured network structure during heating. A second relaxation is indicated at 197°C, this time by the sharp decline in both E" and E'. The first relaxation has an activation energy of 180 kJ/mole while the second process has an E_a of about 725 kJ/mole. When the sample was cooled from the upper temperature limit of 250°C, only a single relaxation near 190°C was observed. For resin II, $T_{g\infty}$ equals 210°C at 3.5 Hz and 218°C at 110 Hz.

A comparison of samples cured at several temperatures is evidence for the occurrence of additional reaction that takes place above the initial T_g. Figure 3-12 gives a comparison of the loss tangent at 11 Hz as a function of temperature for resin II samples cured from 83 to 112°C while Table 3-6 summarizes transition temperature and activation energy data. As the temperature of curing increases, the temperature of the T_g' maximum can be seen to increase. The height of this loss maximum decreases as T_c increases until it becomes extremely small for the 112°C cure. The second loss peak in Figure 3-11, corresponding to $T_{g\infty}$ for the fully developed network structure, is observed in all cases at about 213°C.

Discussion

Isothermal cures. The existence of a loss process associated with curing can be explained by the rapid increase in viscosity of the epoxy resin as its molecular weight increases. DSA studies on low molecular weight polystyrene samples, discussed in Chapter II, have shown that

Figure 3-12. Temperature Variation of the Loss Tangent at 11 Hz of Resin II for Several Cure Temperatures.

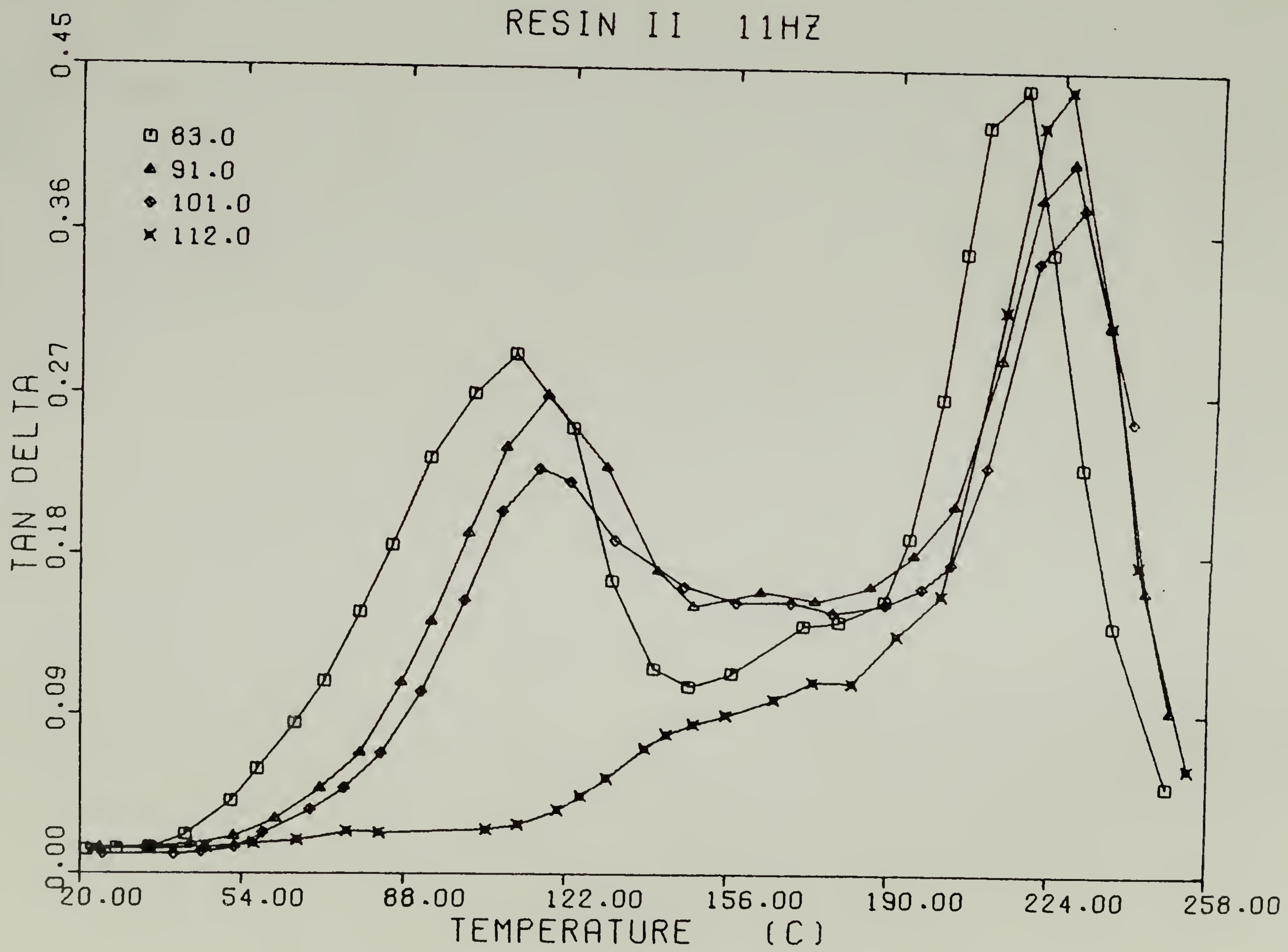
RESIN II 11HZ
83.0
91.0
101.0
112.0
TAN DELTA
0.00
0.09
0.18
0.27
0.36
0.45
20.00
54.00
88.00
122.00
156.00
190.00
224.00
258.00
TEMPERATURE (C)

TABLE 3-6

TRANSITION TEMPERATURES AND ASSOCIATED ACTIVATION ENERGIES FOR PARTIALLY CURED RESIN II FILMS

CURE TEMPERATURE (°C)	CURE TIME (Min)	T'_g (°C)	E_a (kJ/mole)	$T_{g\infty}$ (°C)	E_a (kJ/mole)
83 ± 3	340	92*	180 ± 95**	200*	725 ± 280**
91 ± 1	150	99	230 ± 50	213	440 ± 130
101 ± 2	90	104	300 ± 90	210	590 ± 170
112 ± 2	75	---	---	213	460 ± 100

*At 11 Hz from E''_{max}.

**To the 95% confidence level.

a loss maximum occurs at a critical viscosity for composite samples in the liquid region, which can be attributed to a coupling between the support and the liquid sample. The same process is thought to be occurring during the curing reaction. An increasing degree of cure causes the resin viscosity to rise and achieve a critical level at the relaxation maximum. A model for this phenomenon asserts that the product of sample viscosity and forced oscillation frequency is a constant for a particular composite system. For an isothermal experiment, the loss maximum should occur at a longer time for a lower frequency determination as the viscosity, or alternatively the molecular weight, must be greater in order that constancy of the viscosity-frequency product be maintained. Such behavior can be noted for the loss maximum associated with curing. The relaxation shown in Figures 3-3 and 3-4 is not of molecular origin, however it can be used to characterize the curing reaction of epoxy resins.

In the study of the gelation of an epoxy resin, Gillham (1) observed two loss maxima in a torsional braid experiment. The first peak was attributed to gelation and the second to vitrification. In the DSA studies previously described, no well defined relaxation attributable to vitrification was observed. This can be explained by the lack of sensitivity of the DSA technique to changes in modulus of a high modulus material, as discussed in Chapter I. It was assumed, therefore, that the loss peak observed in the present work was due to an increase in viscosity caused by the curing reaction and not to the network glass transition.

The time to the TBA gelation loss maximum can be seen to coincide well with the DSA curing loss process in cases where the cure temperatures are similar, as can be noted in Figures 3-7 and 3-8. The viscosity at the TBA gelation maximum was calculated to be about 3 kPa·s from T_{11} relaxation data for low molecular weight polystyrene (15). This was accomplished with the aid of an empirical relation of polystyrene melt viscosity to temperature and molecular weight (16) for samples over the molecular weight range of 2,000 to 20,400. Frequencies of the measurements were not given but were assumed to be the same at both polystyrene T_{11} and TBA gelation maxima, about 0.3 Hz. TBA cure times at the gelation maximum of 70 and 17.6 min for resin II at 92 and 112°C respectively (17) fall quite closely to the DSA isothermal cure data obtained at 91.6 and 111.6°C. This indicates that the TBA loss maximum attributed to gelation is identical in nature to the DSA loss process associated with sample-support coupling at a critical sample viscosity and is not of molecular origin.

An additional factor which complicates the determination of kinetic rate constants by the DSA method is the dependence of viscosity on molecular weight. Studies of a phenol-formaldehyde resin (3) indicate that two regions occur in a viscosity-reaction time curve. The initial viscosity increase allowed the polymerization rate constant to be calculated. In the second linear region, the viscosity rose at a factor of 3.9 times the initial rate. The latter behavior was attributed to a change in the viscosity dependence on molecular weight in the region of chain entanglement. A survey of the literature on network systems has shown that viscosity is proportional to the molecular weight raised to a power varying from 1 to 2.6 depending on the chemical nature of the system studied (20). The rate constants reported in this study may therefore not equal the actual rate of polymerization but be proportional to it. The factor of proportionality could be determined from a study of the viscosity-molecular weight relationships of these resins.

Partially cured thin films. The temperature of the T_g' relaxation, determined as a maximum in both the loss modulus E" and the loss tangent as well as by a rapid decrease in the storage modulus E', corresponds closely to the isothermal cure temperature, as can be seen from Figures 3-9 through 3-12. This behavior agrees with Gillham's observation (1) that the glass transition temperature of a thermoset system is equal to the temperature of the cure if the sample is cured below its ultimate T_g. As the temperature increases above T_g', the polymer network becomes increasingly rubbery and further curing takes place, thereby raising T_g'. Although the crosslinking reaction occurs more rapidly as the temperature increases the number of unreacted functional groups continually decreases, limiting the upper value of the glass transition temperature that can be attained, $T_{g\infty}$. The effect of this continuous curing process can be seen in the width of the E" peak, which extends over a 100°C range of temperature for each frequency studied in Figures 3-9 and 3-11. The high magnitude of E" throughout this region confirms the occurrence of a reaction process.

Figure 3-12 indicates that as the temperature of curing increases the temperature of the T_g' relaxation increases while its magnitude decreases. This effect can be attributed to the greater coherence of the network which achieves a higher degree of crosslinking as T_c increases. Furthermore, less unreacted material is available above the initial softening temperature as T_c is increased, and the small degree of additional reaction possible also contributes to the decline in intensity of the first loss maximum with increasing T_c.

It is apparent from Table 3-6 that the activation energy of the $T_{g\infty}$ relaxation is much greater than that of the T_g' relaxation. These activation energies characterize the network mobility in different states of cure assuming that the measurement procedure results in a state of cure at T_g which is independent of frequency. As the degree of crosslinking increases, the free volume of the network decreases leading to an increasingly cooperative relaxation process at the glass transition. This is reflected as an increase in both the temperature and activation energy of the T_g' relaxation as the extent of cure increases. Similar effects of an increase in crosslink density on the glass transition in vulcanized natural rubber have been found by Scott and coworkers (18) in a dielectric relaxation study. The activation energy for the $T_{g\infty}$ relaxation is much greater than that of the T_g' relaxation, as the fully developed network requires a greater degree of cooperativity for long range main chain motion. The higher $T_{g\infty}$ and activation energy of $T_{g\infty}$ for resin II suggest that this epoxy is more highly crosslinked than resin I.

Comparison of the storage modulus curves of the two resins cured at similar temperatures, Figures 3-9 and 3-11, shows that the resins behave differently above the initial T_g' relaxation. Resin I maintains a plateau in modulus between T_g' and $T_{g\infty}$ while resin II increases in modulus after the initial decrease at T_g'. Resin II samples cured at 91 and 101°C also exhibit this behavior. The increase in modulus following T_g' for resin II indicates that a great deal of additional crosslinking is taking place, much more so than for the case of resin I above T_g'. Kline (19) has previously observed an increase in the modulus of undercured bisphenol A resins as the test temperature was increased above the initial cure temperature. The modulus increase was attributed to a further degree of reaction at these temperatures.

Conclusions

Studies of the curing behavior of two epoxy resins by DSA show that the technique is well suited to the determination of the onset of gelation under isothermal curing conditions but that the method is not useful for monitoring later stages of reaction when the resin becomes more rigid. The activation energy for the curing of two commercially formulated resins is determined from time to the onset of gelation and reaction rate constants as 87.9 kJ/mole for resin I and 84.9 kJ/mole for resin II, in good agreement with results of DSC and TBA studies on the same materials. The loss maxima associated with the onset of gelation in DSA and TBA experiments result from the rapid increase in resin viscosity, with increasing conversion, to a critical level which depends on the frequency of the experiment. Films cured at temperatures below the ultimate T_g display two relaxation processes during the initial heating run. The first relaxation occurs near the original isothermal cure temperature and has an apparent activation energy on the order of 250 kJ/mole. Following this relaxation the resins softened and additional curing occurred, producing a more highly crosslinked structure. A second relaxation associated with the ultimate T_g of the epoxy networks occurs at about 140°C for resin I and 215°C for resin II with an activation energy of 500-650 kJ/mole. The large increase in activation energy for the T_g relaxation is attributed to the reduction in molecular mobility caused by increasing crosslink density.

REFERENCES

1. J.K. Gillham, Polym. Eng. Sci., 16, 353 (1976).
2. J.K. Gillham, A.I.Ch.E.J., 20, 1066 (1974).
3. F.G. Mussatti and C.W. Macosko, Polym. Eng. Sci., 13, 236 (1973).
4. S. Naganuma, T. Sakurai, Y. Takahashi, and S. Takahashi, Kobunshi Kagaku, 29, 105 (1972).
5. S. Naganuma et al., Kobunshi Kagaku, 29, 519 (1972).
6. S. Naganuma et al., Shikizai Kyokaishi, 45, 297 (1972).
7. G.A. Senich, W.J. MacKnight, and N.S. Schneider, Amer. Chem. Soc., Prepr., Div. Org. Coat. Plas. Chem., 38, 510 (1978).
8. G.A. Senich, W.J. MacKnight, and N.S. Schneider, Polym. Eng. Sci., accepted for publication.
9. N.S. Schneider and J.K. Gillham, Amer. Chem. Soc., Prepr., Div. Org. Coat. Plas. Chem., 38, 491 (1978).
10. N.S. Schneider and J.K. Gillham, Polym. Eng. Sci., to be published.
11. S.H. Maron and C.F. Prutton, "Principles of Physical Chemistry," p. 552, The Macmillan Co., London (1970).
12. P. Eyerer, J. Appl. Polym. Sci., 15, 3067 (1971).
13. E. Sacher, Polymer, 14, 91 (1973).
14. T.F. Saunders, M.F. Levy, and J.F. Serino, J. Polym. Sci., A-1, 5, 1609 (1967).
15. J.K. Gillham and R.F. Boyer, J. Macromol. Sci. Phys., 13, 497 (1977).
16. T.G. Fox and P.J. Flory, J. Polym. Sci., 14, 315 (1954).
17. J.K. Gillham, personal communication.
18. A.H. Scott, A.T. McPherson, and H.L. Curtis, J. Res. Nat. Bur. Stds., 11, 173 (1933).

19. D.E. Kline, J. Polym. Sci., 47, 237 (1960).

20. S.D. Lipshitz and C.W. Macosko, Polym. Eng. Sci., 16, 803 (1976).

CHAPTER IV

PHASE SEGREGATION IN TOLUENE DIISOCYANATE BLOCK POLYURETHANES

Introduction

Linear polyurethane block copolymers have been objects of considerable research interest over recent years. These materials are composed of three parts, a diisocyanate, a monomeric chain extender (usually a diol but sometimes a diamine), and a low molecular weight rubbery polymer frequently a polyether or polyester. The soft segment is composed of the rubbery polymer while the diisocyanate and the chain extender form the hard segment. These materials are classified as thermoplastic elastomers since their resiliency at room temperature is characteristic of elastomers while their linear nature allows them to be processed with the ease of thermoplastics at higher temperatures.

Dynamic mechanical property studies have been successful in elucidating the molecular mechanisms underlying the mechanical behavior of these materials. Kajiyama and MacKnight (1,2) proposed mechanisms for low temperature and glass transition region relaxations of three model hard segment polyurethanes extended with diols containing from two to ten methylene units. They observed relaxations attributable to motion of side chains, short length main chain structures, and long main chain segments, as well as crystal-crystal transitions. Dynamic mechanical investigations by Huh and Cooper (3) demonstrated the existence of a two phase structure in 4,4'-diphenylmethane diisocyanate, MDI, polyurethanes and examined the effects of composition, soft segment molecular weight and thermal history upon the relaxation mechanisms of this class of copolymers. Relaxations, in their notation, corresponding to a soft segment T_g, α_a, soft segment crystalline melting, α_c, hard segment T_g, δ, and hard segment melting, δ', were observed in the polyurethanes studied. They concluded that the α_a and δ relaxations were influenced by the degree of crystallinity and the nature of the domain structure. The magnitudes of the α_c, δ, and δ' relaxations were found to be related to the size of the domain structures present. Similar studies were carried out on polyurethanes synthesized with structures that eliminated hydrogen bonding effects and which allowed blocks of controlled molecular weight distribution to be incorporated (4,5). The major conclusions from this work are that a narrow hard segment molecular weight distribution in the phase segregated systems increases the hard segment glass transition, α_h, and the modulus between the hard and soft segment T_g while having little effect on the soft segment glass transition, α_s. An examination of low temperature dynamic mechanical properties of MDI polyurethanes with various soft segments was reported by Illinger and coworkers (6). They found that as urethane concentration increased, α_s remained constant but crystallization of the soft segment was inhibited. Ferguson and coworkers (7) have examined MDI-polyether block polyurethane chains extended with 1,3-diaminopropane as a function of hard segment content.

Systematic studies on MDI polyurethanes with polycaprolactone soft segments over a wide range of soft segment molecular weight and hard segment concentration have been carried out by Seefried, Koleske and Critchfield (8,9). The glass transition was observed to shift to lower temperatures as the soft segment chain length increased and soft segment crystallization was found to occur for the highest molecular weight polyester sample. The T_g of lower molecular weight soft segment samples increased as the hard segment concent increased while the T_g of polyurethanes containing higher molecular weight soft segments was unchanged until extreme amounts of hard segments were introduced. The authors attributed the latter behavior to a high degree of phase separation between blocks. This group has also made a comparison of MDI and toluene diisocyanate, TDI, hard segments over a more limited compositional range and studied the effects of different chain extenders on TDI polyurethane properties (10,11). All TDI-containing polyurethanes studied by these workers displayed little or no phase segregation.

Schneider, Paik Sung and coworkers have completed an extensive study of TDI polyurethanes (12-15). This work differs from previous studies by the separate characterization of block polyurethanes prepared from the two isomers of TDI. These materials have been studied by thermomechanical analysis, TMA, DSC, x-ray scattering and infrared analysis in order to elucidate the structure of this particular class of polyurethanes. Their findings can be briefly summarized in terms of the degree of phase segregation exhibited. The glass transition temperature of 2,4-TDI polyurethanes with polyether soft segments of about 1000 $\overline{M}_n$ showed a strong dependence on composition. Extensive hard and soft segment mixing was postulated in these materials. Similar polyurethanes based on the 2,6-TDI structural isomer displayed a highly ordered domain structure, indicated by a concentration invariant T_g and a strong high temperature transition attributed to melting of the easily crystallizable hard segment. An increase in soft segment molecular weight from 1000 to 2000 induced phase segregation in the 2,4-TDI series and improved phase segregation in the 2,6-TDI series to the point that the soft segment exhibited some crystallinity. The soft segment glass transition temperature, T_{gs}, was found to be a sensitive measure of the degree of phase segregation in these materials.

The systematic dynamic mechanical study reported here was undertaken to gain additional insight into the molecular relaxation processes which occur in TDI polyurethanes as well as to test the generality of findings developed from investigations of other chemical classes of segmented polyurethanes. Portions of this work have been previously published (16,17).

Experimental

Samples. Linear polyurethane block copolymers with hard segments composed of 2,4- or 2,6-TDI and 1,4-butanediol, BD, and either 1040 or 2060 molecular weight poly(tetramethylene oxide), PTMO, soft segments were supplied through the courtesy of Dr. N.S. Schneider of the Army Materials and Mechanics Research Center, Watertown, MA. These polymers were prepared by a two step process, first an endcapping of the PTMO with a 5% molar excess of TDI followed by chain extension with BD and additional TDI. All were found to be soluble in N,N-dimethylformamide. Hard and soft segment model polymers were also supplied. These materials were made in a one step condensation reaction of a 2.5% molar excess of TDI with either BD or PTMO of 1090 molecular weight. Figure 4-1 shows a schematic representation of the polymers studied while Table 4-1 summarizes sample composition data. The hard segment is the material contained within the brackets with subscript m. The approximate value of the index i corresponds to 14, 15, and 28 for 1040, 1090, and 2060 molecular weight PTMO, respectively. For the pure hard segment material, the index i is, of course, zero while for the soft segment polymer, m is likewise zero. Overall polymer $\overline{M}_n$ was estimated to be on the order of 13,000-25,000. Hard and soft segment polymers are designated first by the TDI isomeric structure followed by either BD for the hard segment or PTMO for the soft segment polymers. For example, 2,4-TDI/PTMO refers to the 1090 molecular weight PTMO soft segment, which contains 14 wt.% 2,4-TDI. The nomenclature used throughout the discussion for the block polyurethanes first refers to the TDI isomeric structure followed by the molecular weight of PTMO in thousands and finally the hard segment content in weight percent if a specific polymer is designated. For example, 2,6-T-2P-60 indicates a block polyurethane with 60 wt.% 2,6-TDI/BD hard segments and a 2060 molecular weight PTMO soft segment.

Characterization. Film samples about 0.25 mm thick were prepared by compression molding the polyurethanes under dry nitrogen flow at 180°C and 3 MPa pressure. After molding for 20 minutes, the samples were allowed to cool slowly in the press under dry nitrogen flow. Figure 4-2

Figure 4-1. Structure of the Block Polyurethane Elastomers.

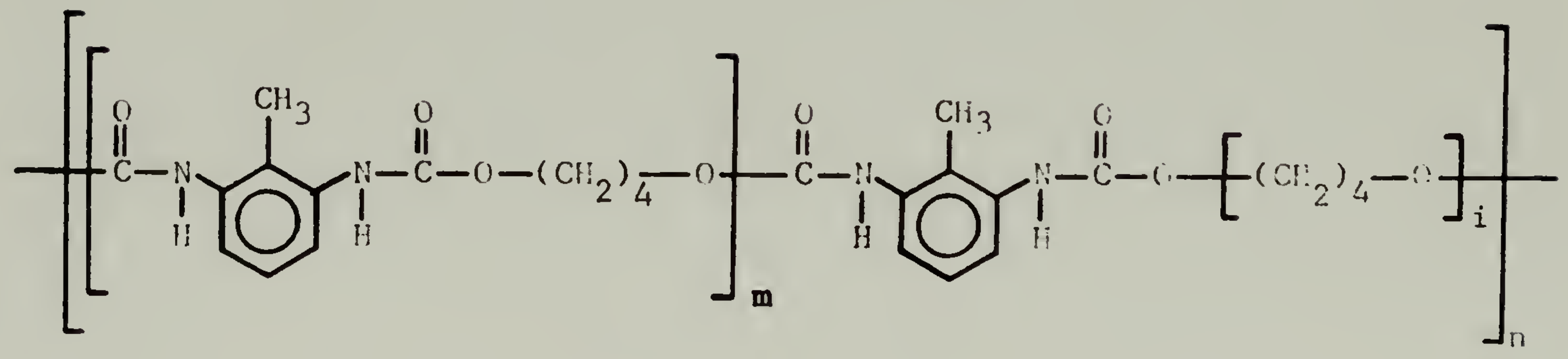

2,6-T-xP Block Polyurethane

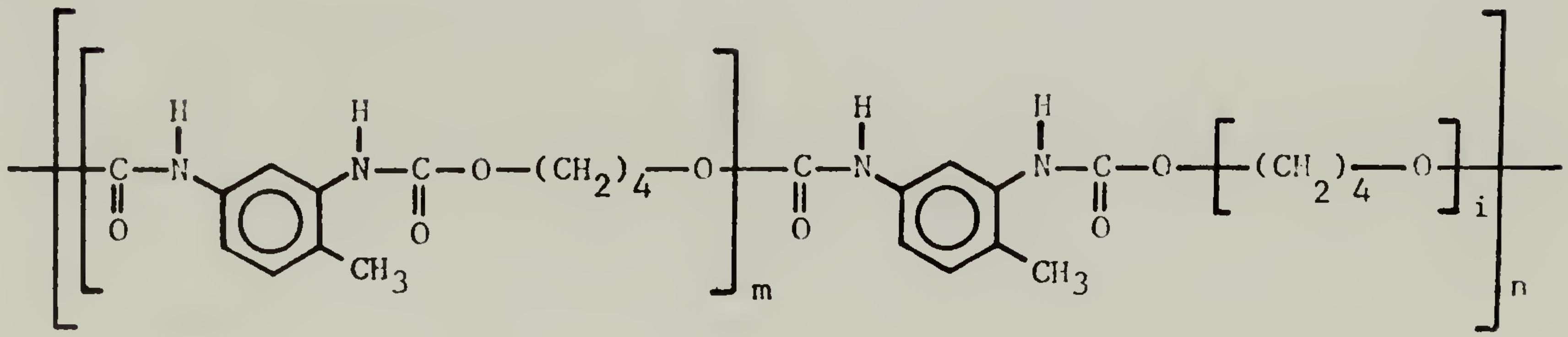

2,4-T-xP Block Polyurethane

TABLE 4-1

TOLUENE DIISOCYANATE POLYURETHANE COMPOSITIONS

MOLAR RATIO TDI/BD/PTMO	MOLECULAR WEIGHT PTMO	WT.% TDI	WT.% URETHANE
2.10/1/1	1040	24.6	31.0
3.15/2/1	1040	31.1	41.7
4.20/3/1	1040	35.9	49.6
5.25/4/1	1040	39.5	55.5
6.30/5/1	1040	42.4	60.3
2.10/1/1	2060	14.6	18.5
3.15/2/1	2060	19.8	26.5
4.20/3/1	2060	24.0	33.2
5.25/4/1	2060	27.5	38.7
6.30/5/1	2060	30.5	43.4
1.025/1/0	--	67.2	100.0
1.025/0/1	1090	14.2	14.2

Figure 4-2. Thermal History of Compression Molded Polyurethane Films.

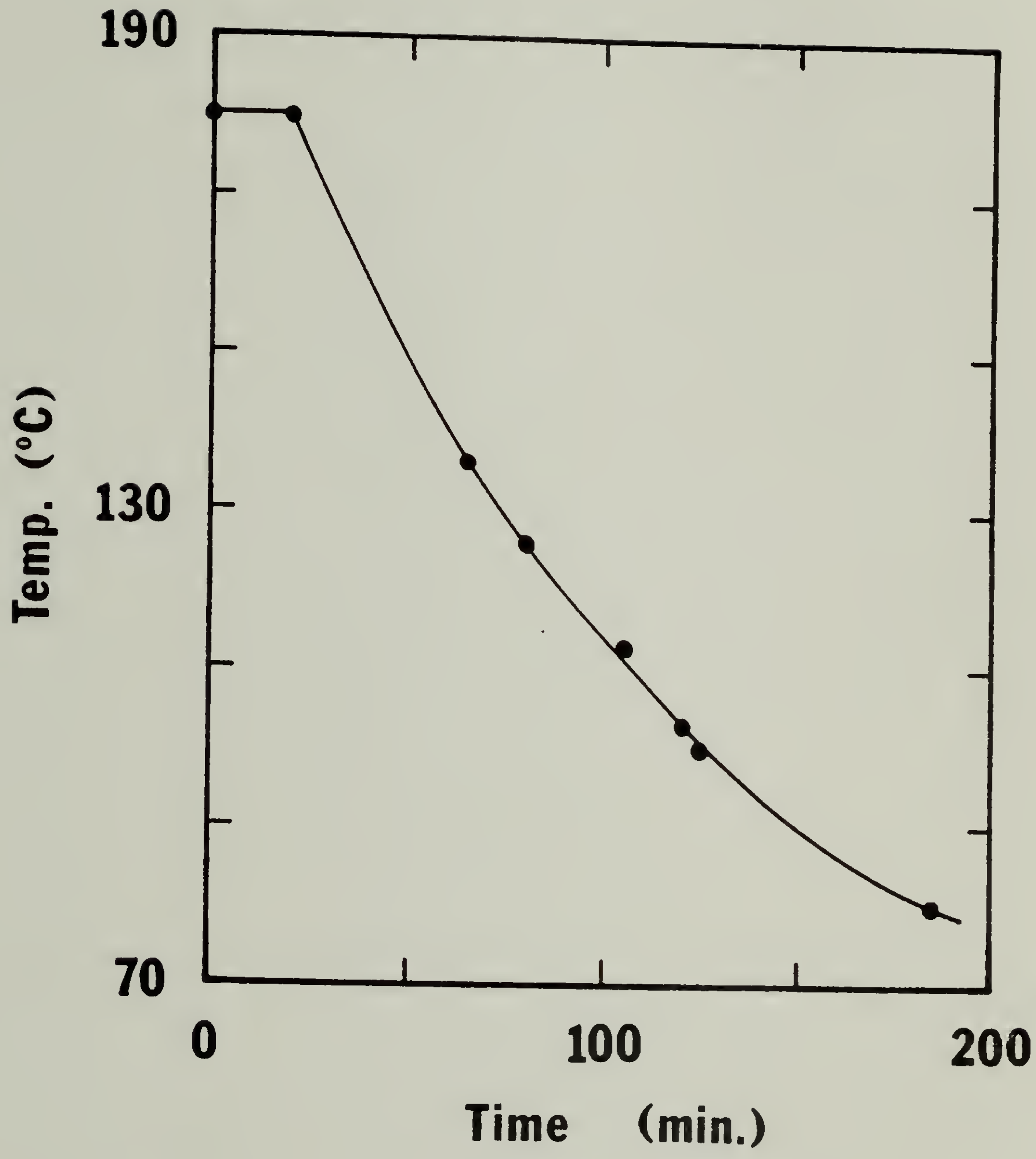
190
130
70
Temp. (°C)
0
100
200
Time (min.)

shows the thermal history of the 180°C molded films. No discoloration was observed when the samples were removed from the mold. The two soft segment polyurethanes were compression molded at 120°C. The films were allowed to stand at least one week at room temperature in a desiccator before being evaluated with the Rheovibron DDV-IIB Dynamic Viscoelastometer (Toyo Baldwin Co.). Samples were tested sequentially at 3.5, 11, 35, and 110 Hz while heating from -135°C to 195°C at a nominal heating rate of 1.5°C/min under a dry nitrogen atmosphere. Several samples were re-examined by the same procedure about 60 days after the first test. Thermal studies of the compression molded films were carried out on a Perkin-Elmer DSC-2 differential scanning calorimeter at a heating rate of 20°C/min and with a sensitivity of 5 mcal/sec. Scans above room temperature were conducted in a nitrogen atmosphere and indium and tin references were employed for calibration. Subambient runs were carried out in a helium atmosphere with two transitions of a cyclohexane reference used for calibration.

DSA samples were prepared by casting polyurethane films from N,N'-dimethylformamide solution onto steel springs stretched to a pitch of 0.1 mm. The springs employed were typically 20 turns in length and made from 0.3 mm diameter wire formed into a coil of 3.3 mm outer diameter. The film casting took place at 55°C, followed by drying in a vacuum oven at the same temperature. These composite samples were evaluated with the Rheovibron DDV-IIB at several frequencies at a nominal heating rate of 1.5°C/min under a dry nitrogen atmosphere. In addition to the isochronal DSA studies, several experiments were conducted at constant temperature over a frequency range of 0.1 to

110 Hz. At frequencies of 0.1 to 1.5 Hz, the oscillating load was provided by a Kikusui Electronics Corporation Model 454A signal generator and the stress and strain gauge output monitored graphically with a Toyo Measuring Instruments Model SS-205D strip chart recorder. Determinations at or above 3.5 Hz were accomplished with the instrument in its normal operating configuration. Temperature was held constant to within 1°C throughout these studies.

Several computer programs were used to facilitate data reduction. Vibfig was employed to analyze and plot thin film dynamic mechanical data. Dsafig served a similar purpose for the DSA determinations. Apparent activation energies were determined for major relaxations from the Arrhenius dependence of frequency on inverse temperature with the program Arrhea. Least squares lines were fitted to plots of log(frequency) vs. inverse temperature and the activation energies to the 95% confidence level determined from the slopes. Losmax was used to calculate and plot curves of normalized loss modulus vs. inverse temperature from thin film dynamic mechanical data. Copies of these programs and instructions for their use can be found in Appendix A.

Results

Hard and soft segments. The hard segment polymer composed of 2,4-TDI/BD exhibited a single major α relaxation associated with the glass transition. The relaxation occurred at 108°C (11 Hz) as determined from the position of the loss modulus maximum. The storage modulus decreased from about 1.5 GPa to 50 MPa during the relaxation and the loss of mechanical integrity and onset of flow was indicated by a rapid and unabated rise in tan(δ) as the temperature rose above T_g. The apparent activation energy, E_a, determined from an Arrhenius dependent of frequency, ν, on temperature as shown below, was 600 kJ/mole.

$$\ln(\nu) = \frac{-E_a}{RT} + C \tag{4-1}$$

The activation energy for the α relaxation agrees within experimental error with the value of 480 kJ/mole determined by Kajiyama (18). No crystallinity is present in this hard segment material, as indicated by the DSC scan in Figure 4-3 which shows no evidence of a melting endotherm.

The dynamic mechanical behavior of 2,6-TDI/BD was found to be similar to that of the 2,4-TDI/BD hard segment at low temperatures. Both showed a secondary γ relaxation at about -115°C to -135°C with an activation energy of about 33 kJ/mole. These processes correspond to the γ_1 and/or γ_2 relaxations, involving motions of methylene sequences, which were observed for model hard segments by Kajiyama and MacKnight (2) and will not be subsequently considered. The α or glass transition relaxation for 2,6-TDI/BD occurred at 105°C (11 Hz) with an activation energy of 510 kJ/mole. Above the α loss peak, the storage modulus remained at a level of about 300 MPa, as can be seen in Figure 4-4. This phenomenon can be attributed to the presence of crystallinity in the 2,6-TDI/BD hard segment. The magnitude of the plateau in modulus was found to be highly dependent upon the thermal history of the sample. The results in Figure 4-4 represent the steady

Figure 4-3. DSC Thermogram of Hard Segment Polymers.

a. 2,4-TDI/BD

b. Quenched 2,6-TDI/BD

c. 2,6-TDI/BD annealed for 1 hour at 423°K

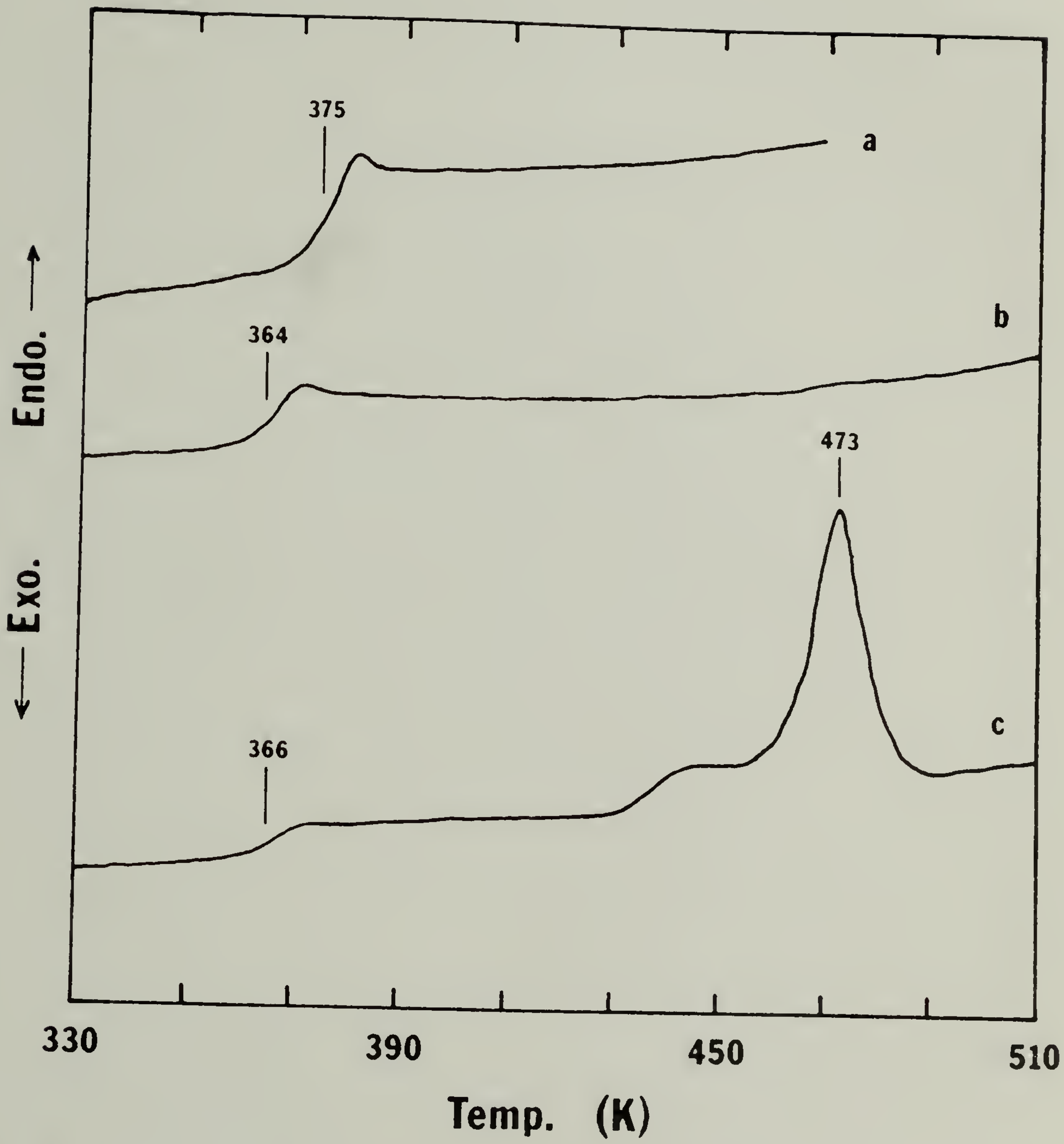
375
a
364
b
473
366
c
Endo.
Exo.
330
390
450
510
Temp. (K)

Figure 4-4. Storage and Loss Modulus of 2,6-TDI/BD as a Function of Temperature at 110, 35, 11, and 3.5 Hz.

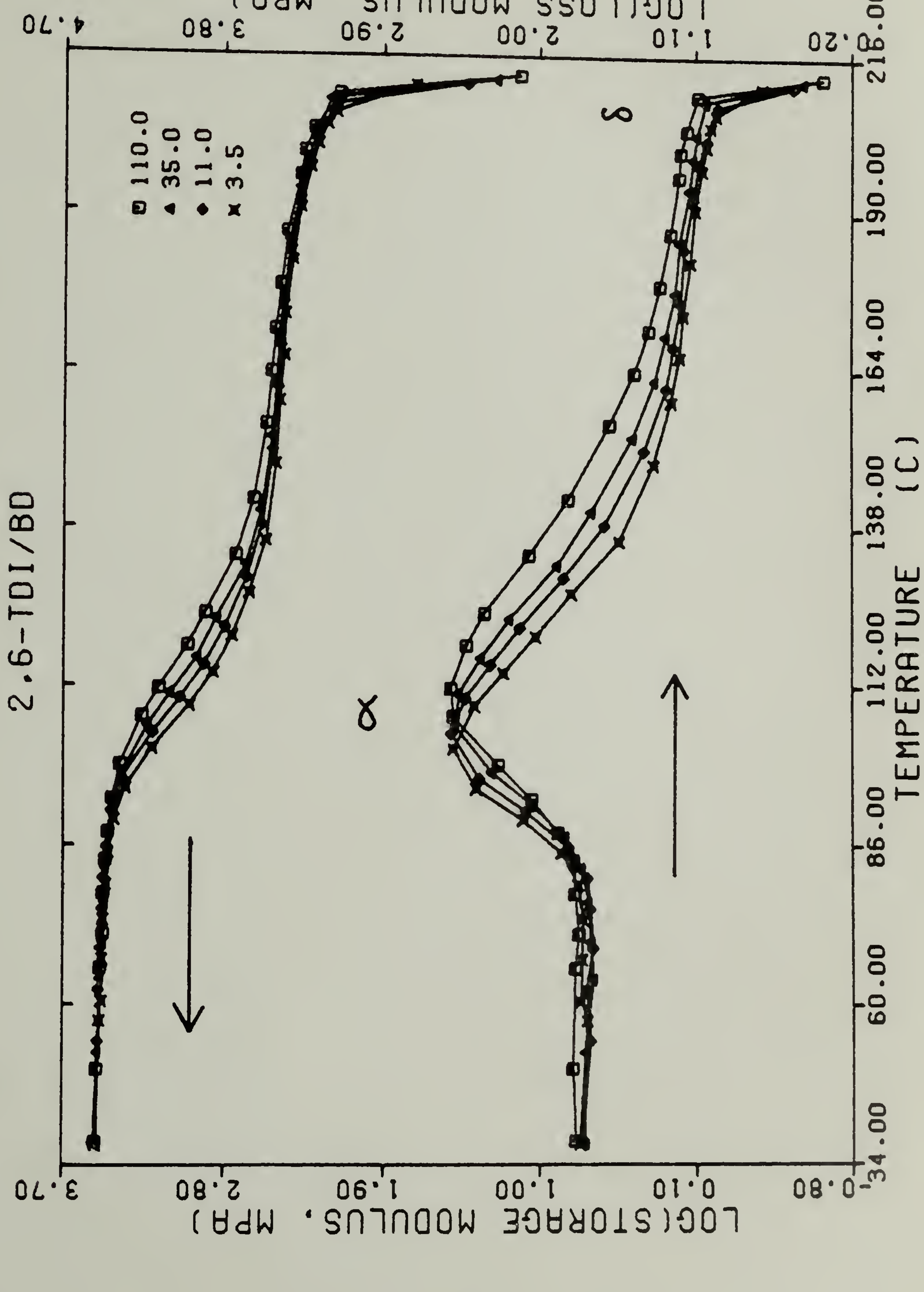
2.6-TDI/BD
110.0
35.0
11.0
3.5
α
δ
LOG(STORAGE MODULUS, MPA)
LOG(LOSS MODULUS, MPA)
TEMPERATURE (C)
34.00
60.00
86.00
112.00
138.00
164.00
190.00
216.00
-0.80
0.10
1.00
1.90
2.80
3.70
0.20
1.10
2.00
2.90
3.80
4.70

state behavior of the fully annealed polymer. The width of the α loss peak is about twice that of the 2,4-TDI/BD α relaxation maximum. Broadening of the α loss maximum by the introduction of crystallinity has been similarly observed for PET and PTFE (19). Crystalline structure in the 2,6-TDI/BD hard segment polymer remained until the onset of the α relaxation in dynamic mechanical experiments, about 212°C. The melting point, as determined from the maximum of the melting endotherm in Figure 4-3, was found to be 200°C. The positions of the α relaxations for 2,4- and 2,6-TDI/BD are in good agreement with T_g values found from DSC studies, 102°C and 93°C, respectively.

The model soft segment composed of 2,4-TDI/PTMO exhibited a single major α relaxation at -55°C (11 Hz) accompanied by a drop in the level of the storage modulus of two and one half orders of magnitude. An activation energy of 200 kJ/mole was determined for this relaxation. The 2,6-TDI/PTMO soft segment displayed quite different behavior from the 2,4-TDI/PTMO polymer, as can be seen from Figure 4-5. An α relaxation can be observed to occur at -59°C (11 Hz) with an apparent activation energy of 260 kJ/mole. A subsequent α_c loss process with a corresponding increase in the storage modulus by a factor of 3 can be seen to occur at about -30°C. This second relaxation can be attributed to crystallization of the soft segment above T_g followed by annealing and finally complete melting at 9 to 13°C. Crystallization in the material during cooling to -135°C was inhibited by the rapid quenching process employed for cooling the sample chamber. The DSC results for the 2,6-TDI/PTMO soft segment in Figure 4-6 confirm the interpretation of the dynamic mechanical relaxation processes. A glass transi-

Figure 4-5. Temperature Dependence of the Storage and Loss Modulus of 2,6-TDI/PTMO at 110, 35, 11, and 3.5 Hz.

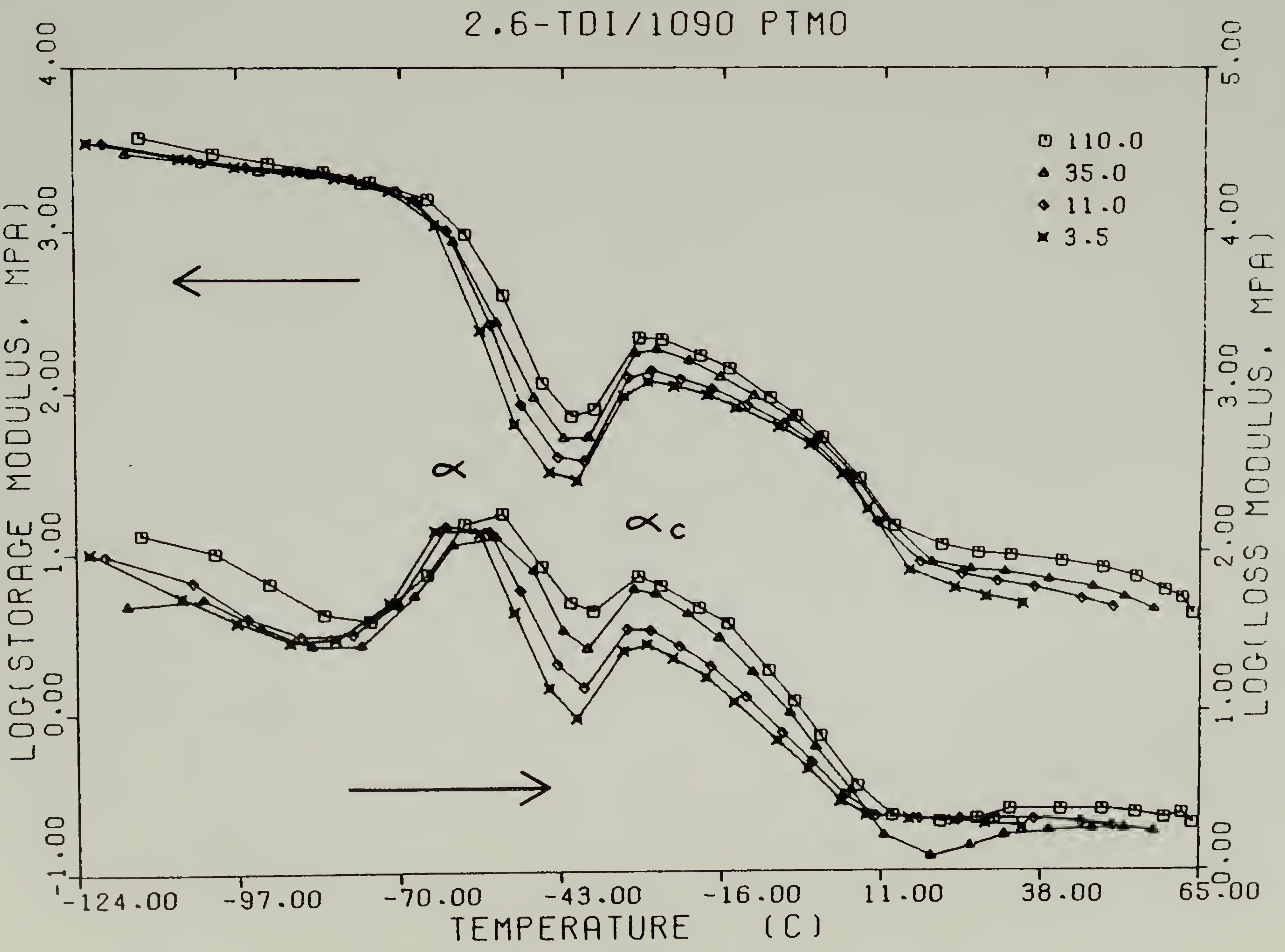
2.6-TDI/1090 PTMO
□ 110.0
▲ 35.0
◇ 11.0
✱ 3.5
α
α
c
LOG(STORAGE MODULUS, MPA)
LOG(LOSS MODULUS, MPA)
TEMPERATURE (C)
-124.00
-97.00
-70.00
-43.00
-16.00
11.00
38.00
65.00
-1.00
0.00
1.00
2.00
3.00
4.00
5.00

Figure 4-6. DSC Thermogram of Soft Segment Polymers.

a. 2,4-TDI/PTMO

b. 2,6-TDI/PTMO

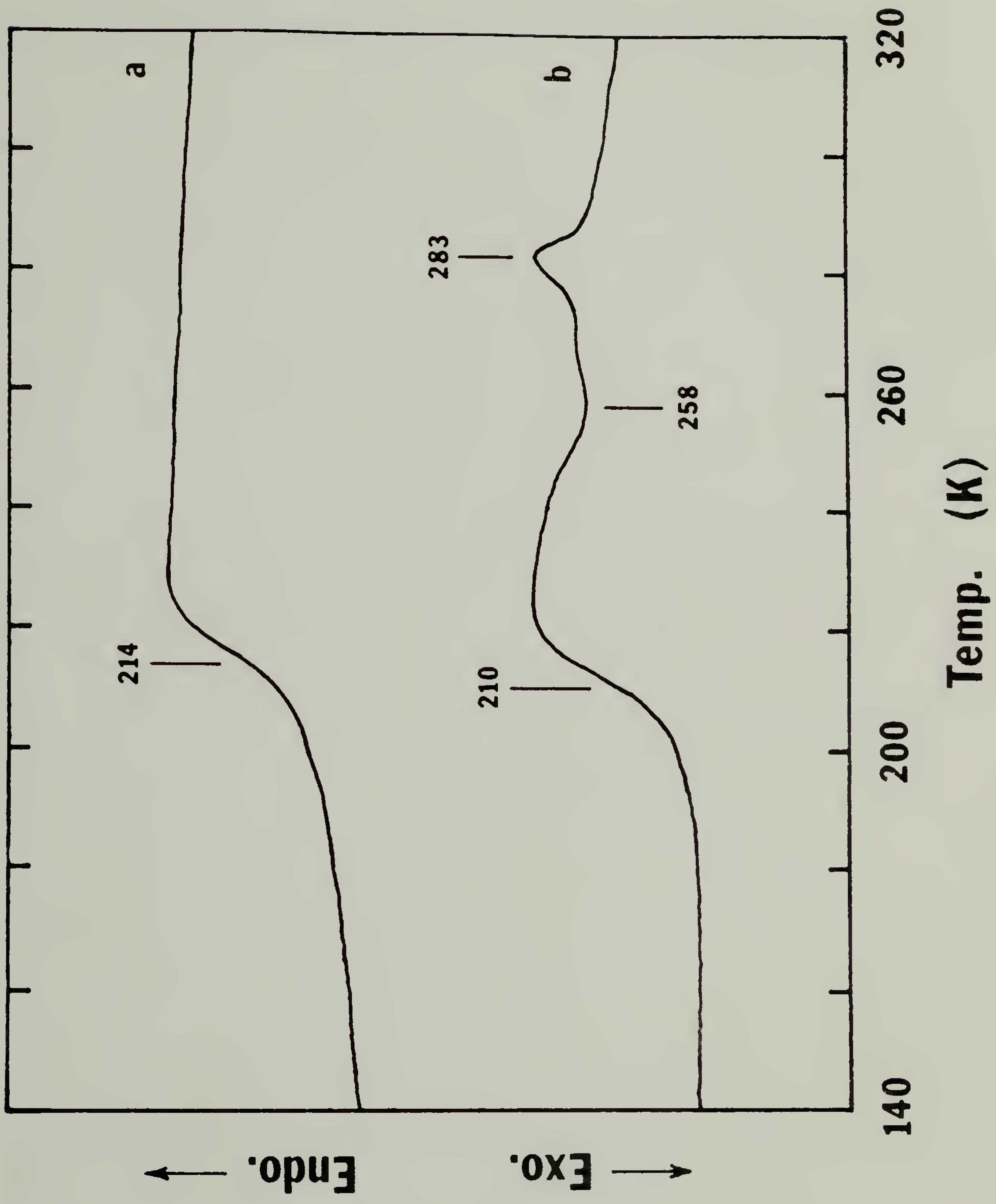
Endo.
Exo.
a
b
214
210
258
283
140
200
260
320
Temp. (K)

tion is indicated at -63°C followed by a broad crystallization exotherm centered at -30°C and finally a melting endotherm at 10°C. The behavior of the 2,6-TDI/PTMO soft segment, containing no chain extender, is similar to that noted by Illinger (6) for an MDI/BD/PTMO polyurethane containing 24 wt.% hard segments and 2000 $\overline{M}_n$ PTMO. The glass transition occurred at -100°C (110 Hz) followed by crystallization, completed at -45°C, and finally melting at 30°C. The dynamic mechanical test results for the hard and soft segments are summarized in Table 4-2.

2,4-TDI polyurethanes. Two 2,4-T-1P samples with different hard segment concentrations were studied and found to display a broad α relaxation maximum, also characterized by a decline in storage modulus of about two and one half orders of magnitude as shown in Figure 4-7, a plot of storage and loss modulus vs. temperature at 11 Hz. The position of the α relaxation varied with hard segment content, ranging from 22°C for 2,4-T-1P-56 to 38°C for 2,4-T-1P-60, both at 11 Hz. The activation energies found for each sample are comparable as can be seen from Table 4-2, a summary of 2,4-TDI polyurethane data, on the order of 290 kJ/mole. The results from dynamic mechanical studies agree with the glass transition temperatures found by Schneider and coworkers (12) from a TMA study of the same polyurethanes, as can be seen from Figure 4-8, a comparison of both sets of data.

The dynamic mechanical response of three 2,4-T-2P samples at 11 Hz is shown in Figure 4-9 for three hard segment concentrations. A low temperature relaxation maximum, α_s, in the region of -68 to -54°C

TABLE 4-2

RELAXATIONS OF HARD AND SOFT SEGMENT POLYMERS

SAMPLE	RELAXATION	TEMPERATURE* (°C)	ACTIVATION ENERGY (kJ/mole)
2,4-TDI/BD	α	108	600 ± 140
2,6-TDI/BD	α	105	510 ± 70
2,6-TDI/BD	δ	212	---
2,4-TDI/PTMO	α	-53	200 ± 40
2,6-TDI/PTMO	α	-59	260 ± 50
2,6-TDI/PTMO	α_c	-30	---

*α and α_c determined from position of E''_{max}, δ from $\log(E') = 1.25$ MPa, all at 11 Hz.

Figure 4-7. Storage and Loss Modulus as a Function of Temperature at 11 Hz for 2,4-T-1P with 56 and 60 wt.% Hard Segments.

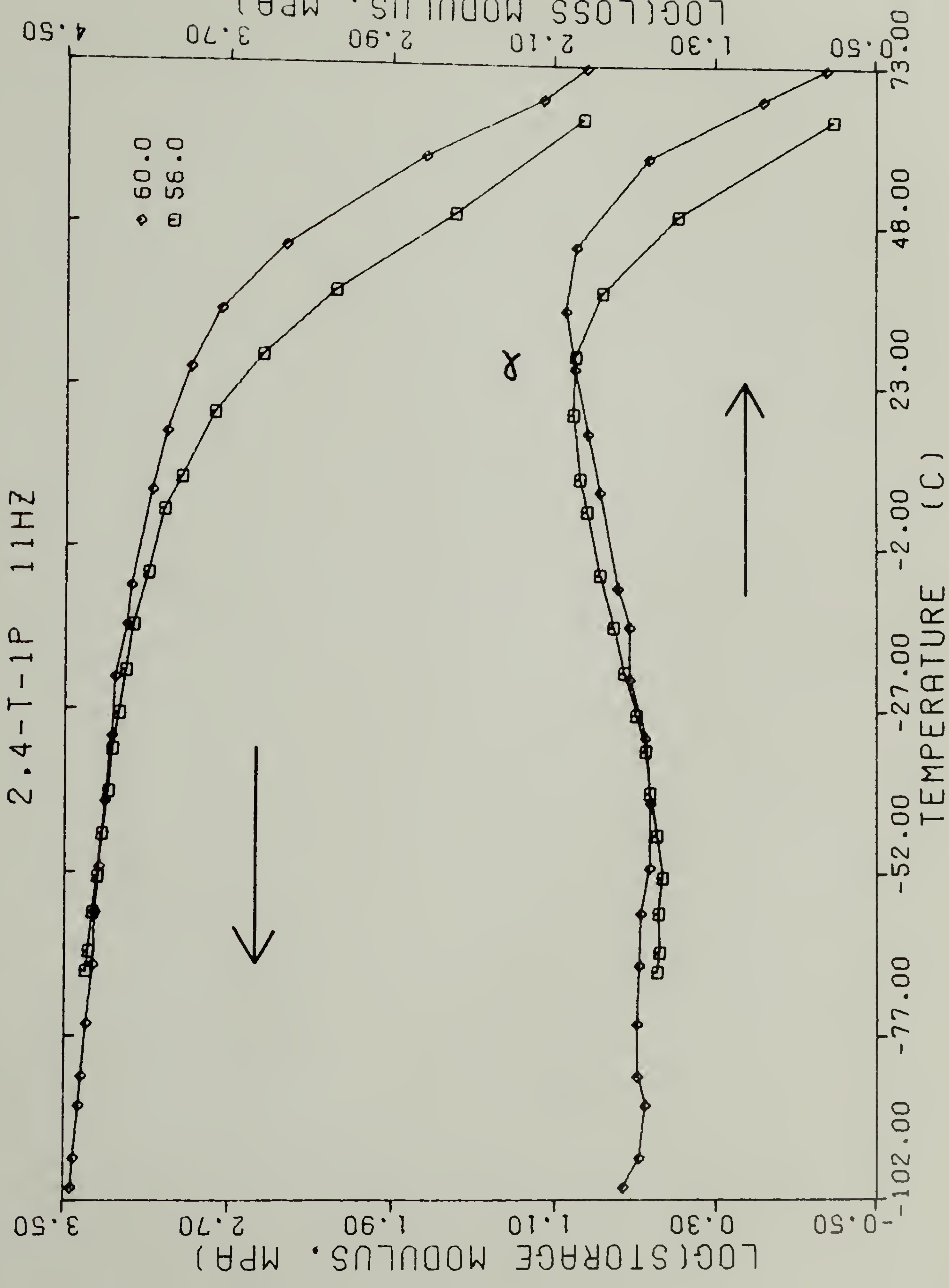
2.4-T-1P 11HZ
◇ 60.0
⊡ 56.0
γ
LOG(LOSS MODULUS, MPA)
4.50
3.70
2.90
2.10
1.30
0.50
LOG(STORAGE MODULUS, MPA)
3.50
2.70
1.90
1.10
0.30
-0.50
TEMPERATURE (C)
-102.00
-77.00
-52.00
-27.00
-2.00
23.00
48.00
73.00

Figure 4-8. Comparison of 11 Hz Dynamic Mechanical (Open Points) and DSC or TMA Transition Temperatures (Filled Points, Ref. 14) of 2,4-T-1P (Triangles) and 2,4-T-2P (Squares) Polyurethanes as a Function of Hard Segment Wt.%.

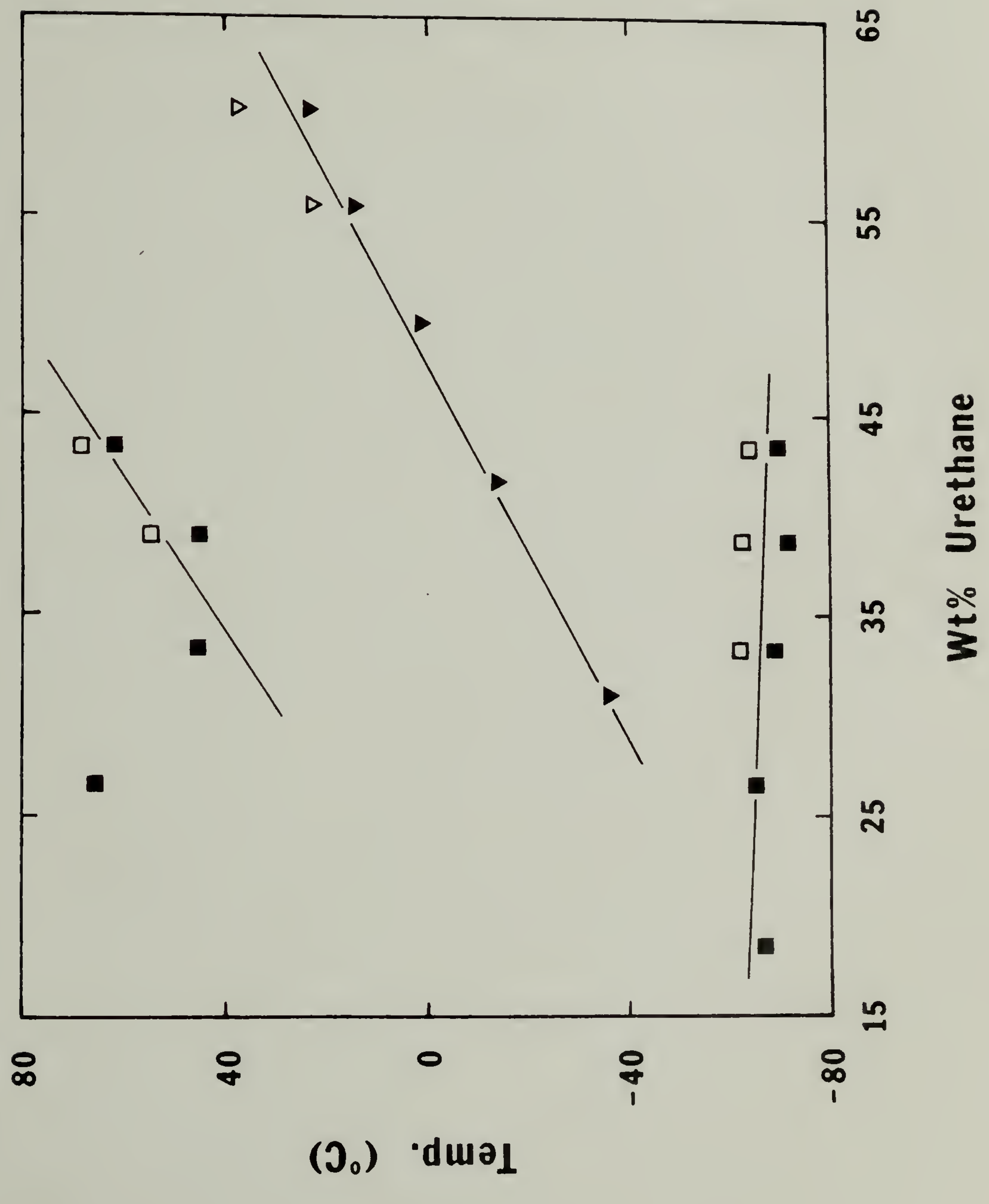
Temp. (°C)
80
40
0
-40
-80
15
25
35
45
55
65
Wt% Urethane

Figure 4-9. Temperature Dependence of the Storage and Loss Modulus of 2,4-T-2P at 11 Hz for 33, 39, and 43 wt.% Hard Segment Concentration.

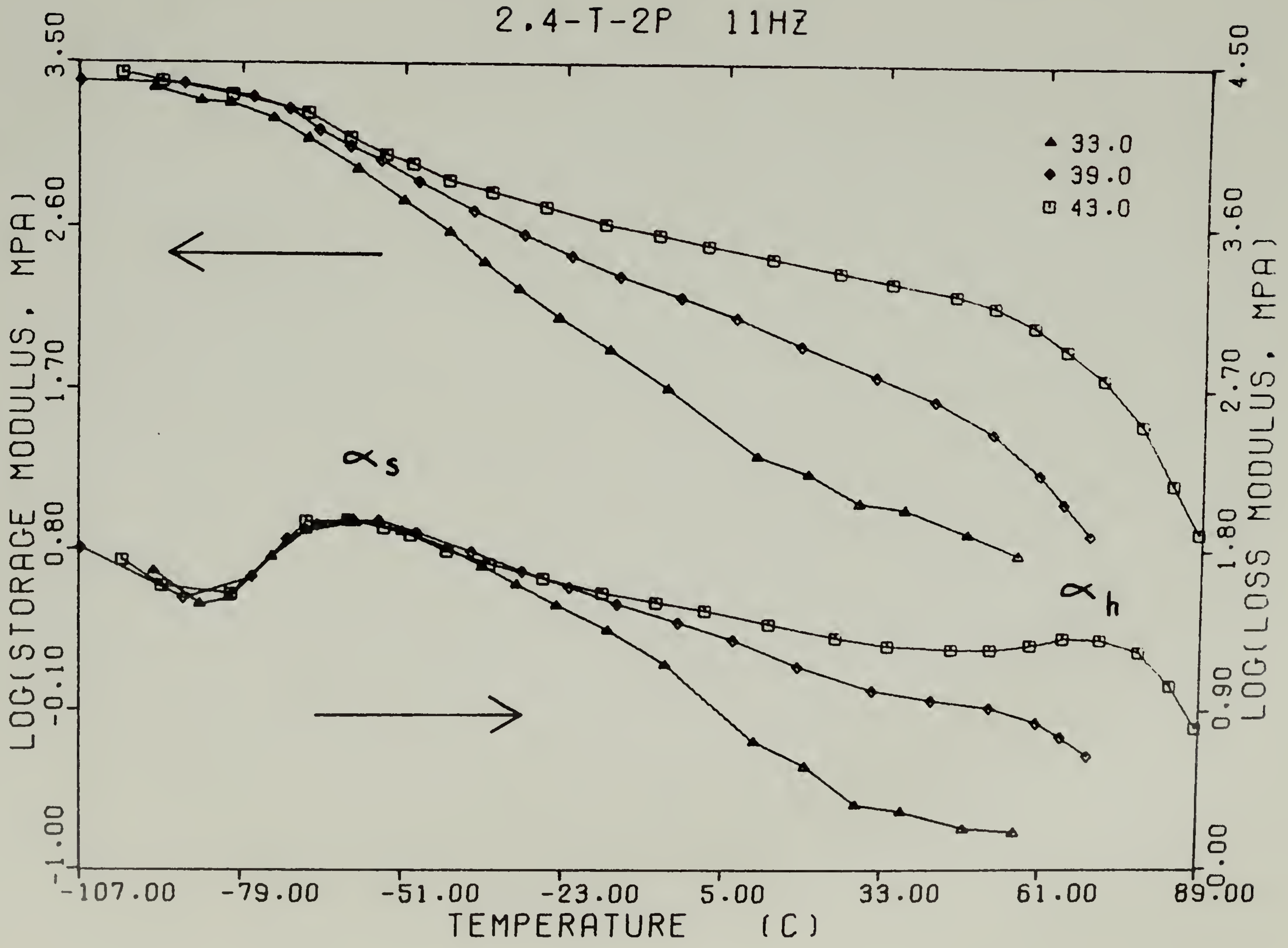
2.4-T-2P 11HZ
▲ 33.0
◆ 39.0
▫ 43.0
αs
αh
LOG(STORAGE MODULUS, MPA)
3.50
2.60
1.70
0.80
-0.10
-1.00
LOG(LOSS MODULUS, MPA)
4.50
3.60
2.70
1.80
0.90
0.00
-107.00
-79.00
-51.00
-23.00
5.00
33.00
61.00
89.00
TEMPERATURE (C)

with an activation energy of 120 kJ/mole is apparent for each sample. The position of the α_s relaxation maximum, given in Table 4-3, can be seen to decrease slightly with increasing concentration of hard segments. Again, the dynamic mechanical data compare favorably with results from DSC studies on these materials by Schneider and Paik Sung (14) as can be seen in Figure 4-8. The same small decrease in transition temperature with increasing hard block content is evident from both determinations. The storage modulus above the α_s relaxation can be seen to be highly dependent upon the hard segment content. At 0°C, for example, the storage modulus of 2,4-T-2P-43 is twice that of 2,4-T-2P-39 which in turn has a modulus five times that of 2,4-T-2P-33.

On further examination of Figure 4-9, an α_h relaxation can be noted and becomes increasingly prominent as hard segment content increases from 33 to 43 wt.%. The α_h loss process for 2,4-T-2P-43 is comparable in breadth to the α_s relaxation and has an apparent activation energy of about 270 kJ/mole. The position of α_h rose about 13°C as the hard segment content increased from 39 to 43 wt.%.

Several 2,4-T-2P samples were reevaluated and gave results identical within experimental error to the first determination, indicating that thermal history has a negligible effect on these polyurethanes.

DSA studies of 2,4-TDI polyurethanes revealed the occurrence of two loss processes above ambient temperature, as shown in Figure 4-10 for 2,4-T-1P-60. The first maximum occurred at 64°C (11 Hz) with an activation energy of 290 ± 100 kJ/mole, somewhat higher in temperature than the α relaxation observed in the thin film analysis

TABLE 4-3

RELAXATIONS OF 2,4-TDI BLOCK POLYURETHANES

SAMPLE	APPROXIMATE MOLAR RATIO TDI/BD/PTMO	RELAXATION	TEMPERATURE* (°C)	ACTIVATION ENERGY (kJ/mole)
2,4-T-1P-56	5/4/1	α	22	320 ± 50
2,4-T-1P-60	6/5/1	α	38	280 ± 20
2,4-T-2P-33	4/3/1	α_s	-62	120 ± 20
2,4-T-2P-39	5/4/1	α_s	-63	120 ± 20
2,4-T-2P-39	5/4/1	α_h	55	260 ± 30
2,4-T-2P-43	6/5/1	α_s	-64	120 ± 20
2,4-T-2P-43	6/5/1	α_h	68	270 ± 40

*Determined from position of E''_{max} at 11 Hz.

Figure 4-10. DSA Storage and Loss Modulus of 2,4-T-1P-60 vs. Temperature at Three Frequencies.

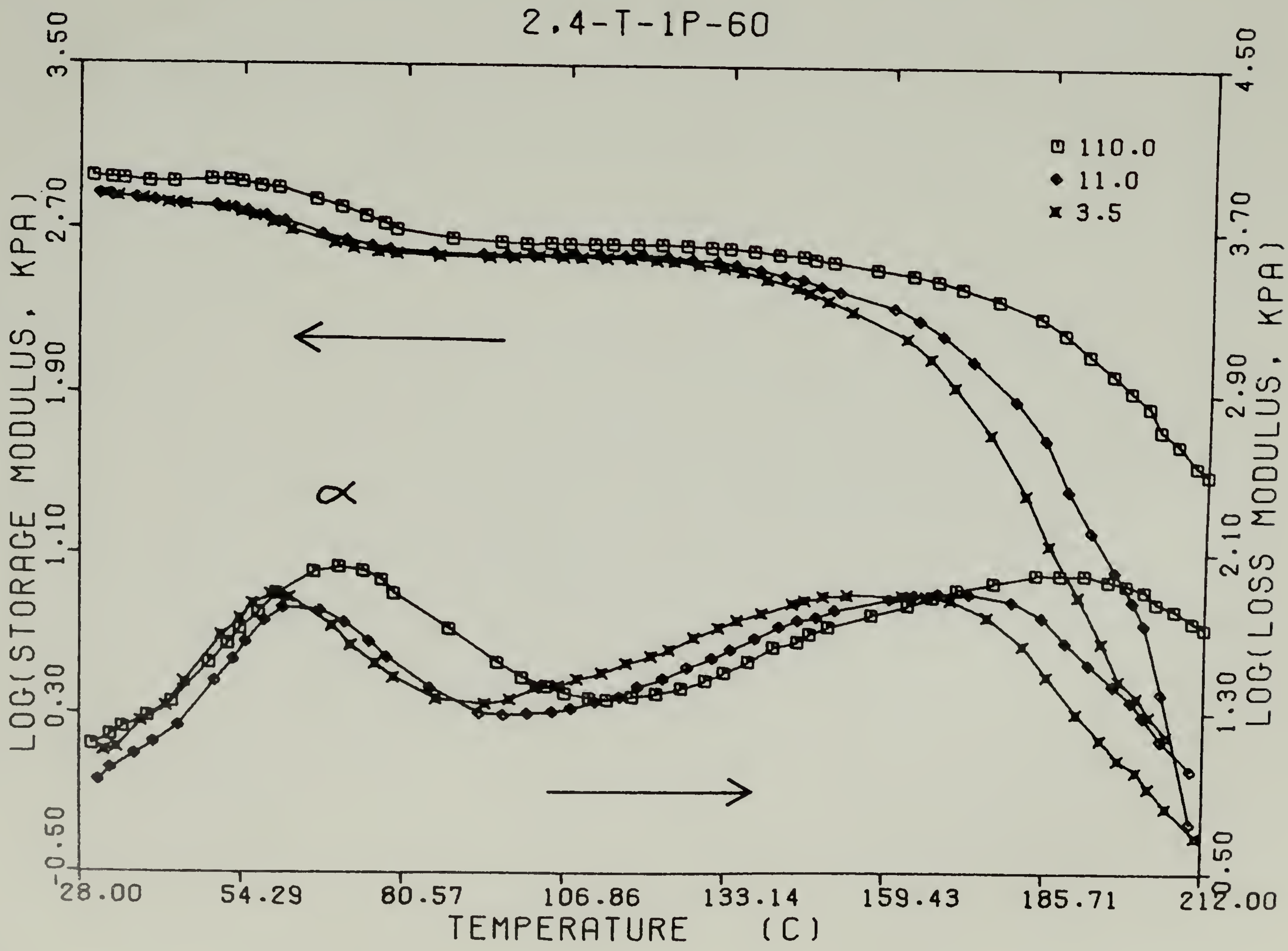
2.4-T-1P-60
□ 110.0
◆ 11.0
✖ 3.5
α
LOG(STORAGE MODULUS, KPA)
3.50
2.70
1.90
1.10
0.30
-0.50
LOG(LOSS MODULUS, KPA)
4.50
3.70
2.90
2.10
1.30
0.50
TEMPERATURE (C)
28.00
54.29
80.57
106.86
133.14
159.43
185.71
212.00

but with the same activation energy. A second loss process is evident at 170°C (11 Hz), with an activation energy of 200 ± 20 kJ/mole. Experiments at constant temperature were conducted to determine if sample degradation was responsible for the higher temperature loss process. Figure 4-11 shows that the relaxation is evident at a temperature of 154°C, well below temperatures where decomposition is likely to occur at significant rates (20).

The DSA results for 2,4-T-2P-43, shown in Figure 4-12, are similar to those of 2,4-T-1P-60. An α_h relaxation can be noted at 83°C (11 Hz) with an activation energy of 370 ± 180 kJ/mole followed by a higher temperature relaxation at 173°C (11 Hz) with a lower activation energy, 275 ± 130 kJ/mole. Additional studies were conducted on several 2,4-T-2P-43 samples to determine if the high temperature relaxation could be attributed to degradation. Samples prepared at 60 and 110°C exhibited a dynamic mechanical response identical to that of Figure 4-12. Heat treatment at 180°C for 260 min under vacuum caused only minor changes, while 3 hr at 190°C led to a major change in viscoelastic response. The latter sample had a high storage modulus to 230°C and displayed no high temperature relaxation, behavior most likely attributable to crosslinking at 190°C.

For 2,4-T-1P-60 and 2,4-T-2P-43, the DSA α or α_h relaxation, respectively, occurs 20 to 30°C above that of the corresponding compression molded film while the higher temperature relaxation is apparent at similar temperatures for both. This relaxation is not attributable to either degradation or crosslinking of the polymer during the test procedure.

Figure 4-11. DSA Loss Modulus (Filled Points) and Loss Tangent (Open Points) vs. Frequency for 2,4-T-1P-60 at Two Temperatures (154°C triangles, 167°C circles).

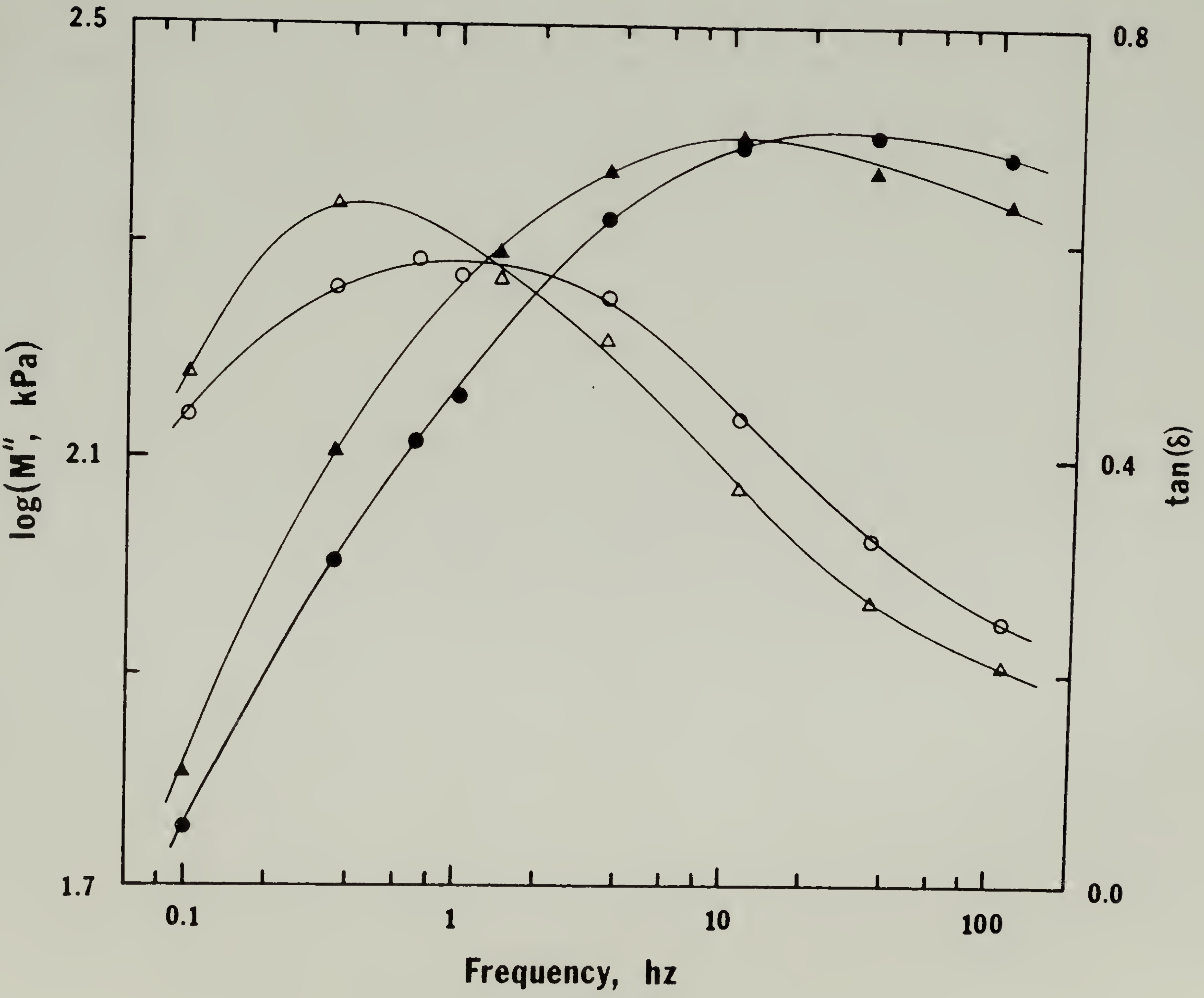
2.5
2.1
1.7
log(M″, kPa)
0.8
0.4
0.0
tan(δ)
0.1
1
10
100
Frequency, hz

Figure 4-12. DSA Storage and Loss Modulus of 2,4-T-2P-43 vs. Temperature at Three Frequencies.

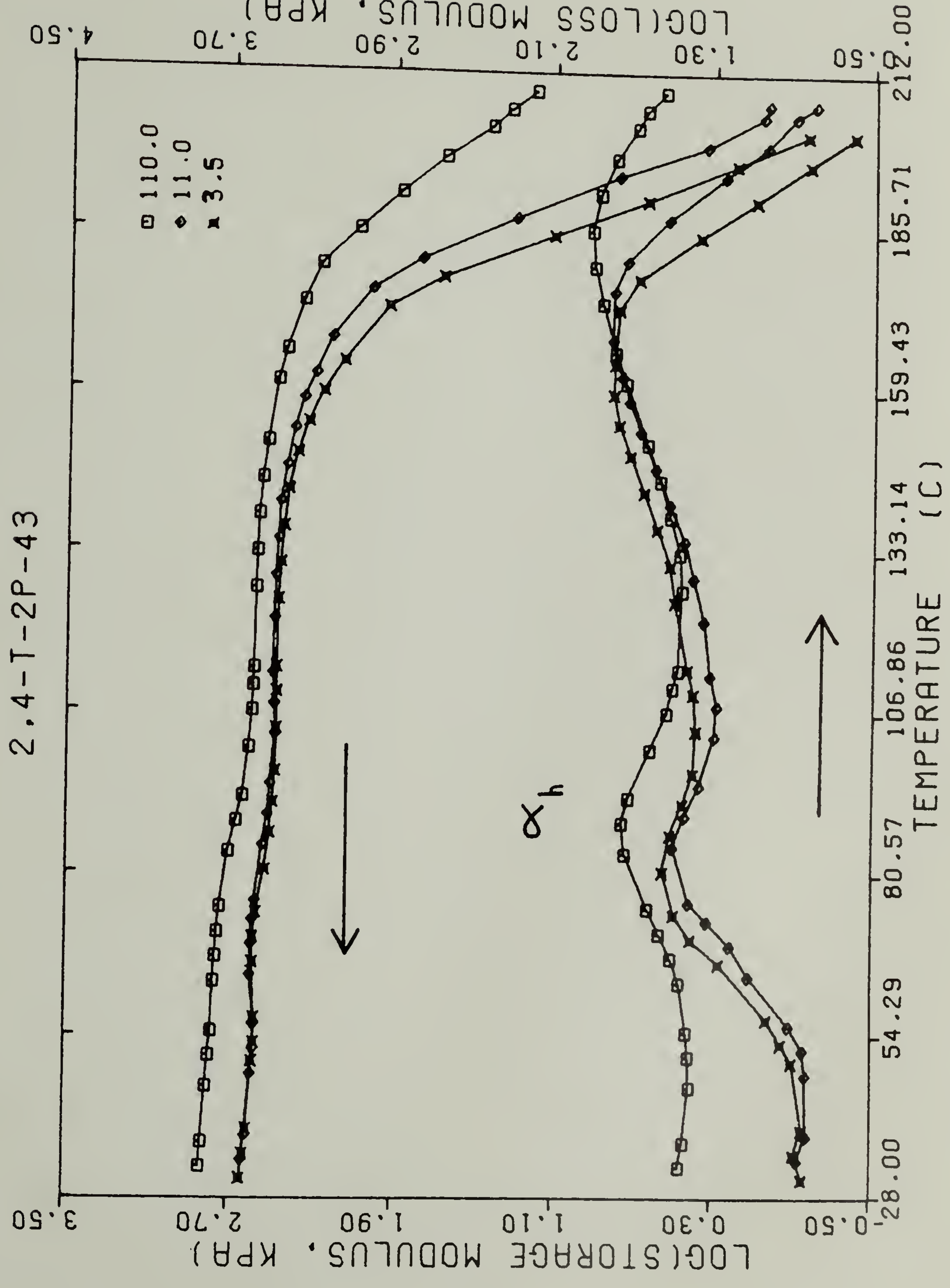
2.4-T-2P-43
LOG(LOSS MODULUS, KPA)
0.50
1.30
2.10
2.90
3.70
4.50
LOG(STORAGE MODULUS, KPA)
-0.50
0.30
1.10
1.90
2.70
3.50
TEMPERATURE (C)
28.00
54.29
80.57
106.86
133.14
159.43
185.71
212.00
⊡ 110.0
◇ 11.0
✱ 3.5
α_h

2,6-TDI polyurethanes. Three 2,6-T-1P samples of varying hard segment content were studied and exhibited the dynamic mechanical response displayed in Figure 4-13. An α_s relaxation can be noted at -64°C (11 Hz) for 2,6-T-2P-31 which progressively broadens as the quantity of hard segments incorporated into the polyurethane increased. The activation energy of the α_s process was found to decrease as hard segment content increased, as can be noted from Table 4-4. The level of the storage modulus above α_s was found to be highly dependent upon the composition of the polyurethane, increasing from 2,6-T-1P-31 to 2,6-T-1P-42 by about 250% at 0°C and by a like amount from 2,6-T-1P-42 to the next member of the series. A final point to note is the high temperature behavior of these polyurethanes. The storage modulus shows a region of rapid decline not matched by the loss modulus. This leads to a rapid rise in the loss tangent at high temperatures corresponding to the onset of a softening or flow α relaxation process. The temperature at which the storage modulus reached a value of 1.25 MPa was taken as an arbitrary indication of the loss of mechanical integrity and melting of the hard segments of these polyurethanes. The temperatures of both α_s and δ relaxation processes are plotted against hard segment content and compared to the data of Schneider and coworkers (12) in Figure 4-14. The α_s relaxation occurs at increasingly higher temperatures as hard segment content increases while the T_{gs} determined from DSC measurements shows a slight decrease. Both sets of data show the same trend for the higher temperature hard segment melting transition.

The dynamic mechanical properties of four 2,6-T-2P samples

Figure 4-13. Storage and Loss Modulus of 2,6-T-1P vs. Temperature at 11 Hz for Polyurethanes Containing 31, 42, and 56 wt.% Hard Segments.

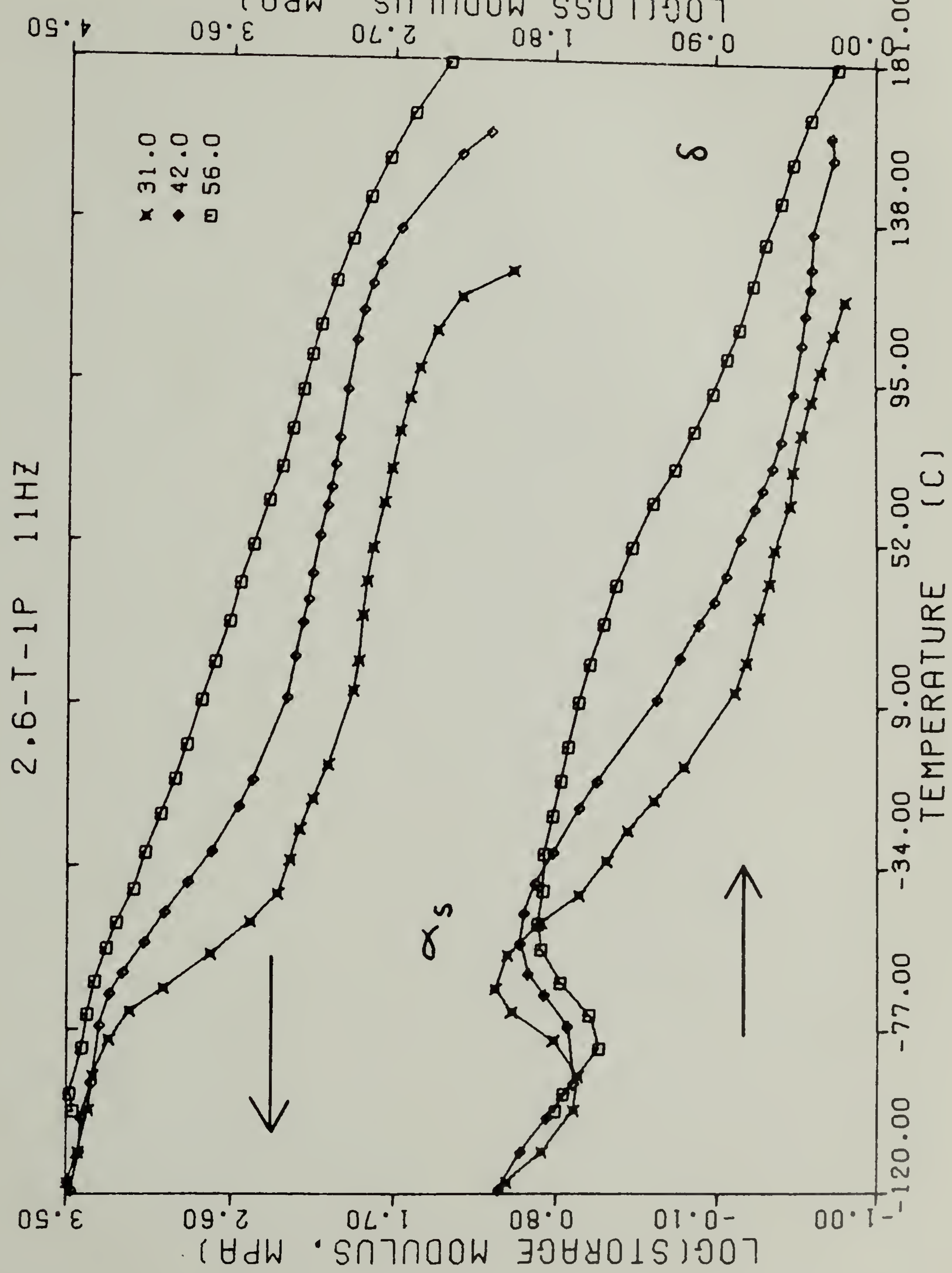
2.6-T-1P 11HZ
LOG(STORAGE MODULUS, MPA)
3.50
2.60
1.70
0.80
-0.10
-1.00
LOG(LOSS MODULUS, MPA)
4.50
3.60
2.70
1.80
0.90
0.00
TEMPERATURE (C)
-120.00
-77.00
-34.00
9.00
52.00
95.00
138.00
181.00
✱ 31.0
◆ 42.0
⊡ 56.0
δ
α_s

TABLE 4-4

RELAXATIONS OF 2,6-TDI BLOCK POLYURETHANES

SAMPLE	APPROXIMATE MOLAR RATIO TDI/BD/PTMO	RELAXATION	TEMPERATURE* (°C)	ACTIVATION ENERGY (kJ/mole)
2,6-T-1P-31	2/1/1	α_s	-64	170 ± 20
2,6-T-1P-31	2/1/1	δ	120	---
2,6-T-1P-42	3/2/1	α_s	-54	120 ± 40
2,6-T-1P-42	3/2/1	δ	157	---
2,6-T-1P-56	5/4/1	α_s	-48	70 ± 20
2,6-T-1P-56	5/4/1	δ	183	---
2,6-T-2P-19	2/1/1	α_s	-69	140 ± 20
2,6-T-2P-19	2/1/1	δ	97	---
2,6-T-2P-27	3/2/1	α_s	-71	180 ± 20
2,6-T-2P-27	3/2/1	α_c	-31	---
2,6-T-2P-27	3/2/1	δ	137	---
2,6-T-2P-33	4/3/1	α_s	-71	180 ± 30
2,6-T-2P-33	4/3/1	α_c	-19	---
2,6-T-2P-33	4/3/1	δ	160	---
2,6-T-2P-39	5/4/1	α_s	-72	160 ± 20
2,6-T-2P-39	5/4/1	α_c	-9	---
2,6-T-2P-39	5/4/1	δ	154	---
2,6-T-2P-43	6/5/1	α_s	-66	70 ± 20
2,6-T-2P-43	6/5/1	α_c	-8	---
2,6-T-2P-43	6/5/1	α_h	60	270 ± 90
2,6-T-2P-43	6/5/1	δ	177	---

*α_s determined from E''_{max}, α_c and α_h from $\tan(\delta)_{max}$, δ from $\log(E') = 1.25$ MPa, all at 11 Hz.

Figure 4-14. Comparison of 11 Hz Dynamic Mechanical (Open Points) and DSC or TMA Transition Temperatures (Filled Points, Ref. 13) of 2,6-T-1P Polyurethanes as a Function of Hard Segment Content.

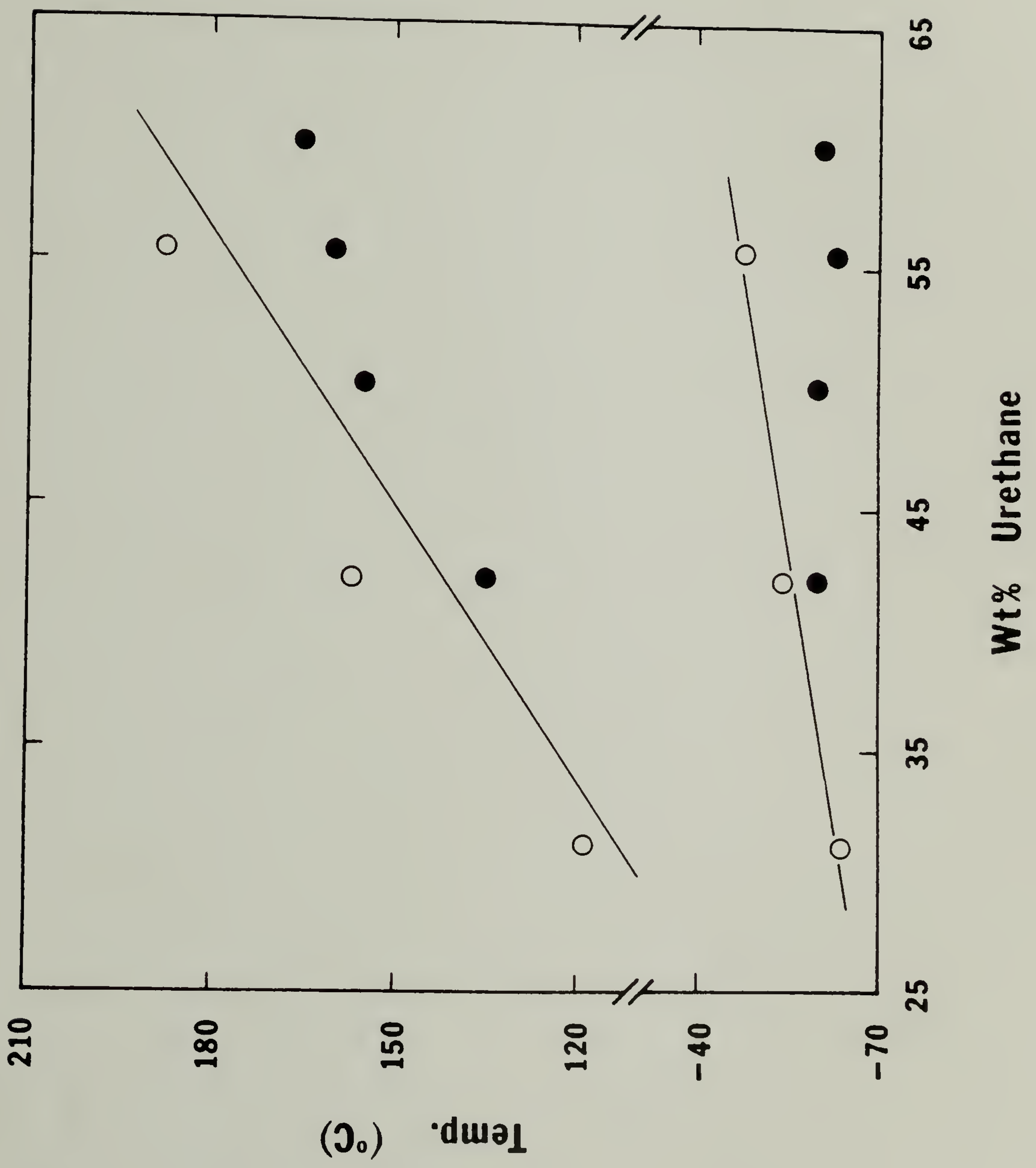
Temp. (°C)
210
180
150
120
−40
−70
25
35
45
55
65
Wt% Urethane

containing from 19 to 43 wt.% hard segments are summarized in Figure 4-15. A low temperature α_s relaxation is apparent at about -70°C for all compositions examined. The transition temperatures of these loss maxima and the associated activation energies are given in Table 4-4. A second process, the α_c relaxation, can be noted as a shoulder on the high temperature side of the α_s loss maximum. The conclusion of this relaxation is marked by a change in slope of the loss modulus vs. temperature plots at about 2 to 7°C. This relaxation is also apparent in loss tangent vs. temperature curves, shown in Figure 4-16. The insity of the α_s relaxation is approximately equal to that of the α_c relaxation from the tan(δ) data and the two processes exhibit considerable overlap. The α_c relaxation can be more clearly observed in a plot of storage and loss modulus vs. temperature at 11 Hz for two polyurethanes, 2,6-T-1P-31 and 2,6-T-2P-33, shown in Figure 4-17. These polymers have about the same hard segment content and differ only in the soft segment molecular weight. The α_c relaxation peak can be observed in the 2,6-T-2P polyurethane as an elevation in the loss modulus over the region from about -40 to 7°C. The storage modulus of the sample with a higher molecular weight soft segment can be seen to be about double that of 2,6-T-1P over the same temperature range. The increase in storage modulus above α_s can be attributed to reinforcement of the soft segment phase by crystallization above its T_g. This enhancement of strength continues up to a temperature of about 7°C, the region where soft segment melting was found to occur in the 2,6-TDI/PTMO soft segment polymer. The presence of soft segment crystallinity in 2,6-T-2P-33 is confirmed by the DSC thermogram in

Figure 4-15. Temperature Dependence of the Storage and Loss Modulus of 2,6-T-2P at 11 Hz for Polyurethanes Containing 19, 27, 33, and 43 wt.% Hard Blocks.

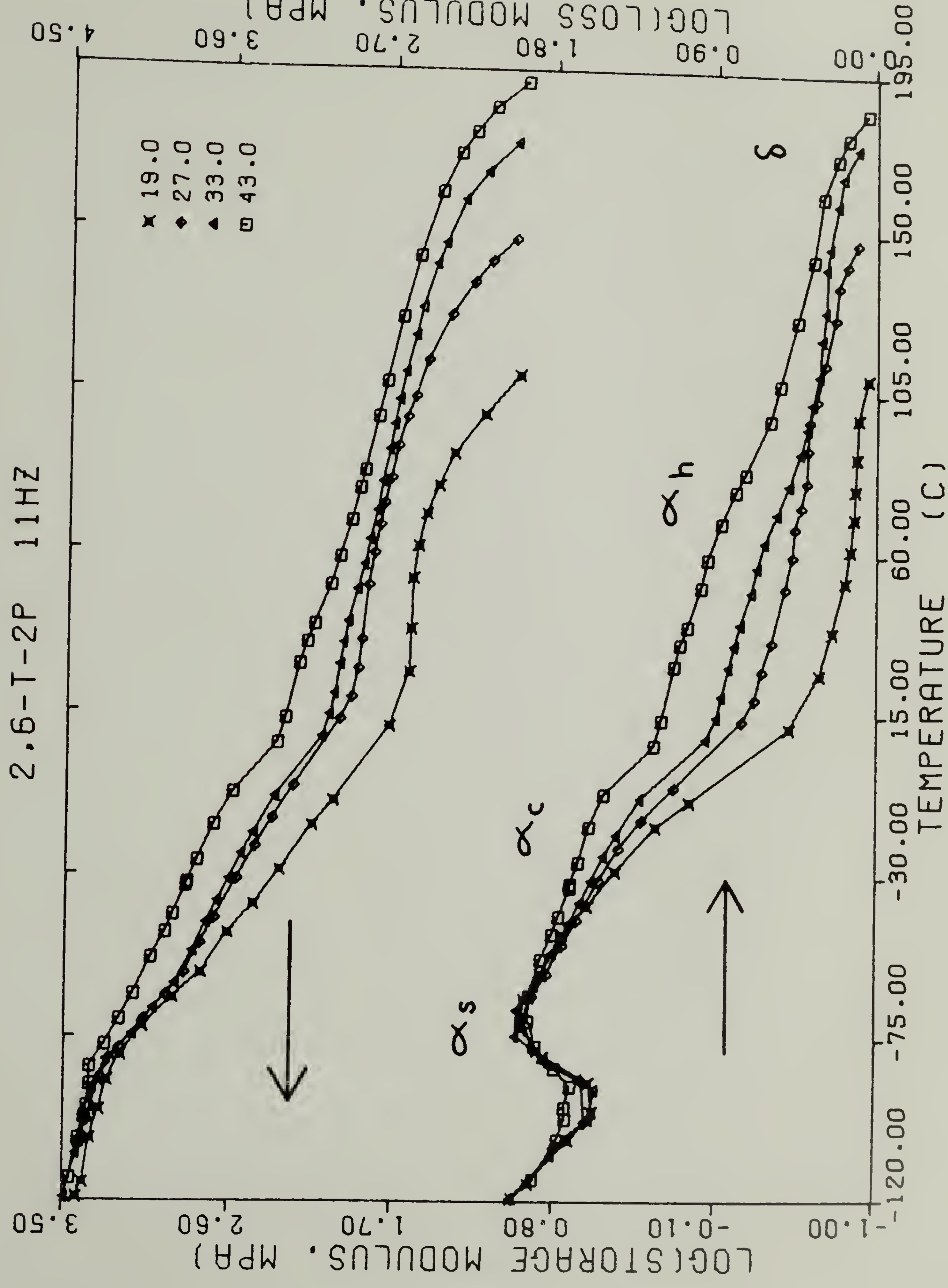
2.6-T-2P 11HZ
LOG(STORAGE MODULUS, MPA)
3.50
2.60
1.70
0.80
-0.10
-1.00
LOG(LOSS MODULUS, MPA)
4.50
3.60
2.70
1.80
0.90
0.00
TEMPERATURE (C)
-120.00
-75.00
-30.00
15.00
60.00
105.00
150.00
195.00
× 19.0
◆ 27.0
▲ 33.0
□ 43.0
α_s
α_c
α_h
δ

Figure 4-16. Temperature Dependence of the Loss Tangent of 2,6-T-2P at 11 Hz for Polyurethanes Containing 19, 27, 33, and 43 wt.% Hard Blocks.

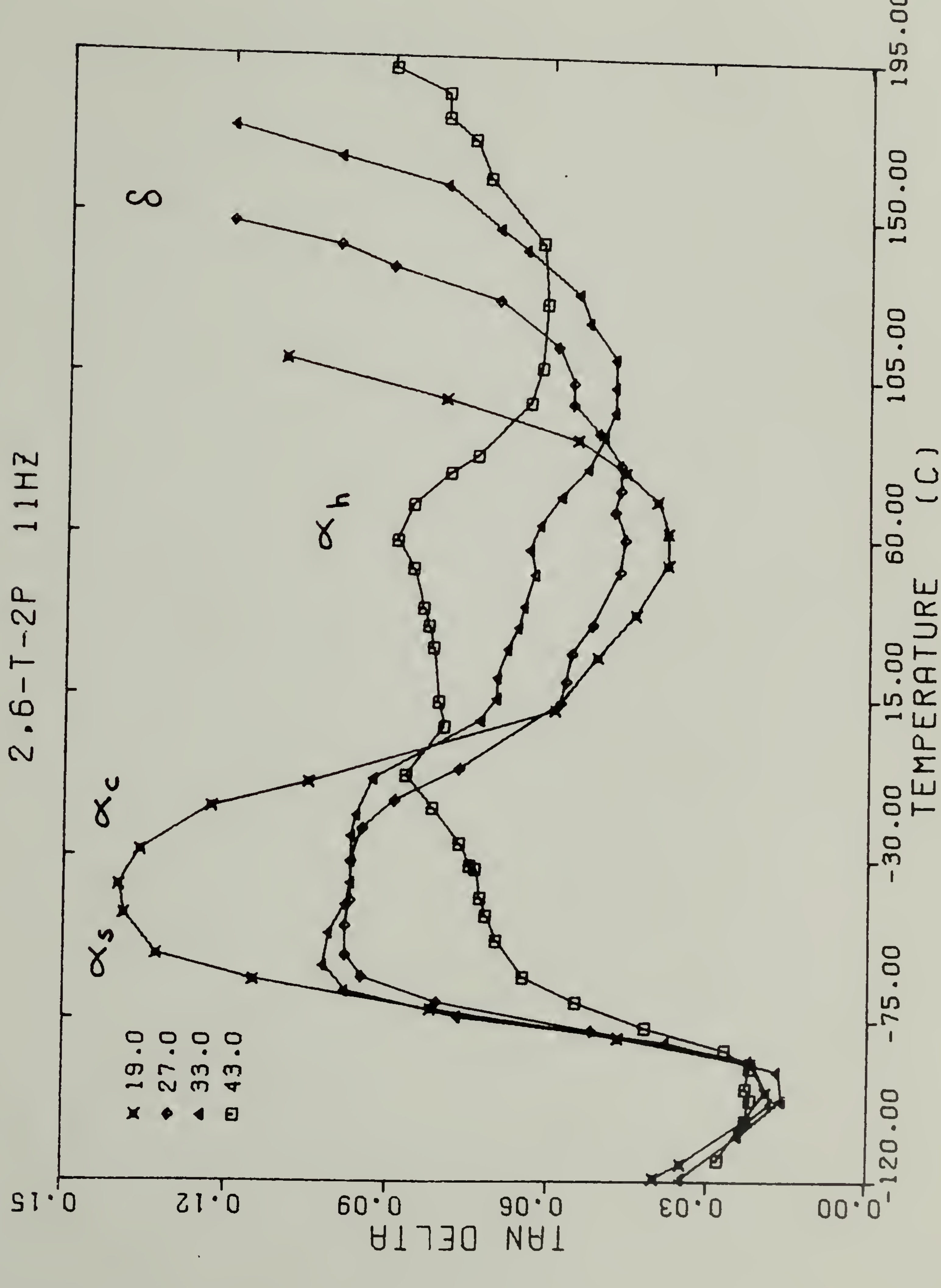
2.6-T-2P 11HZ
× 19.0
◆ 27.0
▲ 33.0
⊡ 43.0
α_s
α_c
α_h
δ
TAN DELTA
0.00
0.03
0.06
0.09
0.12
0.15
TEMPERATURE (C)
-120.00
-75.00
-30.00
15.00
60.00
105.00
150.00
195.00

Figure 4-17. Comparison of the Storage and Loss Modulus of 2,6-T-1P-31 and 2,6-T-2P-33 as a Function of Temperature at 11 Hz.

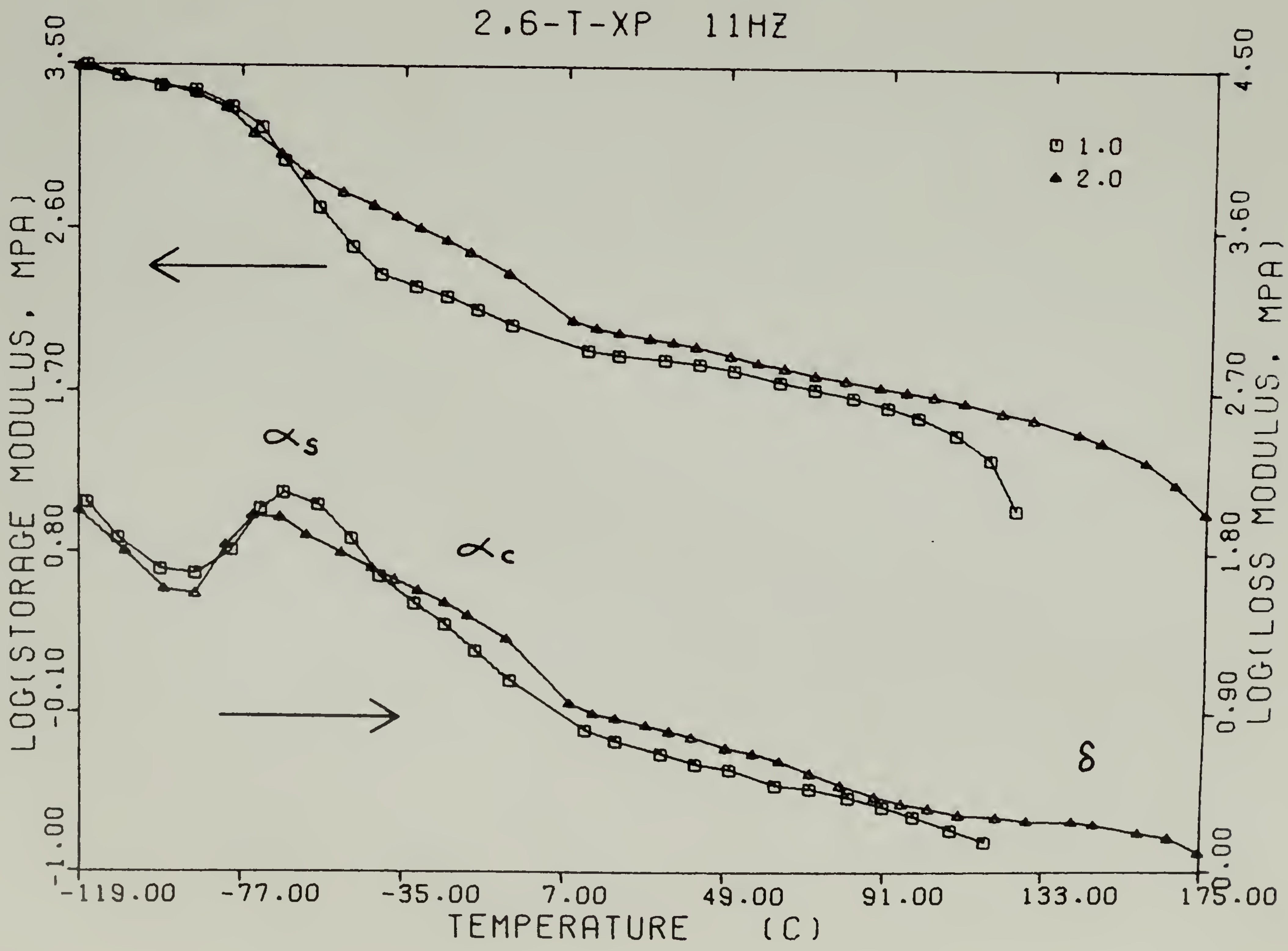
2.6-T-XP 11HZ
▫ 1.0
▲ 2.0
α_s
α_c
δ
LOG(STORAGE MODULUS, MPA)
3.50
2.60
1.70
0.80
-0.10
-1.00
LOG(LOSS MODULUS, MPA)
4.50
3.60
2.70
1.80
0.90
0.00
-119.00
-77.00
-35.00
7.00
49.00
91.00
133.00
175.00
TEMPERATURE (C)

Figure 4-18. The 2,6-T-1P-31 polyurethane displays only a glass transition while a quenched sample of 2,6-T-2P-33 shows evidence for crystallization above T_g followed by melting at 286°K. The region of recrystallization and melting, from 232 to 286°K, corresponds to the temperature range of the α_c relaxation of 2,6-T-2P-33 in Figure 4-17, thereby confirming the mechanism assigned to this relaxation.

An additional relaxation can be detected in plots of the loss tangent as a function of temperature for 2,6-T-2P-43, shown in Figure 4-16. The α_h relaxation occurred at 60°C (11 Hz) in the first examination of this sample. A weak α_h relaxation can be detected in the loss modulus vs. temperature plots in Figure 4-15 but the process is more readily apparent in the tan(δ) data.

Returning to the 2,6-T-2P comparison in Figure 4-15, the storage modulus above α_c and the position of the δ relaxation, the temperature at which the storage modulus reached 1.25 MPa, can be seen to depend upon hard segment concentration in a manner similar to that observed for the 2,6-T-1P polyurethanes. The α_s and δ relaxation temperatures at 11 Hz are plotted as a function of hard segment content in Figure 4-19 and compared to TMA and DSC results of Schneider and Paik Sung (14). There is good agreement between the α_s loss process and the T_{gs} transition, and both the δ relaxation and the hard segment melting transition show a similar trend, with the exception of 2,6-T-2P-39.

Thermal history was found to have an effect on 2,6-T-2P dynamic mechanical properties. For the two samples retested after the first experiment to 190°C, the α_s relaxation was shifted to a higher tempera-

Figure 4-18. DSC Thermogram of: (a) 2,6-T-1P-31, and (b) 2,6-T-2P-33, Both Quenched to 123°C.

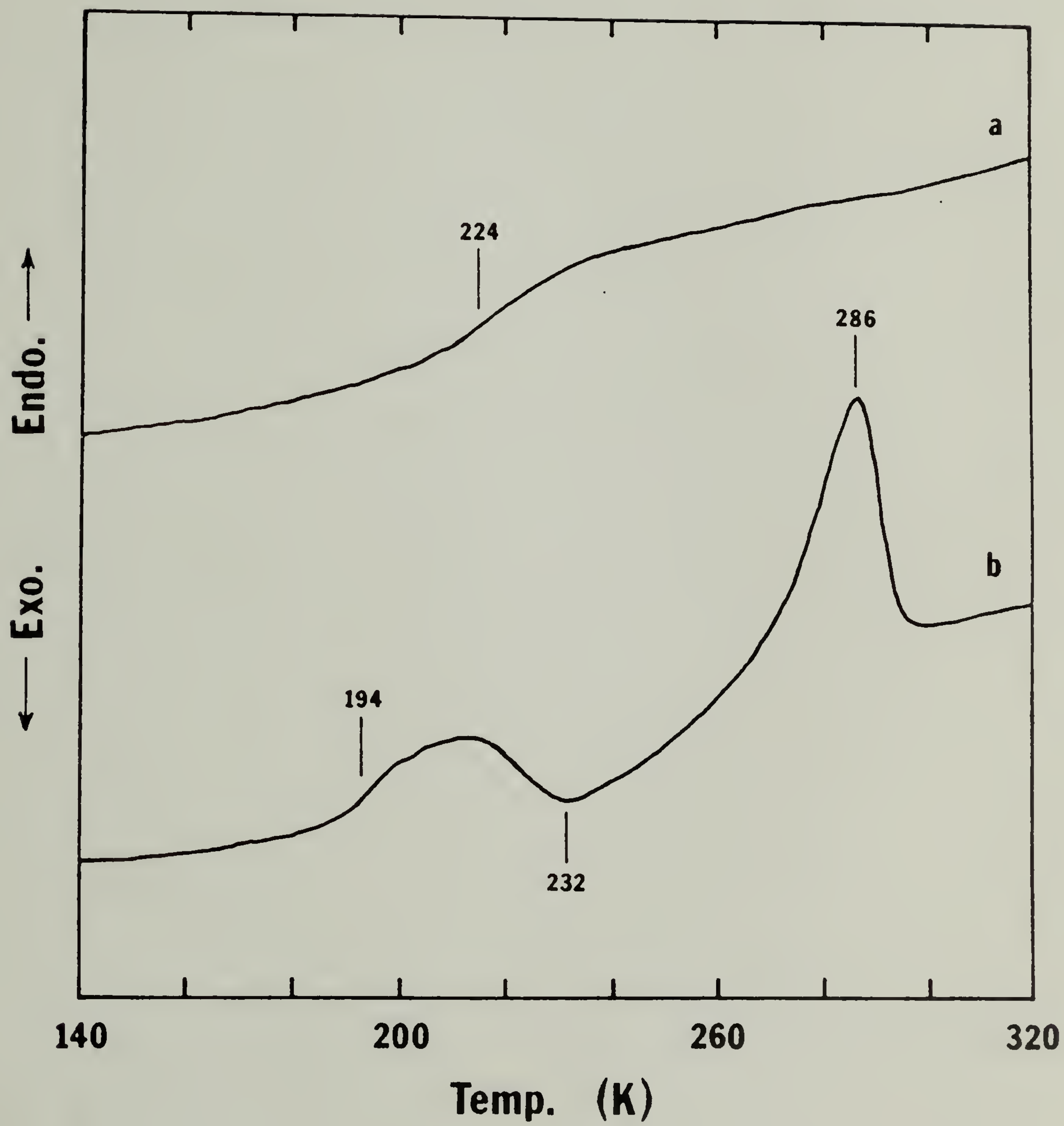
a
224
286
b
194
232
Endo. ⟶
⟵ Exo.
140
200
260
320
Temp. (K)

Figure 4-19. Comparison of 11 Hz Dynamic Mechanical (Open Points) and DSC or TMA Transition Temperatures (Filled Points, Ref. 14) of 2,6-T-2P Polyurethanes as a Function of Hard Segment Concentration.

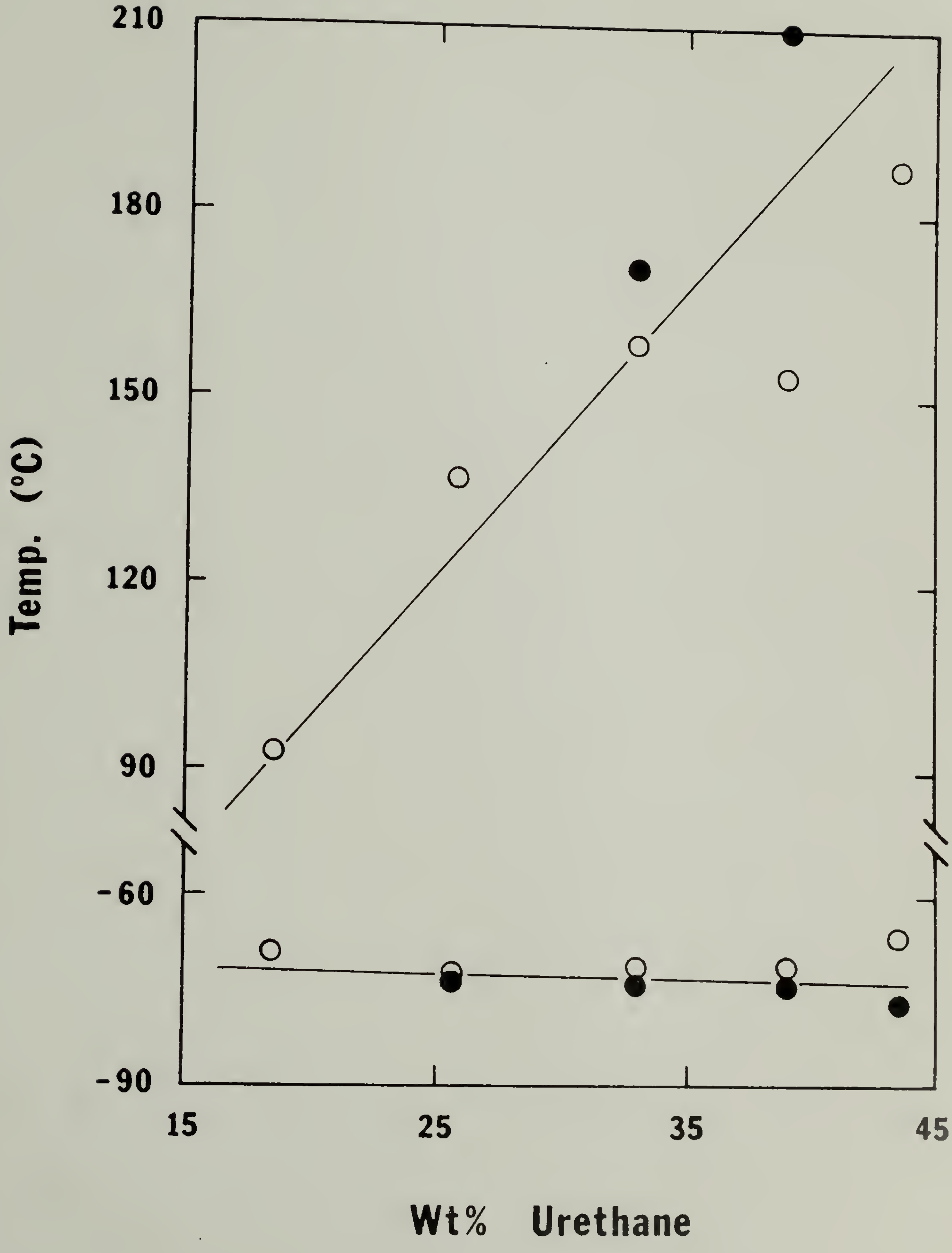
210
180
150
120
90
-60
-90
Temp. (°C)
15
25
35
45
Wt% Urethane

ture after thermal treatment while the storage modulus increased by about 50% over the temperature interval from -80 to 130°C. The δ relaxation was not affected by heating to 190°C. These differences are illustrated for 2,6-T-2P-43 in Figure 4-20 while Table 4-5 summarizes the dynamic mechanical data for both of the retested 2,6-T-2P polyurethanes. The shift of the α_h relaxation from 60 to 71°C is more readily apparent in Figure 4-21. This relaxation was extremely weak or undetectable in 2,6-T-2P samples which contained less than 43 wt.% hard segments. Its activation energy did not change significantly with thermal history. The apparent activation energy of the α_s relaxation increased significantly after the first determination, as can be seen from Figure 4-22, a plot of activation energy vs. hard segment content.

Several DSA experiments were conducted with 2,6-TDI polyurethanes. Studies of 2,6-T-1P-56 and 2,6-T-2P-39 showed a constant storage modulus with increasing temperature to 215°C and 190°C, respectively, where the runs were terminated. The upper limit of these studies is 30 to 35°C over the δ relaxation temperature, yet the DSA experiments showed no indication that melting had taken place. A DSA study of 2,6-T-2P-43 resulted in an essentially constant storage modulus with increasing temperature to 220°C. The α_h relaxation was not apparent in the loss modulus or the loss tangent curves. At a temperature of about 235°C the storage modulus began a decline of about half an order of magnitude to the temperature limit of the experiment, 250°C. The sample was examined after the run and found to have discolored to a dark brown hue. In addition, degradation was indicated by the ease at which the material flowed at room temperature.

Figure 4-20. Comparison of 2,6-T-2P-43 Dynamic Mechanical Response on Initial (Squares) and Second Run (Triangles).

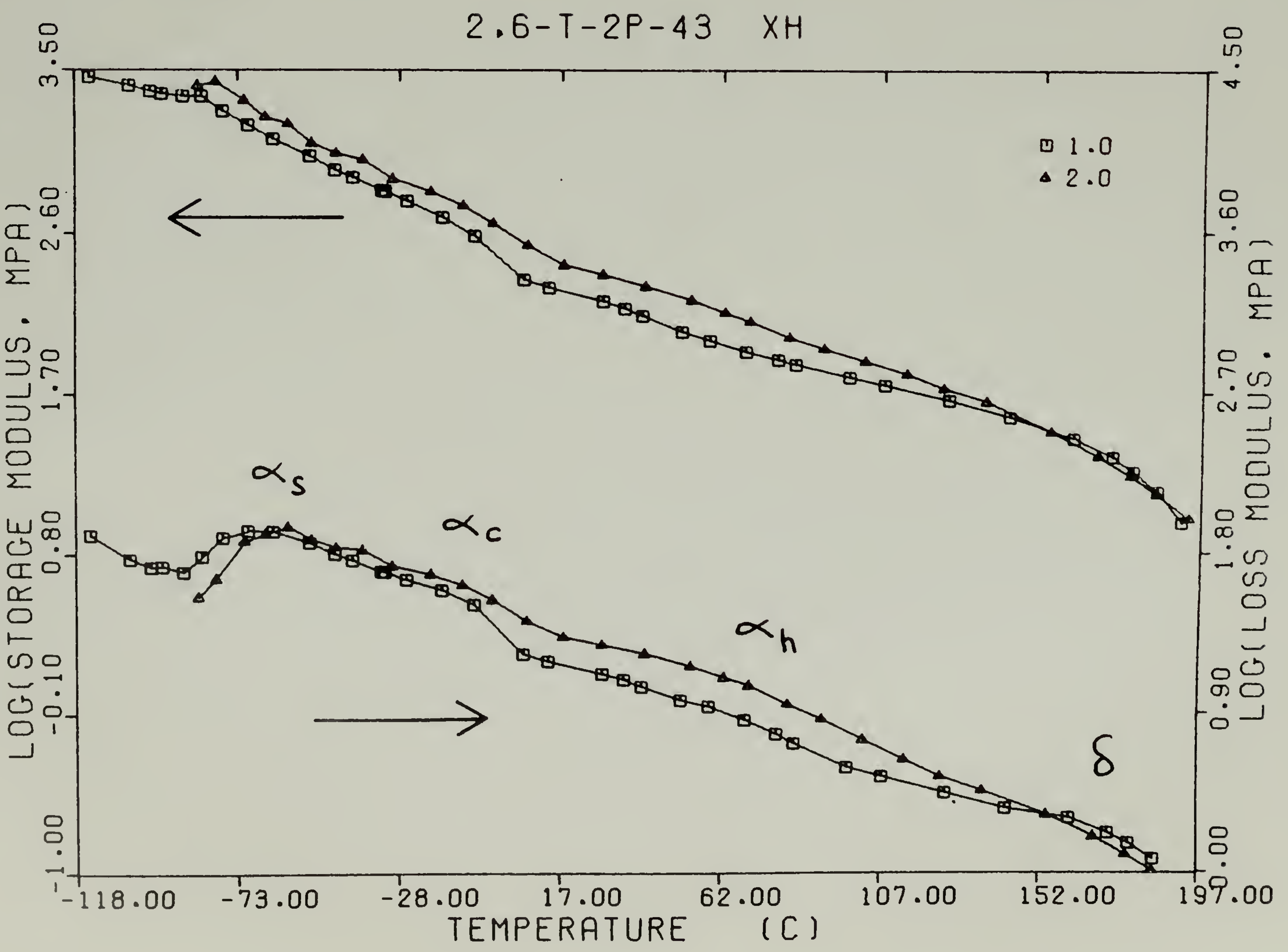
2.6-T-2P-43 XH
1.0
2.0
α_s
α_c
α_h
δ
LOG(STORAGE MODULUS, MPA)
3.50
2.60
1.70
0.80
-0.10
-1.00
LOG(LOSS MODULUS, MPA)
4.50
3.60
2.70
1.80
0.90
0.00
TEMPERATURE (C)
-118.00
-73.00
-28.00
17.00
62.00
107.00
152.00
197.00

TABLE 4-5

RELAXATIONS OF THERMALLY TREATED 2,6-TDI POLYURETHANES

SAMPLE	RELAXATION	TEMPERATURE* (°C)	ACTIVATION ENERGY (kJ/mole)
2,6-T-2P-39	α_s	-64	310 ± 40
2,6-T-2P-39	α_c	-3	---
2,6-T-2P-39	δ	154	---
2,6-T-2P-43	α_s	-64	200 ± 30
2,6-T-2P-43	α_c	-2	---
2,6-T-2P-43	α_h	71	310 ± 50
2,6-T-2P-43	δ	174	---

*α_s determined from E''_{max}, α_c and α_h from $\tan(\delta)_{max}$, δ from $\log(E') = 1.25$ MPa, all at 11 Hz.

Figure 4-21. Comparison of 2,6-T-2P-43 Loss Tangent vs. Temperature Response on Initial (Squares) and Second Run (Triangles).

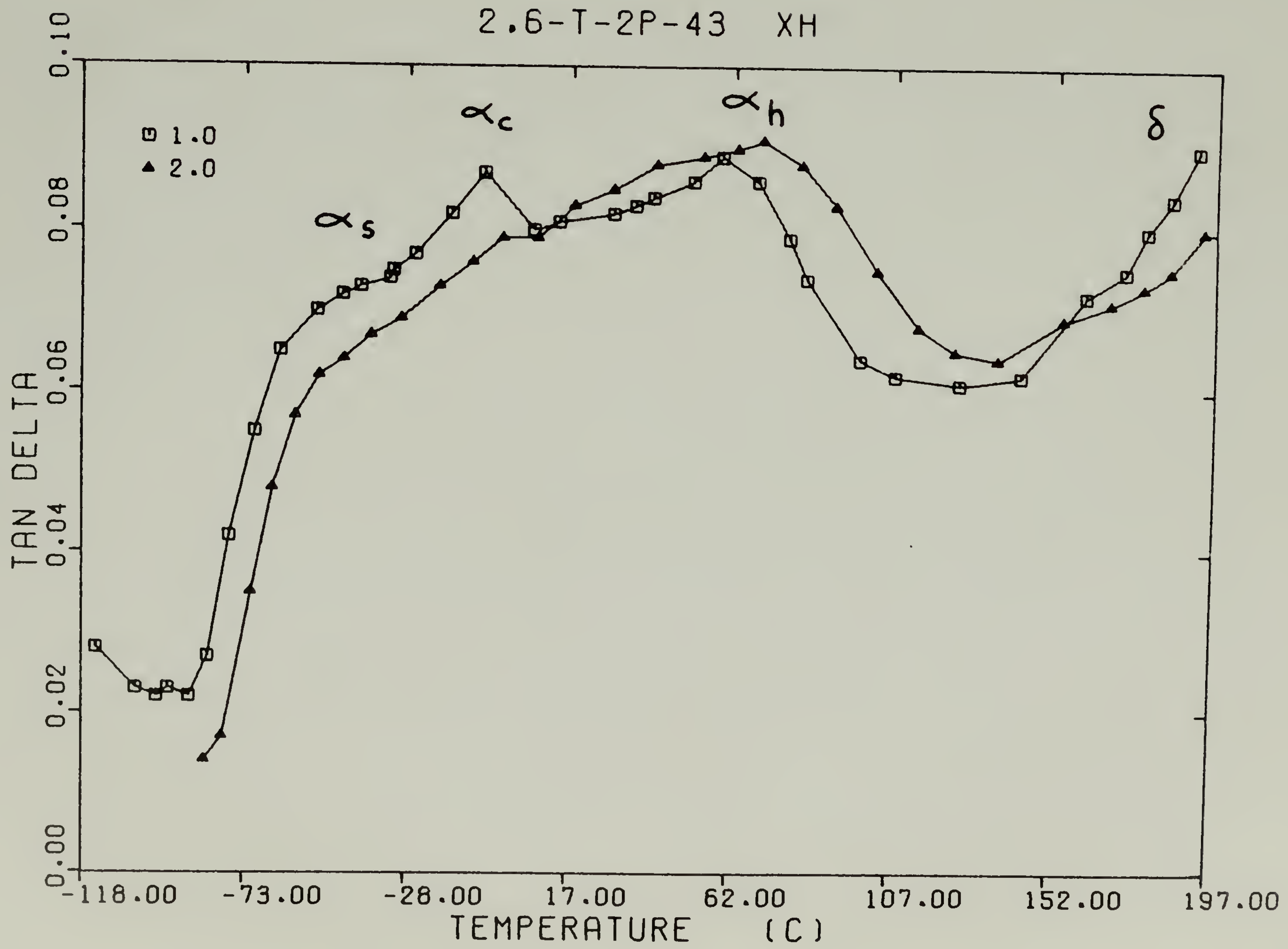
2.6-T-2P-43 XH
▢ 1.0
▲ 2.0
α_s
α_c
α_h
δ
TAN DELTA
0.00
0.02
0.04
0.06
0.08
0.10
TEMPERATURE (C)
-118.00
-73.00
-28.00
17.00
62.00
107.00
152.00
197.00

Figure 4-22. Apparent Activation Energy of the α_s Relaxation in 2,6-T-2P Polyurethanes as a Function of Hard Segment Content from the First (Filled Points) and Second Determination (Open Points).

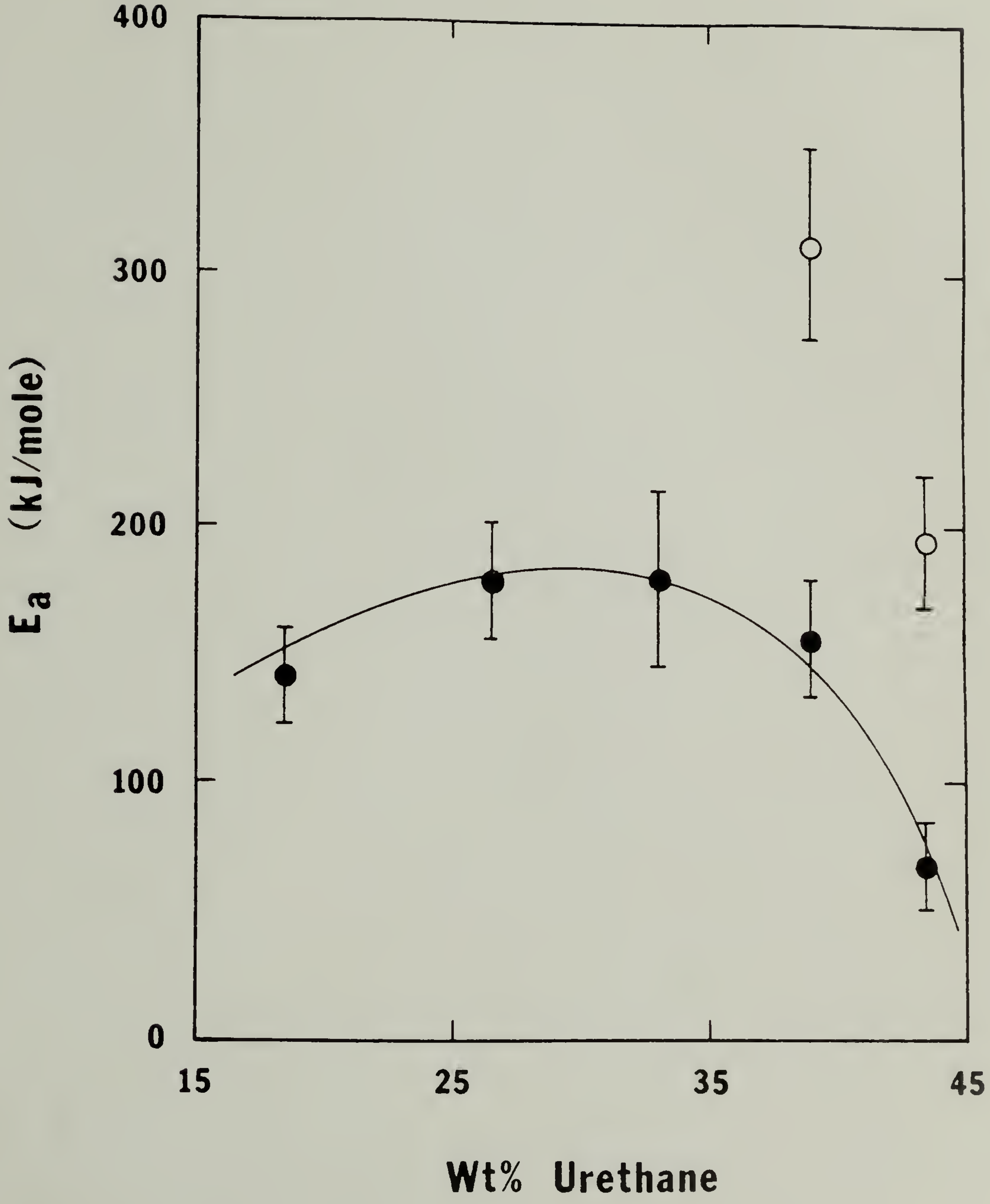
400
300
200
100
0
15
25
35
45
E_a (kJ/mole)
Wt% Urethane

The insensitivity of the DSA technique to hard segment melting and the increasing likelihood of polyurethane degradative reactions at high temperatures precluded further DSA study of 2,6-TDI copolymers.

Discussion

Hard and soft segment polymers. The structure of the diisocyanate component has a significant influence on dynamic mechanical properties of both hard and soft segment polymers. Both 2,4- and 2,6-TDI/BD α relaxations occur at about the same temperature and have a comparable activation energy. However, the symmetrical structure of 2,6-TDI/BD facilitates crystallization of the hard segment polymer, which has the effect of broadening the α relaxation when compared to that of the totally amorphous 2,4-TDI/BD. The semicrystalline nature of the 2,6-TDI hard segment provides modulus reinforcement above the α relaxation to about 212°C. This behavior can be compared with that of an MDI/BD hard segment studied by Illinger et al. (6), which displayed an α relaxation at 110°C (110 Hz) and a second relaxation, attributed to melting, at about 170°C (110 Hz). The symmetrical TDI hard segment maintained a higher modulus above the α relaxation to a higher temperature than did the MDI/BD hard segment studied by these workers.

The soft segment polymers studied consisted of 1090 $\overline{M}_n$ PTMO chains, corresponding to about 75 carbon and oxygen atoms each, in an alternating arrangement with diisocyanate molecules. This material was thought to be representative of the soft segment, as the single urethane units do not function as hard segments in block polyurethanes (21). The glass transition for both isomers was found to be in the region of -50 to -60°C, above the literature value for high molecular weight PTMO, -84°C (22). The elevation of the soft segment T_g over that of the pure PTMO homopolymer can be attributed to a combination of the copolymer effect and effective crosslinking of the PTMO ether oxygens by hydrogen bonding with the diisocyanate amine group, an association which has been found to be significant for block copolyurethanes (13-15).

Above the α relaxation process, the 2,4-TDI/PTMO polymer displayed a short rubbery plateau at a storage modulus of about 5 MPa while 2,6-TDI/PTMO was capable of crystallization, as evidenced by the α_c loss process. This difference in dynamic mechanical properties demonstrates the effect of a symmetric diisocyanate structure upon soft segment properties. As previously discussed, single urethane links can sometimes be incorporated into the soft segment phase. The introduction of only one of these diisocyanate molecules between two 1090 $\overline{M}_n$ PTMO chains inhibits crystallization if the diisocyanate is asymmetric. In the case of a symmetric diisocyanate, soft segment crystallization above T_g can readily occur. The crystals formed were found to melt about 30°C below the reported melting point for PTMO homopolymer, 37 to 43°C (22), possibly due to disruption of the crystal structure by the bulky diisocyanate units.

The α relaxation of 2,4-T-1P. Only the 2,4-T-1P block polyurethanes exhibited a single major α relaxation which had a strongly composition dependent position. Similar behavior was observed by Seefried and coworkers (10) for polyurethanes containing a TDI/BD hard segment and a 2100 $\overline{M}_n$ polycaprolactone soft segment. The extreme dependence of the

α process on hard segment content suggests that the amount of hard urethane segments mixed with the soft segment is extensive. The location of the α relaxation cannot be predicted from the hard and soft segment polymer relaxation temperatures and polyurethane composition by the use of the copolymer equation. Schneider and Paik Sung (14) have shown that the difference between the observed T_g and that predicted from the copolymer equation can be accounted for by considering hydrogen bonds between hard and soft segments as crosslinks which elevate the glass transition of the soft segment phase. Hydrogen bond crosslinking should affect the soft segment main chain micro-Brownian motion through a reduction in free volume. A corresponding increase in the temperature and activation energy of the α relaxation process is predicted with increasing crosslink density, and these two effects can indeed be observed in the dielectric relaxation data of Scott and coworkers (23) on a series of increasingly crosslinked natural rubber samples. An increase in the activation energy for the α process in 2,4-T-1P by about 50% over that for 2,4-TDI/PTMO can be noted. These results are consistent with the crosslinking assumption of Schneider and Paik Sung.

Estimates of the quantity of hard segments incorporated in the soft segment phase do not approach the total hard segment content of the 2,4-T-1P polyurethanes. These materials were found to give rise to a small angle x-ray scattering intensity maximum which became more pronounced as the hard segment content increased (15). The x-ray results indicate that these materials display some phase segregation, but no hard segment relaxation could be detected by dynamic mechanical testing of thin film samples due to the low modulus of these materials above the α relaxation. TMA studies by Schneider and coworkers (12) have shown that a second transition, termed T_2, is found about 45 to 55°C above the soft segment glass transition in 2,4-T-1P polyurethanes. This transition has been interpreted as arising from a domain structure with limited short range order. The domain structure is thought to improve in stability and organization with increasing hard segment length as indicated by its monotonic increase with increasing urethane concentration. Such a T_2 transition is not evident in the DSA curves for 2,4-T-1P-60 in Figure 4-10. The second relaxation region in the DSA curves corresponds to the sample-support coupling relaxation described in detail in Chapter II and does not represent a feature of the block polyurethane morphology.

Soft segment relaxations. The remaining polyurethanes studied exhibited low temperature α_s relaxations much less sensitive to sample composition than the α relaxation of 2,4-T-1P polyurethanes. The α_s relaxation process can be attributed to the glass transition which occurs in soft segment domains of the phase separated structure. The α_s relaxation of 2,4-T-2P occurred at about -63°C and was not strongly dependent on hard segment content over the concentration range examined. An increase in soft segment block length caused a dramatic improvement in phase separation of 2,4-TDI polyurethanes. The width of the α_s relaxation is greater than that of the α relaxation of 2,4-TDI/PTMO as can be seen in Figure 4-23. The breadth of a plot of the dynamic mechanical loss modulus vs. reciprocal temperature has been found to be inversely proportional to the activation energy of the relaxation

Figure 4-23. Normalized Loss Modulus vs. Inverse Temperature for 2,4-TDI/PTMO (14 wt.% Hard Segments) and Three 2,4-T-2P Concentrations.

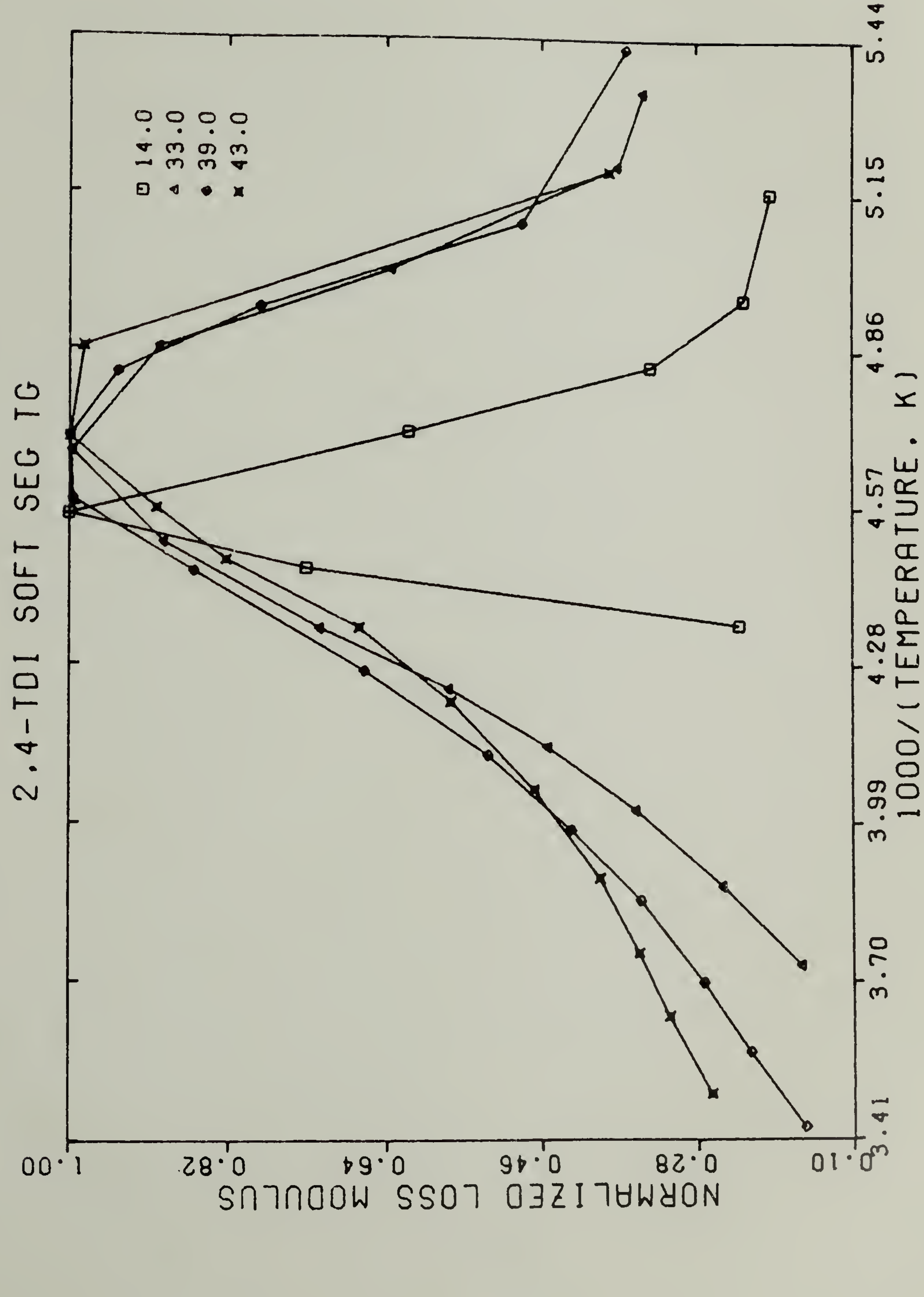
2.4-TDI SOFT SEG TG
1000/(TEMPERATURE. K)
3.41
3.70
3.99
4.28
4.57
4.86
5.15
5.44
NORMALIZED LOSS MODULUS
1.00
0.82
0.64
0.46
0.28
0.10
14.0
33.0
39.0
43.0

(24). At lower temperatures the relationship is not exact since the curves may be asymmetric. The width of the α_s relaxation at half maximum is three times larger than that of the α relaxation. The activation energy was found to decrease from 200 kJ/mole for the α to 120 kJ/mole for the α_s relaxation process. The width of the α_s peak is constant over the hard segment concentration range examined. This indicates that the development of a well organized hard segment phase, which gives rise to an α_h relaxation for 2,4-T-2P-43, has no effect on the mechanism of the α_s relaxation.

The increase in the α_s relaxation temperature for 2,6-T-1P samples with increasing hard segment content is caused by extreme broadening of the relaxation maximum due to increasing hard block crystallinity. This is readily apparent in Figure 4-24. Huh and Cooper (3), Seefried and coworkers (9,10), and Ferguson (7) have observed similar effects in dynamic mechanical studies of MDI polyurethanes. This behavior is similar to changes in dynamic mechanical and dielectric glass transition relaxation processes in nylon, PET and other semicrystalline polymers as the amount of crystallinity increases (25). The activation energy of the α_s process in 2,6-T-1P was found to decrease significantly as the hard segment content increased, again reflecting the influence of the increasingly crystalline hard segment on soft segment motions. Similar results have been noted for the decrease in activation energy of the PET α relaxation with increasing degree of crystallinity (25,26). The activation energy decrease corresponds to the increase in the width at half maximum of the loss peaks in Figure 4-24.

Figure 4-24. Normalized Loss Modulus vs. Inverse Temperature for 2,6-TDI/PTMO (14 wt.% Hard Segments) and Three 2,6-T-1P Concentrations.

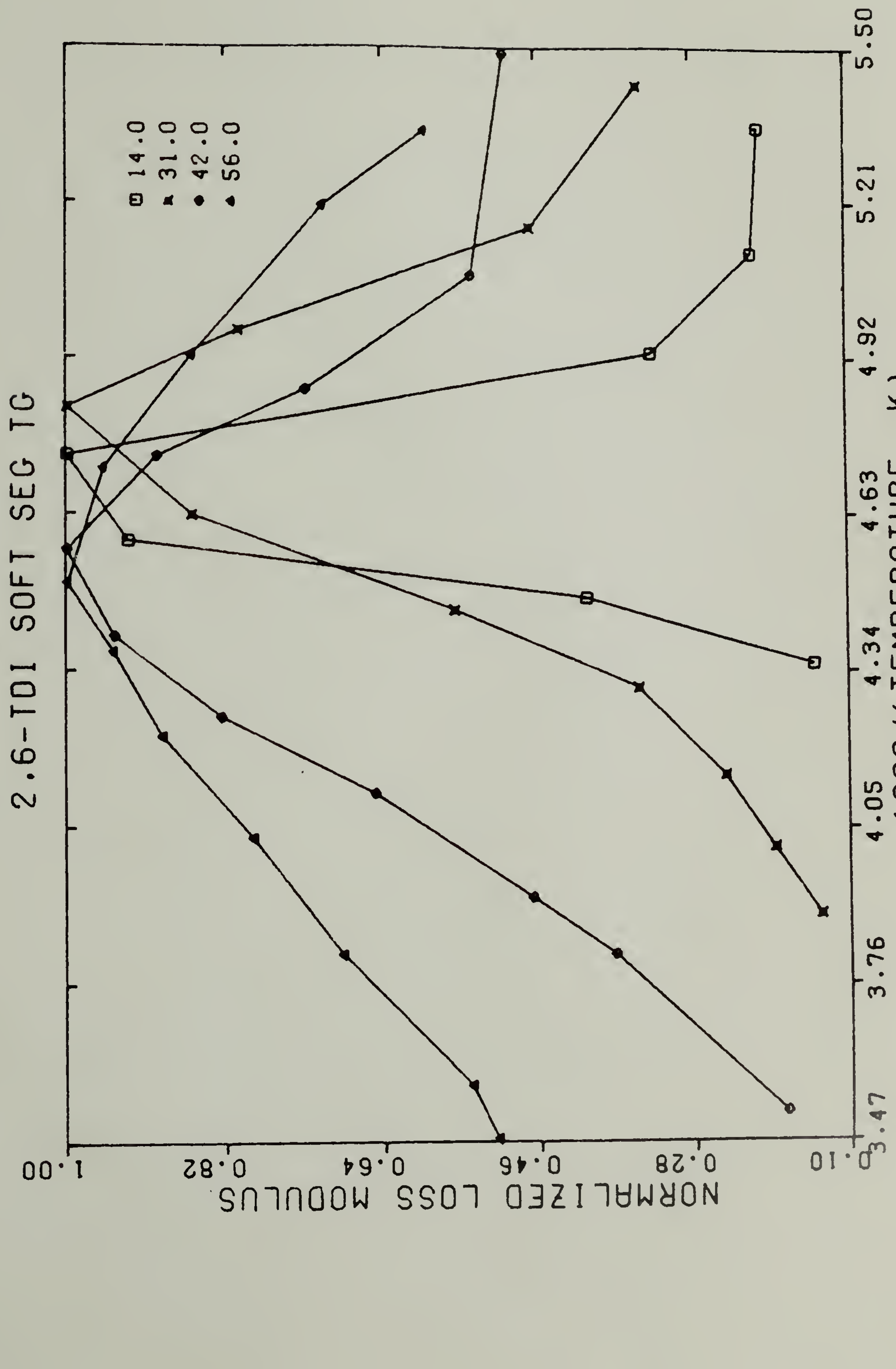
2.6-TDI SOFT SEG TG
NORMALIZED LOSS MODULUS
1.00
0.82
0.64
0.46
0.28
0.10
1000/(TEMPERATURE. K)
3.47
3.76
4.05
4.34
4.63
4.92
5.21
5.50
□ 14.0
✕ 31.0
● 42.0
▲ 56.0

The 2,6-T-2P polyurethanes exhibited the lowest temperature α_s relaxation of any of the block polyurethanes studied. A slight rise in activation energy and decrease in the temperature of the α_s relaxation occurred when the hard segment content increased from 19 to 27 wt.%. This behavior can be attributed to the increasing purity of the soft segment phase. As the hard segment content increases the hard block sequence length also increases, and the longer hard segments display a greater tendency to form a more highly organized separate phase in preference to mixing with the soft segment material. When a well developed hard segment phase has formed in 2,6-T-2P-43, these crystalline regions exert a similar broadening effect on the α_s relaxation to that noted for highly crystalline 2,6-T-1P polymers. The activation energy was found to decrease significantly and the α_s relaxation temperature increased when the hard segment content reached 43 wt.%.

Upon repetition of the dynamic mechanical tests, the activation energy for the α_s relaxation of the two highest hard segment content 2,6-T-2P polyurethanes showed an increase of about 250% over the first determination, as can be seen from Figure 4-22. The increase in activation energy and corresponding narrowing of the α_s relaxation can be understood in terms of a change in composition of the soft segment phase on heating. Longer length hard segments are transferred from the soft segment to the hard segment phase during the thermal treatment. This leads to a narrower distribution of relaxation times and a corresponding narrowing of the α_s loss process when the same samples are reevaluated. Changes in the α_s relaxation temperature from run to run may not be significant in light of the change in breadth of the loss process.

Only the 2,6-T-2P polyurethanes exhibited a relaxation associated with crystallization, and later melting, of the soft segments. The position of the crystallization maximum was estimated from the location of tan(δ) at the relaxation maximum and was somewhat difficult to characterize accurately due to extreme overlapping of the α_s and α_c relaxations, as evident in Figure 4-16. Melting occurred over the region from 2-7°C in all samples. Phase segregation in 2,6-T-2P samples is well developed to the point that the small amount of hard segment mixing in the soft segment results in freedom from restrictions imposed hard segment hydrogen bonding. The soft segment is then able to crystallize above the glass transition after being quenched to below T_g from above the melting temperature.

Hard segment relaxations. For the 2,6-TDI polyurethanes, the δ relaxation temperature increased with increasing hard segment content as did the α_h relaxation temperature of 2,4-T-2P. This effect can more accurately be ascribed to an increase in hard block length as hard segment content increased. The longer hard segment lengths can form a more ordered structure which melts or dissociates at higher temperatures. Peebles (27) has shown that the hard block length is actually greater than that which would be predicted on a molar basis for a two stage polyurethane reaction similar to the procedure used to synthesize the materials characterized in this study. Employing the number average hard segment length at 99% conversion and a μ value of 3 from Peebles' results, the equation given by Flory (28) can be used to obtain the melting temperature for an infinite chain.

$$\frac{1}{T_m} = \frac{2R}{n\Delta H_n} + \frac{1}{T_m^{\infty}} \tag{4-2}$$

T_m is the melting temperature of a chain n units long, T_m^{∞} the melting temperature for infinite molecular weight material, and ΔH_n the heat of fusion per repeat unit. A plot of the inverse of the δ relaxation temperature against the inverse of the hard segment length, n, is shown in Figure 4-25. The δ relaxation temperatures for both 2,6-TDI polyurethanes were found to fit a straight line with identical values of T_m^{∞}, within experimental error, of 222°C for 2,6-T-2P and 227°C for 2,6-T-1P. The hard segment δ relaxation is dependent upon chain length, and is depressed over the value for an infinite chain only by the presence of end groups, in this case the soft segments, which cannot enter the hard segment crystals.

From the slope of the lines, the heat of fusion per repeat unit, ΔH_n, was calculated as 64 J/g for 2,6-T-2P and 82 J/g for 2,6-T-1P. The hard segment in 2,6-T-1P is more highly organized, as the heat of fusion per segment, the unit contained within the brackets with subscript m in Figure 4-1, is about 25% higher than the value for 2,6-T-2P. This could occur if a greater amount of soft segment is mixed in the hard segment phase of 2,6-T-2P. Such an event is unlikely according to current polymer-polymer thermodynamic theories, which maintain that the degree of mixing of two components decreases as molecular weight increases (29,30). Some caution should be exercised in the interpretation of the

Figure 4-25. Reciprocal of Average Hard Segment Length vs. 1/T for the 2,6-TDI Polyurethane δ Relaxation.

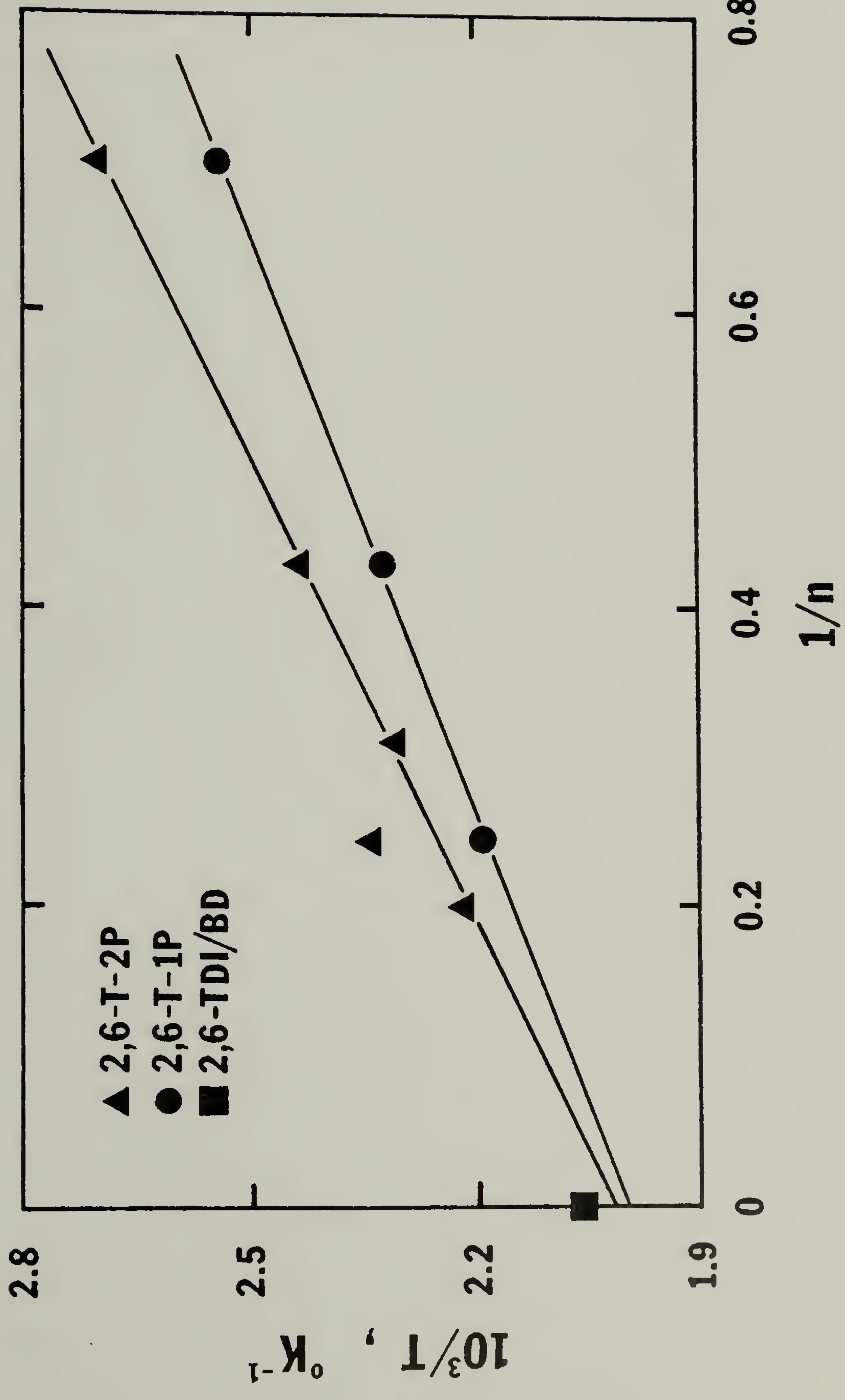
▲ 2,6-T-2P
● 2,6-T-1P
■ 2,6-TDI/BD
$10^3/T$, °K^{-1}
2.8
2.5
2.2
1.9
0
0.2
0.4
0.6
0.8
1/n

heat of fusion results, as the equation given by Flory applies to the melting temperature while the δ relaxation temperature, which has no thermodynamic basis, was employed in this study.

Harrell (21) has noted that the melting point increased with hard block length while the degree of crystallinity did not change in a DSC study of nonhydrogen bonding polyurethane elastomers. The degree of organization in a hard segment polymer was found to be superior to that of a hard segment in a block polyurethane. A value of ΔH_n of about 40 J/g was determined for these materials, considerably less than for the 2,6-TDI hard segments due to the absence of hydrogen bonding interactions in Harrell's piperazine-containing samples.

The δ relaxation, as defined in this study, did not exceed 185°C while the 2,6-TDI/BD hard segment had a melting temperature of about 200°C. The crystalline hard segment domains in 2,6-TDI polyurethanes can be seen to be more poorly organized than in the hard segment polymer due to their shorter lengths and the possibility of inclusion of soft segments into the hard segment domain regions. Similar results that show an increasing hard segment melting relaxation temperature have been reported by Ferguson and coworkers (7) for MDI polyurethanes of increasing hard segment concentration.

The increase in the α_h relaxation temperature with increasing hard segment content for 2,4-T-2P parallels the results of Kraus and Rollman (31) who studied S-B-S and S-I-S block copolymers of varying block molecular weight. They found that as block length increased, the hard segment relaxation shifted to higher temperatures while the soft block relaxation shifted to lower temperatures. They also demonstrated that the hard segment relaxation can be lowered by mixing of soft segment into the hard segment phase at a given hard block length. By employing the theory of Meier (32), they concluded that samples which contained no compositionally pure phases could still give rise to typical block copolymer dynamic mechanical relaxation behavior. The existence of compositionally pure phases in 2,4-T-2P polyurethanes is doubtful. Schneider and Paik Sung (14) have estimated that about 11 to 19 wt.% hard segment is mixed into the soft phase in 2,4-T-2P polyurethanes. The hard segment α_h relaxation occurs at a much lower temperature in 2,4-T-2P polyurethanes than in the pure hard segment, indicating that a compositionally pure hard segment phase may not be present. The existence of specific interactions of the hard and soft segment by hydrogen bonding further enhances the presumption that 2,4-T-2P polyurethanes contain no pure hard or soft phase but consist primarily of interlayer material.

The α_h relaxation in 2,6-TDI block polyurethanes could only be clearly observed for 2,6-T-2P-43. This sample contained sufficiently well developed hard segment domains that both an amorphous α_h and a crystalline melting δ relaxation were detectable. During the second examination of this sample, shown in Figure 4-21, the α_h relaxation increased by about 10°C but did not change in intensity, an effect which can be attributed to the presence of a slightly greater degree of crystallinity in the hard segment after thermal treatment.

Degree of phase segregation. The relative degree of phase segregation of the various block polyurethanes studied can be estimated from their dynamic mechanical response. The 2,4-T-1P samples displayed the least amount of phase segregation by virtue of the highly composition dependent α relaxation. The 2,6-T-2P polyurethanes possessed the soft segment phase of greatest purity as evidenced by the temperature of the α_s relaxation, closest to that of the PTMO homopolymer, as well as the ability of the soft segment to crystallize above its T_g. The soft segment domains in 2,4-T-2P and 2,6-T-1P polyurethanes were intermediate in purity, with the 2,6-T-1P samples containing a slightly greater amount of hard segment mixed into the soft segment than 2,4-T-2P, which inhibited soft segment crystallization. Hard segment domains in 2,4-T-1P were not detected in this study. Of the hard segment domains found, those in 2,4-T-2P were clearly the least organized. A large hard segment concentration was found to be necessary in order for a well defined α_h relaxation process to occur. The 2,6-TDI polyurethanes contained highly ordered hard segments, due to the ability of the hard blocks to crystallize. The 2,6-T-1P polyurethanes appear to be the more highly ordered of the two, as these materials exhibited a higher temperature δ relaxation for a given hard segment length and a higher heat of fusion per segment. The degree of phase segregation in the polyurethanes studied is not nearly as well developed as in some nonpolar block copolymers of higher block molecular weight. The polyurethanes displayed broad relaxation processes characteristic of poorly defined phases. No pure component phases are thought to exist in these materials. From their dynamic mechanical response, the degree of mixing in each phase can be seen to depend on soft block molecular weight and hard segment structure.

Effects of phase segregation on modulus. The magnitude of the modulus between α_s and α_h for 2,4-T-2P or δ for 2,6-TDI block polyurethanes was found to be highly dependent upon hard segment content. The presence of a plateau region in modulus-temperature plots has been attributed to phase segregation in block copolymers (33). The hard phase can act to reinforce the plateau modulus in a manner similar to that of fillers in crosslinked elastomers. The hard phase is also thought to act as a crosslinking or anchoring region for the soft segments, a mechanism which gives rise to a plateau in modulus above the soft segment T_g. An increase in hard segment content can induce a higher value of the plateau modulus through either of these mechanisms.

The nature of the hard segment domains, either crystalline or amorphous, does not appear to be important to plateau modulus enhancement in TDI block polyurethanes, provided that the hard block length is sufficient. This is illustrated in Figure 4-26, a modulus vs. temperature comparison of 2,4- and 2,6-T-2P-43. Both polyurethanes exhibit identical storage moduli in the region between the 2,6-T-2P-43 α_c and 2,4-T-2P-43 α_h relaxations. The difference in modulus between α_s and α_c can be accounted for by crystallinity of the soft segment in the 2,6- sample. A comparison of these two polyurethanes containing 39 wt.% hard segments indicates that the plateau modulus is much lower for 2,4-T-2P-39. A well developed α_h relaxation maximum was not present in this sample. A hard segment capable of crystallization can increase the temperature range of plateau modulus enhancement or be a more efficient method of increasing the plateau modulus, but an equal effort can be provided by a well developed glassy urethane domain structure.

Figure 4-26. Comparison of the Storage and Loss Modulus of 2,4-T-2P-43 and 2,6-T-2P-43 as a Function of Temperature at 11 Hz.

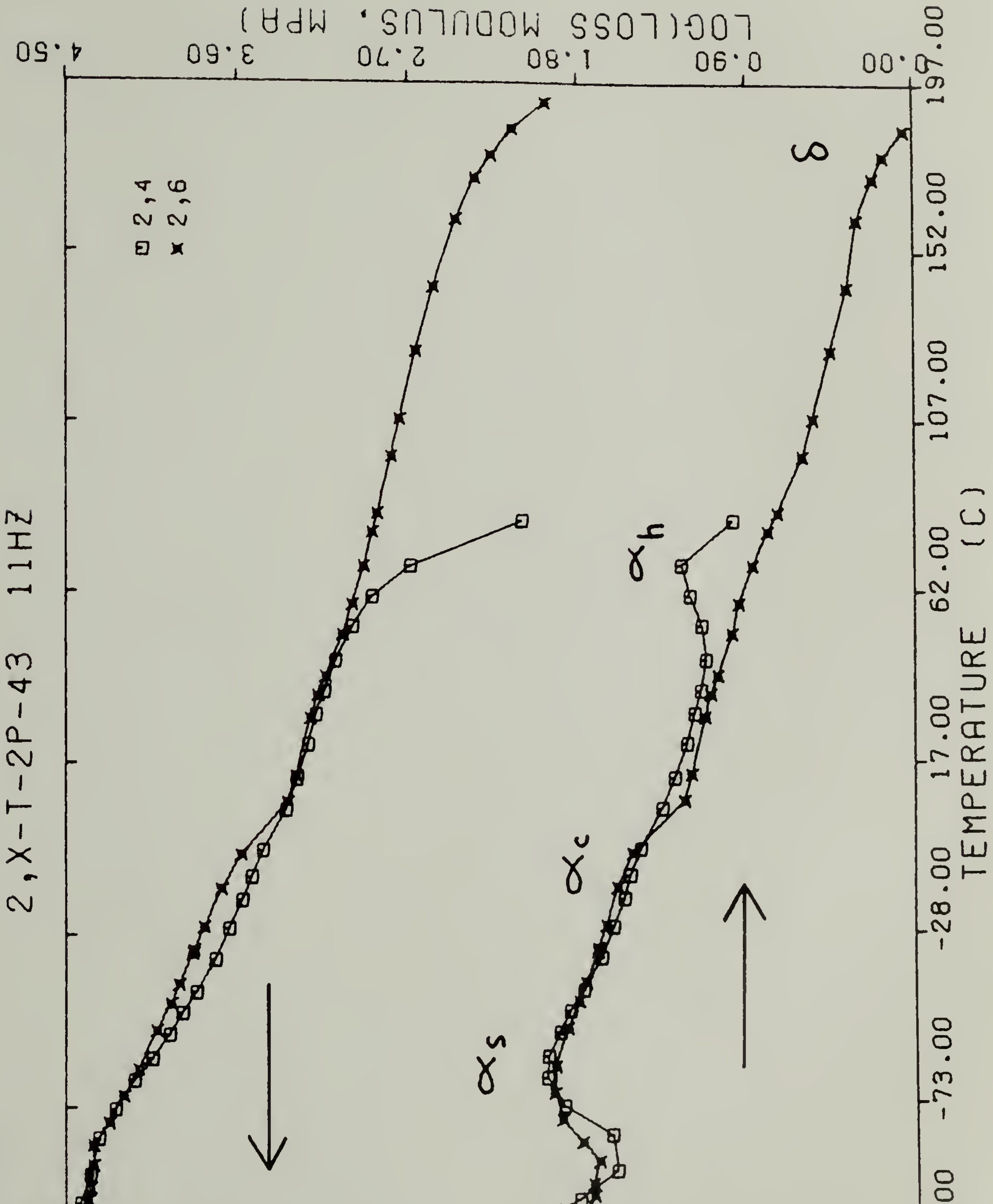
2,X-T-2P-43 11HZ
□ 2,4
✖ 2,6
LOG(STORAGE MODULUS, MPA)
3.50
2.60
1.70
0.80
-0.10
-1.00
LOG(LOSS MODULUS, MPA)
4.50
3.60
2.70
1.80
0.90
0.00
TEMPERATURE (C)
-118.00
-73.00
-28.00
17.00
62.00
107.00
152.00
197.00
α_s
α_c
α_h
δ

The plateau modulus in 2,6-TDI polymers was found to be dependent on hard segment content rather than on hard block length. Comparisons of the modulus levels between two 2,6-TDI samples with the same hard segment content, such as in Figure 4-17, show that the plateau modulus of the 2,6-T-2P polyurethane is only about 10% higher at temperatures above the soft segment melting point. In contrast, for two block polyurethanes with the same hard block length, such as 2,6-T-1P-42 and 2,6-T-2P-27, the plateau modulus of the 2,6-T-1P sample is about 250% greater.

Conclusions

The structure of the diisocyanate moiety has a significant effect on hard and soft segment dynamic mechanical response, which is also reflected in the properties of the block polyurethanes studied. An asymmetric 2,4-TDI hard segment displays only an amorphous α relaxation while a symmetric 2,6-TDI hard segment has a broadened glass transition relaxation and is capable of crystallization, retaining a high modulus to the melting temperature, about 212°C. Similarly for soft segment polymers, the relaxation associated with the glass transition occurs at low temperatures for both 2,4- and 2,6-TDI/PTMO but the latter crystallizes above T_g and later melts at about 10°C.

The dynamic mechanical response of TDI block polyurethanes is sensitive to the degree of phase segregation in these materials. Polyurethanes composed of 2,4-T-1P contain a highly nonhomogeneous soft segment phase, as evidenced by the compositionally dependent α relaxation temperature. A doubling in the soft segment molecular weight causes phase segregation to occur in 2,4-T-2P, as a relaxation process associated with each phase is evident. The 2,6-TDI block polyurethanes studied are also phase segregated, displaying an α_s relaxation corresponding to the soft segment T_g and a δ relaxation, associated with hard block melting. The α_s relaxation temperature is affected by soft segment phase purity and the degree of crystallinity. The δ relaxation temperature increases with increasing hard block length. The level of the plateau modulus between the low and high temperature relaxations in phase segregated polyurethanes is strongly dependent upon hard segment content.

The 2,6-T-2P samples display an additional α_c relaxation associated with crystallization of the soft segment above its glass transition, suggesting that the soft segment phase is relatively free of intermixed hard blocks. A hard segment glass transition was observed for the polyurethane sample in this series with the highest hard segment content, indicating that hard block organization is also well developed in these materials. The 2,6-T-1P polyurethanes, however, contain fewer soft segments mixed in the hard block domains than the 2,6-T-2P samples.

Comparison of the block copolyurethane relaxations with corresponding loss processes of the hard and soft segment polymers indicates that the organization of phases in block polyurethanes is inferior due to the short block length and significant amount of intersegmental mixing in the domains. Samples with crystallizable hard segments and the higher block length amorphous samples are composed of domains with a sufficiently small degree of mixing that typical block copolymer dynamic mechanical response is exhibited.

REFERENCES

1. T. Kajiyama and W.J. MacKnight, Trans. Soc. Rheol., 13, 527 (1969).
2. T. Kajiyama and W.J. MacKnight, Macromol., 2, 254 (1969).
3. D.S. Huh and S.L. Cooper, Polym. Eng. Sci., 11, 369 (1971).
4. H.N. Ng, A.E. Allegrezza, R.W. Seymour, and S.L. Cooper, Polymer, 14, 255 (1973).
5. S.L. Samuels and G.L. Wilkes, J. Polym. Sci., C, 43, 149 (1973).
6. J.L. Illinger, N.S. Schneider, and F.E. Karasz, Polym. Eng. Sci., 12, 25 (1972).
7. J. Ferguson, D.J. Hourston, R. Meredith, and D. Patsavoudis, Eur. Polym. J., 8, 369 (1972).
8. C.G. Seefried, J.V. Koleske, and F.E. Critchfield, J. Appl. Polym. Sci., 19, 2493 (1975).
9. C.G. Seefried, J.V. Koleske, and F.E. Critchfield, J. Appl. Polym. Sci., 19, 2503 (1975).
10. C.G. Seefried, J.V. Koleske, and F.E. Critchfield, J. Appl. Polym. Sci., 19, 3185 (1975).
11. C.G. Seefried, J.V. Koleske, F.E. Critchfield, and J.L. Dodd, Polym. Eng. Sci., 15, 646 (1975).
12. N.S. Schneider, C.S. Paik Sung, R.W. Matton, and J.L. Illinger, Macromol., 8, 62 (1975).
13. C.S. Paik Sung and N.S. Schneider, Macromol., 8, 68 (1975).
14. N.S. Schneider and C.S. Paik Sung, Polym. Eng. Sci., 17, 73 (1977).
15. C.S. Paik Sung and N.S. Schneider, Macromol., 10, 452 (1972).
16. G.A. Senich and W.J. MacKnight, Polymer Preprints, 19(1), 11 (1978).
17. G.A. Senich and W.J. MacKnight, Amer. Chem. Soc., Adv. Chem. Series, S.L. Cooper, ed., accepted for publication.

18. T. Kajiyama, Ph.D. Dissertation, University of Massachusetts (1969).

19. I.M. Ward, "Mechanical Properties of Solid Polymers," p. 177, Wiley-Interscience, London (1971).

20. J.H. Saunders and K.C. Frisch, "Polyurethanes: Chemistry and Technology," p. 106, Interscience Publishers, New York (1962).

21. L.L. Harrell, Macromol., 2, 607 (1969).

22. J. Brandrup and E.H. Immergut, Eds., "Polymer Handbook," p. III-43, John Wiley & Sons, New York (1975).

23. A.H. Scott, A.T. McPherson, and H.L. Curtis, J. Nat. Bur. Stds., 11, 173 (1933).

24. B.E. Read and G. Williams, Trans. Faraday Soc., 57, 1979 (1961).

25. N.G. McCrum, B.E. Read, and G. Williams, "Anelastic and Dielectric Effects in Polymeric Solids," p. 511, John Wiley & Sons, London (1967).

26. S. Saito, Kolloid Z., 189, 116 (1963).

27. L.H. Peebles, Macromol., 7, 872 (1974).

28. P.J. Flory, "Principles of Polymer Chemistry," p. 570, Cornell University Press, Ithaca, New York (1953).

29. L.P. McMaster, Macromol., 6, 760 (1973).

30. R.H. Lacombe and I.C. Sanchez, J. Phys. Chem., 80, 2568 (1976).

31. G. Kraus and K.W. Rollman, J. Polym. Sci., Phys., 14, 1133 (1976).

32. D.J. Meier, Polym. Preprints, 15(1), 171 (1974).

33. G.M. Estes, S.L. Cooper, and A.V. Tobolsky, J. Macromol. Sci., Rev. Macromol. Chem., C4, 313 (1970).

CHAPTER V

FOURIER TRANSFORM INFRARED THERMAL ANALYSIS OF A BLOCK POLYURETHANE

Introduction

Several types of hydrogen bonds can be formed in polyurethane elastomers. In all cases the hydrogen of the N-H group in the urethane linkage serves as the proton donor. A number of acceptor sites are possible; the carbonyl group and the oxygen atom α to the carbonyl in the urethane linkage and polyester and the ether group of the polyether. Early work on urethane elastomers led to the conclusion that ester carbonyl groups are predominantly involved in polyester urethane hydrogen bonding while for polyether urethanes the urethane carbonyl is most likely to act as the proton acceptor (1). The presence of hydrogen bonding was detected by absorption bands lower in frequency than the free N-H and C=O stretching absorbances. Studies on association of low molecular weight urethanes and ethers conclude that hydrogen bonding to ether oxygen and the urethane carbonyl is possible in these systems, with a high concentration of urethane favoring the latter (2). A subsequent publication estimates that about 85% of the N-H groups form hydrogen bonds in a 2,4-TDI (2,4-toluene diisocyanate) polyester urethane (3).

Block or segmented polyurethanes have also been studied. These materials consist of three components, a diisocyanate, a low molecular weight diol and a high molecular weight diol, typically a polyether or polyester. The first two components combined form the hard segment, responsible for crosslinking and reinforcement of the elastomers. The polyether or ester soft segment gives the material a rubbery response at room temperature. Studies of a series of polyether containing block polyurethanes by Nakayama et al. (4) confirm the observations with model compounds that increasing hydrogen bonding to the ether oxygen occurs as the concentration of the ether links increases, accomplished in this case by an increase in the polyether molecular weight. Seymour and coworkers (5) found that virtually all N-H groups were hydrogen bonded but that only 60% of the urethane carbonyl groups were similarly associated in a series of MDI (p,p'-diphenylmethane diisocyanate) segmented polyurethanes. They suggest that the N-H groups also hydrogen bond to the soft segment at the interface of the phase separated structure or in the soft segment itself due to incomplete separation. Stretching experiments to 300% elongation led them to conclude that changes in the extent of hydrogen bonding do not play an important role in determining elastic properties of these materials.

A study of model TDI hard segments by Sung and Schneider (6) demonstrates that the oxygen α to the carbonyl in the urethane linkage, the urethane alkoxyl oxygen, is bonded to a fraction of the N-H protons. This complicates the quantitative determination of hard and soft segment interactions. About 95% of the N-H groups were found to be hydrogen bonded at room temperature, but only 50 and 80% of the carbonyl groups were hydrogen bonded in 2,4-TDI and 2,6-TDI polyurethanes, respectively. The greater degree of urethane to ether hydrogen bonding in

2,4-TDI polyurethanes was assumed to crosslink the soft segment phase and the resulting elevation of the glass transition temperature predicted from a crosslinking model correlates with that observed as the composition varied from 31 to 61 wt.% hard segments (7).

The temperature dependence of hydrogen bonding in polyurethanes has been studied in order to relate hydrogen bond dissociation to structural organization. MacKnight and Yang (8) determined that a series of TDI and MDI polyurethanes are hydrogen bonded to the extent of 75% or less below T_g. They were able to show that the temperature dependence of the integrated absorbance of the N-H stretching band exhibits transitions corresponding to the glass transition and melting point of these materials. A study of 2,4- and 2,6-TDI block polyurethanes by Sung and Schneider (9) concludes that hydrogen bond dissociation bears little relation to the state of structural organization. The onset temperature for dissociation of hydrogen bonded N-H and carbonyl of 2,6-TDI polyurethanes occurred at about 65°C, independent of urethane content. For 2,4-TDI elastomers, hydrogen bonded N-H began to dissociate at temperatures of 40 to 60°C while the bonded carbonyl fraction changed insignificantly to 150°C. These results suggest that hydrogen bonding to the 4 position of the TDI ring is stronger than to the 2 position due to some steric hindrance at the latter. A recent systematic study of the temperature variation of hydrogen bonding in polyether and polyester MDI segmented elastomers (10) revealed that the extent of interurethane hydrogen bonding is higher in materials having better phase separation. Hard to soft segment hydrogen bonding is weaker and dissociates first when these polyurethanes are heated. The ΔH of hydrogen bond dissociation can be used as an indication of hard domain perfection, and it was found to increase with increasing hard and soft segment length.

This study was undertaken to determine if the technique of Fourier Transform infrared spectroscopy (FT-ir) could be applied to a thermal study of hydrogen bonding in segmented polyurethanes. Previous thermal studies have employed curve resolving techniques, not without some drawbacks, to decompose overlapping absorption bands. It was hoped that the subtractive capabilities of the FT-ir and its inherently greater resolution could give additional information about the state of hydrogen bonding in these materials.

Experimental

A linear block copolymer with 43 wt.% of a hard segment composed of 2,6-TDI and 1,4-butanediol (BD) and a 2060 molecular weight poly(tetramethylene oxide) (PTMO) soft segment was supplied through the courtesy of Dr. N.S. Schneider of the Army Materials and Mechanics Research Center, Watertown, MA. This polyurethane corresponds to 2,6-T-2P-43 employed in the dynamic mechanical study of phase segregation in block polyurethanes detailed in Chapter IV. The polymer was cast from N,N-dimethylformamide solution onto a 25 mm diameter NaCl plate. The resulting film, about 3 μm in thickness, was subjected to a thermal treatment similar to that described in Chapter IV with the exception that the film was slowly cooled in an oven under vacuum.

A room temperature survey spectrum of the polyurethane film was recorded on a Perkin-Elmer model 283 infrared spectrophotometer.

For the temperature scans the sample was placed in an aluminum block containing two resistance heaters and insulated with asbestos sheathing. Sample temperature was maintained to within 1°C with a Versatherm temperature controller and monitored by a copper-constantan thermocouple junction placed directly on the film. The temperature was held constant for about five minutes before collection of the spectra was initiated. Infrared spectra were recorded with a Digilab FTS-15 Fourier Transform spectrometer by averaging 256 scans at a resolution of 2 cm^{-1}. A dry nitrogen flow was maintained over the film throughout the experiments.

Results

A survey spectrum of the block polyurethane studied is shown in Figure 5-1. A strong absorption attributed to the stretching of hydrogen bonded amines is present at 3283 cm^{-1}. The free N-H stretch is not resolvable as a separate band in this spectrum but may be noted as the broadened region on the high frequency side of the bonded amine absorption. Several C-H stretching vibrations can be noted between 3100 and 2600 cm^{-1}. The asymmetric stretching of methylene units at 2942 cm^{-1} was used as an internal standard, as will be discussed later. Two very strong carbonyl peaks are evident, the band at 1733 cm^{-1} attributed to stretching of free carbonyl while the absorption centered at 1691 cm^{-1} arises from stretching of hydrogen bonded carbonyl groups. A band at 1595 cm^{-1}, attributed to C=C stretching in the aromatic ring structure, was also employed as an internal standard. Other band assignments for TDI polyurethanes have been summarized in several

Figure 5-1. Infrared Spectrum of 2,6-T-2P-43 at 25°C.

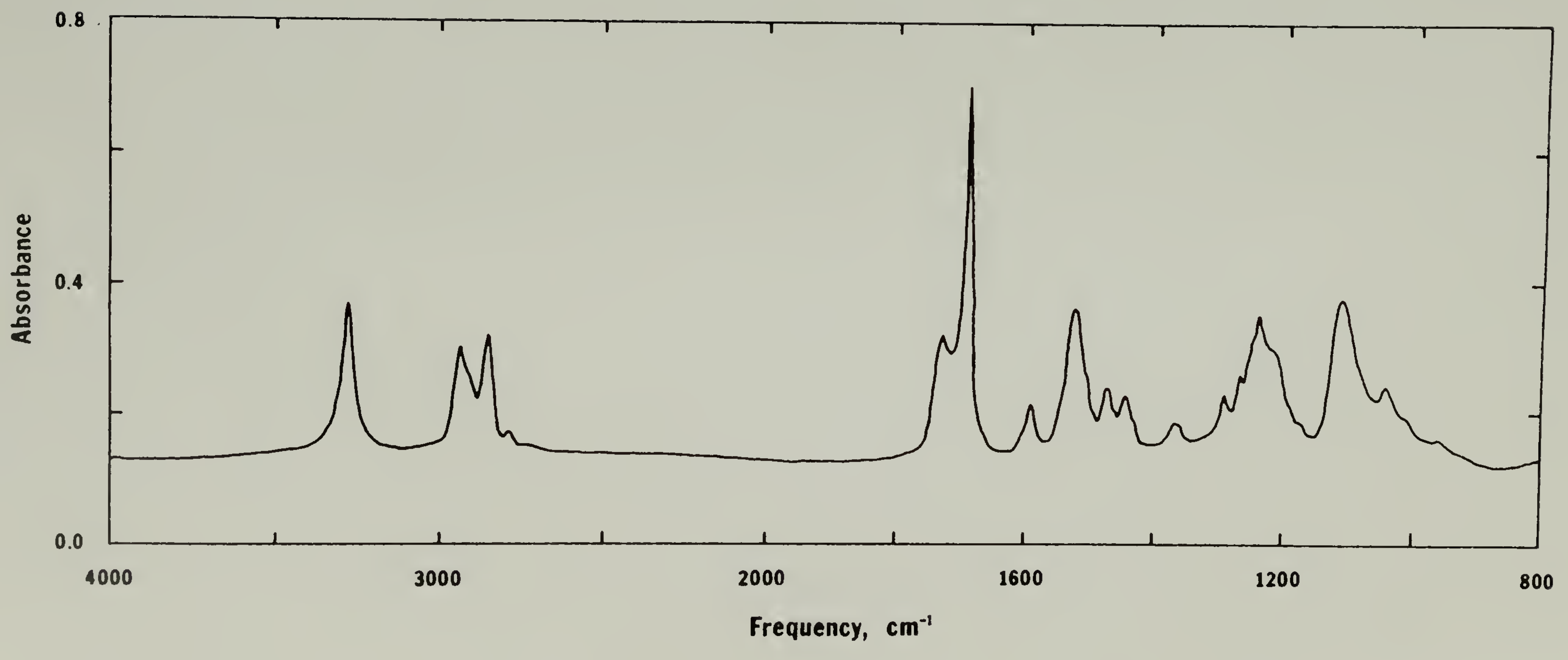
0.8
0.4
0.0
Absorbance
4000
3000
2000
1600
1200
800
Frequency, cm^{-1}

publications (6,8,11).

The infrared spectra of 2,6-T-2P-43 at two temperatures are shown in Figure 5-2. The bonded amine stretching intensity can be seen to decrease at the higher temperature with a corresponding increase in the free N-H stretching absorption. A shift of the bonded N-H maximum from 3283 to 3290 cm^{-1} occurs over this temperature range. A similar increase in the intensity of the free carbonyl absorption at the expense of bonded carbonyl is apparent at the higher temperature. The location of the free amine and both carbonyl absorbance maxima did not change significantly over the course of the investigation.

Quantitative infrared measurements usually employ Beer's law which may be written in the form:

$$A = \varepsilon b c \tag{5-1}$$

where A is the peak absorbance, ε the molar extinction coefficient, b the path length and c the molar concentration. When studying the temperature dependence of infrared absorptions, the band half width and therefore the absorbance can change as a function of temperature. A better measure is the integrated absorbance, that is the area under the absorbance-wavenumber curve, which does not vary with temperature assuming that ε, b and c are not temperature dependent. The total area of the N-H stretch from 3180 to 3470 cm^{-1} and the C=O stretch from 1830 to 1630 cm^{-1} was determined by planimetry at each temperature. Plots of the results, normalized to the 29°C absorptions, vs. temperature are presented in Figure 5-3. The data at 167°C show a decrease in both carbonyl and amine absorbance. This decrease could be

Figure 5-2. Infrared Spectra of 2,6-T-2P-43 in the N-H and C=O Stretching Region at 29 and 98°C.

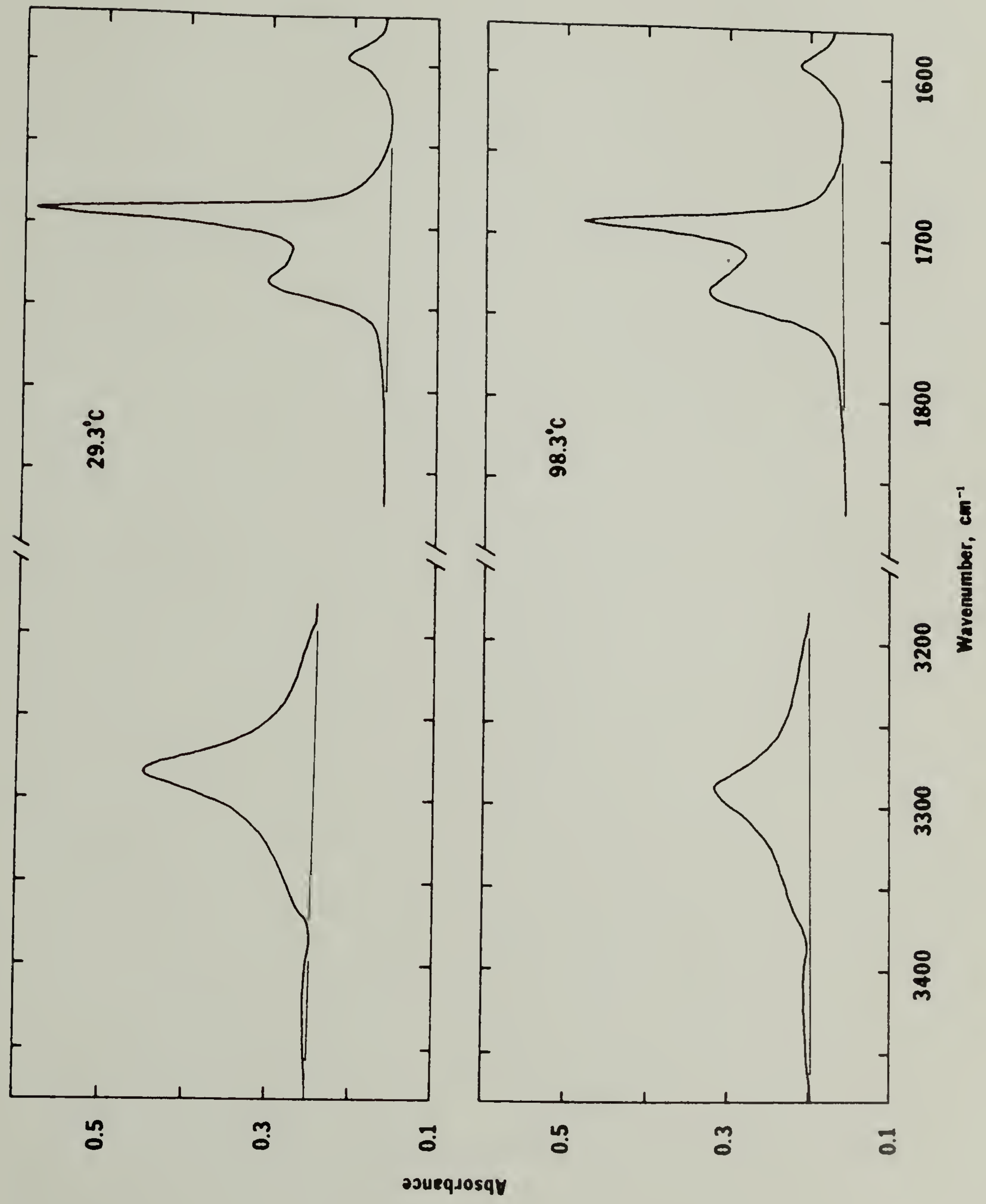
29.3°C
98.3°C
Absorbance
0.5
0.3
0.1
0.5
0.3
0.1
Wavenumber, cm⁻¹
3400
3300
3200
1800
1700
1600

Figure 5-3. Integrated Absorbance Normalized to that at 29°C vs. Temperature (circles C=O stretch; squares N-H stretch).

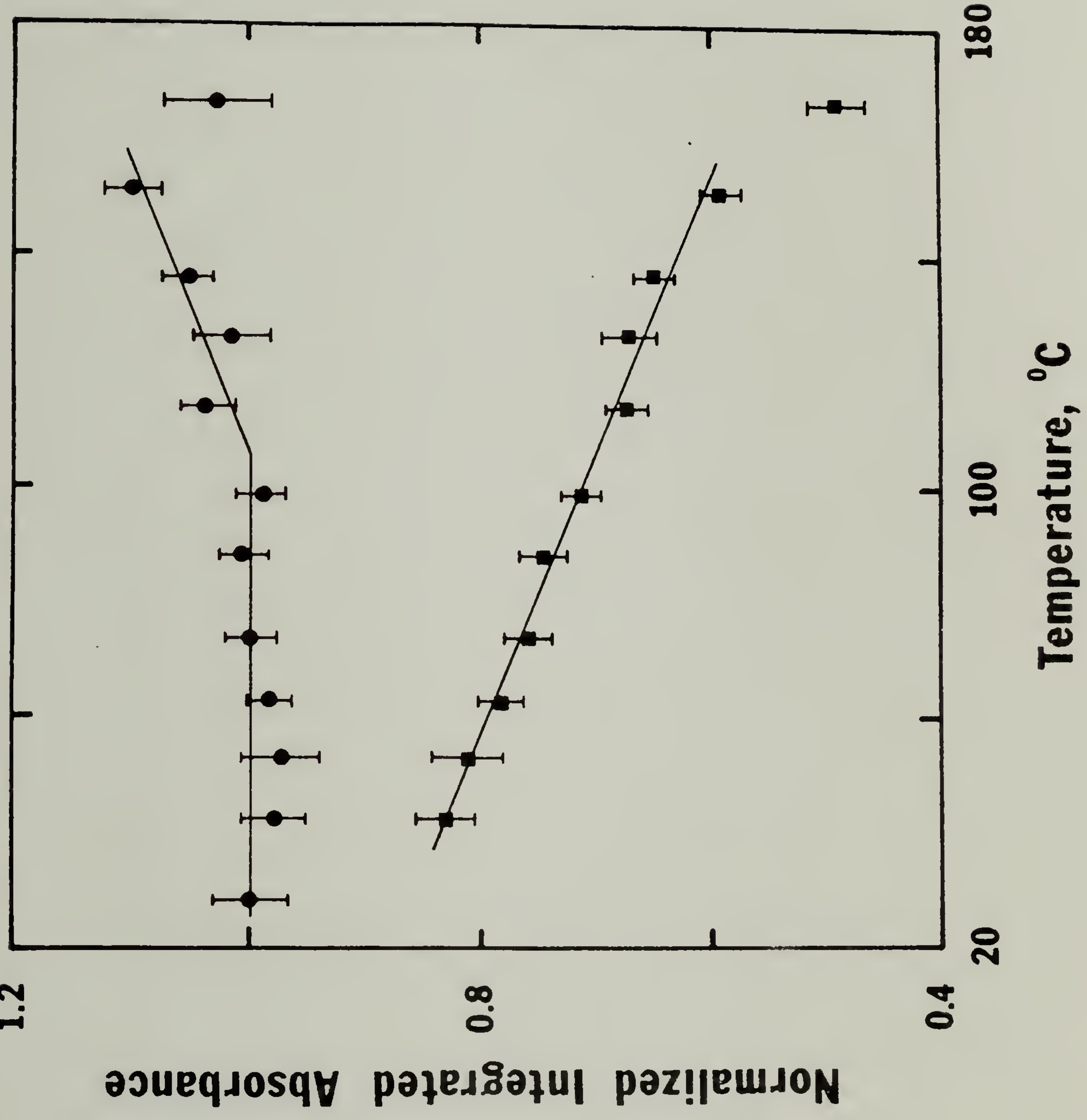
Normalized Integrated Absorbance
1.2
0.8
0.4
20
100
180
Temperature, °C

attributable to a reduction of the amount of material exposed to the incident radiation due to flow of the polymer at this temperature, near the melting point of this polyurethane, determined to be 177°C in a dynamic mechanical study (Table 4-4). In addition, two weak absorbance bands were observed at about 2270 and 2340 cm^{-1}. These absorptions could arise from carbon dioxide or the lower wavenumber peak from free isocyanate. Carbon dioxide and an amine are thought to form during the thermal degradation of the TDI urethane linkage (12,13) and the loss of carbon dioxide on high temperature aging has previously been observed (14,15). For these reasons, the 167°C determination was excluded from further calculations. The decrease in the total amine absorbance can be understood in light of the ratio of the hydrogen bonded to free extinction coefficient for the N-H absorption in urethane model compounds. This ratio has been determined to be about three for several systems (8,11). As the temperature increases, the amount of bonded N-H decreases causing a decrease in the overall amine absorption area. No discontinuity is evident in the slope of the plot of N-H area vs. temperature. Such discontinuities have at times been observed in similar plots for other polyurethanes (8,10). These discontinuities in hydrogen bonding behavior are thought to reflect molecular transitions occurring in the materials. The 2,6-T-2P-43 polyurethane exhibited a weak hard segment glass transition relaxation at 60°C in a dynamic mechanical property study (Table 4-4). No evidence of a discontinuity at the hard segment glass transition is present in Figure 5-3.

The infrared spectra collected at various temperatures were used to study the temperature variation of hydrogen bonding in this block polyurethane. This can be illustrated by the spectra in Figure 5-2 which were used to determine the difference in hydrogen bonding at 29 and 98°C by subtraction of the 98°C spectrum from that at the lower temperature. Figure 5-4 shows the results in the N-H stretching region. Subtraction was accomplished by adjusting the weighting factor for the higher temperature spectrum until the asymmetric C-H stretching band at 2942 cm^{-1} was eliminated in the difference spectrum. The weighting factors employed ranged from 1.11 to 1.06 over the temperature region examined. Such subtractive techniques have been described elsewhere (16). The baseline drawn in Figure 5-4 is constructed over the same frequency region as that for the N-H stretch in Figure 5-2. It is apparent that the bonded N-H absorption is greater in the 29°C spectrum while the free N-H absorption is greater at 98°C, the same results as evident from Figure 5-2. While the shape of the bonded N-H absorption peak changes somewhat as the temperature increases, the position of the bonded N-H maximum remains at a constant position in all the difference spectra collected.

A similar procedure was employed to determine differences in the C=O stretching region. Spectra collected at temperatures up to 151°C were referenced to a 29°C spectrum. Subtraction results obtained from the 98°C determination in the carbonyl region are shown in Figure 5-5. In this instance elimination of the 1595 cm^{-1} band was used as a criterion for subtraction. Scaling factors ranged from 1.05 to 0.95 over the temperature region examined. As in the case of the N-H vibrations, excess bonded carbonyl is present at 29°C while more free

Figure 5-4. Difference Between the 29°C and 98°C Spectra in the N-H Stretching Region.

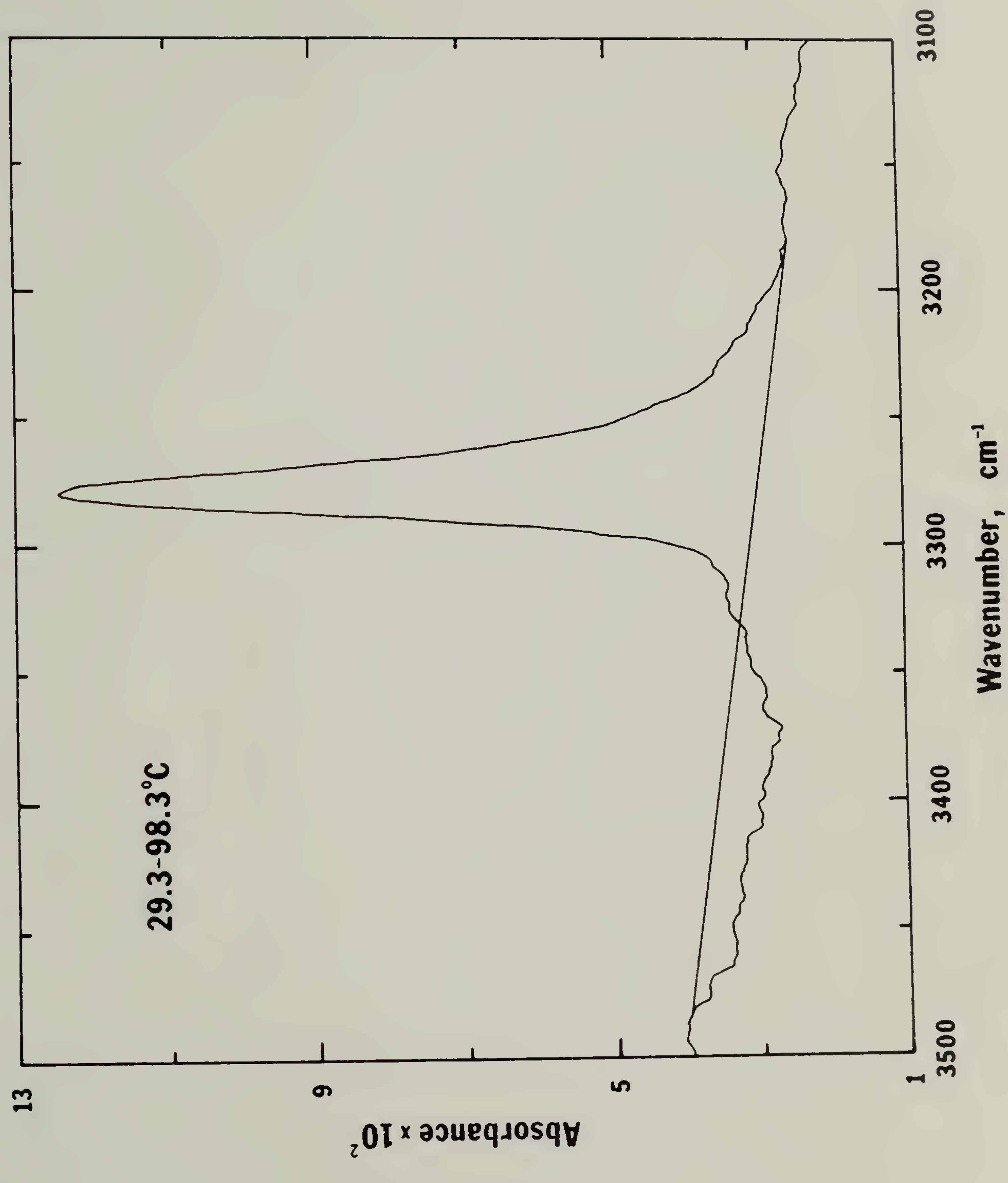
29.3-98.3°C
Absorbance x 10²
13
9
5
1
3500
3400
3300
3200
3100
Wavenumber, cm⁻¹

Figure 5-5. Difference Between the 29°C and 98°C Spectra in the C=O Stretching Region.

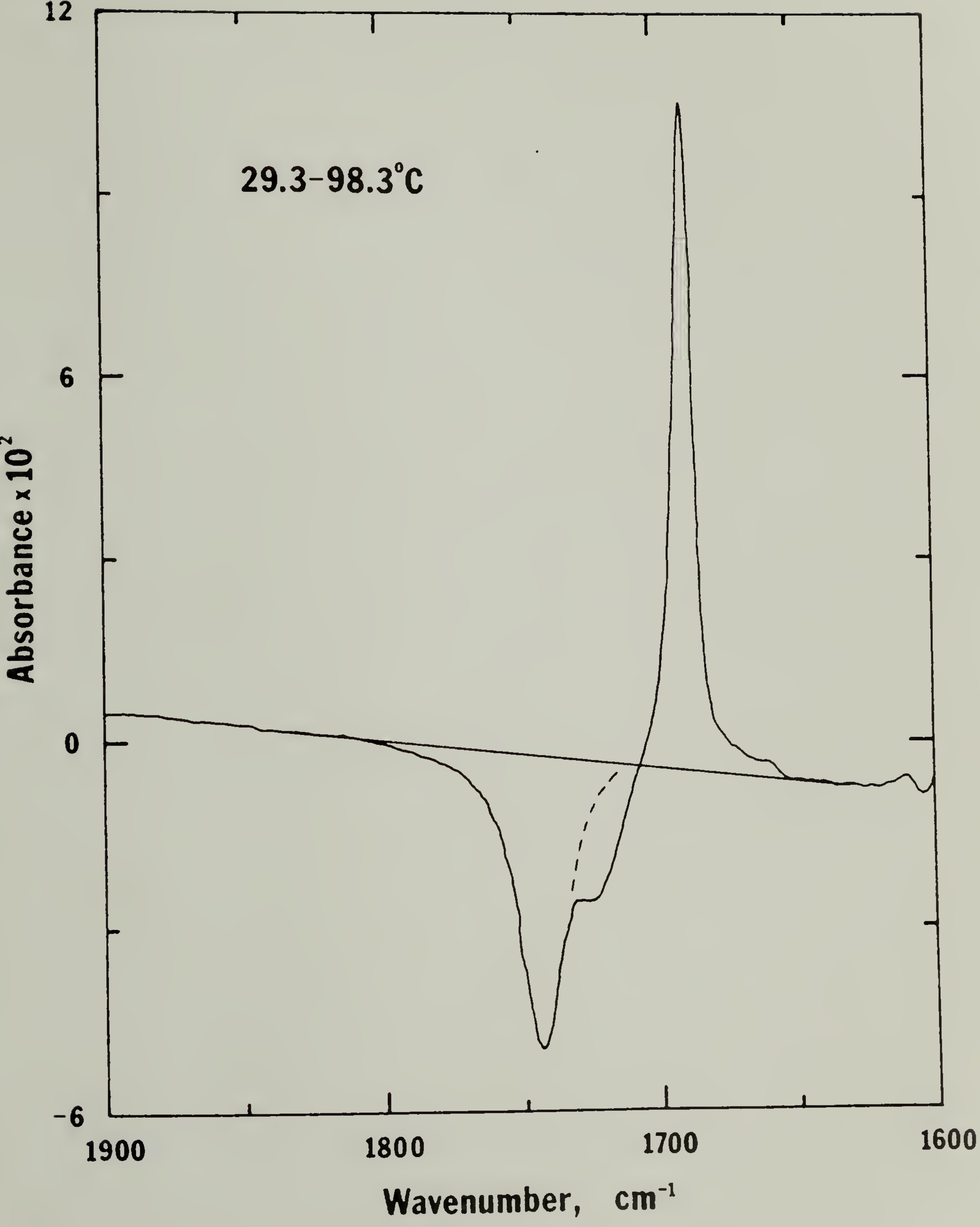
12
6
0
-6
Absorbance x 10^2
29.3-98.3°C
1900
1800
1700
1600
Wavenumber, cm^{-1}

carbonyl is indicated at the higher temperature. An additional feature is present as a shoulder at 1726 cm^{-1}. This shoulder was retained as a negative absorption over a wide variation in the scaling parameter for the subtraction, indicating that it was not an artifact produced by subtraction of bands of differing frequency but a real difference between the spectra at the two temperatures (17).

The area of the bonded N-H and C=0 absorbance difference above the baseline in Figures 5-4 and 5-5 can be taken as a measure of the decrease in concentration of hydrogen bonded species at the temperature of measurement over that at the reference temperature of 29°C. Similarly, the area below the baseline of the free N-H and carbonyl, excluding the contribution of the shoulder at 1726 cm^{-1}, is a measure of the concentration increase in the nonbonded species. These areas were determined by planimetry for each difference spectrum and the results are shown plotted as a function of temperature in Figure 5-6. For each of the bands studied, the integrated absorbance varied linearly with temperature. The slope of the bonded N-H absorption is much greater than that of the free N-H. The slope of the bonded C=0 absorption is about equal to that of the free carbonyl. Since the sample thickness and total N-H concentration is adjusted to be constant at each temperature by variation in the subtraction scaling parameter, the ration of the absorbances was assumed to equal the ratio of the extinction coefficients. This is not generally the case, as the extinction coefficient varies with temperature as:

$$\varepsilon = \varepsilon_0 + \alpha(T - T_0) \qquad (5\text{-}2)$$

Figure 5-6. Integrated Absorbance (arbitrary units) of the Difference Spectra in Four Spectral Regions vs. Temperature. (Reference temperature 29°C; filled points free absorption; open points bonded absorption; circles C=O stretch; triangles N-H stretch.)

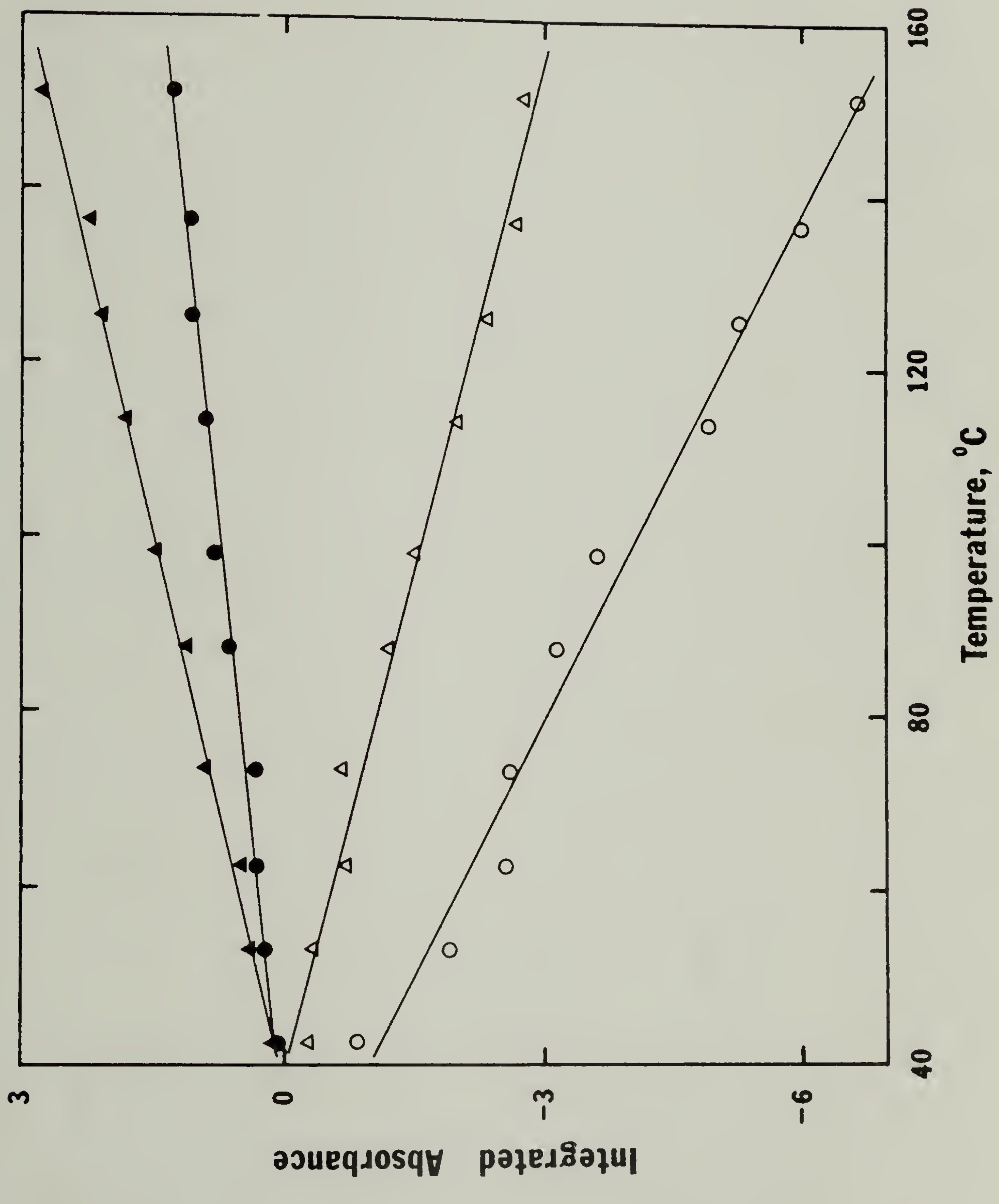
Integrated Absorbance
3
0
-3
-6
Temperature, °C
40
80
120
160

where ε_0 has been experimentally determined at temperature T_0 and the temperature coefficient α is expected to be negative (18). Values of α have been determined experimentally (19) to be about 0.003 ε_0/°C. Since there is no method to determine α for the bonded and free absorptions, the ratio $\alpha_{bonded}/\alpha_{free}$ was assumed to equal the ratio of the extinction coefficients. The ratio of bonded to free N-H stretching extinction coefficients was determined to be 4.60 ± 10%. MacKnight and Yang (3) have determined values from 3.84 to 3.08 for other TDI polyurethanes. The ratio of bonded to free carbonyl stretching extinction coefficients was calculated to be 1.05 ± 10%. This value is similar to results found for other types of carbonyls capable of hydrogen bonding (20-22), which have a bonded to free extinction coefficient ratio between 1.0 and 1.3.

The previous discussion has focused on the spectral differences between the absorbance at a given temperature to that at 29°C, the reference temperature. In order to obtain the fraction of hydrogen bonded N-H and C=O groups as a function of temperature, the amount of bonded and free N-H and C=O at the reference temperature must be known. For the N-H case, this was accomplished by direct integration of the bonded and free absorbance of the 29°C spectrum in Figure 5-2. After taking into account the extinction coefficient difference discussed previously, 87.5% of the N-H groups in the 2,6-T-2P-43 polyurethane were found to be hydrogen bonded. Bonded N-H contents of 75 to 95% have been found for other polyurethanes at room temperature (3,5,6,9, 10). The fraction of bonded N-H at any other temperature can be determined from the reference spectrum by subtracting the integrated absorbance of the difference spectrum from that of the reference. In this fashion, the fraction of bonded N-H was obtained as a function of temperature. A similar procedure was followed to obtain the fraction of bonded carbonyl groups. In this case, the overlapping absorptions in the 29°C reference spectrum of Figure 5-2 were resolved by a trial and error fit of two gaussian peaks. From the fit it was estimated that 60% of the carbonyl groups were hydrogen bonded at room temperature. Values of the bonded N-H and C=O fractions as a function of temperature are collected in Table 5-1.

The heat and entropy of hydrogen bonding can be determined from the temperature variation of the equilibrium constant K_d which in turn can be calculated from the concentration of free and bound species. The hydrogen bonding equilibrium can be written as:

$$\mathrm{B \cdots H\text{-}N} \overset{K_d}{\rightleftharpoons} \mathrm{B + H\text{-}N} \tag{5-3}$$

where B is a proton acceptor. From previous studies of thermal effects on hydrogen bonding (8-10) the expression for the equilibrium constant is given by the expression:

$$K_d = \frac{[\mathrm{B}][\mathrm{NH}]}{[\mathrm{B \cdots H\text{-}N}]} = \frac{(1 - X_{NHb})^2}{X_{NHb}} \tag{5-4}$$

where X_{NHb} is the fraction of hydrogen bonded N-H groups. In this determination, the equilibrium constant for dissociation is calculated per mole of N-H. The dissociation constant can be expressed as:

$$K_d = \exp(-\Delta H/RT + \Delta S/R) \tag{5-5}$$

TABLE 5-1

VARIATION OF HYDROGEN BONDING WITH TEMPERATURE

TEMPERATURE, °C	FRACTION BONDED N-H	FRACTION BONDED C=O	FRACTION N-H BONDED TO OTHER ACCEPTORS
29	.875	.600	.275
42	.845	.585	.260
53	.790	.570	.220
63	.770	.560	.210
74	.760	.545	.215
88	.695	.520	.175
98	.650	.500	.150
114	.605	.470	.135
126	.565	.450	.115
136	.550	.430	.120
151	.500	.410	.090

where the variables in the above expression have their usual thermodynamic meaning. This expression can be rewritten as:

$$-\ln(K_d) = \Delta H/RT - \Delta S/R \tag{5-6}$$

A plot of $-\ln(K_d)$ vs. inverse temperature will yield the heat of dissociation from the slope and the corresponding entropy from the intercept. The slope at temperatures above the glass transition should be used, as the dissociation equilibrium does not hold in the vitrified state below the glass transition (23). Such a plot has been constructed from the data in Table 5-1 and is shown in Figure 5-7. A least squares fit to the 95% confidence level gave ΔH = 29.3 kJ/mole ± 2% and ΔS = 64.0 J/mole-°K ± 1%. The uncertainty in these quantities is undoubtedly much greater than indicated from the fit due to other sources of error which will be discussed later. These results are comparable to values determined in this manner for a similar MDI polyurethane (10) (ET-38-2) of ΔH = 32.6 kJ/mole and ΔS = 70.7 J/mole-°K.

Discussion

The subtraction procedure employed in the analysis relies on the removal of the reference bands at 2942 and 1595 cm^{-1} to normalize the amount of material in the infrared beam. These bands were found to maintain a constant position with temperature, however their intensity variation with temperature according to equation 5-2 was not taken into account. This could introduce an error of 7 to 35% in the subtraction of the 151°C spectrum depending on the value of α. Some absorbance bands, however, appear to have no dependence on temperature

Figure 5-7. Van't Hoff Plot for 2,6-T-2P-43 Hydrogen Bonding Equilibrium.

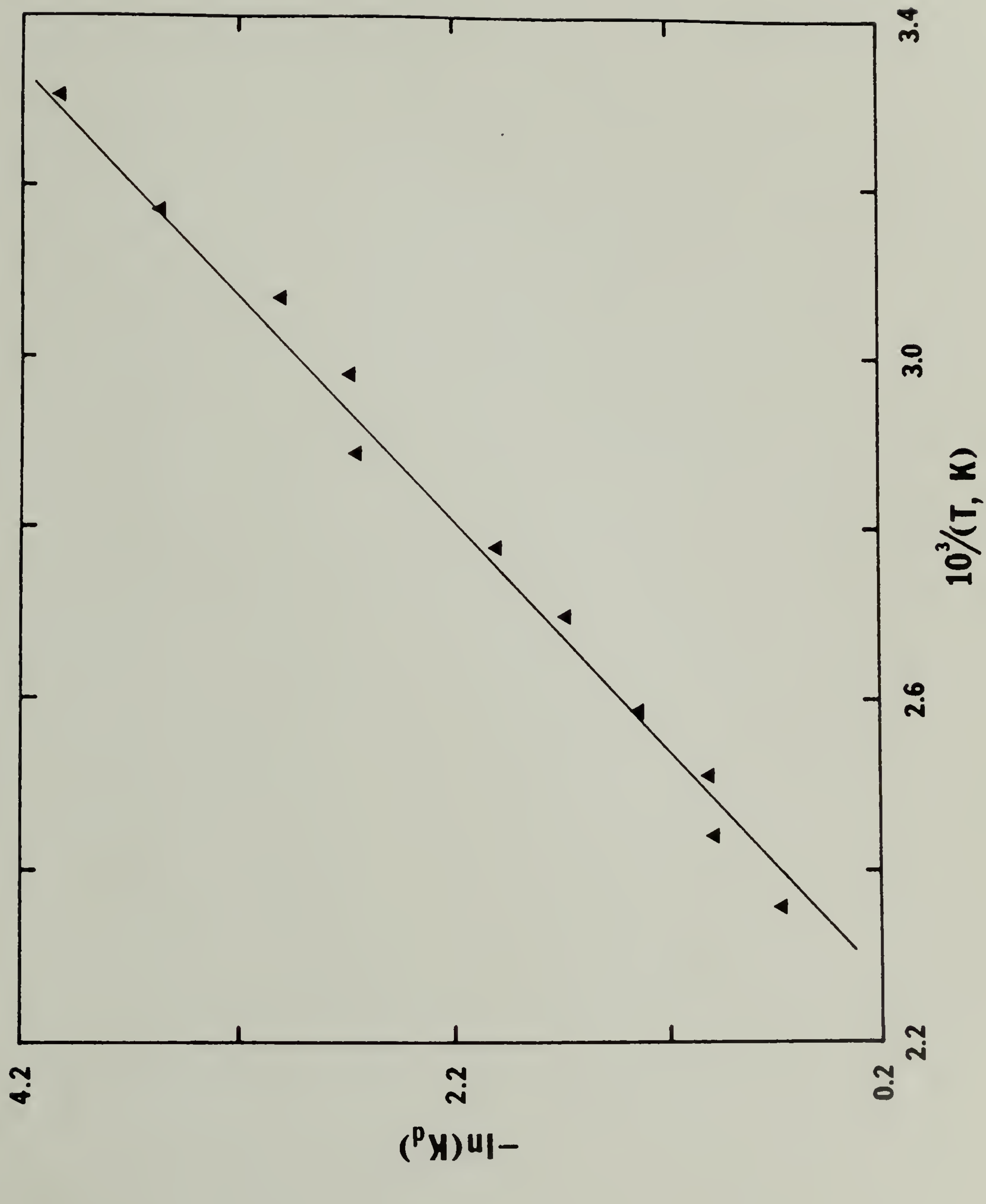
$-\ln(K_d)$
4.2
2.2
0.2
$10^3/(T, K)$
2.2
2.6
3.0
3.4

(19). The contribution of this source of error to the intensity of the N-H, C=O and reference band absorptions cannot readily be determined. For this reason, the errors estimated for ΔH and ΔS may be greater than those given for the fit of a least squares line.

The frequency shift of the bonded N-H absorption with increasing temperature does not present a serious problem, as the position of the bonded N-H maximum in the difference spectrum remained constant with temperature. The change in bonded N-H band shape with temperature appears to have had little effect on the difference spectra, as evidenced by the constant position of this peak in these spectra.

The resolution of the bonded and free carbonyl groups into a single symmetrical peak for each is probably an incorrect assumption. Other studies have used two bands to account for the bonded carbonyl owing to its asymmetric shape at the lower wavenumbers (10). An additional carbonyl absorption appears to be present in the 29°C spectrum, intermediate in wavenumber between the bonded and free carbonyl and amounting to about 5% of the total area of the bonded plus the free carbonyl band. This carbonyl is thought to be due to oxidation of the polyether soft segments during the heat treatment to 180°C. Such oxidation would introduce a ketone or internal ester into the polyether chain, with absorption maxima at 1715 and 1735 to 1750 cm^{-1} respectively (24). Polyether urethanes are known to suffer from thermal instability if suitable additives are not incorporated (25). An internal ester carbonyl formed by oxidation would be indistinguishable from the free urethane carbonyl, however a ketone absorbance would appear at a position between the free and bonded urethane carbonyl. The shoulder at 1726 cm^{-1} in Figure 5-5 is thought to be attributable to a ketone group formed from oxidation, shifted toward higher wavenumbers by the dominant free urethane carbonyl absorption. The shoulder is evident in the 74°C subtraction and continually increases in prominence to 151°C, where it is estimated to be 10 to 15% of the area of the bonded plus nonbonded carbonyl absorption. Formation of this carbonyl species during the initial thermal treatment is likely and the resulting presence of a third C=O absorbance band complicates the decomposition of the reference spectrum into bonded and free C=O absorptions.

Calculation of the equilibrium constant for dissociation of hydrogen bonding by equation 5-4 is probably incorrect, owing to the number of possible proton acceptors in block polyurethanes, as discussed in the introduction. Equation 5-4 assumes that the concentration of free N-H is equal to that of free C=O. The data in Table 5-1 show this to be far from the case. A greater fraction of N-H is bonded at any temperature so the free carbonyl concentration will always be greater. The bound N-H groups not bonded to carbonyl groups are bonded to either urethane alkoxyl oxygen or soft segment ether moieties. This fraction is given in the last column of Table 5-1. From these data, two equilibrium constants can be calculated. The N-H to urethane carbonyl equilibrium constant can be determined from the following expression:

$$K_c = \frac{(1 - X_{COb})(1 - X_{NHb})}{X_{COb}} \qquad (5\text{-}7)$$

where X_{COb} is the fraction of bonded carbonyl groups and X_{NHb} the total fraction of bonded N-H groups. A van't Hoff plot of this data yielded ΔH = 19.1 kJ/mole ± 2% and ΔS = 42.3 J/mole-°K ± 2% from a least squares fit for the N-H to urethane carbonyl hydrogen bond.

A second dissociation equilibrium between N-H and the urethane alkoxyl or ether oxygen can also be examined. This equilibrium constant can be written as:

$$K_e = \frac{(E - X_{NHbe})(1 - X_{NHb})}{X_{NHbe}} \qquad (5\text{-}8)$$

where X_{NHbe} is the fraction of N-H bonded to acceptors other than the urethane carbonyl (column 4 of Table 5-1) and E is a measure of the relative concentration of other acceptors to that of urethane carbonyl groups. By stoichiometry of the formulation, there are 27 ether oxygens for every 12 urethane linkages. If urethane alkoxyl oxygen atoms are considered to be the only proton acceptor other than the urethane carbonyl involved then $E = 1$. If soft segment ether oxygens are considered to be the only other proton acceptors $E = 2.25$. If both of these groups are likely to be proton acceptors $E = 3.25$. All three cases were considered here. The magnitude of E has a considerable effect on the value of the equilibrium constant, however the temperature dependence of the equilibrium constant varies little in the three cases. Thermodynamic parameters of ΔH = 23.0 kJ/mole ± 5% and ΔS = 73.1 J/mole-°K ± 7% were determined for the N-H to alkoxyl or ether oxygen hydrogen bond.

The ΔH values calculated for these two hydrogen bond dissociation equilibria are in reasonable agreement with values of 16 to 18 kJ/mole found in the literature (26). These authors also suggest that the two-fold difference in ΔS values for the equilibria need not be accompanied by a similar change in ΔH. Values calculated for the equilibrium of equation 5-4 are much higher than the literature results, ranging from 21.5 to 32.5 kJ/mole for several MDI-polyether urethanes (10). The similarity of the heat of dissociation for N-H bonded to carbonyl and alkoxy or ether oxygen atoms supports the suggestion of Sung and Schneider (9) that the urethane alkoxyl oxygen and carbonyl groups form hydrogen bonds to N-H of comparable strength in 2,6-TDI polyurethanes.

The morphological implications of these findings will now be considered. Previous infrared thermal studies (9) of 2,6-TDI polyurethanes with a 1000 molecular weight polyether soft segment concluded that dissociation of N-H to C=O hydrogen bonds begins at about 65°C, independent of the urethane content. No thermodynamic transitions were found in this temperature region which could cause the onset of this dissociation (27). Such a point of discontinuity is not at all obvious in plots of the bonded N-H and C=O fraction vs. temperature as the data exhibit considerable scatter. It seems more likely that a continuous dissociation process is occurring throughout the temperature range studied. For the 2,6-T-2P-43 polyurethane studied here, a weak hard segment glass transition occurs at about 60°C, however this transition has no effect on the hydrogen bonding dissociation equilibrium from plots of X_{NHb}, X_{NHbe}, and X_{COb} vs. temperature, not shown. Within experimental error of the data, dissociation appears to be continuous over the temperature range studied. The concentration of the hard segment glass must be low in order for it to exert no effect on the hydrogen bond equilibrium below T_g. The low intensity of the hard segment α_h relaxation in dynamic mechanical experiments (Figure 4-15) supports this argument.

Dynamic mechanical studies of Chapter IV have also shown that the soft segment phase in 2,6-T-2P-43 is relatively free of intermixed hard segments. This suggests that most N-H bonding to acceptors other than the urethane carbonyl is to the urethane alkoxyl oxygen in a well segregated copolymer. The value of E in equation 5-8 should therefore be close to unity. It may be somewhat greater than one if soft segments, containing ether acceptor sites, are mixed into the hard segment phase.

A more reasonable explanation for the continuous dissociation of the X_{NHbe} fraction lies in consideration of a significant amount of interfacial material of variable composition between relatively pure hard and soft segment phases. Such a phase could contain soft segments and short hard segment sequences not included in the hard segment crystalline or paracrystalline structures. Hydrogen bonding between N-H and both acceptors of the urethane linkage as well as soft segment ether oxygens would be possible with more bonding likely to the latter due to its greater concentration of bonding sites. The dissociation of these bonds is not likely to be restricted, over the temperature range studied here, by the glass transition, which would vary with composition across the width of the interlayer but remain below the value for the pure hard segment across much of the interface.

The interfacial thickness in segmented polyurethanes has been studied by small angle x-ray scattering. Bonart and Müller (28) find that interfaces about 1.9 nm in thickness exist between phases of an MDI-polyether urethane. This corresponds to an interfacial volume fraction of about 15%. Koberstein (29) has obtained interfacial thicknesses of 3 to 5 nm on MDI polyurethanes with a crosslinked polyether soft segment, corresponding to about 30 volume percent of interlayer material. No wide angle x-ray studies have been reported on 2,6-TDI polyurethanes. The existence of a significant amount of interlayer material in 2,6-TDI polyurethanes is likely, as the hard segment domains are more poorly organized than in MDI materials, shown by the difficulty in obtaining clear melting endotherms in the former case (7) which are clearly evident for the latter (10). A large amount of hydrogen bond dissociation from a significant fraction of bonded N-H in the interlayer could obscure any effect of the hard segment T_g on the equilibrium.

Infrared dichroism studies of MDI-polyether urethanes by Seymour and coworkers (30) can be interpreted to corroborate some of the points just discussed. They determined the orientation function for bonded N-H, C-H (methylene), and bonded and free carbonyl at elongations up to 250%. The bonded N-H and C=O behave in a similar fashion, the orientation function increasing markedly with elongation. The orientation function of the methylene groups of the soft segment is about four times less than that of the bonded N-H and C=O. The free C=O has an orientation function intermediate between the bonded C=O and the soft segments at all elongations studied. A large number of free C=O groups should be located in the interlayer material, as the N-H groups in the interlayer will preferentially bond to ether oxygens due to their greater concentration. Orientation of this interlayer material would be expected to be greater than in the soft segment domains but not as high as that of the hard domains.

A considerable amount of bonded N-H and C=O remain at the highest temperature studied, 151°C. This is attributable to hard segment crystallinity, which does not dissociate until temperatures of about 177°C have been reached. Similar results have been found by other workers (9,10).

Conclusions

Infrared thermal analysis of block polyurethanes by Fourier Transform spectroscopy has proven to be a useful method for the study of hydrogen bonding equilibria. The ratio of hydrogen bonded to free extinction coefficients is determined to be 4.6 for the N-H stretch and 1.05 for the carbonyl stretching absorptions. The dissociation equilibrium for N-H to C=O hydrogen bonding has a heat of dissociation of 19 kJ/mole and an entropy of dissociation of 42 J/mole-°K. A second equilibrium between N-H and other proton acceptors, either the soft segment ether or the urethane alkoxyl oxygen, is described by the following thermodynamic parameters: ΔH = 23 kJ/mole, ΔS = 73 J/mole-°K. No discontinuities are found in hydrogen bonding equilibria in the region of the hard segment glass transition temperature. This behavior can be attributed to dissociation of a large amount of hydrogen bonding in the interlayer material, dissociation which is not affected by the weak hard segment glass transition.

REFERENCES

1. Yu M. Boyarchuk; L. Ya Rappoport; V.N. Nikitin; and N.P. Apukhtina, Polym. Sci. USSR, 7, 859 (1965).
2. T. Tanaka; T. Yokoyama; and Y. Yamaguchi, J. Polym. Sci. A-1, 6, 2137 (1968).
3. T. Tanaka; T. Yokoyama; and Y. Yamaguchi, J. Polym. Sci. A-1, 6, 2153 (1968).
4. K. Nakayama; T. Ino; and I. Matsubara, J. Macromol. Sci. Chem., A3, 1005 (1969).
5. R.W. Seymour; G.M. Estes; and S.L. Cooper, Macromol., 3, 579 (1970).
6. C.S. Paik Sung and N.S. Schneider, Macromol., 8, 68 (1975).
7. N.S. Schneider and C.S. Paik Sung, Polym. Eng. Sci., 17, 73 (1977).
8. W.J. MacKnight and M. Yang, J. Polym. Sci. C., 42, 817 (1973).
9. C.S. Paik Sung and N.S. Schneider, Macromol., 10, 452 (1977).
10. V.W. Srichatrapimuk and S.L. Cooper, J. Macromol. Sci. Phys., B15, 267 (1978).
11. M. Yang, Ph.D. Dissertation, University of Massachusetts (1971).
12. O.G. Tarakanov; V.A. Orlov; and V.K. Beljakov, J. Polym. Sci. C., 23, 117 (1968).
13. M.L. Matusak and K.C. Frisch, J. Polym. Sci. A, 11, 637 (1973).
14. H.C. Beach and C.P. Ngoc Son, J. Appl. Polym. Sci., 7, 2217 (1963).
15. V.A. Orlov and O.G. Tarakanov, Plastichekie Massy, 6, 12 (1965).
16. J.L. Koenig, Appl. Spectrosc., 29, 293 (1975).
17. K. Krishnan, private communication.
18. L.N. Ovander, Opt. Spect., 11, 68 (1961).

19. M.P. Lisitsa and Yu P. Tsyashchenko, Opt. Spect., 9, 99 (1960).

20. G.C. Pimentel and A.L. McClellan, "The Hydrogen Bond," p. 139, W.H. Freeman and Co., San Francisco (1960).

21. G.J. Boobyer and W.J. Orville-Thomas, Spectrochim. Acta, 22, 147 (1966).

22. G.M. Barrow, J. Chem. Phys., 21, 2008 (1953).

23. M.W. Wolkenstein and O.B. Ptitsyn, in "Hydrogen Bonding," D. Hadzi, Ed., Pergamon Press, London (1959).

24. R.M. Silverstein and G.C. Bassler, "Spectrometric Identification of Organic Compounds," p. 263, John Wiley and Sons, New York (1967).

25. D.C. Allport and W.H. Janes, "Block Copolymers," p. 251, John Wiley and Sons, New York (1973).

26. G.C. Pimentel and A.L. McClellan, "The Hydrogen Bond," pp. 214-224, W.H. Freeman and Co., San Francisco (1960).

27. N.S. Schneider and C.S. Paik Sung, Macromol., 8, 62 (1975).

28. R. Bonart and E.H. Müller, J. Macromol. Sci. Phys., B10, 345 (1974).

29. J.T. Koberstein, private communication.

30. R.W. Seymour; G.M. Estes; and S.L. Cooper, Polym. Sci. Technol., 4, 225 (1974).

CHAPTER VI

SUGGESTIONS FOR FUTURE WORK

Several potential areas of inquiry have become apparent and could form the basis for future studies. The geometry of the DSA method could be altered to provide better transfer of the applied deformation to the polymer and coil. Substituting springs formed from rectangular wire would also simplify the procedure. More complex models could be employed to predict the mechanical behavior of the polymer in the composite sample. Surface tension contributions should also be considered in an effort to improve the agreement with results from unsupported techniques.

A conclusive demonstration that the above T_g relaxation found by DSA is not of molecular origin could be carried out. The model outlined predicts that the relaxation maximum can be shifted to other temperatures for a given material at will by altering the values of the spring constants employed in the model. Such an experiment would clearly show the instrumental origin of the process.

An informative study would involve comparing the kinetic parameters determined by DSA, particularly rate constants, to those obtained from the same reactants under identical conditions by conventional means, i.e., spectroscopy or titration. Such a study would determine the usefulness of the DSA method in this application. Additional dynamic mechanical studies of epoxy resin films cured then postcured, both isothermally, would better simulate the actual curing conditions employed in commercial use.

Additional studies of the block polyurethane elastomers would be useful in further defining the morphology of these materials. A small angle x-ray study would give information on the size of segregated phases and the amount of interfacial material present. The amorphous 2,4-T-2P series would be ideal candidates for such an approach. Electron microscopy might also be used to complement the x-ray determinations. The melting transition of the hard segment domains in 2,6-TDI polyurethanes should be investigated by other methods to ascertain the validity of the heat of fusion results determined mechanically. These findings are contrary to those expected from thermodynamic theories of polymer-polymer mixing. Melt viscosity determinations may prove useful in the study of the hard segment transitions in 2,4-T-1P polyurethanes.

The infrared thermal studies should certainly be extended to other representative polyurethanes examined by dynamic mechanical methods. Such a systematic study could better relate the hydrogen bonding behavior to the morphology of these elastomers and complement dynamic mechanical and x-ray findings to form a complete structural picture of these elastomers. An FT-ir thermal study of the hard and soft segment polymers would be informative in defining the hydrogen bonding equilibria in the pure phases. The change in absorbances other than the N-H and C=O stretch, particularly the ether associated bands, could be studied as this information is also made available by the FT-ir technique. Experimentally, the methods described here could be improved by following the hydrogen bonding equilibria to much lower temperatures, perhaps 0°C, carefully preparing the thin samples to avoid oxidation and employing more sophisticated curve resolving procedures in the carbonyl stretching region of the reference spectrum.

APPENDIX

COMPUTER PROGRAMS

```
      PROGRAM ARRHEA(INPUT,OUTPUT)
C   BATCH FORTRAN PROGRAM ARRHEA       4/28/78
C   CALCULATES ARRHENIUS ACTIVATION ENERGY FROM FREQUENCY
C   DEPENDENCE OF RELAXATION MAXIMA BY A LINEAR LEAST SQUARES
C   FIT
      REAL INTRCPT,M95
      DIMENSION FREQ(20),T025(30),TEMP(20),X(20),Y(20)
      DATA(T025(I),I=1,30)/12.706,4.303,3.182,2.776,2.571,
     +2.447,2.365,2.306,2.262,2.228,2.201,2.179,2.160,2.145,
     +2.131,2.12,2.11,2.101,2.093,2.086,2.08,2.074,2.069,
     +2.064,2.06,2.056,2.052,2.048,2.045,1.96/
      PRINT 5
    5 FORMAT(/,* NUMBER OF RUNS*)
      READ *,M
      DO 4  K=1,M
      SX=0.$SY=0.$SXY=0.$SX2=0.$SY2=0.
      PRINT 10
   10 FORMAT(/,* NUMBER OF FREQUENCIES*)
      READ *,N
      PRINT 15
   15 FORMAT(/,* DATA POINTS; T1,W1,T2,W2,...*)
      READ *,(TEMP(I),FREQ(I),I=1,N)
      DO 3  I=1,N
      X(I)=1./(TEMP(I)+273.15)
      Y(I)=ALOG(FREQ(I))
    3 CONTINUE
C BEGIN LINEAR LEAST SQUARES
      DO 1 I=1,N
      SX=SX+X(I)
      SY=SY+Y(I)
      SXY=SXY+X(I)*Y(I)
      SX2=SX2+X(I)**2
      SY2=SY2+Y(I)**2
    1 CONTINUE
```

```
      SSQ=0.
      DO 2 I=1,N
      SSQ=((SX/N)-X(I))**2+SSQ
    2 CONTINUE
      SLOPE=(N*SXY-SX*SY)/(N*SX2-SX**2)
      INTRCPT=(SX2*SY-SX*SXY)/(N*SX2-SX**2)
      SIGMAB=SQRT(ABS(SY2-INTRCPT*SY-SLOPE*SXY)/(N-2.))
      SIGMAM=SQRT((SIGMAB**2)/SSQ)
      COD=SXY-SX*SY/N
      COD=COD/SQRT(SX2-SX**2/N)
      COD=COD/SQRT(SY2-SY**2/N)
      COD=COD**2
C END LINEAR LEAST SQUARES
      ENERGY=-1.*SLOPE*.00831425
      SIGMAE=SIGMAM*.00831425
      J=N-2
      IF(N.GE.32)J=30
      EN=N*1.
      M95=T025(J)*SIGMAE/SQRT(EN)
      B95=T025(J)*SIGMAB/SQRT(EN)
      PRINT 20,(FREQ(I),I=1,N)
   20 FORMAT(//,3X,*FREQ (HZ)*,10F7.1)
      PRINT 25,(TEMP(I),I=1,N)
   25 FORMAT(3X,*TEMP (C) *,10F7.1)
      PRINT 30
   30 FORMAT(/,3X,*EA (KJ/MOL)    95% CONF    INTERCEPT*,
     +4X,8H95% CONF,3X,9HCOEF DETN)
      PRINT 35,ENERGY,M95,INTRCPT,B95,COD
   35 FORMAT(1X,4(1PE12.3),0PF11.5)
      PRINT 40
   40 FORMAT(//)
    4 CONTINUE
      END
      PROGRAM DSAFIG(INPUT,OUTPUT,TAPEM=INPUT,TAPE20=OUTPUT,
     +DATA1,TAPE1=DATA1,DATA2,TAPE2=DATA2,DATA3,TAPE3=DATA3,DATA4,
     +TAPE4=DATA4)
C     FORTRAN PROGRAM DSAFIG II            7/2/78
C     PROGRAM TO ANALYZE AND PLOT DSA DATA AND DO TIME-
C     TEMPERATURE SUPERPOSITION; VF NOT USED IN CALCULATIONS
C     (MODIFIED TO READ ANY NUMBER OF FREQUENCY SETS)
C     INPUT MODULI LIMITS IN KPA;(DYNES/SQ.CM.)/10**4=1KPA
C          INPUT DATA FILES
C     FIRST LINE: INTEGER VARIABLES PLOTOPT(=0 DOES CALCULATIONS ONLY
C     =1 DOES CALCULATIONS
C     AND PLOTS); NFREQ, THE NUMBER OF FREQUENCY SETS IN THE RUN;
C     TG, THE GLASS TRANSITION TEMPERATURE IN C
C     SECOND LINE: TMAX AND TMIN, SET MAXIMUM AND MINIMUM VALUES FOR
C     PLOT TEMPERATURE SCALE
C     LGMOMAX AND LGMOMIN, SET MAXIMUM AND MINIMUM VALUES FOR PLOT LOG
C     MODULUS SCALE; TANMAX,
C     SETS MAXIMUM VALUE FOR PLOT TAN DELTA SCALE
C     THIRD LINE: UP TO 30 ALPHANUMERIC CHARACTERS WHICH IDENTIFY THE
C     SAMPLE, THE LAST 20 FORM THE TITLE
C     FOURTH LINE OF FIRST FREQUENCY SET AND BEGINNING OF SUBSEQUENT
C     FREQUENCY SETS:
C     RHEOVIBRON ERROR CONSTANT AT AF=30 EK; AMP FACTOR OF THE SPRING
C     ASPR; DYNAMIC FORCE VALUE OF THE SPRING DSPR; DIAMETER OF SPRING
C     WIRE WD, IN MILS;
C     OUTER DIAMETER OF COIL OD, IN MILLS; DISTANCE STRETCHED STRETCH
C     IN CM.; NUMBER OF TURNS
C     TURNS, DIMENSIONLESS; VOLUME FRACTION POLYMER VF, DIMENSIONLESS
C     ; FREQUENCY OMEGA, IN HZ.
C     FIFTH LINE OF FIRST FREQUENCY SET AND SECOND LINE OF SUBSEQUENT
C     FREQUENCY SETS:
C     TEMPERATURE T, IN C; AMPLITUDE FACTOR OF COMPOSITE ACOM; DYNAMIC
C     FORCE VALUE OF COMPOSITE DCOM; TAN DELTA OF THE COMPOSITE TAND
C     LAST LINE OF EACH FREQUENCY SET CONTAINS: "0.,999.,0.,0."
C     LAST LINE OF FINAL FREQUENCY SET CONTAINS: "0.,1000.,0.,0."
C     INTERNAL DATA: WLF CONSTANTS C1 AND C2
C          OUTPUT DATA
C     ALL MODULI IN KPA
       REAL LGLOSM,LGSTOM,LOSSM,LOSSG,LEN,LGMOMAX,LGMOMIN
      INTEGER PLOTOPT
       COMMON/INITIAL/T(100),LGLOSM(100),LGSTOM(100),TAND(100)
       DIMENSION HEADING(3),PTITLE(2)
      M=1
 1100 IF(M-MOLD.EQ.1)READ(M,*)N,PLOTOPT,NFREQ,TG
       IF(M-MOLD.EQ.1)READ(M,*)N,TMAX,TMIN,LGMOMAX,LGMOMIN,TANMAX
       IF(PLOTOPT.NE.1)GO TO 1110
      IF(NPIC.NE.0)GO TO 1110
       CALL PLOTS(40)
       CALL PLOT(0.,-11.,-3)
1110  IF(M-MOLD.EQ.1)READ(M,2180)N,(HEADING(I),I=1,3),(PTITLE(I),I=1,2)
2180  FORMAT(F5.0,5A10)
      MOLD=M
       WRITE(20,2200)(HEADING(I),I=1,3),(PTITLE(I),I=1,2)
2200  FORMAT(1H1,/,5A10)
      IF(PLOTOPT.EQ.0)WRITE(20,2210)
2210  FORMAT(1H0,29X,20H*........+.........*)
       WRITE(20,1150)
1150  FORMAT(1H0)
      READ(M,*)N,EK,ASPR,DSPR,WD,OD,STRETCH,TURNS,VF,OMEGA
      IF(ASPR.EQ.10.)GO TO 1360
      IF(ASPR.EQ.20.)1220,1260
1220        ASPR=SQRT(10.)
      GO TO 1360
1260        IF(ASPR.EQ.30.)1280,1320
1280  ASPR=1.
      GO TO 1360
1320        WRITE(20,2340)
2340        FORMAT(1H0,2X,40HINCORRECT VALUE OF AMPLITUDE FACTOR USED)
      GO TO 2600
1360        EKSPR=EK/ASPR
      SPRK=(2.*10.**9)/(ASPR*(DSPR-EKSPR))
      WD=WD*.00254
      OD=OD*.00254
      AREA=3.14159*WD*(OD-WD)
      LEN=TURNS*WD+STRETCH
      SPRM=SPRK*LEN/(AREA*TURNS)
      WRITE(20,2240)
2240        FORMAT(10H ERROR CON,3X,10HVF POLYMER,3X,10HSPRING MOD,
     +5X,4HFREQ,7X,2HTG)
      WRITE(20,2220)EK,VF,SPRM,OMEGA,TG
2220        FORMAT(F8.1,F12.3,1PE16.3,0PF10.2,F10.1)
      WRITE(20,1150)
      J=1
1560        READ(M,*)N,T(J),ACOM,DCOM,TAND(J)
      IF(ACOM.GE.999.)GO TO 2400
      IF(ACOM.EQ.10.)GO TO 1780
      IF(ACOM.EQ.20.)1640,1700
1640        ACOM=SQRT(10.)
      GO TO 1780
1700  IF(ACOM.EQ.30.)1710,1740
1710        ACOM=1.
      GO TO 1780
1740        WRITE(20,2340)
      GO TO 2140
1780        EKCOM=EK/ACOM
      RELM=(ASPR*(DSPR-EKSPR))/(ACOM*(DCOM-EKCOM))
      DEL=ATAN(TAND(J))
      STORM=SPRM*(RELM*COS(DEL)-1.)/10.**(4)
      IF(STORM.LE.0.)STORM=10.**(-10)
      LOSSM=SPRM*RELM*SIN(DEL)/10.**(4)
      IF(LOSSM.LE.0.)LOSSM=10.**(-10)
      LGLOSM(J)=ALOG10(LOSSM)
      LGSTOM(J)=ALOG10(STORM)
      C1=-13.3
      C2=47.5
        IF(T(J).LE.TG)2000,2020
2000  IF(J.EQ.1)WRITE(20,2280)
2280  FORMAT(1X,5H TEMP,3X,7HTAN DEL,3X,8HLOSS MOL,2X,7HLOGLOSS,3X,
     +8HSTOR MOD,2X,7HLOGSTOR,2X,10HSHIFT*FREQ,2X,9HRED LOSSM,3X,
     +9HRED STORM)
      WRITE(20,2320)T(J),TAND(J),LOSSM,LGLOSM(J),STORM,LGSTOM(J)
2320  FORMAT(F7.1,F8.3,1PE12.3,0PF8.3,1PE12.3,0PF8.3,1P3E12.3)
      GO TO 2140
2020  AT=10.**(C1*(T(J)-TG)/(C2+T(J)-TG))
      TTS=AT*OMEGA
      LOSSG=LOSSM*(TG+273.15)/(T(J)+273.15)
      STORG=STORM*(TG+273.15)/(T(J)+273.15)
      IF(J.EQ.1)WRITE(20,2280)
      WRITE(20,2320)T(J),TAND(J),LOSSM,LGLOSM(J),STORM,LGSTOM(J),
     +TTS,LOSSG,STORG
2140  LGLOSM(J)=LGLOSM(J)-1.
      J=J+1
      GO TO 1560
2400  IF(PLOTOPT.EQ.1)2450,2500
2450  IF(PLOTOPT.EQ.1)CALL PIC(L,NPIC,HEADING,J-1,TMAX,TMIN,
     +LGMOMAX,LGMOMIN,TANMAX,OMEGA,PTITLE)
      NPIC=NPIC+1
2500  L=L+1
      IF(L.EQ.NFREQ)M=M+1
      IF(L.EQ.NFREQ)L=0
      IF(ACOM.EQ.999.)GO TO 1100
2600  IF(NPIC.GT.0)CALL PLOT(END,0.0,999)
       STOP
       END
      SUBROUTINE PIC(L,M,NHEAD,N,TMAX,TMIN,LGMOMAX,LGMOMIN,TANMAX,
     +FREQ,PTITLE)
       REAL LGLOSM,LGSTOM,LGMOMAX,LGMOMIN
       COMMON/INITIAL/T(100),LGLOSM(100),LGSTOM(100),TAND(100)
       DIMENSION NHEAD(3),PTITLE(2),NS(8)
      DATA(NS=0,2,5,10,4,3,11,12)
       BOG=(TMAX-TMIN)/7.
      YP=.2
      IF(FREQ.EQ.110.)KF=1
      IF(FREQ.EQ.35.)KF=2
      IF(FREQ.EQ.11.)KF=3
      IF(FREQ.EQ.3.5)KF=4
      IF(L+M.EQ.0)5,10
    5 K=1
      CALL PLOT(0.,-11.,-3)
      CALL PLOT(0.,2.75,-3)
      GO TO 40
10    K=L+1
      IF(K.GT.1)GO TO 20
      CALL PLOT(11.,0.,-3)
      GO TO 40
20    CALL PLOT(-11.,0.,-3)
40    CONTINUE
      IF(K.GT.1)GO TO 50
      CALL AXIS(0.,0.,17HTEMPERATURE   (C),-17,7.,0.,TMIN,BOG)
      CALL AXIS(0.,0.,25HLOG(STORAGE MODULUS, KPA),
     +25,5.,90.,LGMOMIN,(LGMOMAX-LGMOMIN)/5.)
      CALL AXS(0.,5.,-7.,1.,0.)
      CALL AXIS(7.,0.,22HLOG(LOSS MODULUS, KPA),-22,5.,90.,LGMOMIN+1.,
     +(LGMOMAX-LGMOMIN)/5.)
      CALL SYMBOL(2.,7.5,.14,NHEAD,0.0,30)
      CALL SYMBOL(2.4,5.2,.14,PTITLE,0.,20)
50    CALL SYMBOL(6.,(4.7-YP*K)+.05,.07,NS(KF),0.,-1)
      CALL NUMBER(6.14,(4.7-YP*K),.1,FREQ,0.,1)
      T(N+1)=TMIN $ T(N+2)=BOG
      LGSTOM(N+1)=LGLOSM(N+1)=LGMOMIN
      LGSTOM(N+2)=LGLOSM(N+2)=(LGMOMAX-LGMOMIN)/5.
      CALL PSYM(T,LGSTOM,N,NS(KF),TMIN,TMAX,LGMOMIN,LGMOMAX)
      CALL PSYM(T,LGLOSM,N,NS(KF),TMIN,TMAX,LGMOMIN,LGMOMAX)
      CALL PLOT(11.,0.,-3)
      IF(K.GT.1)GO TO 70
      CALL AXIS(0.,0.,17HTEMPERATURE   (C),-17,7.,0.,TMIN,BOG)
      CALL AXIS(0.,0.,9HTAN DELTA,9,5.,90.,0.,TANMAX/5.)
      CALL AXS(0.,5.,-7.,1.,0.)
      CALL AXS(7.,0.,5.,1.,90.)
      CALL SYMBOL(2.,7.5,.14,NHEAD,0.0,30)
      CALL SYMBOL(2.12,5.2,.14,PTITLE,0.,20)
70    CALL SYMBOL(.4,(4.7-YP*K)+.05,.07,NS(KF),0.,-1)
      CALL NUMBER(.54,(4.7-YP*K),.1,FREQ,0.,1)
      TAND(N+1)=0.0        $ TAND(N+2)=TANMAX/5.
      CALL PSYM(T,TAND,N,NS(KF),TMIN,TMAX,0.,TANMAX)
      RETURN
      END
      SUBROUTINE PSYM(X,Y,N,NS,X1,X2,Y1,Y2)
      DIMENSION X(100),Y(100)
      J=-1
      DO 10      LP=1,N
      IF((X(LP)+.001).LT.X1)GO TO 10
      IF((X(LP)-.001).GT.X2)GO TO 10
      IF((Y(LP)+.001).LT.Y1)GO TO 10
      IF((Y(LP)-.001).GT.Y2)GO TO 10
      CALL SYMBOL((X(LP)-X(N+1))/X(N+2),(Y(LP)-Y(N+1))/Y(N+2),
     +.07,NS,0.0,J)
      J=-2
10    CONTINUE
      RETURN
      END
      PROGRAM ISOFIG(INPUT,OUTPUT,TAPE10=INPUT,TAPE20=OUTPUT,
     +DATA1,TAPE1=DATA1,DATA2,TAPE2=DATA2,DATA3,TAPE3=DATA3,DATA4,
     +TAPE4=DATA4)
C     FORTRAN PROGRAM ISOFIG II           10/13/77
C     VF NOT USED IN CALCULATIONS
C     (MODIFIED TO READ ANY NUMBER OF FREQUENCY SETS)
C     INPUT MODULI LIMITS IN KPA; (DYNES/SQ.CM.)/10**4=1KPA
C          INPUT DATA FILES
C     FIRST LINE: INTEGER VARIABLE PLOTOPT(=0 DOES CALCULATIONS ONLY
C     =1 DOES CALCULATIONS
C     AND PLOTS); NFREQ, THE NUMBER OF FREQUENCY SETS IN THE RUN
C     SECOND LINE: LGTIMAX AND LGTIMIN, SET MAXIMUM AND MINIMUM VALUES
C     FOR PLOT LN TIME SCALE;
C     LGMOMAX AND LGMOMIN, SET MAXIMUM AND MINIMUM VALUES FOR PLOT
C     LOG MODULUS SCALE; TANMAX,
C     SETS MAXIMUM VALUE FOR PLOT TAN DELTA SCALE
C     THIRD LINE: 30 ALPHANUMERIC CHARACTERS TO IDENTIFY THE SAMPLE;
C     30 TO FORM THE PLOT TITLE
C     THE LAST 30 FORM THE PLOT TITLE
C     FOURTH LINE OF FIRST FREQUENCY SET AND BEGINNING OF SUBSEQUENT
C     FREQUENCY SETS
C     RHEOVIBRON ERROR CONSTANT AT AF=30 EK; AMP FACTOR OF THE SPRING
C     ASPR; DYNAMIC FORCE VALUE OF THE SPRING DSPR; DIAMETER OF SPRING
C     WIRE WD, IN MILS;
C     OUTER DIAMETER OF COIL OD, IN MILLS; DISTANCE STRETCHED STRETCH
C     IN CM.; NUMBER OF TURNS
C     TURNS, DIMENSIONLESS; VOLUME FRACTION POLYMER VF, DIMENSIONLESS
C     ; FREQUENCY OMEGA, IN HZ.
C     FIFTH LINE OF FIRST FREQUENCY SET AND SECOND LINE OF SUBSEQUENT
C     FREQUENCY SETS:
C     AMPLITUDE FACTOR OF COMPOSITE ACOM; DYNAMIC FORCE VALUE OF
C     COMPOSITE DCOM; TAN DELTA OF COMPOSITE TAND; TIME WHEN DATA
C     POINT WAS TAKEN IN
C     THREE VARIABLES, HOU, MIN, SEC
C     LAST LINE OF EACH FREQUENCY SET CONTAINS: "999.,0.,0.,0.,0.,0."
C     TO CLOSE READING OF THAT
C     PARTICULAR FREQUENCY
C     LAST LINE OF FINAL FREQUENCY SET CONTAINS: "1000.,0.,0.,0.,0.,
C     0." TO END PROGRAM
C          OUTPUT DATA
C      ALL MODULI IN KPA; TIME IN SEC.
       REAL MIN,LGLOSM,LGSTOM,LOSSM,LGTIMAX,LGTIMIN,LEN,LGMOMAX,LGMOMIN
      INTEGER PLOTOPT
       COMMON/INITIAL/Z(100),LGLOSM(100),LGSTOM(100),TAND(100)
       DIMENSION HEADING(3),PTITLE(3)
      M=1
 1100 IF(M-MOLD.EQ.1)READ(M,*)N,PLOTOPT,NFREQ
      IF(M-MOLD.EQ.1)READ(M,*)N,LGTIMAX,LGTIMIN,LGMOMAX,LGMOMIN,TANMAX
       IF(PLOTOPT.NE.1)GO TO 1110
      IF(NPIC.NE.0)GO TO 1110
       CALL PLOTS(40)
C      CALL FACTOR2(.85,.64)
       CALL PLOT(0.,-11.,-3)
 1110 IF(M-MOLD.EQ.1)READ(M,2180)N,(HEADING(I),I=1,3),(PTITLE(I),I=1,3)
 2180 FORMAT(F5.0,6A10)
      MOLD=M
       WRITE(20,2200)(HEADING(I),I=1,3),(PTITLE(I),I=1,3)
 2200 FORMAT(1H1,/,6A10)
      IF(PLOTOPT.EQ.0)WRITE(20,2210)
 2210 FORMAT(1H0,29X,20H*.........+.........*)
       WRITE(20,1150)
 1150 FORMAT(1H0)
      READ(M,*)N,EK,ASPR,DSPR,WD,OD,STRETCH,TURNS,VF,OMEGA
      IF(ASPR.EQ.10.)GO TO 1360
      IF(ASPR.EQ.20.)1220,1260
 1220      ASPR=SQRT(10.)
      GO TO 1360
 1260      IF(ASPR.EQ.30.)1280,1320
 1280 ASPR=1.
      GO TO 1360
 1320      WRITE(20,2340)
 2340      FORMAT(1H0,2X,40HINCORRECT VALUE OF AMPLITUDE FACTOR USED)
      GO TO 2600
 1360      EKSPR=EK/ASPR
      SPRK=(2.*10.**9)/(ASPR*(DSPR-EKSPR))
      WD=WD*.00254
      OD=OD*.00254
      AREA=3.14159*WD*(OD-WD)
      LEN=TURNS*WD+STRETCH
      SPRM=SPRK*LEN/(AREA*TURNS)
      WRITE(20,2240)
 2240      FORMAT(10H ERROR CON,3X,10HVF POLYMER,3X,10HSPRING MOD,
     +5X,4HFREQ)
      WRITE(20,2220)EK,VF,SPRM,OMEGA
 2220      FORMAT(F8.1,F12.3,1PE16.3,0PF9.1)
      WRITE(20,1150)
      J=1
 1560      READ(M,*)N,ACOM,DCOM,TAND(J),HOU,MIN,SEC
      IF(ACOM.GE.999.)GO TO 2400
      IF(ACOM.EQ.10.)GO TO 1780
      IF(ACOM.EQ.20.)1640,1700
 1640      ACOM=SQRT(10.)
      GO TO 1780
 1700 IF(ACOM.EQ.30.)1710,1740
```

```
1710      ACOM=1.
     GO TO 1780
1740      WRITE(20,2340)
     GO TO 2140
1780      EKCOM=EK/ACOM
     RELM=(ASPR*(DSPR-EKSPR))/(ACOM*(DCOM-EKCOM))
     DEL=ATAN(TAND(J))
     STORM=(SPRM*(RELM*COS(DEL)-1.))/10000.
     IF(STORM.LE.0.)GO TO 1560
     LOSSM=(SPRM*RELM*SIN(DEL))/10000.
     IF(LOSSM.LE.0.)GO TO 1560
     LGLOSM(J)=ALOG10(LOSSM)
     LGSTOM(J)=ALOG10(STORM)
     TIME=SEC+60.*MIN+3600.*HOU
     Z(J)=ALOG(TIME)
2000 IF(J.EQ.1)WRITE(20,2280)
2280 FORMAT(1X,7H TIME S,4X,6HLNTIME,4X,4HTAND,4X,8HLOSS MOD,
    +2X,7HLOGLOSS,3X,8HSTOR MOD,2X,7HLOGSTOR)
     WRITE(20,2320)TIME,Z(J),TAND(J),LOSSM,LGLOSM(J),STORM,LGSTOM(J)
2320 FORMAT(1PE10.3,0P2F8.3,2(1PE12.3,0PF8.3))
2140 LGLOSM(J)=LGLOSM(J)-1.
     J=J+1
     GO TO 1560
2400 IF(PLOTOPT.EQ.1)2450,2500
2450 IF(PLOTOPT.EQ.1)CALL PIC(L,NPIC,HEADING,J-1,LGTIMAX,LGTIMIN,
    +LGMOMAX,LGMOMIN,TANMAX,OMEGA,PTITLE)
     NPIC=NPIC+1
2500 L=L+1
     IF(L.EQ.NFREQ)M=M+1
     IF(L.EQ.NFREQ)L=0
     IF(ACOM.EQ.999.)GO TO 1100
2600 IF(NPIC.GT.0)CALL PLOT(END,0.0,999)
      STOP
      END
     SUBROUTINE PIC(L,M,NHEAD,N,TMAX,TMIN,LGMOMAX,LGMOMIN,TANMAX,
    +FREQ,PTITLE)
      REAL LGLOSM,LGSTOM,LGMOMAX,LGMOMIN
      COMMON/INITIAL/T(100),LGLOSM(100),LGSTOM(100),TAND(100)
      DIMENSION NHEAD(3),PTITLE(3),NS(8)
     DATA(NS=0,2,5,10,3,4,11,12)
     YP=.2
      BOG=(TMAX-TMIN)/7.
     IF(FREQ.EQ.81.)KF=1
     IF(FREQ.EQ.91.6)KF=2
     IF(FREQ.EQ.100.)KF=3
     IF(FREQ.EQ.111.6)KF=4
     IF(FREQ.EQ.110.)KF=1
     IF(FREQ.EQ.35.)KF=2
     IF(FREQ.EQ.11.)KF=3
     IF(FREQ.EQ.3.5)KF=4
     IF(L+M.EQ.0)5,10
   5 K=1
     CALL PLOT(0.,-11.,-3)
```

```
C       CALL PLOT(0.,3.,-3)
      CALL PLOT(0.,2.75,-3)
      GO TO 40
   10 K=L+1
      IF(K.GT.1)GO TO 20
      CALL PLOT(11.,0.,-3)
      GO TO 40
   20 CALL PLOT(-11.,0.,-3)
   40 IF(K.GT.1)GO TO 50
      CALL AXIS(0.0,0.0,13HLN(TIME, SEC),-13,7.,0.,TMIN,BOG)
      CALL AXIS(0.,0.,25HLOG(STORAGE MODULUS, KPA),
     +25,5.,90.,LGMOMIN,(LGMOMAX-LGMOMIN)/5.)
      CALL AXS(0.,5.,-7.,1.,0.)
      CALL AXIS(7.,0.,22HLOG(LOSS MODULUS, KPA),-22,5.,90.,
     +LGMOMIN+1.,(LGMOMAX-LGMOMIN)/5.)
      CALL SYMBOL(2.,7.5,.14,NHEAD,0.0,30)
      CALL SYMBOL(2.,5.2,.14,PTITLE,0.,30)
   50 CALL SYMBOL(.4,(4.7-YP*K)+.05,.07,NS(KF),0.0,-1)
      CALL NUMBER(.54,4.7-YP*K,.10,FREQ,0.0,1)
      T(N+1)=TMIN $ T(N+2)=BOG
      LGSTOM(N+1)=LGLOSM(N+1)=LGMOMIN
      LGSTOM(N+2)=LGLOSM(N+2)=(LGMOMAX-LGMOMIN)/5.
      CALL PSYM(T,LGSTOM,N,NS(KF),TMIN,TMAX,LGMOMIN,LGMOMAX)
      CALL PSYM(T,LGLOSM,N,NS(KF),TMIN,TMAX,LGMOMIN,LGMOMAX)
      CALL PLOT(11.,0.,-3)
      IF(K.GT.1)GO TO 70
      CALL AXIS(0.,0.,13HLN(TIME, SEC),-13,7.,0.,TMIN,BOG)
      CALL AXIS(0.0,0.0,9HTAN DELTA,9,5.0,90.,0.,TANMAX/5.)
      CALL AXS(0.,5.,-7.,1.,0.)
      CALL AXS(7.,0.,5.,1.,90.)
      CALL SYMBOL(2.,7.5,.14,NHEAD,0.0,30)
      CALL SYMBOL(2.,5.2,.14,PTITLE,0.,30)
   70 CALL SYMBOL(.4,(4.7-YP*K)+.05,.07,NS(KF),0.0,-1)
      CALL NUMBER(.54,4.7-YP*K,.10,FREQ,0.0,1)
      TAND(N+1)=0.0       $ TAND(N+2)=TANMAX/5.
      CALL PSYM(T,TAND,N,NS(KF),TMIN,TMAX,0.,TANMAX)
      RETURN
      END
      SUBROUTINE PSYM(X,Y,N,NS,X1,X2,Y1,Y2)
      DIMENSION X(100),Y(100)
      J=-1
      DO 10      LP=1,N
      IF((X(LP)+.001).LT.X1)GO TO 10
      IF((X(LP)-.001).GT.X2)GO TO 10
      IF((Y(LP)+.001).LT.Y1)GO TO 10
      IF((Y(LP)-.001).GT.Y2)GO TO 10
      CALL SYMBOL((X(LP)-X(N+1))/X(N+2),(Y(LP)-Y(N+1))/Y(N+2),
     +.07,NS,0.0,J)
      J=-2
   10 CONTINUE
      RETURN
      END
      PROGRAM LOSMAX(INPUT,OUTPUT,TAPEM=INPUT,TAPE20=OUTPUT,
     +DATA1,TAPE1=DATA1,DATA2,TAPE2=DATA2,DATA3,TAPE3=DATA3,DATA4,
     +TAPE4=DATA4)
C     FORTRAN PROGRAM LOSMAX                         8/8/78
C     INPUT MODULI LIMITS IN MPA; (DYNES/SQ.CM.)/10**7=1MPA
C     INPUT INVERSE TEMPERATURE LIMITS IN 1000/K
C          INPUT DATA FILES
C     SAME AS VIEFIG INPUT FILES WITH THE FOLLOWING EXCEPTIONS:
C     FIRST LINE: INTEGER VARIABLE PLOTOPT(=0 DOES CALCULATIONS ONLY,
C     =1 DOES CALCULATIONS AND PLOTS, =2 DOES CALCULATIONS AND
C     NORMALIZED PLOTS); NFREQ, THE NUMBER OF FREQUENCY SETS IN THE RUN
C     SECOND LINE: ITMAX AND ITMIN, SET MAXIMUM AND MINIMUM VALUES FOR
C     PLOT INVERSE TEMPERATURE SCALE; MODMAX AND MODMIN, SET MAXIMUM
C     AND MINIMUM VALUES FOR PLOT MODULUS OR NORMALIZED MODULUS
C     SCALE; NORMAL(=0. DOES NORMALIZATION CALCULATIONS, =ANY
C     OTHER VALUE DOES NOT NORMALIZE MODULUS)
C     FIFTH LINE OF FIRST FREQUENCY SET AND SECOND LINE OF SUBSEQUENT
C     FREQUENCY SETS ONLY IF NORMAL=0.: MAXLOSS, MAXIMUM LOSS MODULUS
C     OF THE RELAXATION MAXIMUM USED TO NORMALIZE THE LOSS PEAK
C          OUTPUT DATA
C     ALL MODULI IN MPA
      REAL LENZERO,LGLOSM,LGSTOM,LOSSM,LEN,MODMAX,MODMIN
      REAL NORLOS,MAXLOSS,IT,ITMIN,ITMAX,NORMAL
      INTEGER PLOTOPT
      COMMON/POINTS/IT(100),LOSSM(100)
      COMMON/LIMITS/ITMAX,ITMIN,MODMAX,MODMIN
      COMMON/HEADER/HEADING(3),PTITLE(2)
      DIMENSION T(100),NORLOS(100)
      M=1$  L=0$  NFIG=0
 1100 IF(M-MOLD.EQ.1)READ(M,*)N,PLOTOPT,NFREQ
      IF(M-MOLD.EQ.1)READ(M,*)N,ITMAX,ITMIN,MODMAX,MODMIN,NORMAL
      IF(PLOTOPT.LT.1)GO TO 1200
      IF(NFIG.NE.0)GO TO 1200
      CALL PLOTS(40)
      CALL PLOT(0.,-11.,-3)
 1200 IF(M-MOLD.EQ.1)READ(M,1300)N,(HEADING(I),I=1,3),(PTITLE(I),I=1,2)
 1300 FORMAT(F5.0,5A10)
      MOLD=M
      WRITE(20,1400)(HEADING(I),I=1,3),(PTITLE(I),I=1,2)
 1400 FORMAT(1H1,/,5A10)
      IF(PLOTOPT.EQ.0)WRITE(20,1500)
 1500 FORMAT(1H0,29X,20H*.........+.........*)
      WRITE(20,1600)
 1600 FORMAT(1H0)
      READ(M,*)N,EK,LEN,WIDTH,THICK,OMEGA
      XAREA=WIDTH*THICK*6.4516*10.**(-6)
      WRITE(20,1700)
 1700 FORMAT(10H ERROR CON,3X,6HLENGTH,3X,5HWIDTH,3X,5HTHICK,
     +4X,4HFREQ,6X,5HE"MAX)
 1800 FORMAT(F8.1,F11.3,F8.1,F8.2,F9.2,F10.2)
      J=1
```

```
1900 IF((NORMAL.EQ.0.).AND.(J.EQ.1))READ(M,*)N,MAXLOSS
     READ(M,*)N,T(J),ACOM,DCOM,TAND,DLEN
     IF(J.GT.1)GO TO 2000
     LENZERO=LEN+DLEN*10.**(-3)
     IF(NORMAL.NE.0.)WRITE(20,1800)EK,LENZERO,WIDTH,THICK,OMEGA
     IF(NORMAL.EQ.0.)WRITE(20,1800)EK,LENZERO,WIDTH,THICK,OMEGA,
    +MAXLOSS
     WRITE(20,1600)
2000 IF(ACOM.GE.999.)GO TO 3100
     IF(ACOM.EQ.10.)GO TO 2600
     IF(ACOM.EQ.20.)2100,2200
2100        ACOM=SQRT(10.)
     GO TO 2600
2200 IF(ACOM.EQ.30.)2300,2400
2300        ACOM=1.
     GO TO 2600
2400        WRITE(20,2500)
2500        FORMAT(1H0,2X,40HINCORRECT VALUE OF AMPLITUDE FACTOR USED)
     GO TO 3000
2600        EKCOM=EK/ACOM
     DEL=ATAN(TAND)
     COMPMOD=2.*10.**(9)*(LEN+DLEN*10.**(-3))**(2)/(ACOM*(DCOM-EKCOM)*
    +XAREA*LENZERO)
     STORM=COMPMOD*COS(DEL)/10.**(7)
     LOSSM(J)=COMPMOD*SIN(DEL)/10.**(7)
     LGLOSM=ALOG10(LOSSM(J))
     LGSTOM=ALOG10(STORM)
     IT(J)=1000./(T(J)+273.15)
     IF(NORMAL.NE.0.)GO TO 2700
     NORLOS(J)=LOSSM(J)/MAXLOSS
2700 IF(J.EQ.1)WRITE(20,2800)
2800 FORMAT(1X,7H TEMP,C,1X,7HTAN DEL,4X,6HE' MPA,3X,7HLOG(E'),4X,
    +6HE" MPA,3X,7HLOG(E"),3X,7H1/(T,K),4X,7HNORM E")
     IF(NORMAL.NE.0.)WRITE(20,2900)T(J),TAND,STORM,LGSTOM,LOSSM(J),
    +LGLOSM,IT(J)/1000.
     IF(NORMAL.EQ.0.)WRITE(20,2900)T(J),TAND,STORM,LGSTOM,LOSSM(J),
    +LGLOSM,IT(J)/1000.,NORLOS(J)
2900 FORMAT(F7.1,F8.3,1PE12.3,0PF8.3,1PE12.3,0PF8.3,1PE12.3,0PF9.4)
3000 J=J+1
     GO TO 1900
3100 IF(PLOTOPT.EQ.0)3500,3200
3200 IF(PLOTOPT.EQ.1)CALL FIG(L,NFIG,J-1,OMEGA,PLOTOPT)
     IF(PLOTOPT.NE.2)GO TO 3400
     IDO=J-1
     DO 3300 I=1,IDO
     LOSSM(I)=NORLOS(I)
3300 CONTINUE
3400 IF(PLOTOPT.EQ.2)CALL FIG(L,NFIG,J-1,OMEGA,PLOTOPT)
     NFIG=NFIG+1
3500 L=L+1
     IF(L.EQ.NFREQ)M=M+1
     IF(L.EQ.NFREQ)L=0
     IF(ACOM.EQ.999.)GO TO 1100
3600 IF(NFIG.GT.0)CALL PLOT(END,0.0,999)
     STOP
     END
```

```
      SUBROUTINE FIG(L,M,N,FREQ,F)
      REAL LOSSM,MODMAX,MODMIN
      REAL ITMAX,ITMIN,IT
      COMMON/POINTS/IT(100),LOSSM(100)
      COMMON/LIMITS/ITMAX,ITMIN,MODMAX,MODMIN
      COMMON/HEADER/NHEAD(3),PTITLE(2)
      DIMENSION NS(8)
      DATA(NS=0,2,5,10,3,4,11,12)
      DELIT=(ITMAX-ITMIN)/7.
      SPACE=.2
      IF(FREQ.EQ.110.)KF=1
      IF(FREQ.EQ.35.)KF=2
      IF(FREQ.EQ.11.)KF=3
      IF(FREQ.EQ.3.5)KF=4
      IF(L+M.NE.0)GO TO 10
      K=1
      CALL PLOT(0.,-11.,-3)
      CALL PLOT(0.,2.75,-3)
      GO TO 20
   10 K=L+1
      IF(K.GT.1)GO TO 50
      CALL PLOT(11.,0.,-3)
   20 CALL AXIS(0.,0.,21H1000/(TEMPERATURE, K),-21,7.,0.,ITMIN,DELIT)
      IF(F.NE.1.)GO TO 30
      CALL AXIS(0.,0.,17HLOSS MODULUS, MPA,
     +17,5.,90.,MODMIN,(MODMAX-MODMIN)/5.)
      GO TO 40
   30 CALL AXIS(0.,0.,23HNORMALIZED LOSS MODULUS,
     +23,5.,90.,MODMIN,(MODMAX-MODMIN)/5.)
   40 CALL AXS(0.,5.,-7.,1.,0.)
      CALL AXS(7.,0.,5.,1.,90.)
      CALL SYMBOL(2.,7.5,.14,NHEAD,0.0,30)
      CALL SYMBOL(2.,5.2,.14,PTITLE,0.,20)
   50 CALL SYMBOL(6.,(4.7-SPACE*K)+.05,.07,NS(KF),0.,-1)
      CALL NUMBER(6.14,(4.7-SPACE*K),.1,FREQ,0.,1)
      IT(N+1)=ITMIN $ IT(N+2)=DELIT
      LOSSM(N+1)=MODMIN
      LOSSM(N+2)=(MODMAX-MODMIN)/5.
      CALL WINDOW(N,NS(KF))
      RETURN
      END
      SUBROUTINE WINDOW(N,NS)
      COMMON/LIMITS/X2,X1,Y2,Y1
      COMMON/POINTS/X(100),Y(100)
      J=-1
      DO 10      LP=1,N
      IF((X(LP)+.001).LT.X1)GO TO 10
      IF((X(LP)-.001).GT.X2)GO TO 10
      IF((Y(LP)+.001).LT.Y1)GO TO 10
      IF((Y(LP)-.001).GT.Y2)GO TO 10
      CALL SYMBOL((X(LP)-X(N+1))/X(N+2),(Y(LP)-Y(N+1))/Y(N+2),
     +.07,NS,0.0,J)
      J=-2
   10 CONTINUE
      RETURN
      END
      PROGRAM RATECON(INPUT,OUTPUT)
C  BATCH FORTRAN PROGRAM RATECON       6/1/78
C  CALCULATES FIRST ORDER REACTION RATE CONSTANTS FROM DSA
C  ISOTHERMAL CURE DATA BY A LEAST SQUARES FIT
C  VISCOSITY AT THE LOSS MAXIMUM FOR EACH FREQUENCY IS ENTERED
C  IN A DATA STATEMENT
C  LOG TIME TO THE LOSS MAXIMUM IS ENTERED FOR EACH RUN IN THE SAME
C  ORDER OF FREQUENCIES AS THE VISCOSITIES IN THE DATA STATEMENT
      REAL INTRCPT,M95
      DIMENSION VISC(20),T025(30),TIME(20),X(20),Y(20)
      DATA(T025(I),I=1,30)/12.706,4.303,3.182,2.776,2.571,
     +2.447,2.365,2.306,2.262,2.228,2.201,2.179,2.160,2.145,
     +2.131,2.12,2.11,2.101,2.093,2.086,2.08,2.074,2.069,
     +2.064,2.06,2.056,2.052,2.048,2.045,1.96/
      DATA(VISC(I),I=1,4)/1920.5,6035.7,19204.5,60357.1/
      PRINT 5
    5 FORMAT(/,* NUMBER OF RUNS*)
      READ *,M
      DO 4  K=1,M
      SX=0.$SY=0.$SXY=0.$SX2=0.$SY2=0.
C     PRINT 10
C  10 FORMAT(/,* NUMBER OF VISCOSITIES*)
C     READ *,N
      N=4
      PRINT 15
   15 FORMAT(/,* LOG10(TIME,SEC): T110,T35,T11,T3.5*)
      READ *,(TIME(I),I=1,N)
      DO 3  I=1,N
      X(I)=10.**(TIME(I))
      Y(I)=ALOG10(VISC(I))
    3 CONTINUE
C BEGIN LINEAR LEAST SQUARES
      DO 1 I=1,N
      SX=SX+X(I)
      SY=SY+Y(I)
      SXY=SXY+X(I)*Y(I)
      SX2=SX2+X(I)**2
      SY2=SY2+Y(I)**2
    1 CONTINUE
      SSQ=0.
      DO 2 I=1,N
      SSQ=((SX/N)-X(I))**2+SSQ
    2 CONTINUE
      SLOPE=(N*SXY-SX*SY)/(N*SX2-SX**2)
      INTRCPT=(SX2*SY-SX*SXY)/(N*SX2-SX**2)
      SIGMAB=SQRT(ABS(SY2-INTRCPT*SY-SLOPE*SXY)/(N-2.))
      SIGMAM=SQRT((SIGMAB**2)/SSQ)
      COD=SXY-SX*SY/N
      COD=COD/SQRT(SX2-SX**2/N)
      COD=COD/SQRT(SY2-SY**2/N)
      COD=COD**2
C END LINEAR LEAST SQUARES
      J=N-2
      IF(N.GE.32)J=30
      EN=N*1.
      M95=T025(J)*SIGMAM/SQRT(EN)
      B95=T025(J)*SIGMAB/SQRT(EN)
      PRINT 20,(VISC(I),I=1,N)
   20 FORMAT(//,3X,*VISC (POISE)*,10F8.1)
      PRINT 25,(X(I),I=1,N)
   25 FORMAT(3X,*TIME (SEC)  *,10F8.1)
      PRINT 30
   30 FORMAT(/,3X,* RATE  CON     95% CONF   INTERCEPT*,
     +4X,8H95% CONF,3X,9HCOEF DETN)
      PRINT 35,SLOPE,M95,INTRCPT,B95,COD
   35 FORMAT(1X,4(1PE12.3),0PF11.5)
      PRINT 40
   40 FORMAT(//)
    4 CONTINUE
      END
      PROGRAM VIBFIG(INPUT,OUTPUT,TAPEM=INPUT,TAPE20=OUTPUT,
     +DATA1,TAPE1=DATA1,DATA2,TAPE2=DATA2,DATA3,TAPE3=DATA3,DATA4,
     +TAPE4=DATA4)
C     FORTRAN PROGRAM VIBFIG II                4/8/78
C     (MODIFIED TO READ ANY NUMBER OF FREQUENCY SETS)
C     INPUT MODULI LIMITS IN MPA; (DYNES/SQ.CM.)/10**7=1MPA
C          INPUT DATA FILES
C     FIRST LINE: INTEGER  VARIABLE PLOTOPT(=0 DOES CALCULATIONS ONLY
C     =1 DOES CALCULATIONS
C     AND PLOTS); NFREQ, THE NUMBER OF FREQUENCY SETS IN THE RUN
C     SECOND LINE: TMAX AND TMIN, SET MAXIMUM AND MINIMUM VALUES FOR
C     PLOT TEMPERATURE SCALE;
C     LGMOMAX AND LGMOMIN, SET MAXIMUM AND MINIMUM VALUES FOR PLOT LOG
C     MODULUS SCALE; TANMAX,
C     SETS MAXIMUM VALUE FOR PLOT TAN DELTA SCALE
C     THIRD LINE: 30 ALPHANUMERIC CHARACTERS TO IDENTIFY THE SAMPLE;
C     20 FOR THE PLOT TITLE
C     FOURTH LINE OF FIRST FREQUENCY SET AND BEGINNING OF SUBSEQUENT
C     FREQUENCY SETS:
C     RHEOVIBRON ERROR CONSTANT AT AF=30 EK; INITIAL LENGTH OF SAMPLE
C     LEN,
C     IN CM; WIDTH OF THE FILM WIDTH, IN MILLS; THICKNESS OF THE FILM
C     THICK, IN MILLS; FREQUENCY
C     OMEGA, IN HZ.
C     FIFTH LINE OF FIRST FREQUENCY SET AND SECOND LINE OF SUBSEQUENT
C     FREQUENCY SETS:
C     TEMPERATURE T, IN C; AMPLITUDE FACTOR ACOM; DYNAMIC FORCE DCOM;
C     TAN
C     DELTA OF FILM TAND; CHANGE IN LENGTH OVER INITIAL LENGTH DLEN,
C     IN .01MM.
C     LAST LINE OF EACH FREQUENCY SET CONTAINS: "0.,999.,0.,0.,0."
C     LAST LINE OF FINAL FREQUENCY SET CONTAINS: "0.,1000.,0.,0.,0."
C     INTERNAL DATA: WLF CONSTANTS C1 AND C2; GLASS TRANSITION TEM-
C     PERATURE TG, IN C
C          OUTPUT DATA
C     ALL MODULI IN MPA
       REAL LGLOSM,LGSTOM,LOSSM,LOSSG,LEN,LGMOMAX,LGMOMIN
      INTEGER PLOTOPT
       COMMON/INITIAL/T(100),LGLOSM(100),LGSTOM(100),TAND(100)
       DIMENSION HEADING(3),PTITLE(2)
      M=1$  L=0$  NPIC=0
 1100 IF(M-MOLD.EQ.1)READ(M,*)N,PLOTOPT,NFREQ
       IF(M-MOLD.EQ.1)READ(M,*)N,TMAX,TMIN,LGMOMAX,LGMOMIN,TANMAX
      IF(PLOTOPT.NE.1)GO TO 1110
      IF(NPIC.NE.0)GO TO 1110
       CALL PLOTS(40)
      CALL PLOT(0.,-11.,-3)
1110 IF(M-MOLD.EQ.1)READ(M,2180)N,(HEADING(I),I=1,3),(PTITLE(I),I=1,2)
2180 FORMAT(F5.0,5A10)
     MOLD=M
      WRITE(20,2200)(HEADING(I),I=1,3),(PTITLE(I),I=1,2)
2200 FORMAT(1H1,/,5A10)
     IF(PLOTOPT.EQ.0)WRITE(20,2210)
2210 FORMAT(1H0,29X,20H*.........+.........*)
      WRITE(20,1150)
1150 FORMAT(1H0)
     READ(M,*)N,EK,LEN,WIDTH,THICK,OMEGA
     XAREA=WIDTH*THICK*6.4516*10.**(-6)
2340       FORMAT(1H0,2X,40HINCORRECT VALUE OF AMPLITUDE FACTOR USED)
     WRITE(20,2240)
2240 FORMAT(10H ERROR CON,3X,6HLENGTH,3X,5HWIDTH,3X,5HTHICK,
    +4X,4HFREQ)
2220 FORMAT(F8.1,F11.3,F8.1,F8.2,F9.2)
     J=1
1560       READ(M,*)N,T(J),ACOM,DCOM,TAND(J),DLEN
     IF(J.EQ.1)WRITE(20,2220)EK,LEN+DLEN*10.**(-3),WIDTH,THICK,
    +OMEGA
     IF(J.EQ.1)WRITE(20,1150)
     IF(ACOM.GE.999.)GO TO 2400
     IF(ACOM.EQ.10.)GO TO 1780
     IF(ACOM.EQ.20.)1640,1700
1640       ACOM=SQRT(10.)
     GO TO 1780
1700 IF(ACOM.EQ.30.)1710,1740
1710       ACOM=1.
     GO TO 1780
1740       WRITE(20,2340)
     GO TO 2140
1780       EKCOM=EK/ACOM
     DEL=ATAN(TAND(J))
     COMPMOD=2.*10.**(9)*(LEN+DLEN*10.**(-3))/(ACOM*(DCOM-EKCOM)*XAREA)
     STORM=COMPMOD*COS(DEL)/10.**(7)
     LOSSM=COMPMOD*SIN(DEL)/10.**(7)
     LGLOSM(J)=ALOG10(LOSSM)
     LGSTOM(J)=ALOG10(STORM)
     C1=-13.3
     C2=47.5
     TG=10000.
       IF(T(J).LE.TG)2000,2020
2000 IF(J.EQ.1)WRITE(20,2280)
2280 FORMAT(1X,5H TEMP,3X,7HTAN DEL,4X,6HE" MPA,3X,7HLOG(E"),4X,
    +6HE' MPA,3X,7HLOG(E'),2X,10HSHIFT*FREQ,2X,9HREDUCE E",3X,
     +9HREDUCE E!)
      WRITE(20,2320)T(J),TAND(J),LOSSM,LGLOSM(J),STORM,LGSTOM(J)
2320  FORMAT(F7.1,F8.3,1PE12.3,0PF8.3,1PE12.3,0PF8.3,1P3E12.3)
      GO TO 2140
2020  AT=10.**(C1*(T(J)-TG)/(C2+T(J)-TG))
      TTS=AT*OMEGA
      LOSSG=LOSSM*(TG+273.2)/(T(J)+273.2)
      STORG=STORM*(TG+273.2)/(T(J)+273.2)
      IF(J.EQ.1)WRITE(20,2280)
      WRITE(20,2320)T(J),TAND(J),LOSSM,LGLOSM(J),STORM,LGSTOM(J),
     +TTS,LOSSG,STORG
2140  LGLOSM(J)=LGLOSM(J)-1.
      J=J+1
      GO TO 1560
2400  IF(PLOTOPT.EQ.1)2450,2500
2450  IF(PLOTOPT.EQ.1)CALL PIC(L,NPIC,HEADING,J-1,TMAX,TMIN,
     +LGMOMAX,LGMOMIN,TANMAX,OMEGA,PTITLE)
      NPIC=NPIC+1
2500  L=L+1
      IF(L.EQ.NFREQ)M=M+1
      IF(L.EQ.NFREQ)L=0
      IF(ACOM.EQ.999.)GO TO 1100
2600  IF(NPIC.GT.0)CALL PLOT(END,0.0,999)
       STOP
       END
      SUBROUTINE PIC(L,M,NHEAD,N,TMAX,TMIN,LGMOMAX,LGMOMIN,TANMAX,
     +FREQ,PTITLE)
       REAL LGLOSM,LGSTOM,LGMOMAX,LGMOMIN
       COMMON/INITIAL/T(100),LGLOSM(100),LGSTOM(100),TAND(100)
       DIMENSION NHEAD(3),PTITLE(2),NS(8)
      DATA(NS=0,2,5,10,3,4,11,12)
       BOG=(TMAX-TMIN)/7.
      YP=.2
      IF(FREQ.EQ.110.)KF=1
      IF(FREQ.EQ.35.)KF=2
      IF(FREQ.EQ.11.)KF=3
      IF(FREQ.EQ.3.5)KF=4
      IF(L+M.EQ.0)5,10
    5 K=1
      CALL PLOT(0.,-11.,-3)
       CALL PLOT(0.,2.75,-3)
       GO TO 40
   10 K=L+1
       IF(K.GT.1)GO TO 20
       CALL PLOT(11.,0.,-3)
       GO TO 40
```

```
20 CALL PLOT(-11.,0.,-3)
40 IF(K.GT.1)GO TO 50
   CALL AXIS(0.,0.,17HTEMPERATURE     (C),-17,7.,0.,TMIN,BOG)
   CALL AXIS(0.,0.,25HLOG(STORAGE MODULUS, MPA),
  +25,5.,90.,LGMOMIN,(LGMOMAX-LGMOMIN)/5.)
   CALL AXIS(0.,5.,-7.,1.,0.)
   CALL AXIS(7.,0.,22HLOG(LOSS MODULUS, MPA),-22,5.,90.,LGMOMIN+1.,
  +(LGMOMAX-LGMOMIN)/5.)
   CALL SYMBOL(2.,7.5,.14,NHEAD,0.0,30)
   CALL SYMBOL(2.,5.2,.14,PTITLE,0.,20)
50 CALL SYMBOL(6.,(4.7-YP*K)+.05,.07,NS(KF),0.,-1)
   CALL NUMBER(6.14,(4.7-YP*K),.1,FREQ,0.,1)
   T(N+1)=TMIN $ T(N+2)=BOG
   LGSTOM(N+1)=LGLOSM(N+1)=LGMOMIN
   LGSTOM(N+2)=LGLOSM(N+2)=(LGMOMAX-LGMOMIN)/5.
   CALL PSYM(T,LGSTOM,N,NS(KF),TMIN,TMAX,LGMOMIN,LGMOMAX)
   CALL PSYM(T,LGLOSM,N,NS(KF),TMIN,TMAX,LGMOMIN,LGMOMAX)
   CALL PLOT(11.,0.,-3)
   IF(K.GT.1)GO TO 70
   CALL AXIS(0.,0.,17HTEMPERATURE     (C),-17,7.,0.,TMIN,BOG)
   CALL AXIS(0.,0.,9HTAN DELTA,9,5.,90.,0.,TANMAX/5.)
   CALL AXIS(0.,5.,-7.,1.,0.)
   CALL AXIS(7.,0.,5.,1.,90.)
   CALL SYMBOL(2.,7.5,.14,NHEAD,0.0,30)
   CALL SYMBOL(2.,5.2,.14,PTITLE,0.,20)
70 CALL SYMBOL(.4,(4.7-YP*K)+.05,.07,NS(KF),0.,-1)
   CALL NUMBER(.54,(4.7-YP*K),.1,FREQ,0.,1)
   TAND(N+1)=0.0        $ TAND(N+2)=TANMAX/5.
   CALL PSYM(T,TAND,N,NS(KF),TMIN,TMAX,0.,TANMAX)
   RETURN
   END
   SUBROUTINE PSYM(X,Y,N,NS,X1,X2,Y1,Y2)
   DIMENSION X(100),Y(100)
   J=-1
   DO 10      LP=1,N
   IF((X(LP)+.001).LT.X1)GO TO 10
   IF((X(LP)-.001).GT.X2)GO TO 10
   IF((Y(LP)+.001).LT.Y1)GO TO 10
   IF((Y(LP)-.001).GT.Y2)GO TO 10
   CALL SYMBOL((X(LP)-X(N+1))/X(N+2),(Y(LP)-Y(N+1))/Y(N+2),
  +.07,NS,0.0,J)
   J=-2
10 CONTINUE
   RETURN
   END
```

```
COMMENT.  PROCEDURE TO WRITE FROM MASS STORAGE TO MAG TAPE
VSN(TAPE1=GAS1)
LABEL(TAPE1,NT,PO=W,SI=EPOXYV,FI=$92500MNP PS 2HDS,G=0205,QN=9999)
GET,I93H2.
COPYEI(I93H2,TAPE1,V)
LABEL(TAPE1,NT,PO=W,SI=EPOXYV,FI=$92500MNP PS 1HDS,G=9227,QN=9999)
GET,I193H1.
COPYEI(I193H1,TAPE1,V)
LABEL(TAPE1,NT,PO=W,SI=EPOXYV,FI=$233000MNM PS 1HDS,G=9208,QN=9999)
GET,233H1.
COPYEI(233H1,TAPE1,V)
LABEL(TAPE1,NT,PO=W,SI=EPOXYV,FI=$233000MNM PS 2HDS,G=9209,QN=9999)
GET,233H2.
COPYEI(233H2,TAPE1,V)
REWIND,TAPE1.
LABEL(TAPE1,NT,PO=W,SI=EPOXYV)
LISTLB(TAPE1,LO=F,SI=EPOXYV,QN=83)
COMMENT.                END MSTONT
COMMENT.LABEL(TAPE1,NT,PO=W,SI=EPOXYV,FI=$CS,G=J,QN=9999)
COMMENT.GET,D.
COMMENT.COPYEI(D,TAPE1,V)
```

```
COMMENT.  PROCEDURE TO READ FROM MAG TAPE TO MASS STORAGE
VSN(TAPE1=GAS1)
LABEL(TAPE1,NT,SI=EPOXYV,PO=R)
LISTLB(TAPE1,SI=EPOXYV,LO=F)
REWIND,TAPE1.
LABEL(TAPE1,NT,PO=R,SI=EPOXYV,QN=23)
COPYEI(TAPE1,V4T2P43,V)
SAVE,V4T2P43.
LABEL(TAPE1,NT,PO=R,SI=EPOXYV,QN=25)
COPYEI(TAPE1,V4T2P39,V)
SAVE,V4T2P39.
LABEL(TAPE1,NT,PO=R,SI=EPOXYV,QN=28)
COPYEI(TAPE1,V4T1P60,V)
SAVE,V4T1P60.
LABEL(TAPE1,NT,PO=R,SI=EPOXYV,QN=29)
COPYEI(TAPE1,V4T1P56,V)
SAVE,V4T1P56.
COMMENT.          END NTTOMS
COMMENT.LABEL(TAPE1,NT,PO=R,SI=EPOXYV,QN=J)
COMMENT.COPYEI(TAPE1,D,V)
COMMENT.SAVE,D.
```